EiABC
Ethiopian Institute of Architecture, Building Construction and City Development
Addis Ababa University

Addis Ababa University
Ethiopian Institute of Architecture, Building Construction, and City Development (EiABC)

Analyzing the impacts of urbanization and climate change on urban flood and planning of resilience-based flood hazard management: A case of Adama City, Ethiopia

By:

Dejene Tesema Bulti

A Dissertation Submitted to the School of Graduate Studies of Addis Ababa University, Ethiopian Institute of Architecture, Building Construction and City Development, in Partial Fulfillment of the Requirements for the Award of Doctor of Philosophy Degree in Urban and Regional Planning.

Supervisors:

Dr. Birhanu Girma

Dr. Zelalem Biru

June 2021

Addis Ababa, Ethiopia

Declaration

I hereby declare that this dissertation is the result of my own original work and has not been submitted at any University/Institutions for any degree or other purpose. All materials other than my own idea used in this study from other sources have been fully acknowledged and cited in the text properly.

Name: Dejene Tesema Bulti

Signature: _____

Date: _____

Approval

As a member of the Examiners board of the PhD Dissertation open defense of Dejene Tesema Bulti, we have read and evaluated the Dissertation prepared by Dejene Tesema Bulti entitled "**Analyzing the impacts of urbanization and climate change on urban flood and planning of resilience-based flood hazard management: A case of Adama City, Ethiopia"** and recommended to Ethiopian Institute of Architecture, Building Construction and City Development, Addis Ababa University to accept the Dissertation as it meets the accepted standards with respect to originality and quality for the partial fulfillment of requirements for the award of Doctor of Philosophy Degree in Urban and Regional Planning.

Board of Examiners:

Dr. Birhanu Girma		
Dr. Zelalem Biru		
Advisors	**Signature**	**Date**
Dr. Mihret Dananto		
External Examiner	**Signature**	**Date**
Professor Hailu Worku		
Internal Examiner	**Signature**	**Date**
Dr. Sisay Seifu		
Chair Person	**Signature**	**Date**
Dr. Dagnachew Adugna		
Graduate Program Director	**Signature**	**Date**

ACKNOWLEDGMENTS

I would like to express my special appreciation and thanks to my supervisors Dr. Birhanu Girma and Dr. Zelalem Biru. Starting from scratch was not very easy and our discussions and their willingness to listen and to read many lines of chapters helped me to finalize the thesis. Thank you for the critical review of my findings.

A special thanks to HydroPraxis company for PCSWMM—modeling software provided for this research.

I would like to extend my appreciation to Adama city administration staffs, Mr. Lijalem Tafese and Mr. Shimelis Regasa for the provided urban drainage system and land use data.

Finally, this dissertation is dedicated to my family

With love and thanks.

ABSTRACT

Urban flooding, which occurs when rainfall exceeds the capacity of urban drainage systems, has become a major concern in many cities across the world. Due to urbanization-driven increases in impermeable surfaces and climate change-induced increases in extreme precipitation, urban flood is anticipated to rising in frequency and intensity in the future. The majority of Ethiopian cities are susceptible to urban floods, although there is little research on the subject. Understanding of the contributions of main drivers at appropriate spatial and temporal scales, features of potential floods under current and future conditions and various flood frequencies, as well as flood adaptation measures at smaller spatial scales can aid efforts to effectively respond to the current problem of urban flooding, as well as consideration of its potential future increase. This study aims to analyze the impacts of urbanization and climate change on urban flood in Adama City and to devise resilience-based flood hazard management strategies.

By mapping LULC of the City at about 5-year interval from 1995 to 2019 and computing the runoff depth at respective years using SCS-CN method, the dynamics of the City's hydrologic characteristics attributable to urbanization-induced spatio-temporal changes of LULC was analyzed. Statistical downscaling model (SDSM) and extreme precipitation indices were, respectively used for downscaling daily precipitation from the projections of two Global Circulation Models (CanESM2 and HadCM3) and for analyzing the impacts of climate change on the historical and future extreme precipitation events. Further, the potential changes in the relationship between intensity-duration-frequency (IDF) of extreme precipitation in present-day and future periods were compared and contrasted. IDF curves and their functions were deduced using Gumbel Type I probability distribution and power-regression model, respectively. Flood inundation model was developed with coupled 1D-2D flood modeling method using PCSWMM, and used for simulating potential floods for a range of return periods and possible combinations of existing and future LULC and climate scenarios. Flood hazard levels were determined based on flow depth-velocity approach, for each scenario. The theory of urban resilience to floods was adopted for assessing the flood resilience level of the study area and for planning resilience-based flood hazard management. Flood-prone area was selected from the 100-yr flood scenarios and under the combined future LULC and climate. Localized flood adaption strategies were identified and their suitability for the selected prone area was assessed.

The findings show that the built-up area undergone 7.9% expansion rate from 1995 to 2019. Likewise, the runoff depth is increased by 9.5 % in the City administration and 12.9 % and 6.9 % within the two sub-watersheds. At all spatial scales, the temporal change of runoff depth is linearly associated with the rise of imperviousness ratio. Moreover, statistically significant trends were obtained for the majority of extreme precipitation indices computed for historical daily rainfall records of 1967-2016, indicating that climate change has had an impact on historical precipitation. Moreover, extreme precipitation is expected to rise in the future up to 2080. The findings also reveal that extreme precipitation intensity over the years 2021-2070 in Adama City would increase up to 49.5% or decrease up to 106.2%, depending on GCM, storm duration and return period considered. Furthermore, the study area is flooded under both existing and future land cover and climate conditions, with increasing in the water depth, flow velocity and inundation extent as the return period increases. Under historical climate and existing land-use scenario, 123.7 (5-yr)-204.3 ha (100-yr) is prone to flood whereas the extent varies from 178.2 to 396.8 ha, under the combined effect of future land use and climate changes. Moreover, the study area is associated with lower level flood resilience. Finally, elevated configuration, dry-proofing, wet-proofing, temporary measures and site and landscape interventions are proposed as effective strategies for building flood resilience of the prone community.

In line with sustainable flood risk management in the City, it is suggested that the stakeholders recognize the level of potential associated risk and improve the awareness of the prone community. Future developments should be guided with impervious surface based land-use regulation in order to better control the hydrological effects of urbanization. Further, the standards and guidelines presently employed by the City for the planning and design of stormwater management infrastructure should be revised in such a way that they reflect global climate change impacts at local level. Designing and updating local development plans on flood-prone areas should also aim to ingrate localized flood adoption strategies to build flood resilience of the prone community. Finally, urban planning policies should aim to promote urban flood modeling as a base for urban flood hazard management operations, and personal responsibility in flood safety.

Keywords: urban flood, climate change, flood modeling, flood hazard, statistical downscaling, flood resilience, extreme precipitation, IDF

TABLE OF CONTENTS

LIST OF FIGURES

LIST OF TABLES

LIST OF ACRONYMS

AHP:	analytical hierarchical process (AHP)
CN:	Curve Number
DEM:	Digital Elevation Model
DN:	Digital Number
DTM:	Digital Terrain Model
ETCCDI:	Expert Team On Climate Change Detection and Indices
FI:	Flood Intensity
GCM:	Global Circulation Model
GHG:	Greenhouse Gases
HSG:	Hydrological soil group
IDF:	Intensity-Duration-Frequency
LDP:	Local Development Plan
LULC:	Land Use Land Cover
MCDA:	Multi-Criteria Decision Analysis (MCDA)
MCDM	Multi-Criteria Decision-Making
NASA:	National Aeronautics and Space Administration
NMA:	National Meteorological Agency
PCSWMM:	Personal Computer Storm Water Management Model
PIA:	Percent Impervious Area
RCP:	Representative Concentration Pathways
SCS-CN:	Soil Conservation Service Curve Number
SDSM:	Statistical Downscaling Model

SWMM: Storm Water Management Model

UFI: Urban Floodability Index

CHAPTER 1: INTRODUCTION

1.1 Background of the study

Around the world, more people are concentrated in towns and cities. In 2017, the proportion of urban population was 55 percent and projected to reach 68 percent in 2050 (UN, 2018). The rise of a number of urban population is among primary drivers of substantial alterations of land cover types around many urban areas to increase impermeable surfaces (Parsasyrat and Jamali, 2015; Berihun et al., 2019). In the context of developing countries, such as Ethiopia, unplanned urban growth is a common scenario (Bajracharya et al., 2015), leading to rapid increase of impervious land areas. Impervious surface reduces infiltration and resistance to flow, leads the volume and flowrate of rainfall-runoff to rise (Mejía & Moglen, 2009; Chen et al., 2017).

Global warming is now being caused by the human-induced changes in the natural environment, and the term "climate change" is frequently used to denote the human-specific consequences (Mekonen and Berlie, 2019; Geremew et al., 2020). With the recent achievements in climate science, several global circulation models (GCMs) have been developed for simulating changes in climatic features of the current and future periods. In order to enable impact studies, climate information on the twenty-first century is projected by several GCMs.

Climate change influences the fundamental characteristics of extreme precipitation, usually described in terms of Intensity-Duration-Frequency (IDF) relationship; as a result it trigger climate-related natural hazards, such as floods (Deb et al., 2018; Natarajan and Radhakrishnan, 2019; Stephenson et al., 2016; Zahiri et al., 2016; Zeder and Fischer, 2020). There has also been the growing recognition that the changes in

global climate are likely to be one of the most drivers of future increasing flood risk (Jha et al., 2011; Zhou et al., 2018).

Urbanization-driven increased impermeable surface, combined with increased intensity of extreme precipitation caused by the changing climate, aggravates flooding in several cities worldwide (Huong & Pathirana, 2013). Recent decades have witnessed a number of severe flood incidents around the globe that led to displacement of millions of people, thousands of deaths and financial loses that amount to billions of Dollars (IFRC, 2014; Parsasyrat & Jamali, 2015; Batica & Gourbesville, 2016; Abshirini et al., 2017). Flooding in urban areas is mostly pluvial flood (urban flood) (Tingsanchali, 2012; Bouvier, et al. 2017; Meng et al., 2019). Urban flood occurs when the volume of rainfall-runoff exceeds the capacity of the urban storm drainage system.

Like many cities in the world, various urban areas of Ethiopia are susceptible to urban flood (NDRMC, 2018; Birhanu et al., 2016; Ogato et al., 2020). In Adama City, a fast-growing Regional City with densely populated floodplain areas, urban flooding has arguably been more widespread (Chemeda, 2020). Since the turn of 21st century, several floods have occurred in the City with a lot of calamity to the residents, although keeping track of such incidents in the context of Ethiopia is uncommon.

Despite its importance, urban flood has received little attention in research and practice, until recent decades. Because there are well-established methods for designing stormwater drainage systems, urban flooding is thought to be a “solved” technical problem. However, the conventional engineering methods for designing of urban flood control infrastructure hinge on time-invariant (stationary assumption) land covers and rainfall distribution (Rosenzweig et al., 2018), which is being challenged by rapid urbanization and global climate change. On the other hand, the impacts of urban

flooding are presumed to be minimal, yet there are examples where it has caused loss of lives, substantial property damage, and disruption of urban critical systems (Douglas et al., 2010; ACFMP, 2016). In addition, the cumulative costs of comparatively minor but frequent flood events can surpass that of less frequent flood events with severe impacts.

In line with growing concern of sustainable development of urban areas, detecting the influences of increased impermeable surface area due to urbanization and climatic change-induced rainfall intensity on urban floods has become the main concern of recent research. Numerous studies have looked at the effects of urbanization on hydrological attributes of urban watersheds, yet the results are inconsistent. Although significant positive linear relationship is found between urbanization driven increased impervious surface and runoff (Sanyal et al., 2014; Ohana-Levi et al., 2017; Li et al., 2018), there are also evidences of deviation from this relationship (Su et al., 2014). Even recent case studies (e.g., Chen et al., 2015) have found indirect correlation urbanization and runoff in some sub-basin of analyzed watershed. The impacts of urbanization, mainly depend on the spatial distribution of impervious surfaces in a given watershed and the scale of the study area.

As more emphasis is placed on evaluating potential circumstances for future climate change at the local scale, attempts have been made to examine the susceptibility of stormwater drainage infrastructure to climate change, with the estimate of future extreme rainfall being the most significant step (Nie et al., 2009; Tran et al., 2011; Amaguchi and Kawamura, 2016). Future design rainfall is forecasted in these research by utilizing hypothetical increments of present-day rainfall information.

By using the outputs of GCMs, several researchers assessed the change in extreme precipitation characteristics attributable to climate change (Buba et al., 2017; Fadhel et al., 2017; Yilmaz et al., 2014; Mirhosseini et al., 2012; Abbasnia and Toros, 2016; Shiferaw et al., 2018; Salvacion et al., 2018; Moses and Gondwe, 2019). The findings of these studies confirmed that the current extreme precipitation characteristics is likely to change, due to the impacts of the change in global climate. moreover, the observed changes are extremely varied across geographic areas, as well as at lower spatial scales, necessitating local scale study to effectively address climate-related hazards.

There are also many studies conducted to explore the implications of climate change on stormwater drainage infrastructure (Rosenberg et al., 2010; Karamouz and Nazif, 2013; Willems, 2013), and revealed that present stormwater drainage systems in the study areas may be insufficient under future design conditions. However, literature on the impacts of change in global climate on urban flooding is scant, though the changes in extreme precipitation intensity may imply variations in pluvial floods in some regions. Furthermore, quantitative evaluation of the effectiveness of urban drainage systems in response to climate change is lacking in Ethiopia.

Urban flood modelling has a key role in a contemporary urban flood hazard and risk management. It provides features of potential floods such as inundation extent, water depth and flow velocity, plays significant role in producing accurate City's flood hazard maps corresponding to various return periods (example 5-yr, 10-yr etc.). Reliable flood hazard maps play critical role in designing sustainable urban plans, protecting properties and lives, and reducing flood risk (Luo et al., 2018; Pinos and Timbe, 2019). Many countries use urban flood modeling to promote flood risk reduction, yet

application of such more scientific approach in urban flooding issue is too often neglected in Ethiopia.

Over the years, the use of flood-control infrastructures has been regarded as a predominant method for urban flood mitigation (Yeo, 2013), as a result, urban design rarely considers the possibility of flooding and assumes urban flood hazard mitigation to be a business of hydraulic engineering. However, structural measures are unlikely reliable under uncertainties arising from climate change and urbanization (Hughes & Sharman, 2015; Barroca & Pacteau, 2018).

Since recent decades, attention is shifting toward resilience-based strategies for flood hazard mitigation and recovery options (Liao, 2012; Rosenzweig et al., 2018). Resilience is a contested concept that has been exposed to different definitions in various disciplines and contexts (Batica et al., 2013; Meerow et al., 2016; Quinlan et al., 2016). Urban flood resilience is interpreted as the capacity of the City to tolerate flooding and to quickly reorganize if physical damage and socioeconomic disruption occur (Liao, 2012). Flood tolerance refers to the capacity to remain undamaged and functional in the event of a flood; essentially not preventing floods altogether. However, the concept still remains theoretical and lacks empirical studies applied in urban flood hazard management (Su, 2016). Moreover, attempts to assess urban flood resilience are largely rested on post-disaster recovery, and the quantitative assessment of the mitigation aspect of flood resilience—flood tolerance—is still largely unexplored.

On the other hand, there is a common belief that cities have no spare room for floodwater, due to their high population density and land values. However, this assumption is no more valid because there are studies that illustrate environmental

design strategies that could allow urban areas to accommodate flooding (Zevenbergen et al., 2011; Serre et al., 2016).

A number of Ethiopian cities, including Adama City, confront comparable difficulties when it comes to (re)development and expansion projects in flood-prone areas, and they realize the need for alternative planning techniques to control present and future flood hazards in the areas. On the other hand, there is a common perception that hazard management is largely the responsibility of the government. It is essential to look for new ways to distribute responsibilities among all sorts of stakeholders so that diverse projects may be implemented at various spatial scales, from individual buildings to watersheds. In this regard, there is a definite need to integrate resilience measures at the lowest spatial level as part of a top-down and bottom-up strategy, yet research to investigate the potential application of strategies to improve localized flood response capacity is scant.

1.2 Statement of the problem

Adama City is one of Ethiopia's fastest growing cities, with densely populated floodplain areas. The City is established on the low-lying flat terrain with mountains and ridge topography surrounding it. It serves as the center of vast region with enormous economic potential. Urban flood has become a regular feature of the City during rainy seasons with a lot of calamity to the residents. In recent past, floods occurred in 2008, 2009, 2013 and 2016 caused significant social, economic and ecological damages in different parts of the City (Bulti et al., 2017; NDRMC, 2018). Flood event in 2013 had affected about 3,000 people and resulted in estimated economic damage of Eth. Birr 23 million. In addition, flood occurred in 2016 resulted in the loss of 4 lives and the displacement of 300 households (ACFMP, 2016).

Efforts to manage flood hazard are targeted at controlling flood by structural measures, which have been identified as ineffective in the face of uncertainty. On the other hand, the City has no stormwater drainage masterplan so far and information on the network and performance of the City's drainage system is limited (ACFMP, 2016). Under combined effects of urbanization and perhaps increasing extreme precipitation events as a result of climate change, such a poorly planned and operated stormwater drainage system would most certainly result frequent and devastating urban flooding overtime, leading the City more vulnerable to flood.

There are limited studies conducted with respect flooding in Adama City. By using Multi-Criteria Decision Analysis (MCDA), Bulti et al. (2017) identified that 10.4% of Adama City administration, comprising different urban land uses, is located in a high flood hazard zone. Bashah (2015) confirmed that the capacity of crossing structures in section of Adama-Asela road in the City is inadequate. It has also been argued that poor solid waste management is the main cause of flooding in Adama City (Hailemariam & Ajeme, 2014; ACFMP, 2016; Woldetsadik, 2017). Detention ponds as flood risk mitigation measure for Boku Shenen area, south-east part of the City, have also been proposed by Aychiluhim (2016). However, in response to the existing flooding problems of Adama City, and the thoughtfulness of a potential increase of the impacts of urbanization and the change in global climate, flooding of the City demands more empirical investigations.

Although scientific study on urban flooding specific to Adama City is limited, flood problem in urban areas has recently been a growing study emphasis in Ethiopia. The relative contribution of land-use and climate changes on flood frequency has been analyzed in two Cities of Ethiopia: Dire Dawa (Billi et al., 2015) and Addis Ababa

(Birhanu et al., 2016). The results reflect, the effects of underlying flood drivers depend on local situation; for example, geographical location, level of planning and socioeconomic level.

Flood-prone areas of different urban areas of the country have been delineated using MCDA approach (Getahun & Gebre, 2015; Bulti et al., 2017; Assefa, 2018; Ogato et al., 2020). However, the results of such methods do not provide physical characteristics of floods—important parameters for flood hazard assessment. Many studies have also employed hydrodynamic simulation models to map flood hazard areas (Alemu, 2015; Erena et al., 2018), yet they deliberated on riverine flood.

By spatially downscaling future climate information from the outputs GCMs, studies have documented the variability in extreme precipitation events attributable to climate change (Dile et al., 2013; Samuale et al., 2014; Rukundo and Doğan, 2016; Mohammed et al., 2020), despite the focus on cities has attracted attention of few scholars, e.g., Feyissa et al. (2018). With more detail, few recent studies (e.g., Gebreigziabher, 2020; Gebremedhin, 2017; Gebru, 2020; Tesfay and Quraishi, 2017) have investigated the impacts of climate change on the relationship between extreme precipitation IDF. In-depth investigation, however, is necessary to acquire a complete understanding of the impacts of the changes in global climate. In this respect, focusing on urban flood hazard can aid in the development of long-term management strategies.

Despite acknowledged studies above provided insight into flooding problem in different urban areas of the country, much more needs to be done to improve understanding and respond effectively to the existing problem of urban flooding, as well as the consideration of its potential increase in the future. In this regard, investigation should address the impact of spatio-temporal changes of LULC on

hydrological characteristic of urban areas and the combined effect of urbanization and climate change on flood. Urban flood modeling also requires consideration of existing storm drainage infrastructures, in order to provide reliable information for a proper flood risk assessment. Moreover, following unreliability of conventional flood prevention measures under uncertainties, operationalization of the concept of resilience in urban flood hazard management has become a concern of research and practice (Rosenzweig et al., 2018; Zhou et al., 2018; Shin et al., 2018). Addressing these problems will have practical benefits for Adama City in developing effective flood hazard management strategies. Moreover, it contributes to understanding of this widespread phenomena. as well as potentially inform future policy objectives.

The purpose of this study is to determine the level of urban flood hazard in Adama City and its future variations as a result of evolving LULC changes due to urbanization and climate change-induced variation in extreme precipitation by simulating flood inundation with coupled drainage flow (1D) and overland flow (2D) models. By employing the theory of urban resilience to flood (Liao, 2012), it also assesses the level of flood resilience of the City and devise a resilience-based urban flood hazard strategies for prone areas.

1.3 Objectives

General objective

To analyze the impacts of urbanization and climate change on urban flood in Adama City and to propose resilience-based flood hazard management.

Specific objectives

- To analyze the changes in storm runoff depth due to spatio-temporal changes of LULC due to urbanization in Adama City from 1995 to 2019
- To downscale future precipitation from GCM outputs and assess the variations in extreme precipitation events in the future periods 2020-2050 and 2051-2080.
- To analyze the climate change-induced variations in relationship between intensity, duration and frequency of extreme precipitation in Adama City
- To assess the level of flood hazard in Awash sub-watershed in the Adama City under existing and future LULC and climate conditions in 2050
- To measure flood resilience level of Awash sub-watershed in Adama City based on theory of urban resilience to flood
- To devise resilience-based flood hazard management strategies suitable for local prone areas

1.4 Research questions

1. How has the storm runoff depth in Adama City been changed due to the changes of LULC from 1995 to 2019?
    - How has the LULC in Adama City administration been changed between 1995 and 2019?
    - How has runoff depth in Adama City administration boundary and in its sub-watersheds been changed due to the LULC changes from 1995 to 2019?
    - What is the relation between the spatio-temporal changes of imperviousness due to urbanization and the runoff depth during 1995 to 2019?

2. How does extreme precipitation events in historical climate changes in the future period due to climate change in Adama City?
    - What was the trend of extreme precipitation events in Adama City over the period of 1967-2016?
    - How can the future period (2021-2080) daily precipitation in Adama City be downscaled from the estimates of GCMs?
    - How does extreme precipitation events in present-day climate changes in the future periods 2021-2050 and 2051-2080?
3. What is the change in the relationship between intensity, duration and frequency of extreme precipitation of future period?
    - How can the observed (1967-2016) and the projected (2021-2070) daily precipitation be disaggregated into sub-daily time resolution
    - What is the relationship between IDF of extreme precipitation in the present-day and future climate conditions?
    - How does the relationship between extreme precipitation IDF in present-day climate changes in the future extreme rainfall for a range of storm durations and return periods?
4. What is the level of urban flood hazard in Awash sub-watershed in Adama City under the current and potential LULC and climate changes in 2050?
    - How can urban flood inundation in Awash sub-watershed be modelled using a coupled one-dimensional drainage flow (1D) and overland flow (2D) models
    - What is the level of urban flood hazard in Awash sub-watershed under the current and future LULC and climate condition?

- How the urban flood hazard in Awash sub-watershed changes under future LULC and climate condition in 2050?

5. What is the flood resilience level of Awash sub-watershed in Adama City in response to flood hazard under the combined effect of LULC and climate changes in 2050?
    - What are potential floodable lands in the existing and proposed land use in Awash sub-watershed
    - What is the level of floodability of Awash sub-watershed under the current and future LULC and climate condition in 2050?
6. What are the available localized flood adaptation techniques, and how can they be employed in resilience-based flood hazard management?

1.5 Delimitation of the study

There are some demarcating lines-ups to which the study extends such as time, theoretical and methodological perspectives, temporal and spatial extent which the analysis uses as inputs to produce the aimed result, and its level of generalizability. Adama City falls in two distinct macro watersheds: Awash sub-watershed and Mermersa sub-watershed. Both watersheds have experienced flooding problem. However, the main problem of flooding in the latter case is mainly related to Mermersa pond whereas in the case of the former is due to exceedance flow in urban drainage infrastructure at the central part of the City. In line with the objective of this study Awash subwatershed deemed appropriate and selected for the case study. The results of this study could be generalizable to urban areas with similar urban flood problem, environmental conditions, socioeconomic status, and under the same urban land-use planning system. Moreover, the assumption taken in this study includes existing

drainage infrastructures function at their full capacity and no infrastructure upgrade is undertaken, as well as the structural plan of the City will be implemented effectively in guiding future development of the City.

1.6 Structure of the dissertation

This dissertation is composed of six chapters. The current chapter presented the background of the study, statement of the problem, objectives, research questions and significance of the study. Chapter 2 presents a review of review of related literature. The methodology used in the study are discussed in chapter 3. Chapter 4 presents the results and discussion of the study. The last chapter presents conclusions drawn from the study and recommendations.

CHAPTER 2: LITERATURE REVIEW

2.1 Introduction

This chapter presents a literature review of the key concepts, which serve as the theoretical and conceptual background to the study. The literature includes scientific and academic journals, conference proceedings, books, and government and international organizations reports. The chapter starts with defining the most important terms to provide the contexts they are used in this study. As the study is related to rain-related urban flooding, the brief explanation of the rainfall-runoff process in urban areas and downscaling of GCMs projections are presented in section 2.3 and 2.4, respectively. Section 2.5 presents conceptualization of urban flood as dual drainage concept. In section 2.6, the main drivers of urban flood and the extent to which they are addressed by local studies is explored. Flood hazard map is key component of flood hazard management. Reliability of information provided by flood hazard map is primarily affected the method used in mapping. Hence, mapping techniques, along with their potential application and limitations are explored in section 2.7. Simulation of urban flood inundation is the centerpiece of this study. The selection of appropriate method demands to balance between the type and quality of the simulation results, model complexity, input data, time, hardware and software required for implementation. By taking these facets into account, features of urban flood modeling approaches are explored in section 2.8. Section 2.9 examines the conventional flood hazard management strategies: structural and nonstructural approaches. The concept of resilience is taken-up in section 2.10. The two distinct interpretations of resilience: engineering and ecological resilience are discussed. The theory of urban resilience to floods is explained in brief. The review of empirical studies and existing literature and

knowledge gaps are presented in section 2.11 and 2.12, respectively. Conceptual framework of the study is presented in the last section of this Chapter.

2.2 Definition of terms

Urbanization

Urbanization is often defined in different ways. In relation to population growth—"Urbanization refers to the increasing number of people that live in urban areas". Sometimes it is taken as local state's territorial expansion. In this study, process-based definition is adopted "a process of artificial land-use alteration during time." Because of socio-economic change and regional economic growth drive land demand, a competition in space, spatial planning, and, consequently, lead to land-use change. In this case, it involves the development of urban infrastructure and public service facilities that supply for the changing economic and social circumstances. The temporal dimension of urbanization is usually established by a planning period—a span of time in which reliable projection of urban changes can be made. It is often between 15 and 25 years.

Climate change

Climate change is defined as a change in the condition of the climate that can be characterized by changes in the mean and/or variability of its attributes—such as temperature and rainfall—in a region over a long period of time. Climate change can be caused by natural internal processes, external forcing, or by long-term human changes in the composition of the atmosphere or land use systems. In this study, it characterized by average long-term changes of precipitation.

Urban flood

Flooding is a natural phenomenon characterized by a great overflow of water submerges normally dry lands. Flood in urban areas can be coastal (surge flood)—due to extreme tidal conditions caused by severe weather; fluvial (river flood)—caused by excessive rainfall over extended period of time, heavy snow melt and ice jams; and pluvial flood—a flood event independent of an overflowing water body. In this study, urban flood refers to a flood occurs when the volume of rain-related runoff exceeds the capacity of urban stormwater drainage system.

Resilience

Resilience is a contested concept that has been exposed to different definitions in various disciplines and contexts. In engineering, resilience refers to a system's ability to resist and return to original state. In ecology, it is associated with the change that the system can tolerate and the capacity to reorganize or renew, irrespective of the state. In this study, the definition used by (Anger et al., 2005; Berkes, 2007) is adopted which defined resilience as the capacity of a system to absorb recurrent hazard impacts and to reorganize while undergoing change so as to maintain fundamental structures, processes, identity, and feedbacks. This definition acknowledges the inevitability of natural hazard, and the emphasis is on how the system will withstand a hazard by making necessary internal adjustments.

2.3 Rainfall-runoff process in urban areas

Flood modeling needs an adequate understanding of important processes that occur in the drainage system from the input (rainfall) to the output (outflow) (Josef, 2012; Jaafar et al., 2015). Figure 2.1 demonstrates the rainfall-runoff process in urban regions.

Rainfall, a prominent type of precipitation, is the main source of runoff in most urban areas (Subramanya, 2008; Butler and Davies, 2011; Tingsanchali, 2012). It is usually expressed as a depth of liquid water measured in millimeters, indicating the water depth that would store on the ground surface, if all the rain remained where it had dropped.

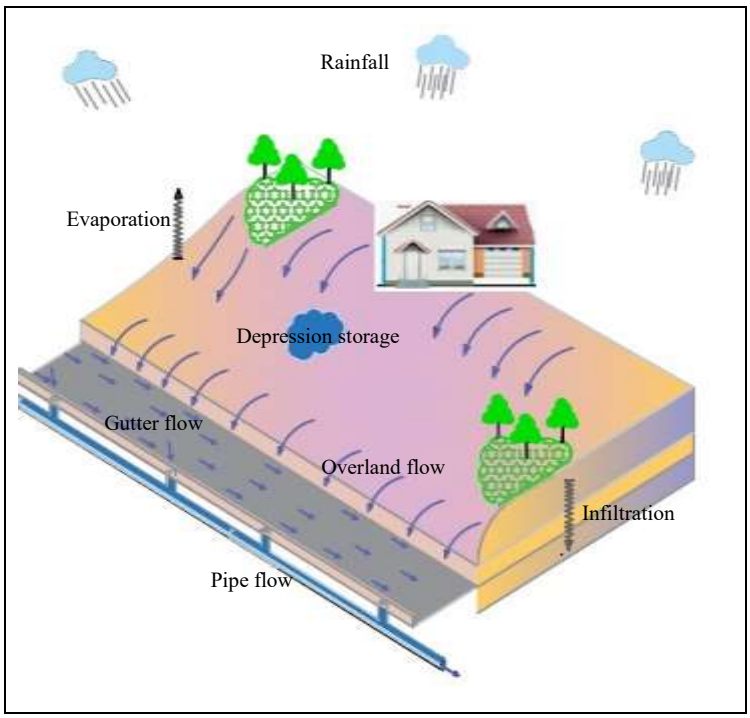

Figure 2.1 Schematic representation of rainfall–runoff processes in urban areas

Not all rainwater falling on the catchment surface is converted to runoff, rather it is subjected to initial and continuing losses. Initial loss refers to the portion of stormwater conserved on vegetation and buildings. It also includes rainwater trapped in surface puddles and ditches occur on any surfaces, paved or otherwise. The volume of initial loss is commonly considered as a minimum quantity of rainfall causing runoff (Loucks et al., 2005). On the other hand, continuing loss occurs as a result of the processes of infiltration and evapotranspiration, and they are assumed to proceed as far as the stormwater is available on the surface of the ground. The amount of both types of losses relies on the catchment characteristics and duration of the storm. In urbanized

catchment with dominant impervious surfaces, the loss prior to runoff is smaller for periods with intense rainfall (Josef, 2012). Infiltration is usually higher at the start of a rain and tends to diminish exponentially, once the soil became saturated (Gupta, 2017).

If the amount of precipitation exceeds the combined initial and continuing losses, the excess rain known as runoff starts flowing across the surface to enter the urban drainage network. The flow will be changed to gutter flow as it reaches streets or natural flow paths. Finally, it becomes channel flow once it enters the storm water drainage system.

2.4 Downscaling large-scale future climate information

Climate information about future period is projected by several Global Circulation Models (GCMs) and readily available up to the end of 21st century. However, the resolution of GCMs is usually quite coarse, about 70-500 kilometers spatial scale and at temporal scales of monthly means and longer (ARCC, 2014; Gharbia et al., 2016; Deb et al., 2018; Navarro-Racines et al., 2020). Hence, downscaling is required in order to derive GCMs' projections at the finer-scale (usually tens or hundreds of square kilometers), the scale at which climate information is usually required for climate change impact studies (Pervez and Henebry, 2014).

Downscaling of climate information from GCMs' outputs is grounded on the assumption that local climate is conditioned by interactions between the local features (e.g., mountain ranges, water bodies, land surface properties, etc.) and the large-scale atmospheric characteristics (e.g., circulation, temperature, moisture, etc.). The process of downscaling adds information to the GCMs' outputs so that the derived information is more realistic at a smaller-scale. Based on the way the information about local

conditions combined with that of large-scale climate projections, downscaling approaches can be grouped into dynamical downscaling and statistical downscaling.

Dynamical downscaling relies on the employment of a regional climate model (RCM), which is based on the same concepts as a global climate model but has a higher resolution. RCMs take the large-scale atmospheric information provided by GCM output at the lateral boundaries and combine it with more complex topography, land-sea contrast, surface heterogeneities, and detailed descriptions of physical processes to produce realistic climate information with a spatial resolution of about 20–50 kilometers. However, climate change impact studies at local area usually requires climate information at finer-scale.

Statistical downscaling method involves the establishment of empirical relationships between historical large-scale atmospheric and local climate variables. Once a relationship has been established, future atmospheric variables projected by GCMs are used to predict future local climate variables. This method provides climate information at any scale, down to station-level with a low computational cost (Wilby and Dawson, 2013; Gharbia, 2016). However, this approach assumes the present-day empirical relationship between the local observed climate variable (e.g., Precipitation) and its estimates by GCMs remains unchanged under the future climatic conditions.

As more emphasis is placed on evaluating potential circumstances for future climate change at local scale, several researchers have downscaled long-term future climate conditions projected by GCMs using statistical downscaling methods (Abbasnia and Toros, 2016; Shiferaw et al., 2018; Salvacion et al., 2018; Moses and Gondwe, 2019). To this point, some attempts have been made to downscale the outputs of GCMs to provide the long-term future climate conditions in Ethiopia for hydrological

applications (Dile et al., 2013; Samuale et al., 2014; Rukundo and Doğan, 2016; Mohammed et al. 2020). However, the downscaling of GCMs estimates for cities is limited, although there is an example to the contrary (Feyissa et al., 2018). Moreover, the statistically downscaled future daily precipitation is also further applied in few studies for assessing the impacts of climate change on IDF relationship in the country (Gebreigziabher, 2020; Gebremedhin, 2017; Gebru, 2020; Tesfay and Quraishi, 2017). They documented the IDF relationship of extreme rainfall in the present-day climate condition likely to change over the future period, with different magnitude and direction for analysis areas.

2.5 Dual-drainage concept for urban flood process

The main processes explained in section 2.3 above are useful in flow modeling in urban settings if the discharge is less than the conveyance capacity of the stormwater drainage system. However, when the capacity is reached or exceeded, the urban flood is induced. Urban flood can occur either before the water reaches the minor drainage system or when outflow from the system occurs, or as the combination of the two cases (Rosenzweig et al., 2018).

The dual-drainage concept is usually used to explain the exceedance flow (Figure 2.2). It divides the urban drainage system into two components: minor system and major system (Maksimović et al., 2009; Simões, 2011; Rao and Ramana, 2015). The minor drainage system encompasses the traditional storm drainage hardware (manholes, gully inlets, storm sewer and roadside ditches) and culverted watercourses. This drainage system is generally capable of conveying the flow during more frequent storm events with the flow kept below the ground surface. The major drainage system is the route followed by stormwater when the conveyance capacity of the minor drainage system is

surpassed (Jahanbazi and Egger, 2014). It consists of the flow pathways along the surface whose primary purpose is generally not to convey flow, such as streets and other artificial and natural channels and temporary storage areas (e.g., Playing Fields).

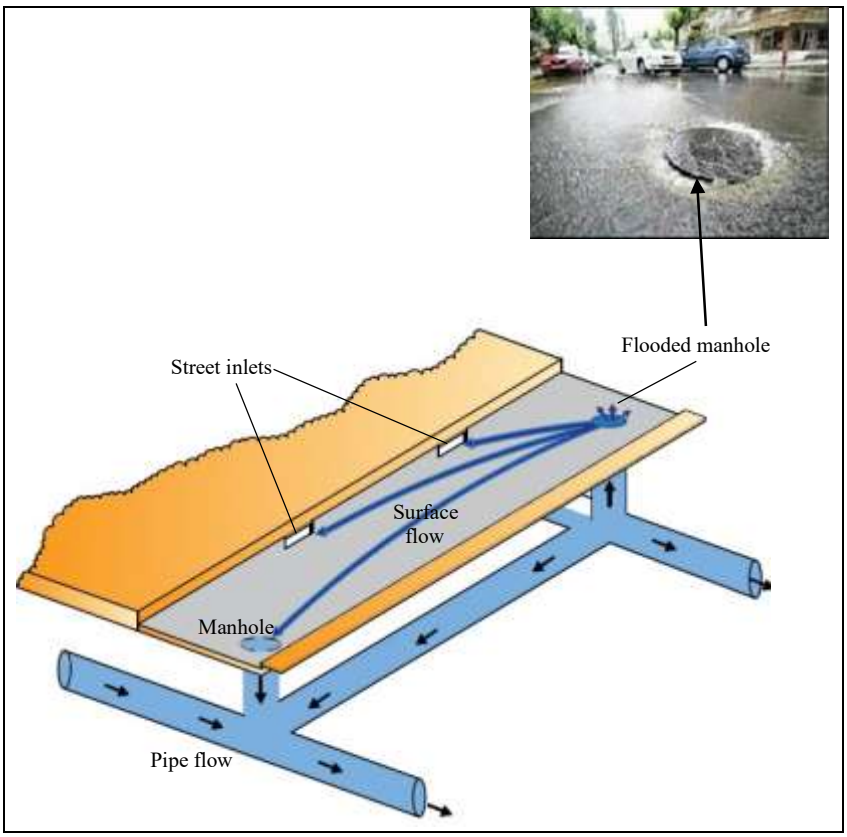

Figure 2.2 Illustration of dual-drainage concept

The interface points of the minor and major systems are vital features of exceedance. The flow exchange between the two systems takes place at gully inlets, manholes and river outfalls (Leandro et al. 2009; Hénonin et al. 2015). Generally, gully inlets are provided for runoff to enter into the storm drainage and manholes are access points for maintenance and services of the storm sewer. Nonetheless, if the conveyance capacity of the storm drainage is reached or the inlets are obstructed, water cannot enter into the system and will be retained on the surface. Likewise, if the capacity of the minor system is surpassed, the water can exit the system at the inlets and manholes. The

river outfalls are also used as outlet points for the minor system, yet if the level of water in the receiving watercourse rises, a backwater can be formed and induces exceedance.

2.6 Drivers of urban flood

Flooding is a function of climatic events such as depth, intensity and temporal and spatial distribution of rainfalls. However, two identical rainfalls do not necessarily create identical runoff, because of possible different antecedent conditions in the drainage basin. According to the existing body of literature, triggers of urban flood can closely be related with urbanization, climate change, and planning and management of urban drainage system or their combination.

Urbanization

Urbanization modifies land use land cover of a watershed and increases impervious surface through provision of roads, sidewalks, parking lots, and buildings etc. Stormwater drainage system is planned to carry the rain-related runoff from these impervious areas, ultimately conveying to the outlet. In developing countries, where unplanned urban growth is the common scenario, urbanization leads to rapid densification and expansion of impervious land areas (Bajracharya et al., 2015). Impervious surfaces reduce infiltration and resistance to flow; consequently, the volume and speed of the runoff rise, thereby exceeding the local drainage capacity (Mejía and Moglen, 2009; Chen et al., 2017). It has also been argued that the spatial heterogeneity of land use change is a potential factor contributing to the existing complex pattern of local runoff response (Sanyal et al., 2014).

Climate change

Urban stormwater infrastructure is usually designed for short and more frequent storms such as 2-yr and 5-yr. There are also well established methods for the design of stormwater drainage infrastructures and rely on time-invariant distribution (i.e., Stationary assumption). In other words, the methods assume that significant changes in the extreme rainfall characteristics in the historical climate condition overtime are less likely (Liao, 2012; Rosenzweig et al., 2018). Such assumption, however is less likely valid under the conditions of potential global climate change (Katz, 2013; Cheng et al., 2014; Tesfay & Quraishi, 2017).

Climate change alters the relationship between intensity, duration and frequency (IDF) of extreme precipitation in historical climate condition with high variability across spatial scales (Buba et al., 2017; Fadhel et al., 2017; Yilmaz et al., 2014; Mirhosseini et al., 2012; Tiepolo, 2014; Emilsson & Ode Sang, 2017). The changes in IDF relationships would have key consequences of the way the current and future urban drainage system is designed, operated and sustained (Cook et al., 2020; Gebru, 2020; Moujahid et al., 2018; Sillmann et al., 2017). Hence, in the case of stormwater drainage system of an urbanized area, uncertainties in extreme rainfall events attributable to climate change are always there to lead to urban flood occurrence. It has also been argued that the impacts of climate change on extreme precipitation are likely to be the most important drivers lead to more frequent and extreme flood events in the future (Jha et al., 2011; Zhou et al., 2018).

Planning and Operation of urban drainage system

Poorly planning and operating urban drainage system is another important factor contributing to urban flood occurrence, mostly in the case of developing countries (Feyissa et al., 2018). In most of the cases, drainage master plan for urban areas to guide

the provision of stormwater drainage infrastructure is not available and information about the network and hydraulic capacity of existing stormwater drainage system is limited (Dibaba, 2018; Zinabie, 2018; Adugna et al., 2019). Stormwater drainage infrastructures are usually provided unsystematic and fragmented way, and designed without hydrologic and hydraulic analysis. On the other hand, urban drainage channels are blocked as a result of poor waste management system and reduce the capacity of the drainage system (Douglas et al., 2008). More of, lack of attention to proper construction and failure to maintain drainage channels in timely manner can lead to frequent flooding of urban areas (Tingsanchal, 2012; Jenkins et al., 2016).

In general, three major drivers of urban flood have been identified. Urbanization is found responsible to increase the volume of rainfall runoff by increasing impervious surface and increase flow speed by reducing the resistance to flow. By influencing the relationship of extreme precipitation attributes, such as intensity, duration and frequency, climate change lead the existing stormwater drainage system insufficient. Poorly planned and operated urban drainage system likely experience frequent flood in the future period.

2.7 Methods of flood hazard mapping

Flood hazard map has been recognized as the main component of sustainable flood risk management (Aryal et al., 2020; Forkuo & Quaye-ballard, 2013; Rangari et al., 2018). It depicts the spatial distribution of prone areas along with the severity of a potentially destructive flood likely to occur with a specific return period. Such information is a key to conduct a proper flood risk assessment (Kulkarni et al., 2014; Patel et al., 2017; Zhang et al. 2015; Vojtek and Vojtekova, 2016; Jiang et al., 2015; Rangari et al., 2018; Sañudo et al., 2020). Flood hazard maps have also played an important role in the

designing of sustainable urban plans, protection for properties and lives, and reduction of flood risk (Luo et al., 2018; Pinos and Timbe, 2019). However, the reliability of the information provided by flood hazard maps primarily affected by the method used for flood hazard assessment, which in turn hinges on the availability of data and resources.

One approach to map flood hazard is using flood inundation information based on remote sensing images and/or ground observational data during post-flood survey (Cao et al., 2016; Alahacoon et al., 2018). However, satellite images of pluvial flood events are limited and records of water depth and extent of past pluvial floods are not well documented in most cases (Khaing et al., 2019).

MCDA is commonly used for flood hazard mapping in urban areas. It involves weighted spatial overlay analysis of flood generating factors such as land-use, slope, drainage density, soil, elevation etc. The relative importance of these factors is usually determined through analytical hierarchical process (AHP) and the factors are combined in GIS environment. AHP is multi-criteria, semi-quantitative approach for representing a decision-making issue hierarchically (Saaty, 2004). The AHP's integration with a GIS improves decision-making technique by providing sophisticated visualization and mapping capabilities, as well as facilitating the creation of hazard maps (Bathrellos et al., 2016). It is widely applied in different regions (Bathrellos et al., 2016; Gigovi´c et al., 2017; Kourgialas and KaratzasScience, 2017; Sepehri et al., 2019; Nigusse and Adhanom, 2019); however, the results of method do not provide the physical characteristics of floods during their occurrence.

In contemporary flood hazard management, a flood-prone area is often defined by predetermined recurrence interval through hydraulic simulation. Several hydrodynamic

models have been developed and their application has been spread (Kourtis et al., 2017; Rangari et al., 2018).

2.8 Urban flood modelling approaches

There are various underlying approaches for modeling urban flood inundation attributed to the existing hydrodynamic models. Focusing on the consideration of stormwater drainage the modeling approaches can be one-dimensional channel (1D), coupled channel-surface (1D-1D and 1D-2D).

2.8.1 One-dimensional channel

One-dimensional (1D) for channel flow modeling approach attempts to simulate the flow in the stormwater drainage and simplify the situations when the system conveyance capacity is exceeded. It represents the minor system as a set of links (represent conduits) and nodes (represent manhole or gullies). With this approach, the overflow is considered as stagnant water temporarily stored in a virtual storage on the top of the manholes (Figure 2.3), and it is supposed that the water starts returning from the storage when the situation of hydraulic head in the node permits (Henonin et al., 2013).

Stormwater drainage network and digital terrain model (DTM) are the main spatial data for modelling flood inundation using this method. The required time for computation ranges from one minute to one hour (Chen et al., 2014; Henonin et al., 2013), allowing to run multiple scenarios. This approach enables to identify the potential overflow locations and the corresponding volume of floodwater accurately. The volume of overflowed water at each node can help to identify the distribution of

hotspots. It can also be used for approximating the average inundation depth over the storage cross-section. Nonetheless, besides the challenges associated to, how to define the dimensions of the virtual storage, the floodwater depth computed in the reservoir rarely represent the realistic behavior of the floodwater (Mark et al., 2004; Jiang et al., 2015). Therefore, the floodwater depth may not be determined precisely.

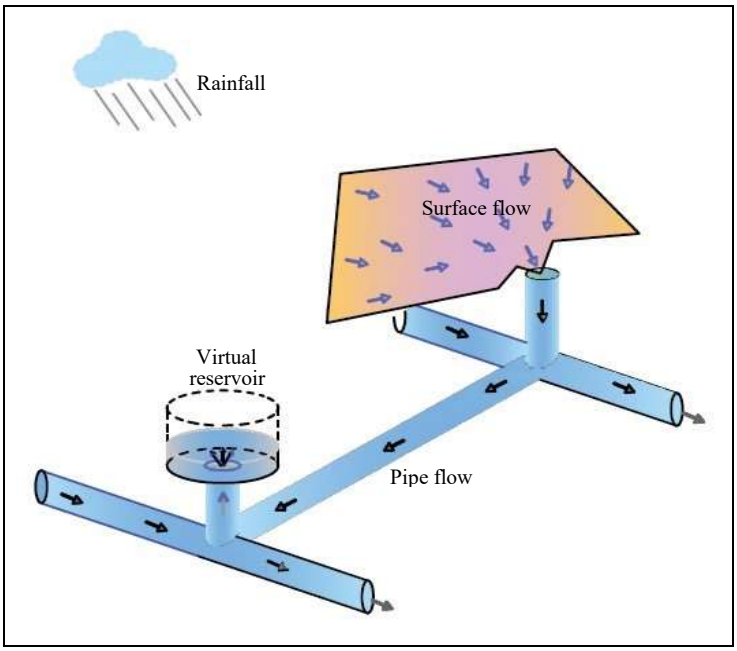

Figure 2.3 Illustration of 1D sewer flow modeling approach, showing the virtual reservoir at the flooded manhole

2.8.2 1D-1D coupled channel-surface

1D-1D (channel-surface) coupling is a condition in which a one-dimensional for minor system flow is coupled with a one-dimensional representation of surface flow, which treats the floodplain as a user-defined network of open channels and ponds connected to the stormwater drainage system (Figure 2.4). This approach enables to capture the interaction between the belowground flow and aboveground flow (Mark et al., 2004). The flow exchanges bi-directionally (i.e., Surcharging and spilling) between the two

systems and takes place through coupling links: gully inlets and manholes (Leandro et al., 2009; Hénonin et al., 2015). In this case, the overflowed water at the nodes is directly discharged on the surface network to surcharge the surface flow.

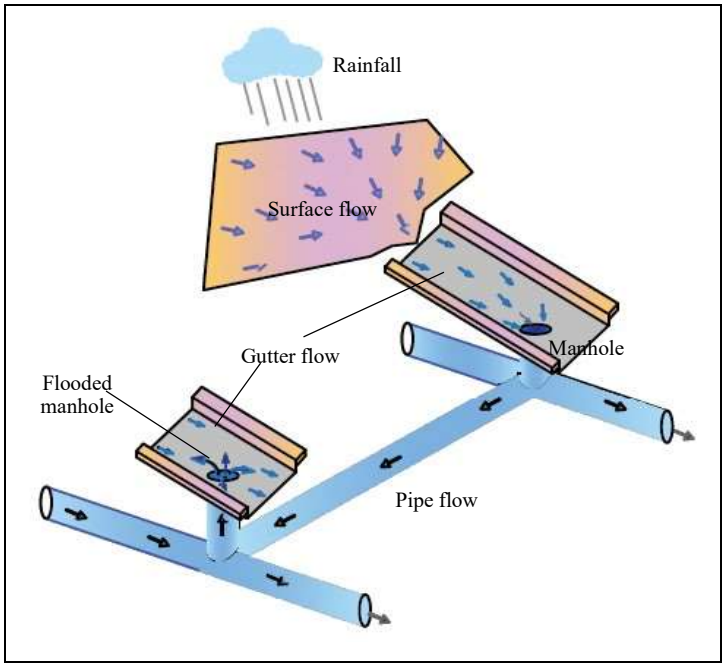

Figure 2.4 Illustration of 1D-1D coupled modeling approach, simulating the flow in major and minor drainage systems

The main input data include surface flow paths, stormwater drainage network and DTM. Using moderate computation time, ranging from 5 minutes to 1 hour, this approach enables to determine overflow location, flow-depth and velocity (one-dimension) with sufficient accuracy, assuming the surface flow paths are well defined (Henonin et al., 2013; Bisht et al., 2016; Kourtis et al., 2017). However, it is not capable of providing the flood information when the water leaves the defined surface flow pathways; for example, when the flow overtops the street curbs.

2.8.3 1D-2D coupled channel-surface

1D-2D coupled method is a condition in which a 1D channel flow is connected with a 2D surface flow representation. The flow interaction between the two systems takes place at the gullies and manholes and 2D grid cells (Jahanbazi and Egger, 2014). In this molding approach, the flow in the minor system is modelled in one-dimensional, whilst the surface flow is modelled as a two-dimensional problem.

This mode of coupling enables to determine the flood information (overflow location, extent, depth, and velocity). The results of the simulations are more accurate than other methods (Hankin et al., 2008; Rangari et al., 2018), yet attain this accuracy at the cost of high computational burden in terms of run-time and data requirements (Bamford et al., 2008; Leandro et al., 2009; Schlauß and Grottker, 2016; Kourtis et al., 2017). Hence, it leads to applications for smaller catchments or the use of a coarser-resolution terrain data in order to have an acceptable period of calculation. The applications of 1D-2D coupled modeling method for a complex urban topography have been realized (Tayefi et al., 2007; Vojinovic and Tutulic, 2009; Leitão, 2009; Aksoy et al., 2016; Schlauß and Grottker, 2016). The outputs of 1D-2D can also be used for calibrating a 1D-1D model in the absence of adequate field data (Leandro et al., 2011).

2.8.4 Strength of model coupling

In model coupling process, the relationship between the belowground and aboveground flows can be defined in a loose or tight manner. For each of the coupling approaches (1D-1D and 1D-2D), both loose and tight coupling is possible. In a loose coupling mode, the 1D model is seen as a preprocessor to create input data for the surface model (Butler and Davies, 2011). Thus, the models can be run independently and the events

of the two models could be derived from different simulation software packages. This mode of coupling has been used in several urban studies (Adeogun et al., 2012; Burns et al., 2015; Bellos et al., 2017; Rangari et al., 2018). It can also be applied for designing and analyzing large systems with lower precision. For instance, the minor system can be designed accurately using 1D, then surface conveyance capacity is defined by flow pathways determined in the field and modelled without detailed consideration of the interaction between the minor and major systems. It can also be used when explicitly modeling of inlet capacity is not required and the level of flood risk is required in terms of areal extent or groups of properties.

In tight coupling mode, the interaction between the channel and surface flow models cannot be split into distinct processes (Sui and Maggio, 1999; WeiFeng et al., 2009), indicating a high level of non-linearity. This way of coupling enables to implement real-time interactions between the two models. Governing equations for network nodes, channel ends, pipes and surface channel flow are solved simultaneously. Tightly coupled models could be described as a single unit (single package). There are several commercial simulation packages that provide such access (e.g., PCSWMM, XPSWMM, MIKE FLOOD, etc.); however, such software packages are expensive that limits their application in low-income countries, like Ethiopia.

In general, by taking factors influencing the choice of an appropriate modelling method for a particular application into account, the state-of-the-art of existing urban flood modeling approaches is reviewed. Each of the methods has benefits and drawbacks for applications in urban areas. The outputs of 1D sewer encompass the overflow locations and maximum floodwater volume. In addition, by simplifying the situation of the overflow using a virtual reservoir, it helps to estimate the maximum

inundation extent and floodwater depth. However, as it is not capable of describing the surface flow, the actual flood conditions could not be predicted precisely. The coupling of sewer-surface models enables to represent the urban dual-drainage system, as it considers the interaction between the major and minor system, and provides accurate descriptions of flood conditions. However, the 1D-1D approach cannot provide information about surface flow velocities when the flow overtops the defined surface networks. On the other hand, although the 1D-2D coupling approach is capable of providing the most accurate and detailed information, it is computationally expensive both in terms of run-time and data requirements. In line with importance of effective flood modeling tasks, the selection of appropriate method demands balancing between the type and quality of the simulation results, model complexity, input data, time, hardware and software required for implementation.

2.9 Flood hazard management

Totally avoiding floods is unrealistic, hence, they have to be managed (Ahmed et al., 2016). Urban flood hazard management refers to the required measures to be undertaken for minimizing the probability of a particular flood hazard and its associated vulnerability at acceptable level (Fratini et al., 2012; Ahmed et al., 2016). Management of flood hazard requires fundamental tasks that include a variety of measures from the policy and planning level to the implementation and operation level. Conventional flood hazard management methods usually involve structural measures and nonstructural measures.

Structural measures

Structural measures have an objective of "keep the flood away from people" by construction of flood control infrastructures. In urban areas, they include structures of delaying of runoff processes, floodwalls, floodways, diversion works, and drainage works. This strategy has been common over the years, and regarded as predominant method for addressing urban flood mitigation that made urban areas to have heavily relied on flood control (Liao, 2012; Yeo, 2013). However, flood-control infrastructures can only resist floods of a certain magnitude and unreliable for the capacity-exceeding extreme floods such as in the face of uncertainties due to nature-human couplings (Smits et al. 2006; Zevenbergen & Gersonius 2007; Liao, 2012; Hughes & Sharman 2015). Moreover, structural measures often cannot evolve with development, require high financial investments for upgrading existing infrastructure, hence not cost effective that more reflected on lower-income countries (Bischiniotis et al., 2018; Adugna et al., 2019).

Nonstructural measures

Nonstructural measures are grounded on strategy of "keeping people away from floods" (Kang et al., 2009). Such measures attempt to avoid the use of flood-prone areas as a central thought and they can be categorized as land-use planning measures, architectural measures and regulatory system measures.

As flood hazard management measures, land use planning has the potential to avoid exposure in the most hazardous zones and to decrease overtime exposure and vulnerability in already urbanized areas (Tingsanchal, 2012; Yeo, 2013; Galderisi & Menoni, 2015; UFCOP, 2017). In other words, it minimizes development in flood-prone zones and reduces storm runoff through development controls, designates routes and open spaces for better response and recovery efforts, and accommodates urban

growth and expansion in flood-safe areas during resettlement and reconstruction. Moreover, it helps to address underlying urban flood drivers, such as unplanned urbanization, poor land management, and weak regulation disaster risk reduction investments.

However, the perception of nonstructural measures—keeping people away from floods—cannot be practicable at full. Because, many valuable developments are located and dense population are living in flood-prone areas, as in most of the cases, they are already urbanized area. Further, Glavovic et al. (2010) and Su (2016) argued that the full potential of land-use planning in urban flood hazard management has not yet been realized. Various studies (Bengston, et al., 2004; Yang & Zhou, 2007; Bulti & Sori, 2017) revealed that several factors counteract the effectiveness of land-use planning, mainly related to planning quality, implementation and contextual characteristics. In most of the cases, land-use plans are prepared based on inventories of basic assessments of quantity and the least attention is given to the natural hazard management (Zevenbergen et al., 2008). On the other hand, well preparation of plan does not necessarily ensure effective implementation (Bulti and Sori, 2017). Essentially, evaluation of plan in the context of flood hazard management to guide enhancement of planning process is rarely done in Ethiopia, and information about consistency of consecutive plans is limited.

Architectural planning measures include elevating the building basement or site, dry and wet flood-proofing techniques, facility maintenance and repair, structural retrofitting or reinforcement, building greening and pavements with water permeability. Except the first measure, they are less effective against a bigger flood (Kang et al., 2009). More importantly, elevating the building basement is less practical for urbanized

flood-prone areas. Regulatory system measures include statutes, ordinances, flood prevention standards, public awareness and education, flood warning systems and flood insurance. Limitation in local resources and skills can affect the accuracy of flood forecasting, particularly in developing countries.

2.10 Resilience-based flood hazard management

The third strategy is based on the acceptance of flooding conditions and concentrates actions for the eventuality of floods to minimize damage and to promote a fast return to normality after the flood has occurred i.e. it follows the strategy of accepting floods and clean afterwards. It certainly can be realized that such an approach is basically unavoidable in flood threatened regions known as flood resilience-based flood hazard management.

2.10.1 Engineering resilience vs Ecological resilience

Resilience is a contested concept that has been exposed to different definitions in various disciplines and contexts (Batica et al., 2013; Quinlan et al., 2016; Meerow et al., 2016). Divergent problem definitions, focuses, and approaches when the concept of resilience is applied to flood hazard management are mostly related to the two interpretation of resilience concept: Engineering and Ecological resilience (Holling, 1996). The conceptual differences can be illustrated by the ball and cup heuristic (Figure 2. 5a &b). The ball denotes the state of the system at any given time. The cup denotes the region in the state space, in which the system tends to stay "basin of attraction", and includes all likely values of the system variables of interest.

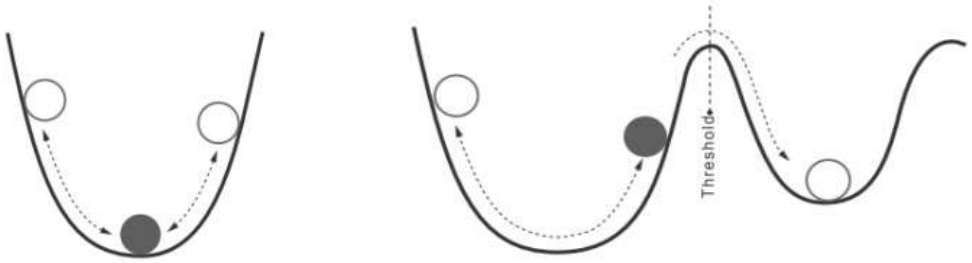

a) Engineering resilience concept b) Ecological resilience concept

Figure 2.5 Illustration of engineering and ecological resilience concepts (Liao, 2012)

In engineering, resilience is conceptualized as a system's ability to resist disturbance and return to original state when relaxed from stress (Wang and Blackmore, 2009). Essentially, it is the capacity to maintain stability—that is, to keep the system state unchanged or to have minimum fluctuation. It assumes only one regime, hence only one possible basin of attraction (Figure 2. 5a). The bottom of the basin of attraction denotes the ideal stable state. The engineering resilience notion is concerned with whether the optimal state of system's functionality can be maintained, presuming only one regime with an idealized stable state as the norm.

Such resilience mainly depends on properties such as robustness—the physical strength to resist a disturbance without degrading the function; resourcefulness—the capacity to recognize problems and mobilize required resources; redundancy—the degree to which the system components can be replaced; and rapidity—the capacity to restore the system quickly (Bruneau et al., 2003). This concept of resilience involves both resistance to and recovery from disturbances, yet the measurement is solely on recovery—the quicker the full functionality is restored the more the resilience (Hollnagel et al., 2008).

Ecological resilience, on the other hand, is defined as a system's capacity to absorb perturbations while still surviving. It emphasizes persistence, or remaining in the same

regime characterized by the same processes, structures, feedbacks, and identities (Walker et al. 2004). As a result, several regimes are assumed, implying more than one basin (Figure 2.5b).

In ecological resilience concept, a system is characterized by diverse sets of structures and processes, and exceedingly difficult to return to previous state—that is the system never settle at the bottom of the basin, may move about in the basin; and it may cross a threshold and become calm in a new basin. Any fluctuation in the regime is normal because systems are inherently dynamic (Holling, 1973). Because systems do not operate in a state of equilibrium, resilience is linked to the system's ability to accept change as well as its capacity to reorganize or renew itself (Carpenter et al., 2001). Ecological resilience concept concerned with whether the system can stay within the current basin (Holling, 1996). It is measured by the degree of the disturbance that the system can withstand before shifting to a new regime (Gunderson and Holling, 2002).

The ecological resilience concept is a better framework for flood hazard management because it is based on a more realistic multi-equilibria paradigm that focuses pragmatically on persistence in a world of flux (Adger et al., 2005). However, as compared to in ecology and in engineering, application of resilience concept in urban planning and natural hazard management is relatively recent (Berkes, 2007; Liao, 2012). Moreover, the notion of urban resilience to flood still remains theoretical and lacks empirical studies applied in urban research (Su, 2016).

2.10.2 Theory of urban resilience to floods

The theory of urban resilience to floods is developed by Liao (2012). The theory emphasizes specific type of system (urban) with a specific problem (flood), mainly to

facilitate operationalization of the resilience theory. By taking the concept of ecological resilience as a framework, urban flood resilience is defined as:

> "The capacity of the City to tolerate flooding and to reorganize should physical damage and socioeconomic disruption occur, so as to prevent deaths and injuries and maintain current socioeconomic identity." (Liao, 2012).

In a nutshell, urban flood resilience is characterized by flood tolerance and rapid reorganization in the event of a disruption. The former is associated with hazard mitigation, whereas the latter is associated with post-disaster recovery. Flood tolerance is the capacity to avoid physical damages and socioeconomic disruptions during a flood; in other words, it is the ability to prevent a flood disaster rather than preventing a flood entirely (Liao, 2014). In this case, the City's floodability, which refers to the physical ability to accommodate—rather than resist—flooding, would be crucial. If there has been damage and disturbance, staying in the regime ensures reorganization—the restoration of socioeconomic order.

2.11 Empirical literature review

In line with growing concern of sustainable development of urban areas, assessing the impacts of urbanization and climate change on urban flooding, as well as seeking alternative flood hazard management methods have become the subjects of recent research. This section presents a review of empirical studies conducted in different regions of the world. The review mainly focused on those studies inspected the impacts of urbanization of hydrological characteristics of urbanized watershed, influences of climate change on extreme rainfall and pluvial floods; existing practice of flood hazard assessment and mapping; application of resilience concept in urban flood hazard

management. It provides understanding on existing knowledge regarding to urban flooding and management at global and local levels.

2.11.1 Global perspectives

Impacts of urbanization on urban hydrology

Among the studies focused on the impacts of urbanization-driven LULC change on hydrological characteristics of urban watersheds, Parsasyrat and Jamali (2015) investigated the impact of land use changes and impermeable surfaces on flooding potential in the Iranian province of Isfahan. According to their results, altering the green urban environment in residential areas increases maximum floodwater output significantly. In shorter return periods, the consequences of the land use shift are stronger on the region's flooding potential. Chen et al. (2017) assessed the effects of urbanization on surface runoff in United States on a nationwide scale during 2001-2011. The authors argued that the contiguous United States experienced non-uniform urbanization across the country, and urban expansion and densification highly influenced surface runoff.

Sanyal et al. (2014) investigated the impact of sub-catchment land-use/cover changes on downstream flood maxima in eastern India. They discovered a modest but statistically significant positive linear correlation between sub-catchment LULC alterations and the magnitude of the flood peak at the catchment outflow, though a number of sub-catchments deviated significantly from this trend. Ohana-Levi et al. (2017) argued that 50% of the watershed in Israel appear to be urbanized with a linear rise in runoff response, by the year 2050. Afforestation and quarrying plans show little effect on runoff. Li et al. (2018) used the urban functional zone (UFZ) as the basic unit for hydrological analysis to investigate the impact of urbanization on direct runoff in

the Shenyang urban area. Urbanization had a significant impact on direct runoff. high-density residential, business, and industrial zones had large runoff volumes and high runoff coefficients for various UFZs. The findings of these studies revealed the modest positive linear relationship between the changes in impervious surface and runoff volume.

According to Hu et al. (2020), in the central area of Beijing, the trend of variation in runoff was consistent with that of impervious land, which augmented during 1984-2009 and reduced during 2009-2019. Furthermore, increases in surface runoff were most significantly linked with changes in impervious surfaces, when compared to the correlation of runoff with other types of land use. By examining the patterns of LULC change in St. Charles County at about 5-year interval, Yingkui & Wang (2009) reported the runoff increase in the study area is highly correlated with urban expansion during 1982-2003. In these studies, the changes in imperviousness are found to be strongly correlated with that of runoff volume.

Chen et al. (2015) investigated the temporal and spatial effects of urbanization on flood events at the catchment level, and concluded that the magnitude of runoff increased in a non-linear relationship with the rate of urbanization. In some sub-basins, urbanization had the opposite effect on runoff. Su et al. (2014) explored how urban land patterns influence urban floods, and argued that the organization of imperviousness and channels, as well as the location of impervious surfaces within a catchment, could affect floods.

Despite the findings of these acknowledged studies are inconsistent with regard to the correlation between the changes of impervious surface and runoff characteristics, they highlighted that the rises in runoff were most significantly associated with changes

in impervious surfaces. Moreover, they provided important insight into spatiotemporal variability of the impacts of urbanization on hydrological attributes.

Impacts of climate change

In regard to increasing concern of urban flood management, assessing the impacts of global climate change at local area have become the growing concern of the recent research. With the estimate of future extreme rainfall being the most significant step, researchers have examined the susceptibility of stormwater drainage infrastructure to climate change in Australia (Amaguchi and Kawamura, 2016), Japan (Tran et al., 2011), and Norway (Nie et al., 2009). However, future design rainfall in these research is estimated by utilizing assumed increments (e.g., 10%, 30%, 50% etc.) of present-day rainfall information. The results of such studies only provided preliminary understanding how drainage systems react to shifting climate inputs.

In line with the recent advancement of climate research, the outputs of General Circulation Models (GCMs) have been applied in climate change impact studies at local scale. Accordingly, numerous studies have investigated the alterations in the extreme rainfall IDF relationship in Nigeria (Buba et al., 2017); England (Fadhel et al., 2017); Australia (Yilmaz et al., 2014); US (Mirhosseini et al., 2012). Majority of these studies concluded that current precipitation intensity is likely to appear in the future, yet with a shorter recurrence interval. The findings indicate the impacts of climate change on extreme rainfall is associated with high variability across the regions.

Many studies have used GCM results to explore the implications of climate change on storm drainage infrastructure. Rosenberg et al. (2010) confirmed that urban stormwater infrastructure in Washington State built on the basis of rainfall records of mid-twentieth century may be subjected to a future precipitation regime that differs

from present design standards. The outputs of ECHAM5 and CCSM3 GCMs were used in the study. Karamouz et al. (2013) were assessed the effects of climate change on stormwater drainage system in Tehran metropolitan area, Iran, in which they used the projections of HadCM3 GCM under A2 scenario. According to their result, the existing state of drainage system performance under anticipated rainfalls in the future reveals that flooding hazards are growing, owing to the increased likelihood of extreme rainfall events in the study area. Based on the analysis conducted using the outputs of multiple RCM/GCM, Willems (2013) claimed that systems intended for a 20-yr recurrence interval flooding in Belgium, might be flooded with a return period of – in the order of magnitude – 5-yr by the end of this century. In general, these studies documented that present stormwater drainage systems of analyzed areas may be insufficient under future design conditions. However, they did not offer thorough analyses in terms of flooding.

In China, Xiong et al. (2018) quantified the impacts of climate change on stormwater drainage performance using the Storm Water Management Model (SWMM). The study used the outputs of five GCMs of the Coupled Model Inter-comparison Project Phase 5 (CMIP5): CanESM2, BCCCSM1.1, MIROC-ESM, CNRM-CM5 and GFDL-ESM 2M. The authors confirmed that existing drainage system in the study area is insufficient that reflected by flooding at multiple nodes and surcharging of different conduits. However, this study provides little information about the potential inundation characteristics (e.g., extent, depth and speed).

Urban flood resilience

Urban resilience to flood moves from the engineering strategy of blocking out floods to the built-environment planning strategy of accommodating floods. Despite the idea of resilience has a long history in ecology and engineering, but its application to urban

planning and natural hazard management is relatively recent, and empirical studies to operationalization of the concept of urban resilience to flood in urban research still in development stage.

Su (2016) analyzed urban flood vulnerability and practices of flood prevention in six global cities in both developed and developing countries. The results underscored the importance of land-use and environmental planning for resilience as well as maintaining up-to-date risk and vulnerability assessment.

There are studies conducted to develop tools for assessing different dimensions of resilience, such as economic, physical, social, environmental etc. (Cutter et al., 2010; Batica and Gourbesville, 2013; Irwin et al., 2016; Keating et al., 2017). However, these studies are focused on post-disaster recovery. Liao (2012) proposed urban floodability index as surrogate measures for assessing flood resilience of urban areas. It mainly indicates the flood tolerance, and focus on flood hazard mitigation aspect. Lhomme et al. (2013) developed methodology for analyzing flood resilience of urban technical networks. Based on the system approach, the three capacities of City's resilience absorption, resistance, recovery were analyzed. Web-GIS was used for the implementation of resilience assessment. The research is focused only on technical aspect of road network.

In Hamburg, Serre et al. (2016) analyzed the potential of neighborhood design in enhancing urban resilience to flood. The study utilized the Spatial Decision Support System DS3. The result revealed that design measures involving transportation infrastructure, land use and buildings can contribute to the flood resilience of the neighborhood. In Philippines, Rivera and Navarra (2015) determined buffer distances

for ecological resilience of settlements along Pampanga River, under different levels of flood hazards.

2.11.2 Local perspective

Impacts of urbanization on hydrology

The effects of urbanization-driven LULC changes on hydrology have been assessed by several studies in different parts of the country, such as Lake Awassa (Shewangizaw and Michael, 2010); Angered watershsd (Getachew and Melesse, 2012); Melka Kuntrie subbasin (Getahun and Van Lanen, 2015); Muga watershed (Demeke and Andualem, 2018); Upper Blue Nile river basin (Mekonnen et al., 2018); Abaya-Chamo basin (Yohannes et al., 2018). However, these studies are deliberated on riverine basin.

Among few studies focusing on urban watershed, Billi et al. (2015) identified that the LULC change in Dire Dawa City during 1985-2006 resulted 4.5% increase of flash flood frequency in the City. According to the results of the study conducted by Birhanu et al. (2016), the peak flow in Addis Ababa City increased by 25% due to an increase of urban land cover class from 16% in 1993 to 26% in 2002. However, these studies did not offer thorough analyses of influences of urbanization on hydrological attributes of the areas in terms of change in imperviousness and runoff depth, as well as smaller spatiotemporal scales.

Attempts have also been made to quantify the expansion of Adama City. Sinha et al. (2016) concluded that built-up area of Adama City administration has increased by 293% during 1984-2015. In their comparative analysis of the growth and spatial patterns of urban development in Ethiopian cities, Terfa et al. (2019) reported that Adama City grew at an annual rate of 8.3% between 1987 and 2017. Moreover, Regassa

et al. (2020) argued that Adama City is expanded by 7.6% during 1973-2010 and by 13.44% during 2000-2010, and the built-up area coverage would reach 60.27% of the total area of the City administration in 2040. The results of these studies indicate significant expansion of built-up area in Adama City has been occurred in the past and would continue to increase in the future period, with high rate. However, the potential environmental impacts associated with the LULC change, particularly on the hydrology have not been investigated.

Impacts of climate change on extreme precipitation

There are studies that have been conducted to assess the impacts of climate change on the extreme precipitation of the past and future periods. Existence of climate change in the past period is explored through analysis of the trend of extreme precipitation in daily time-series records. In their study of the behavior of extreme precipitation in Debre Markos town during 1953-2006, Shang et al. (2011) concluded that there is no statistically significant trend in the observed precipitation time-series in the study area over the analyzed period. In Enebsie Sar Midir district, Geremew et al. (2020) also reported similar results (no significant trend) for rainfall extremes in three climate stations: Gundowoin, Mertu Lemariam and Motta towns over the years 1987-2016.

On the other hand, Mohammed et al. (2018) concluded that the trends of extreme rainfall in the south Wollo zone from 1984 to 2014 did not exhibit any consistent patterns among the analyzed 6 stations). The study revealed significant trend at Dessie, Haik and Mekaneselam climate stations, yet no sufficient evidences were found to support the observed trends for the case of Combolcha, Ambamariam and Wereilu stations. Similar mixed results are reported by Shawul and Chakma (2020), in which they investigated the variability of extreme precipitation indices at 20 climate stations

in Upper Awash basin during 1980-2015. Accordingly, the trends of mean annual and extreme rainfall events for the majority of the analyzed stations were not statistically significant. They also concluded the downstream areas of the basin could experience higher flood risk as the values of extreme 1-day and 5-days annual precipitation were found to be high in this portion of the basin.

The finding of the acknowledge studies show that the variability of extreme rainfall between the analyzed stations is high and obtaining a systematic pattern in trends of extreme rainfall events is less likely. This reflects the impacts of climate change on extreme precipitation of past period, is less uniform when it comes to a smaller spatial scale and different geographic regions, and signify the importance of local scale analysis to adequately address the climate-related risks, at a particular area.

As more emphasis is placed on evaluating potential circumstances for future climate change at local scale, some recent attempts have been made to provide the long-term future precipitation conditions in Ethiopia. Based on the climate projection of HadCM3, Dile et al. (2013) reported that the annual and monthly mean precipitation of Gilgel Abay River is expected to decrease in the near future (2010-2039), while it is projected to increase in the medium (2040-2069) and long-term (2070-2099) timeframes. In the Geba Catchment, Northern Ethiopia, between 2010 and 1999, Samuale et al. (2014) found that monthly rainfall variability is higher than yearly mean precipitation. In addition, the average annual rainfall declines, over the years 2010-2039, followed by a slight increase during 2040-2069 and 2070-2099. In their analysis of climate change impacts using the projections of CanESM2 GCM, Mohammed et al. (2020) confirmed that the precipitation in Tikur Wuha watershed increases up to the end of 21st century. An increase in total annual precipitation in the future period (2011-2100) in Addis

Ababa City has also been reported by Feyissa et al. (2018) based on the projections of CanESM2 and CGCM3 GCMs. The research offered scientific information on the changes that are expected to occur in various locations of Ethiopia in the future. The results of these studies indicate rainfall extreme in the future period would changes as compared to the present-day climate condition for the analyzed areas. However, the results could not provide information about the relationship between extreme precipitation attributes; hence, they are not sufficiently sensitive for the desires of urban drainage system performance analyses, which usually requires the change in rainfall intensity for various durations and frequencies.

In this regard, there are few attempts have been made to develop the rainfall IDF relationship by temporally disaggregating the observed and projected daily precipitation time-series and applied for quantifying the potential changes in extreme rainfall intensity in the future period, as compared to that of the present-day climate condition. Based on their study using the precipitation time-series recorded at Chiro and Hurso climate stations in Eastern Ethiopia, Tesfay and Quraishi (2017) argued that the rainfall intensity in Chiro would rise up to 1.58% in 2010-2039, whereas it is expected to decrease by 20.22% in 2040-2069 and 55.93% in 2070-2099. In Hurso, rainfall intensity is predicted to increase up to 1.74% from 2010 to 2039, but then drop up to 34% and 67% from 2040 to 2069 and 2070 to 2099, respectively.

In Northern part of the country, Gebru (2020) evaluated changes in IDF information in the future period for seven climate stations: Humera, Mekelle, Adigrat, Adwa, Axum, Michew and Shire. According to his findings, rainfall intensity is predicted to drop by 15.9%, 14.7%, and 20.3% for shorter storms and increase by 21.3%, 26.9%, and 18.9% for longer storms during the analyzed future timeframes of 2010-2039, 2040-2069, and

2070-2099, respectively. Another study conducted by Gebreigziabher (2020) has also documented that the intensity of less frequent storms in Mekele City would decrease up to 78.61%, while that of more frequent precipitation would increase up to 65.95%. The findings of these studies highlight an important fact: the relationships of extreme rainfall characteristics in the analyzed areas will undoubtedly alter in the future period as a result of climate change. Although an increase in rainfall intensity could highlight the vulnerability of existing drainage system, quantitative assessment is essential to better understand the impacts of climate-change-induced increased rainfall intensity on existing drainage system, which is not available for Ethiopia.

Performance urban drainage system

Effective planning and operation of stormwater infrastructures of the cities has a key role in urban flood management. Qualitative assessment has been carried out through questioners and interview for Addis Ketema Sub-City of Addis Ababa City (Belete, 2011); Sululta City (Singh et al., 2016); Woliata Soddo town (Adisu & Hailemikael, 2017); Jimma City (Dibaba, 2018); and Adama City (ACFMP, 2016). These studies emphasized that the low performance of drainage system in the analyzed areas is mainly related to lack of regular inspection and maintenance, poor drainage and roads integration and poor solid waste management. These are usually indicators of poorly managed drainage system.

There are also attempts to evaluate hydraulic capacity of existing stormwater management infrastructure at different scales. Based on analysis at smaller scale, Bashah (2015) concluded that the hydraulic capacity of existing crossing structures of Nazareth-Assela road in Adama City are insufficient to convey the design discharge. Similarly, Nora and Reddy (2018) reported that the roadside drainage infrastructures in

some road-section in Burayu Town is inadequate to remove the runoff generated from respective watershed.

With relatively larger spatial scale, Adugna et al. (2019) evaluated the hydraulic capacity of existing drain systems and the management challenges of stormwater in Addis Ababa City taking two sites, namely wereda 4 and wereda 3 as a case studies. According to their findings the capacity of 14% and 28% of analyzed drains in respective study areas are inadequate to remove rainfall-runoff from corresponding catchments, and they are responsible for flash flood occurred in the associated watersheds. According to the study by Zinabie & Kebede (2020), floods occurred in Alamata Town in the past period are due to inadequate hydraulic capacity of the Town's drainage system. The findings of these studies highlight that the design and management practice in analyzed study areas are poor, suggesting stormwater drainage system evaluations in different cities of the country. However, these studies did not offer thorough analyses of the stormwater drainage system's performance in terms of flooding. Moreover, the studies are conducted based on the present-day climate and land cover conditions, and provide little information about the future conditions.

Urban flood hazard mapping

The assessment of urban flood hazards is critical for flood mitigation and is a required step for government policies on urban development. Flood hazard maps were also prepared for different urban areas of the country. Through spatial weighted overlay analysis of flood generating factors such as soil, elevation, slope, land use etc. in GIS environment along with multi-criteria analytical hierarchical process (AHP) techniques flood hazard areas were delineated for Adama City (Bulti et al., 2017), Awash river basin (Getahun and Gebre, 2015) and Ambo Town (Ogato et al., 2020). The results of

the acknowledged studies, however, do not represent important physical characteristics of inundation required for detail flood hazard analysis, such as inundation extent, depth and velocity of the floods during their occurrence.

There are also local studies that have applied hydrodynamic models (e.g., HEC-RAS, FLO-2D) for simulating flood inundation for urban areas, such as Dire Dawa City in relation to Dechatu river (Alemu, 2015; Erena et al., 2018). These studies are focused on fluvial floods, which often occur as a result of a river/stream overflowing. The modeling of urban flood has received limited attention. Above all, attempts to estimate the effects of climate change on urban flood hazard under future climate conditions are limited, despite the fact that the results of such an analysis are acknowledged as being useful in designing effective mitigation and adaptation strategies.

2.12 Literature and research gaps

Several studies have been conducted in relation to urban flooding; however, they are not sufficient, and various significant issues emerge in response to existing urban flood problems and the thoughtfulness of a potential future increase due to urbanization and climate change.

Despite the fact that there has been a lot of study on the effects of urbanization on hydrological attributes of urbanized watershed, the results with regard to the relationship between the changes in imperviousness and surface runoff are inconsistent. The relationship between increase magnitude of runoff and rate of urban area expansion is different for different areas, as other factors or land-use changes could counterbalance the consequences of increased impervious area.

Moreover, available few Ethiopian studies focused on urban watershed did not provide the impacts of urbanization on hydrological attributes at smaller spatiotemporal scales. A particular urban area could encompass distinct macro-watersheds with a number of sub-catchments. Improved understanding about LULC change in each sub-watershed supports formulating effective urban land development control to reduce the hydrological effects of urbanization. On the other hand, results of previous studies rested on changes in long-time scale (e.g., decadal or longer). Consequently, they provided little insight into the impacts of short-time (e.g., 5 years or shorter) changes in urban areas, which is vital under existing rapid urbanization. Rapid urbanization encourages the rapid development of structures and pavement, as well as the expansion of barren land during the construction process.

Importantly, the high rate of built-up area expansion in Adama City is documented, yet the associated impacts on the City's hydrology remain unclear. The more critical scenario is that Adama City is the fast-growing regional City with densely populated floodplain areas. In this context, planning the City's sustainable development demands enhanced understanding of the spatiotemporal effects of urbanization on the hydrological characteristics at the City watershed and its sub-watersheds.

The variations in fundamental characteristics of extreme precipitation due to climate change have been established for different areas, and used to examined the susceptibility of stormwater drainage infrastructure to climate change in Australia, Belgium, China etc. However, literature on the impacts of change in global climate on stormwater drainage flooding is scarce, though the changes in extreme precipitation intensity may imply variations in urban floods in some regions. Particularly, in

Ethiopia, there is no strong evidence for climate change-related increases in the magnitude of urban floods.

Moreover, the present study has been unable to mention to a specific research towards investigating how the existing drainage system respond to future climate change in Ethiopia, regardless of few studies deliberated on quantifying the potential shift in rainfall intensity due to climate change. It has also been argued that the changes in the relationship between attributes of extreme precipitation enables to design climate-resilient urban drainage infrastructures and improves decision-making process, yet such information is not available for flood-vulnerable City of Adama.

In contemporary urban flood hazard and risk management, flood modelling is considered as a key step. It provides physical characteristics of potential floods: inundation extent, water depth and flow velocity, hence plays significant role in producing accurate City's flood hazard maps corresponding to various return periods (example 5-yr, 10-yr etc.). Urban flood modeling is used to promote flood risk reduction in many countries (e.g., the United States, the Netherlands, and the United Kingdom). However, application of such more scientific approach is too often neglected in Ethiopia. The most concerning situation is that a lot of structural measures are being implemented in different cities of the country, yet given the lack of reliable flood data, the reliability of flood control infrastructures has been overlooked. If urban flood modeling is used as the basis for flood management operation, flood-vulnerable urban centers in the country, particularly Adama City will gain the most long-term advantages.

Despite growing acknowledgment that the idea of resilience has a potential to help formulation of flood hazard management measures, empirical studies to operationalize

the concept of urban resilience to flood in urban research are still in the early stages of development. In addition, attempts to assess urban flood resilience are largely rested on post-disaster recovery, and the quantitative assessment of the mitigation aspect of flood resilience—flood tolerance—is still largely unexplored.

2.13 Conceptual framework of the study

The goal of flood hazard management practices across the world is to minimize the chance of flood occurrence and/or its effects. Analysis of the level of urban flood hazard under existing and future scenarios, as well as developing alternative measures become crucial. In this respect, a thorough understanding is essential with regard to the contribution of main drivers, features of potential floods under different scenarios, a proper assessment of associated hazard, appropriate adaption measures, and knowledge-based decision-making.

In cities, urbanization and climate change are the determinant drivers of urban flood in the future (Ohana-Levi et al., 2017; Xiong et al., 2018). Urbanization—artificial alteration of land use, mostly characterized by increases of impermeable surfaces. Impervious surface reduces infiltration and resistance to flow, and leads the volume and flowrate of runoff to rise (Mejía & Moglen, 2009; Chen et al., 2017). Information about the influences of urbanization-driven impervious surfaces on the runoff depth at an appropriate spatial and temporal scales, as well as the relationship between the trends of their change over time, contribute to planning of land (re)development (Li et al., 2019), which are arguably the most direct and effective way to reduce flood hazard.

Climate is the average weather for a particular region over long-time. The climate of a particular area is determined through analysis of climatological variables (e.g.,

rainfall) in a region over the period of 30-years or more. Climate information for the twenty-first century has been projected by several GCMs. Downscaling process enables to generate daily precipitation for the present-day and future periods, from GCMs outputs to local scale (Wilby and Dawson, 2013; Gharbia, 2016). Observed and predicted precipitation time-series are important input for flood simulation models; allow to understand the climate change; to better plan adaption measures to combat the potential impacts of climate change. Moreover, the downscaled daily precipitation helps to establish the relationships between extreme precipitation attributes for the future period.

Climate change affects the fundamental characteristics of extreme rainfall (Tesfay and Quraishi, 2017; Gebru, 2020). The rainfall IDF relationships of the observed and projected precipitation helps to determine the rainfall intensities, and used for comparison. The variations in rainfall IDF are essential for designing, managing and standardizing urban drainage infrastructures, thereby help to reduce the consequences of increased intensity due to climate change. Moreover, rainfall intensities are used to determine design storms of respective duration and flood frequencies, which are key input for urban flood simulation.

Urban flood encompasses intrinsically linked phenomena: runoff, stormwater drainage flow and overland flow. Properly representation and understanding of urban flooding demands modeling these phenomena all together (Butler and Davies, 2011; Mishra and Herath, 2014). The results provide features of the potential floods, including extents, water-depth and flow-velocity, for different flood frequencies. These attributes are key parameters for accurate flood hazard mapping, urban flood resilience assessment, and localized flood adaption planning. Urban flood modeling for existing

and future using different combination scenarios of main drivers allows to identify the consequences of urbanization and climate change. The results of the scenarios can be compared and contrasted in terms of extents of flood-prone areas.

Flood hazard in urbanized floodplains is influenced by climate, built systems, socioeconomic developments, and hydrological processes. They operate like evolving ecosystems and characterized by multifaceted behaviors and will not remain at a predetermined state. In this respect, ecological resilience concept is more appropriate framework for urban flood hazard management, as it works on a more realistic multi-equilibria paradigm that focuses pragmatically on persistence in a world of flux.

Theory of urban resilience to flood (Liao, 2012) is developed based on ecological concept of resilience. It characterizes urban flood resilience by flood tolerance and rapid reorganization in the event of a disruption. Flood tolerance relates to hazard mitigation and quick reorganization relates to post-disaster recovery. Flood tolerance refers to the capacity to remain undamaged and functional in the event of a flood; it is fundamentally the capacity to avoid a flood damage, not preventing floods altogether, which necessitates adapting the built-environment to flood.

Unlike the flood control paradigm that focuses on preventing flooding, the flood adaptation paradigm is concerned with how to tolerate flood. It is worth noting that the term "adaptation" employed here differs from that used in the climate change literature, which frequently refers to all-inclusively means of adjustments to current or projected climatic conditions and their consequences. More flood control is commonly mentioned in the climate change literature as an adaptation tool to climate-change-induced greater flood hazards (Wilby & Keenan, 2013). However, flood adaptation here is to refer to actions to fit for current and predicted flood regime without seeking to change it. In this

regard, flood damage and socioeconomic disruption are avoided by modifying the built environment and livelihoods to reduce flood effect rather than by preventing floods. The conceptual framework of this study is depicted in Figure 2.6.

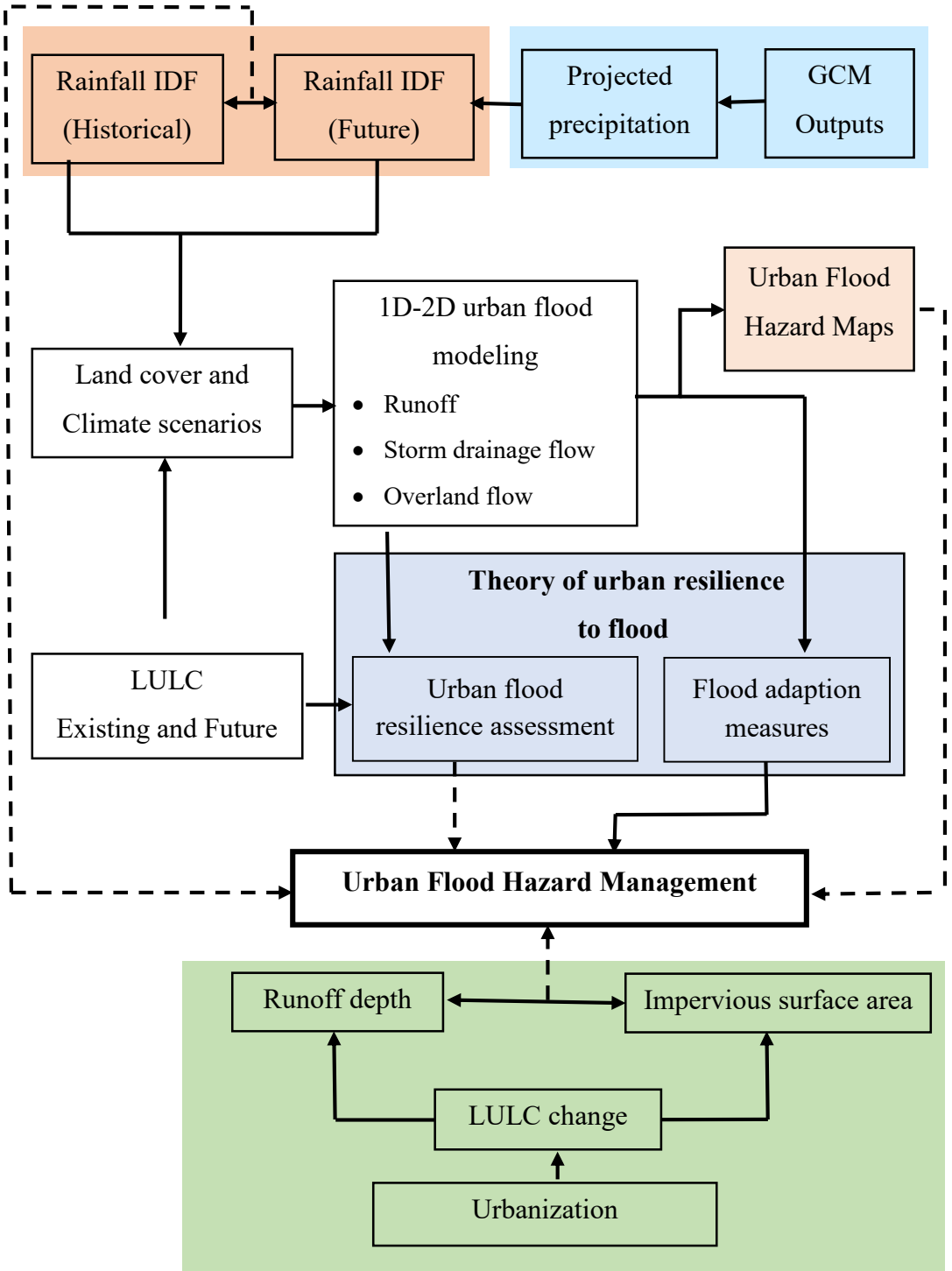

Figure 2.6 Conceptual framework of the study

CHAPTER 3: METHODOLOGY

3.1 Study area

3.1.1 Location

The study area, Adama City is located at latitude 8^0 33' N and longitude 39^0 16' E, at the center of both the National Regional State of Oromia and the country as well. The City is accessible by expressway and railway, and is about 100 km southeast of Addis Ababa City. Moreover, the City is situated in the Rift Valley. The City's administrative boundary consists of fourteen kebeles (Figure 3.1) and spans a total area of 134.1 square kilometers. The term "kebele" refers to the lowest level of the country's administrative structure.

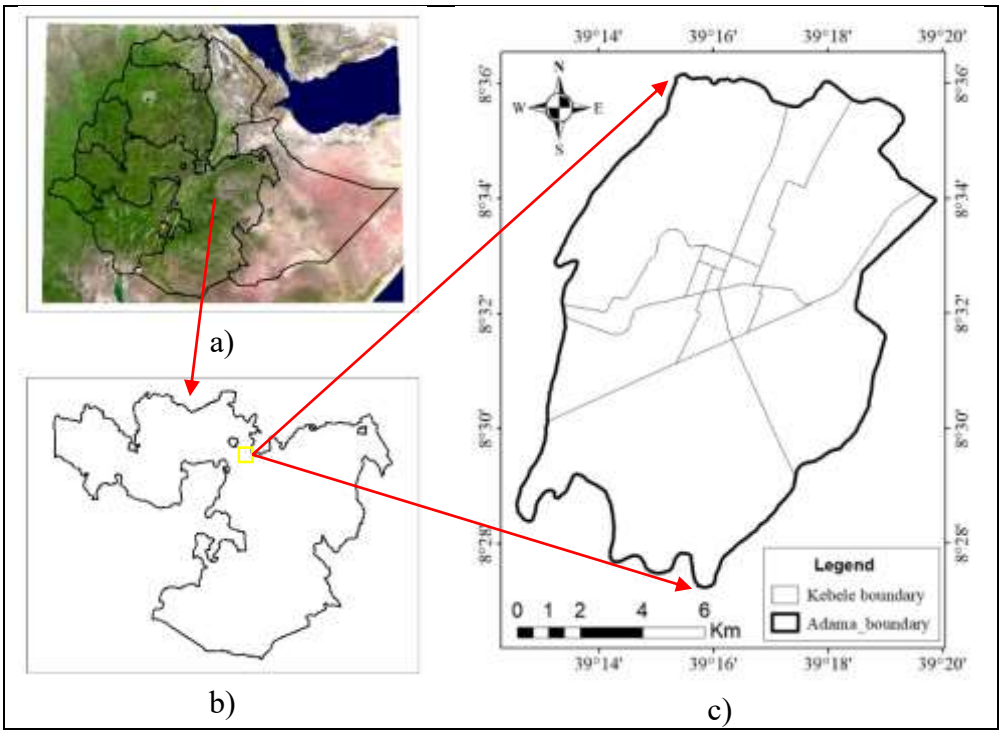

Figure 3.1 Location map of the study area a) Ethiopia regions, b) Oromia regional state, and c) Adama City administration

3.1.2 Urban growth

Adama City is one of the fast-growing cities in Ethiopia in terms of both the number of population and the footprint of built up areas. It has been the capital City of Oromia, the country's largest Regional State since August 2000. On top of this administrative position, its proximity to the national capital city, as well as its expressway and railway accessibility, are often regarded as the primary factors contributing to the City's fast development as a commercial, industrial, residential, and recreational center. Furthermore, the Awash Valley's economic potential and perspective developments are also important aspects in the city's growth, as well as the surrounding region as a whole. As a result, the city serves as the center of vast region with enormous economic potential, attracting stakeholders to invest in the city and its environs (Asfaw et al., 2011). Many civil engineering projects are currently under construction in the city, such as roads, bridges, Industry Park, and high-rise buildings with international hotels and commercial centers. This made rapid expansion of built-up area during last decades (Sinha et al., 2016; Terfa et al., 2019). The city's population growth rate from 2004 to 2016 increased 9 % (Bulti and Assefa, 2019). The floodplain area is densely populated with massive urban development.

3.1.3 Topography and Natural drainage

Figure 3.2 depicts the built-up area and natural drainage overlaid with the topography of the area. The drainage is extracted from ALASKA DEM through hydrological modeling in ArcGIS environment. Overall, the built-up area of the City is laid on the low-lying flat terrain with mountains and ridge topography surrounding it with significant elevation contrast (Figure 3.2). Generally, elevation in the Adama City Administration ranges from 1476 m to 1970 m above mean sea level.

The surface drainage of Adama City could be classified into two distinct macro-watersheds: Western (Awash sub-watershed) and Eastern (Mermersa sub-watershed). Awash sub-watershed collects runoff from western and northwestern parts of the City and finally drains to Awash River located at south of the City administration. Mermersa sub-watershed mainly collects runoff from the Eastern part of the City and the runoff drains northward from minor ridge that found at southeastern part and finally contributes to Mermersa.

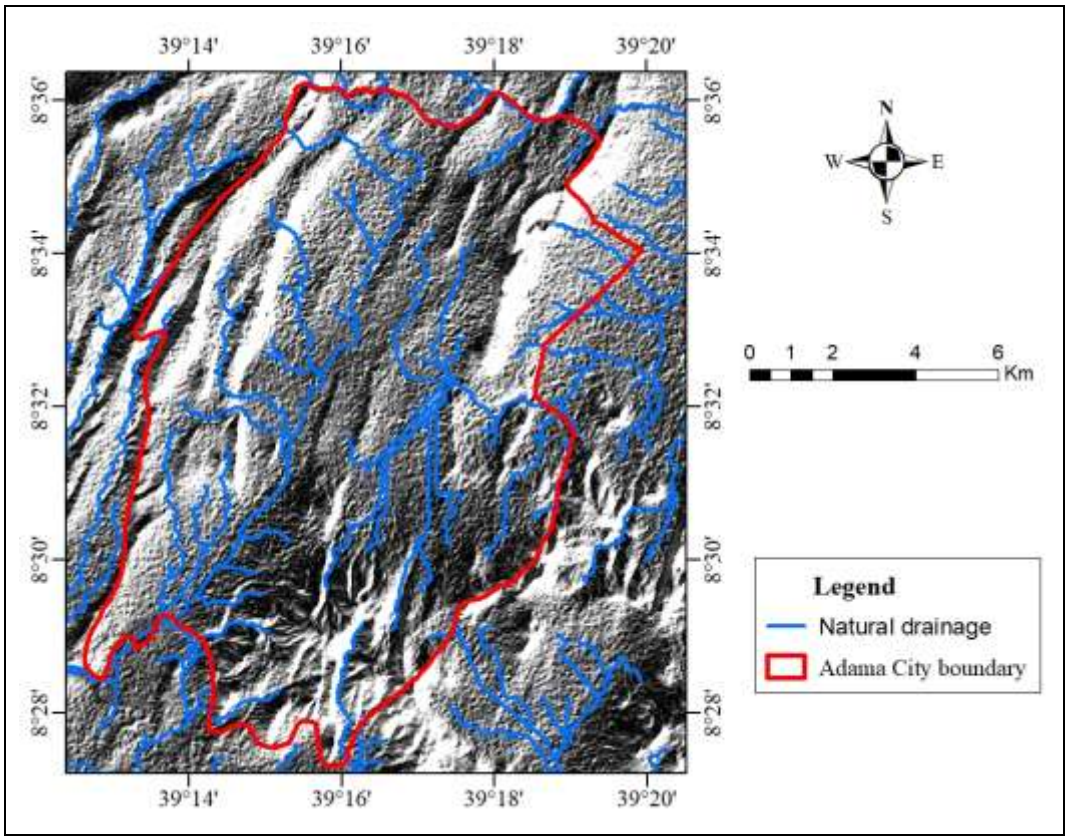

Figure 3.2 Topography and natural surface drainage of Adama City administration

3.1.4 Slope

Figure 3.3 illustrates the slope of the study area extracted from DEM. The slope of the varies between less than 2% to greater than 20 % around the ridges. The built-up area of the City is characterized by slope of 0-5%, and bounded by steep slope ridges. Slope ranging 2-5% covers larger area (37.6%) flowed by areas with 5-10% slope covering 26.8% of the City administration area.

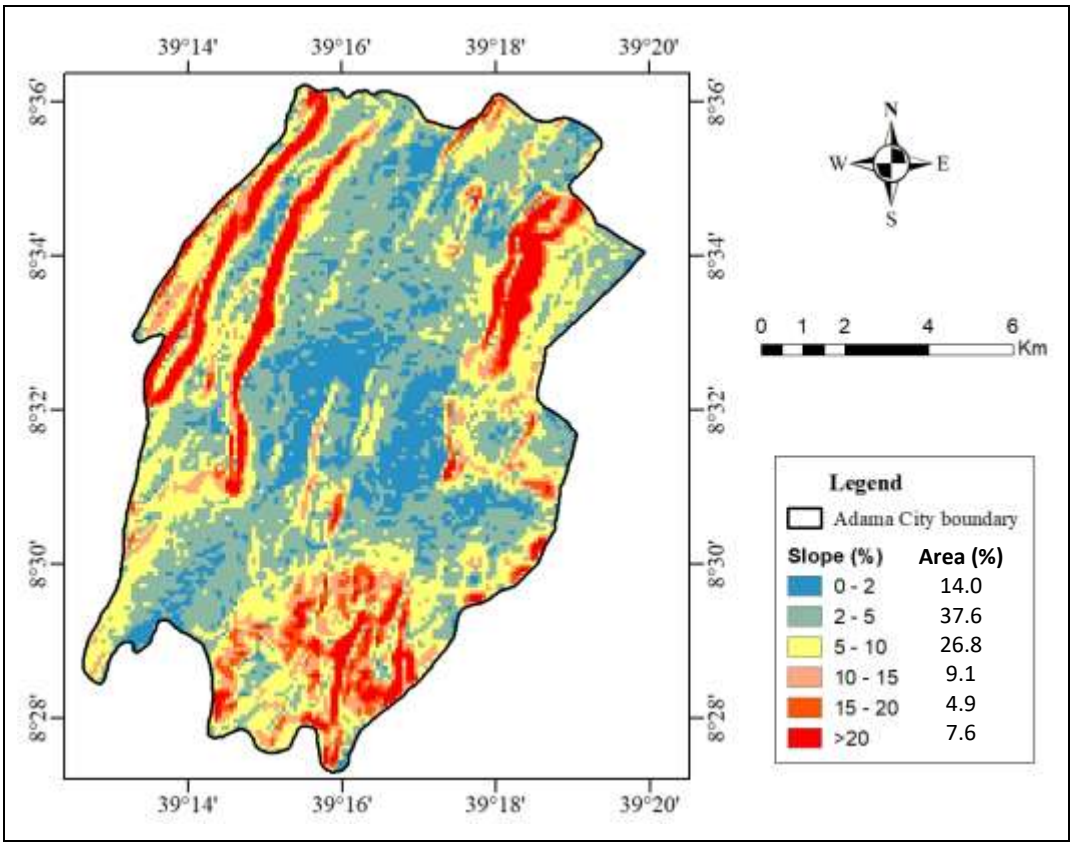

Figure 3.3 Slope of Adama City adminstration and coverage area for each slope range

3.1.5 Soil map

Soil properties influence the relationship between runoff and rainfall since different types soils have different rates of infiltration. Texture of a particular soil type influences

the rate at which water can enter and move through the soil. Permeability and infiltration are commonly used in classification of soils into different Hydrologic Soils Groups (HSG). Soil data of the study area was extracted from Awash Basin Soil map, which was collected from institute of water resource engineering, Adama Science and Technology University. Figure 3.4 shows the textural information the soil in the study area. Texturally, the soil in the City administration is characterized largely by loam (71.8%) and clay loam (24.9%) with small coverage of rock (3.3%). Loam soil has a moderately low runoff potential due to moderate infiltration rates, with moderately fine to moderately coarse textures. Clay loam concentrated at the center of the City with low-lying area and southern part of the City. It has a high runoff potential due to very slow infiltration rates.

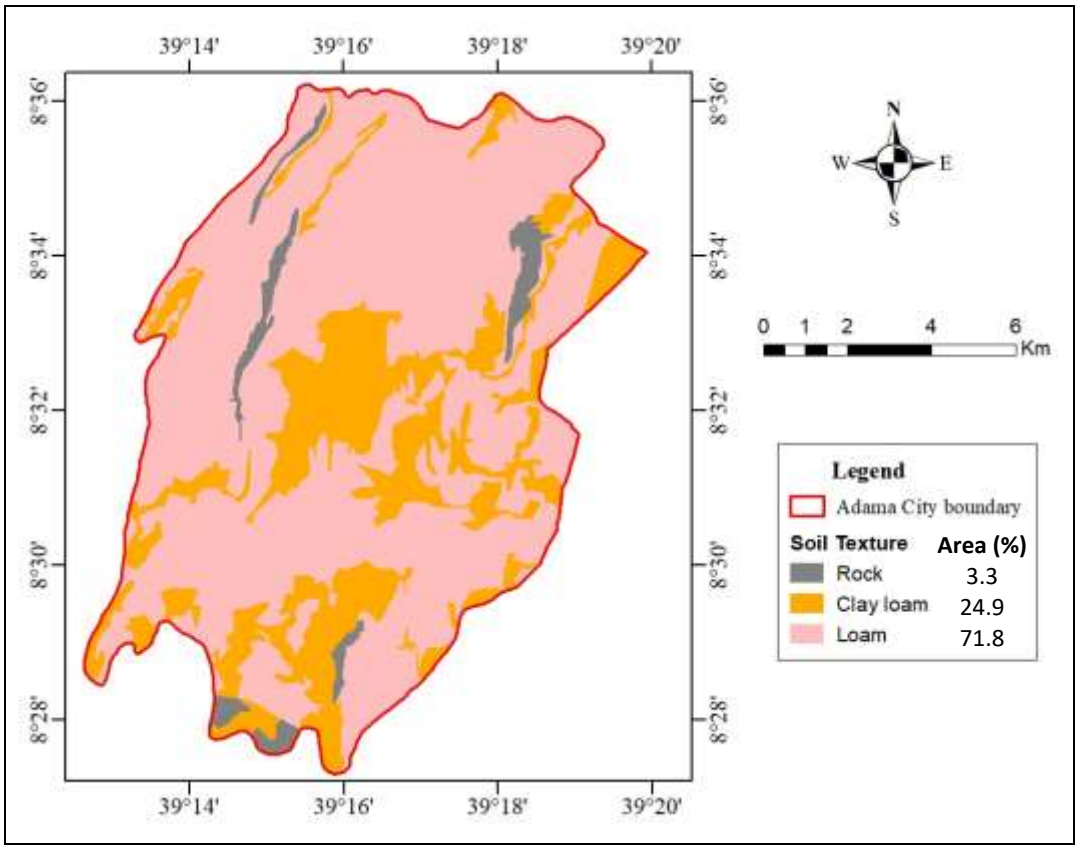

Figure 3.4 Soil map of Adama City administration in terms of textural characteristics with spatial coverage

3.2 Analysis of the changes in runoff depth under spatio-temporal dynamics of LULC

Analyzing how urbanization-induced dynamics of impervious surface has affected the runoff depth in Adama City administration involves a series of steps. Preparation of LULC maps of the City administration in different years to assess the spatio-temporal changes of LULC. Computation of runoff depth corresponding to the respective LULC condition and assessing its variations. Regression analysis to determine how well the spatio-temporal changes of imperviousness due to urbanization and the runoff depth are linearly related. The flow chart depicted in Figure 3.5 shows the general workflow for investigation of effects of urbanization on surface runoff depth. The details of data used and processes and the methods employed are explained in the following sections.

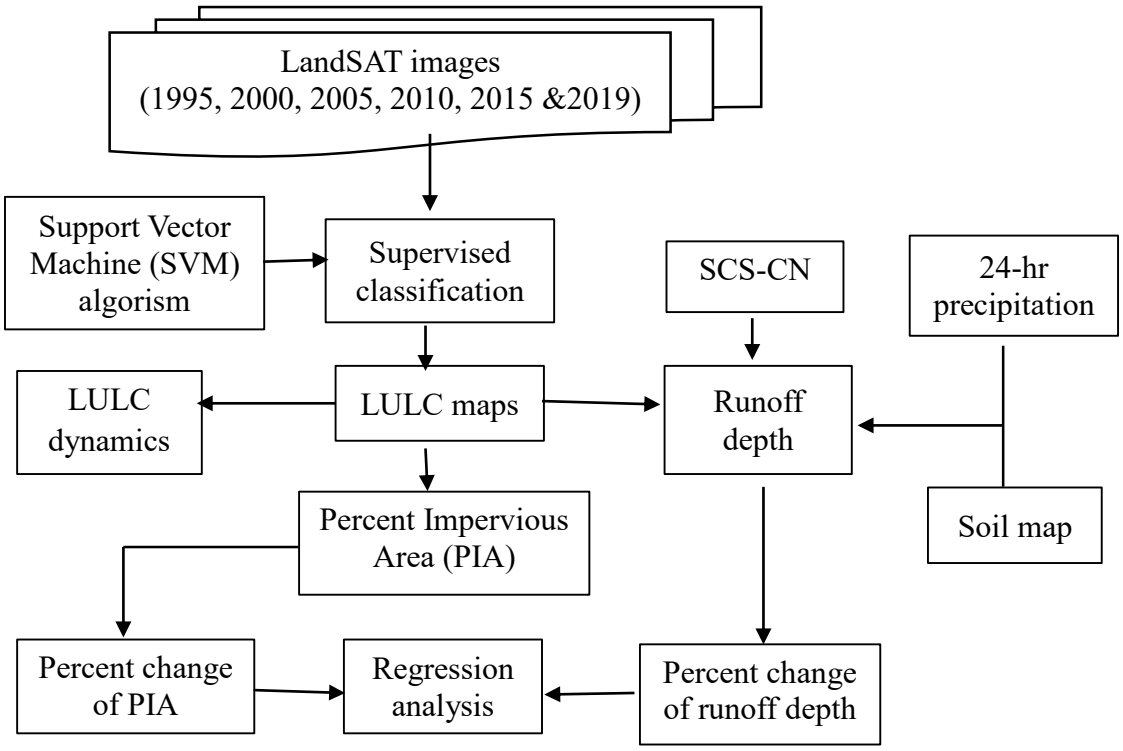

Figure 3.5 Workflow for investigation of effects of urbanization on runoff depth

3.2.1 Data used and image pre-processing

(i) Spatial data

The spatial data used in this study were collected from different sources, including websites, organizations. Landsat 7 TM/ ETM+ (Enhanced Thematic Mapper Plus) (L1TP product of path 168, row 54) was used for mapping LULC of the study area. Landsat image is widely used for urban LULC mapping, despite its medium spatial resolution and mixed pixel problem (Chen et al., 2016). It is freely accessible for multiple dates and considered suitable for time-series analysis. One image from each year with free cloud contamination, except that of 2015 (Table 3.1) was accessed from the United States Geological Survey (USGS) (https://espa.cr.usgs.gov/). All bands of the landsat image have 30 m spatial resolution. In addition, all images are geometrically corrected and orthorectified by the National Aeronautics and Space Administration (NASA) (Gutman et al., 2013).

The LULC maps serve as the base of the analysis, the accuracy of LULC classification has direct significant impact on the reliability of the runoff depth analysis. Accordingly, all images are acquired during the dry season, as the accuracy of landsat image classification during the dry season is found to be higher than during the wet season (Liu et al., 2015). Further, the atmospheric effects were reduced through conversion of raw digital number (DN) values to the surface reflectance in radiometric calibration module in ENVI software.

Soil map of the City administration was collected from institute of water resource engineering, Adama Science and Technology University. Digital orthophoto acquired

in 2014 and 2018 with 15 cm spatial resolution were obtained from Adama City administration.

Table 3.1 Date of acquisition and the cloud cover (%) of landsat images used for LULC mapping

Year	Date of image acquisition	Cloud cover
1995	Jan 30, 1995	-
2000	Feb 05, 2000	-
2005	Feb 18, 2005	-
2010	Jan 15, 2010	-
2015	Feb 14, 2015	1%
2019	Jan 08, 2019	-

(ii) Rainfall data

The daily rainfall data for a period of 1995-2016 recorded at Adama meteorological station was collected from the National Meteorological Agency (NMA) of Ethiopia, Adama branch office. The starting year, 1995, is selected in consistent with that of LULC maps. The data were checked for missing values, and few gaps (91 days about 0.9%) identified in the data were filled using R-based ImputeTS package. Accordingly, the maximum, minimum, and mean annual precipitation over the study period are found to be 1371 mm, 629 mm, and 920 mm, respectively.

In Adama, most of the rain occurs from June to September, whereas the wettest months are July and August. The maximum daily precipitation in rainy season (June – September) was selected for runoff computation for analyzing the impacts of

urbanization on runoff response in the City administration, and its sub-watersheds. It is found to be 99.8 mm, precipitation record corresponding to July 18, 2000. It is used for the study, and helped to distill the impacts of LULC on the surface runoff depth of the study area, by reducing the effect of rainfall variations.

3.2.2 Land use/land cover mapping

Considering the importance of short-term changes in urban areas due to rapid urbanization (Zhang et al., 2018), LULC maps of the study area were prepared at about 5 years' interval (1995, 2000, 2005, 2010, 2015 and 2019) using landSAT images through supervised classification method. It involves defining classification scheme, selection of training samples, running an algorithm to assign each pixel into a class and accuracy assessment. Flooding problem is aggravated since the turn of this century and fast urban developments is perceived after assignment the City new administration position. Urbanization impacts on hydrologic characteristics of the study area in the period of 1995-2019 deemed necessary.

3.2.2.1 Defining classification scheme

The analysis focused on spectral resolution because the spectral dimension is the most important source of cover type information in coarse resolution images. The success of LULC usually measured by the ability to match the spectral classes in the data to the information classes of interest (Weng, 2010). Spectral classes refer to the groups of pixels with similar (or near-similar) brightness values in the diverse spectral bands of the data. Whereas, information classes are those classes of concern that the analyst is attempting to identify within the imagery.

In a complex urban landscape, a particular land use class may have diverse spectral characteristics (e.g., Roof cover of old and new buildings). By contrast, different classes (objects) can have the same spectral characteristics (e.g., Rock and concrete or bright building roofs). Hence, a simple one-to-one relation between the two types of classes is rarely identified. Many times it is found that 2 to 3 spectral classes merge to form one informational class.

Given the importance of the appropriate classification scheme, in this study, initially, by visually analyzing the color composite landsat images with different band combinations, different classes were identified, and aggregated into four: urban, bare land, agriculture and vegetation (Table 3. 2). LULC classes were defined based on their contribution to runoff.

Table 3.2 Land use/land cover classification scheme used in the study

LULC class	**Description**
Urban	Comprises areas with all types of artificial surfaces, including buildings and transportation infrastructure (asphalt, gravel, railway). Areas under construction are also included
Barren land	Includes a surface with no or little vegetation, open land, exposed soil, rocks and sand (eroded gullies)
Agricultural	Includes areas used for cultivation (both annuals and perennials)
Vegetation	Comprises areas with vegetation cover, such as areas covered with both indigenous and exotic tree and shrub land. It also includes green spaces in built-up areas: an area of grass, trees, or other vegetation set apart for recreational or aesthetic purposes inside urban built environment

3.2.2.2 Training Sample Selection

Training samples for each class were collected from each image. In order to reduce the sampling biases, consistency in sample selection was kept by selecting pixels that remained unchanged at different times to train the classifier. First, samples were selected from landsat image of 1995 (first image). Subsequently, these samples were treated as training samples for the first image and used as a base for the adjacent image (2000). Second, the base samples were overlaid with the second image to check if change in class occurred (i.e., different LC in the image than the base image). If changes were observed, new sample with more confidence was substituted from the surrounding area. Similarly, the same procedures were followed by selection of training samples for the rest of the images.

As a general rule, the number of sample pixels for each subclass was determined based on the recommendation of Sertel and Akay (2015), which sate that the number of pixels of training samples for each class should be at least 10 times the number of bands in an image to classify. In this study, the total number of training pixels used for each LULC class alongside the respective years is summarized in Table 3. 3.

Table 3.3 Summary of the number of training samples selected for image classification

Year	Number of pixel per LULC class			
	Agriculture	**Barren**	**Urban**	**Vegetation**
1995	1709	1640	650	610
2000	1430	1276	698	606
2005	1764	1493	883	801
2010	1183	1685	1071	524
2015	1269	1761	1556	1378

3.2.2.3 Classification algorithm

Each image was classified into a set of spectral classes using Support Vector Machine (SVM) algorithm in ENVI software. SVM is non-parametric classifier. Unlike parametric classifiers such as maximum likelihood which assumes that the data is normally distributed, non-parametric classifiers do not base classification on a normality assumption or statistical parameters (Phiri and Morgenroth, 2017). Because of highly heterogeneous land covers data (e.g., Urban areas) are unlikely normally distributed, the distribution of land cover surfaces is associated with various uncertainties which prevents their description based on data distribution (Lu and Weng, 2007). In this respect, non-parametric classifiers provide better results as compared to parametric classifiers in complex landscapes.

3.2.2.4 Accuracy assessment

Accuracy of land use maps is important in urban studies (Sertel and Akay 2015). In thematic mapping from remote sensing data, classification accuracy refers to the level to which the resulting image classification conforms to the 'truth' or agrees with the reality (Foody, 2002). This is usually undertaken by using information collected from the map and the reference sources. Reference sample data is the class label, which derived from sources that are assumed to be correct. Whereas, map sample data refers to the data derived from the map being assessed. A reference sample data for assessing the accuracy of maps created from moderate-resolution satellite imagery (e. g., Landsat) can be collected from a variety of sources, including previously existing maps, aerial photography and Google Earth (Congalton and Green, 2009; Fonji and Taff, 2014; Tilahun and Teferie, 2015; Amani et al., 2019).

In this study, LULC classification accuracy was assessed quantitatively using error matrix which is the commonly used method in LULC classification accuracy assessment (Weng, 2010). In this regard, sample pixels were selected from each of classified images through a stratified random sampling scheme in ENVI software. This enables to undertake unbiased sample selection, as it includes each LULC class in the sample (Congalton and Green, 2009).

The samples were overlaid with the existing map (for 1995), Google Earth image of respective years for 2000, 2005 and 2010 and digital orthophoto (for 2015 and 2019) to visually interpret and determine their respective classes. Based on the error matrix generated for each classified map, overall accuracy, user's accuracy and producer's accuracy were calculated, in addition to kappa variance. The accuracy requirements for change detection analysis were determined based on the suggestion of Congalton and Green (2009). In this case, the value of the Kappa statistics, greater than 0.8, indicates strong agreement between the class label on the map and on the reference data.

3.2.3 Methods of data analysis

3.2.3.1 Analysis of LULC dynamics

The spatio-temporal changes of LULC were identified using areal data generated from LULC maps in GIS environment. Quantitative areal data from the overall LULC changes, as well as gains and losses in each class were compiled to analyze the nature and rate of the changes. The percentages of changes were computed using Equation 3.1. In this case, the positive and negative values suggest a gain and loss in spatial extent, respectively.

$$\Delta_{\mathrm{LULC}} = \frac{A_2 - A_1}{A_1} * 100 \quad (3.1)$$

Where: A_1 *and* A_2 are areas of a LULC class in the consecutive years

3.2.3.2 Analysis of imperviousness change

Imperviousness refers to the areal proportion of impervious surfaces within the defined boundary (e.g., watershed, administrative boundary), i.e., Percent impervious area (PIA). Impervious surface in urban areas, generally comprises anthropogenic features (e.g., Buildings, parking lots, roads, etc.) which rainfall water cannot permeate, and they are usually associated with urban expansion (Tabbutt and Ambrogi, 2013; Zhang et al., 2018). These features are categorized under urban land use class in this study and considered as impervious surfaces, similar to other studies (Parece and Campbell, 2013; Ramamurthy and Bou-Zeid, 2014; Yu et al., 2018). In this regard, the urban class in each watershed was extracted and the area was computed to provide the extent of impervious surface in respective watersheds.

PIA was calculated by using the ratio of impervious surface area at different years to the area of the respective analysis boundaries. The changes of imperviousness were computed with respect to the first year of the analysis (Equation 3.2). This helped to assess the impact of urbanization in increasing the impervious surface in the study area.

$$\Delta PIA_i = \frac{PIA_i - PIA_{1995}}{PIA_{1995}} * 100 \quad (3.2)$$

Where ΔPIA_i: percentage change of imperviousness; PIA_i *:* imperviousness in respective years; PIA_{1995}: imperviousness in the baseline year (1995).

3.2.3.2 Evaluation of spatio-temporal changes of runoff depth

Evaluation of the temporal variations of the runoff depth due to the impacts of LULC changes involves computation of runoff and percentage change with respect to a baseline/reference year. Rainfall-runoff was estimated using the method of soil conservation service curve number (SCS-CN). It is simple and stable conceptual technique for direct runoff depth estimation based on rainfall depth (Subramanya, 2008). SCS-CN is well-established method, having been commonly used for examining the relationship between different land uses and runoff in water resources management and planning (Gunn et al., 2012; Cherian et at., 2017; Rao et al., 2017; Zhang et al., 2018). SCS-CN method provides an adequate result with a minimum information that makes it more useful for ungauged watershed (Chen et al., 2017; Pandey, 2017). The value of CN reflects the impact of land cover on the runoff yield ranging from 0 (100% infiltration) to 100 (0% infiltration). Evapotranspiration losses are insignificant in the storm event (Chen et al., 2015).

Runoff can be easily obtained using three important properties of the watershed: soil permeability, land use and antecedent soil water conditions (Bansode et al., 2014; Chen et al., 2015). Initially, the soil types in the study area were converted to hydrologic soil group (HSG). The CN for each LULC class is determined and found to be 72, 91, 93 and 50 for agriculture, bare land, urban and vegetation, respectively.

The analysis was conducted at the City and sub-catchment levels, and the study watersheds encompass different LULC class alongside different spatial extent. To determine a single curve number for respective analysis boundaries for runoff estimation using SCS-CN method, the catchments were spatially intersected with

LULC maps and the area of each class in each catchment was computed. Then, the weighted CN for respective watersheds was computed using Equation 3.3.

The 5 days' (July 14-18, 2000) rainfall magnitude is found to be 137 mm. Based on Subramanya (2008) recommendation, wet antecedent moisture condition was selected. Based on this, equations 3.4 and 3.5 were applied for converting the average antecedent moisture condition into wet condition and for computing the potential maximum soil retention, respectively. Using daily rainfall, the accumulated runoff depth in respective areas was computed using Equations 3.6.

$$CN_{w\,II} = \frac{\sum_{i=1}^{n} CN_i a_i}{\sum_{i=1}^{n} a_i} \quad (3.3)$$

$$CN_{III} = \frac{CV_{w\,II}}{0.427+0.00573CN_{II}} \quad (3.4)$$

$$S = \frac{25{,}400}{CN_w} - 254 \quad (3.5)$$

$$Q = \frac{(P-0.2S)^2}{(P+0.8S)} \quad (3.6)$$

Where Q: accumulated direct runoff depth (mm); P: accumulated rainfall (mm); S: potential maximum retention (mm).

Using the computed runoff depth for respective years, the temporal variations of the runoff depth due to the impacts of LULC changes were assessed through runoff depth change ratio. By taking the runoff depth of the first year (1995) as a baseline, the percentage changes in runoff for 2000, 2005, 2010, 2015 and 2019 were computed using Equation 3.7. This helped to determine the temporal variations in storm runoff

depth attributable to the changes in LULC of the study area with respect to that of the baseline year.

$$\Delta Q_i = \frac{Q_i - Q_{1995}}{Q_{1995}} * 100 \quad (3.7)$$

Where ΔQ_i Percentage change of runoff depth; Q_i is runoff depth in respective years, Q_{1995} is runoff depth in the reference year (1995).

3.2.3.3 Regression analysis

Regression analysis was carried out to explore the relationship between the spatio-temporal changes of PIA and runoff depth. It is the common method to investigate the relationship between a quantitative outcome and a quantitative explanatory variable (Seltman, 2018).

The validity of the model assumptions was determined by examining the structure of the residuals and the data pattern through graphs. Examination of residual plots is a simple and effective method for validation of standard assumptions in regression analysis (Chattefuee and Hadi, 2006). In this context, the normality assumption was validated using a normal probability plot of standardized residuals which is a plot of the ordered standardized residuals against the normal scores. Under normality assumptions, this plot should resemble a (nearly) straight line with an intercept of zero and a slope of one, and they are equal to mean and standard deviation of the standardized residuals, respectively. In addition, scatter plots of the standardized residual against PIA and fitted values were used to validate the linearity assumption. Under the standard assumptions, the standardized residuals are uncorrelated with the

explanatory variable and with fitted values. The random scatter of points of these plots explains the validity of linearity assumption.

The strength of the linear relationship between the runoff variations and the PIA was determined using the value of Pearson's correlation coefficient (r). It is a dimensionless quantity that commonly used to compare the linear relationships between pairs of variables in different units. Accordingly, the non-zero value of the correlation coefficient indicates the variables are correlated. Further, the positive and negative values indicate direct and indirect relationship, respectively. Moreover, like Bulti and Assefa (2019) the strength of the correlation was described using the absolute value of correlation coefficient: very weak ($|r| < 0.19$), weak ($|r| < 0.39$), moderate ($|r| < 0.59$), strong ($|r| < 0.79$), very strong ($|r| < 1$).

Statistical significance testing was also conducted to offer an objective measure in the decision about the validity of the generalization, and it was determined using a p-value statistic. In this case, the null hypothesis states that there is no significant relationship between the changes in PIA and runoff. In theory, the p-value is a continuous measure of evidence (Gelman, 2012), yet in this study, the term "significant" refers to the 95% confidence level ($p < 0.05$); it is standard in statistical practice in most of the Engineering researches.

3.3 Analysis of trend of extreme precipitation and its future variability under climate change

The trend of extreme precipitation in Adama City and its future variability under climate change was analyzed by (i) assessing the trend of extreme precipitation in the study area over the period of 1967-2016; (ii) downscaling of daily precipitation from

the projections of GCMs; and (iii) investigating the future changes in precipitation extreme in the study area. The general workflow to analyze the change in extreme precipitation under the influence of climate change.

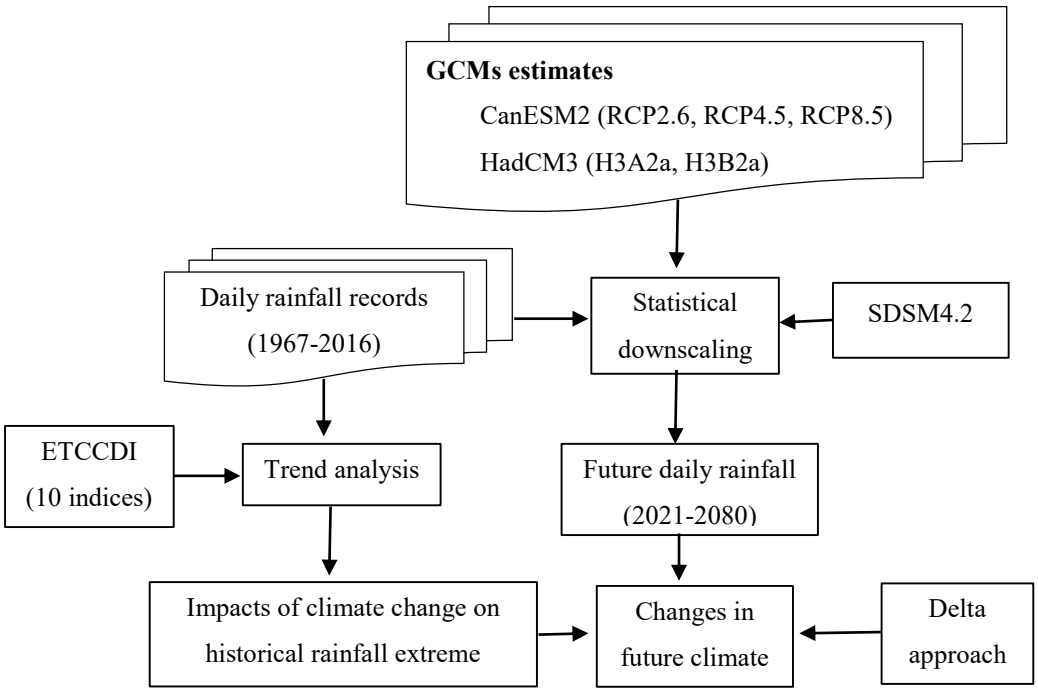

Figure 3.6 Workflow of analysis of trend of extreme precipitation and its future variability under climate change

3.3.1 Precipitation data series and selection of GCMs

Precipitation data used for assessing the trends in historical precipitation records and its future variability were accessed from different sources. The daily rainfall data recorded at Adama weather observation station were obtained from the National Meteorological Agency (NMA). Due to extended missing observation (i.e., more than one year), only 50 years (1967-2016) time-series precipitation data were selected for analysis. First, the proportion of missing observation in the selected time-series data

was checked and found to be 7.47%. It is within the maximum flexible threshold values adopted by other studies (Ngongondo et al., 2011; Mohammed et al., 2018). Next, the missing data were filled using the Kalman Smoothing function in R-based ImputeTS package. This function provides the acceptable results and it is recommended for long time-series data (Steffen, 2019).

In addition, three large-scale datasets (described below) were used: NCEP reanalysis dataset for the calibration and validation, and CanESM2 and HadCM3 datasets for the baseline and climate scenario generation. They are chosen because they are freely available online and predictors are organized in such a way that they can directly be used in statistical downscaling model (SDSM) presented in section 3.4.3. In addition, they have been widely applied in similar studies (Dile et al., 2013; Mekonnen and Disse, 2018; Deb et al., 2018; Mohammed et al., 2020).

CanESM2 (second generation Canadian Earth System Model) is coupled atmosphere-ocean global climate model developed by the Canadian Centre for Climate Modelling and Analysis (CCCma). CanESM2 provided long-term climate simulation based on the three greenhouse gases (GHG) emission scenarios (Representative Concentration Pathways, RCPs), including a stringent mitigation scenario (RCP2.6); medium stabilization scenario (RCP4.5) and high emission scenario (RCP8.5). The CanESM2 model has a resolution of 2.79^0 latitude and 2.81^0 longitude. More descriptions can be found in Intergovernmental Panel on Climate Change IPCC (2014).

HadCM3 (third generation Hadley center Climate Model) is a coupled atmosphere ocean general circulation model developed at the Hadley Centre in the United Kingdom. The model generated climate variable using two emission scenarios in

the future atmosphere: medium-high (A2) and medium-low (B2). This GCM has a resolution of 2.5° latitude by 3.75° longitude. More description can be found in Semenov and Stratonovitch (2010).

NCEP (National Centre for Environmental Prediction) reanalysis dataset contains largescale atmospheric variables representing the present-day condition, and it was used for calibration and validation of the downscaling model in this study. The NCEP dataset was normalized over the complete 1961–1990 period data, and interpolated to the equal grid as CanESM2 and HadCM3 from its horizontal resolution of 2.50 latitude and 2.50 longitude (Mekonnen and Disse, 2018).

The archives of large-scale datasets were downloaded from Environment Canada website (*http://ccdsdscc.ec.gc.ca/?page=pred-canesm2)* for the grid box containing the study area (CanESM2_BOX_015X_36Y and HadCM3_BOX_11X_31Y). The archive of CanESM2 include historical large-scale simulation data (CanESM2_historical_1961_2005) and predicted data corresponding to three emission scenarios (RCP2.6, RCP4.5 and RCP8.5) for the years 2006-2100. HadCM3 archive also include data for both scenarios (H3A2a and H3B2a) spanning from 1961 to 2099 (the "a" in A2a and B2a refers the ensemble member in the HadCM3 A2 and B2 experiments). In addition, archives of both datasets contain reanalysis data (NCEPNCAR_1961_2005 for CanESM2 and NCEP_1961-2001 for HadCM3). The datasets include 26 predictor variables under each of the emission scenarios of respective GCMs and reanalysis data. However, the NCEP-derived predictors data and the predictors supplied for the GCMs were slightly vary (Table 3. 4).

Table 3. 4 Gridded predictors of CanESM2 and HadCM3 datasets

Variable	Description
temp	Mean temperature at 2m
mslp	Mean sea level pressure
p500	500 hPa geopotential height
p850	850 hPa geopotential height
shum	Near-surface specific humidity
rhum [a]	Near-surface relative humidity
prec[b]	Total precipitation
s500[b]	Specific humidity at 500 hPa height
r500[a]	Relative humidity at 500 hPa height
s850[b]	Specific humidity at 850 hPa height
r850 [a]	relative humidity at 850 hPa height
*_f	Geostrophic air flow velocity
*_z	Vorticity
*_u	Zonal velocity component
*_v	Meridional velocity component
*zh	Divergence
*thas	Wind direction

[a] found only for HadCM3, [b] found only for CanESM2, *refers to different atmospheric levels: the surface (p_), 850 hPa height (p8) and 500 hPa height (p5)

3.3.2 Analysis of extreme precipitation

***Extreme precipitation indices*:** Extreme precipitation in Adama City was analyzed using standard indices for the extreme precipitation defined by Expert Team on Climate Change Detection and Indices (ETCCDI). These indices are ease to calculate and understand, and they provide scientifically robust measures of the variability of rainfall

extremes (Zhang et al., 2011). Moreover, they have been widely used in several similar studies in different regions of the world for recent years (e.g., Lima et al., 2015; Gujree et al., 2017; Shawul and Chakma, 2020; Berhane et al., 2020; Geremew et al., 2020). The definitions of the indices used in this study are presented in Table 3.5. The linear trends of the indices were computed from daily precipitation data using the R-based RClimDex software package, and the statistical significance of the trends was assessed at $\alpha = 0.1$ amd $\alpha = 0.05$.

Table 3. 5 Definitions of indices for analysis of extreme precipitation in Adama City

ID	Indicator name	Indicator definitions	Units
PRECTOT	Annual total wet-day precipitation	Total wet-day precipitation ≥ 1 mm	mm
SDII	Simple daily intensity index	Mean precipitation amount on wet-day (≥ 1 mm)	mm/day
Rx1day	Max 1-day precipitation amount	Maximum 1-day precipitation	mm
Rx5day	Max 5-day precipitation amount	Maximum consecutive 5 days precipitation	mm
R10	Number of heavy precipitation days	Annual count when precipitation ≥ 10 mm	days
R20	Number of very heavy precipitation days	Annual count when precipitation ≥ 20 mm	days
CDD	Consecutive dry days	Maximum number of consecutive days when precipitation < 1 mm	days
CWD	Consecutive wet days	Maximum number of consecutive days when precipitation ≥ 1 mm	days
R95p	Very wet days	Annual total precipitation from days > 95th percentile	mm

R99p	Extremely wet days	Annual precipitation days > 99th percentile	total from	mm

***Correlation analysis*:** The linear relationship between extreme precipitation indices was also assessed using Pearson correlation analysis. In essence, it was conducted to compare the precipitation indices for mean conditions (SDII and PRECTOT) and other extreme indices. Such analysis may also help to identify the data with irregular behavior as a result of a few individual, highly faulty daily values in time-series data, which affect overall data statistics (Santo et al., 2013); hence, it helped as an additional tool for examining the data closely. The statistical significance of the correlations was determined using the two-tailed test of the Student's distribution and evaluated at the α = 0.05 level.

3.3.3 Downscaling future precipitation

i) Model description

The choice of proper downscaling method relies on the needed temporal and spatial resolutions of the climate variability, as well as the resource and time constraints. In this study, the Statistical DownScaling Model (SDSM) was selected to downscale local daily precipitation from the outputs of selected GCMs. The structure of the model for climate scenario generation is depicted in Figure 3.7. The downscaling experiment was realized using SDSM4.2 software. It is a freely available Windows–based decision support tool for generating single–site daily climate variables under the current and future regional climate forcing (Wilby and Dawson, 2007). It provides a robust scenario building technique for a specific location for which there are archived GCMs outputs and adequate observed daily local variable for calibrating the model

(Gebrechorkos et al., 2019). In general, downscaling experiment using SDSM in this study involves selection of candidate predictors; model calibration and validation; and synthesizing future precipitation.

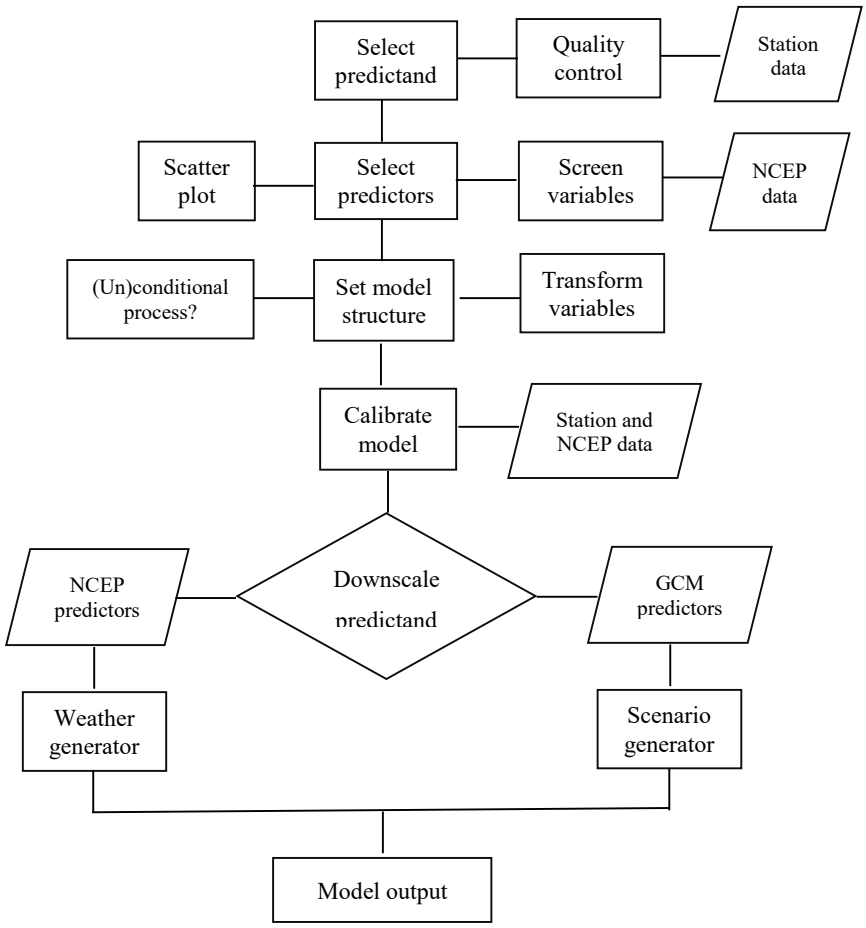

Figure 3. 7 SDSM Version 4.2 climate scenario generation, adopted from Wilby and Dawson (2007)

ii) Selection of predictors

Statistical downscaling methods require appropriate large-scale atmospheric variables that enable identification of robust empirical associations between gridded predictor variables and site-scale predictands. However, choosing a predictor is one of the most challenging tasks, as the explanatory power of each variable varies in both spatial and

temporal scales, indicating the selection process can be exposed to some level of subjectivity. To reduce this, a quantitative approach presented in other similar studies (Huang et al., 2011; Mahmood and Babel, 2014), was used to examine the predictive variables.

Initially, the correlations between the daily rainfall (predictand) and each of the 26 NCEP atmospheric variables (Table 3.4) were identified. Then, 11 variables with relatively large values of absolute correlation were selected, from which the variable with the highest correlation coefficient is assigned as a superior predictor (*SP*). Then, the absolute correlation between predictor variables (*r*), the partial correlation coefficient (*Pr*) and the *P*-values were determined in the presence of *SP*. Then, the percentage reduction (*PR*) for each variable was calculated using Equation 3.8. The second candidate predictor was determined using a combination of the correlation coefficient (*r*), p-value and the percent reduction (*PR*). In this case, a predictor with, $r < 0.7$, $p < 0.05$, and *minimum PR*. By repeating this procedure, further additional predictors were selected. Due to variation in the supplied predictors for the two GCMs, two sets of predictors were selected one for each GCM for calibration of the models. In most cases, 3 to 5 predictors are considered sufficient to detect the variation of a predictand during SDSM calibration (Chu et al., 2010; Feyissa et al., 2018). Because in the regression equation, an increase in the number of predictors can increase the probability of multiple co-linearity (Mahmood and Babel, 2014).

$$PR = \frac{(Pr - r)}{r} * 100 \qquad (3.8)$$

iii) Model calibration and validation

Using the respective sets of selected NCEP predictors, two precipitation models (for each of the GCMs) were developed under conditional processes on the monthly timescale with a fourth root transformation of the predictand. The models were calibrated for daily rainfall data observed over the period of 1967-1990, and used for historical rainfall generation (i.e., downscaling of NCEP reanalysis data). The models were validated over the years 1990-2005 (CanESM2) and 1990-2001 (HadCM3). The variation of the length of the validation periods is due to the availability of NCEP data corresponding to the GCMs. The performance of the models was evaluated using graphical and statistical methods. First, the models were validated by plotting the observed against simulated monthly mean precipitation. Second, two statistical parameters: the coefficient of determination (R^2) and the ratio of standard deviation of the simulated data to the observed data (RSD) were used. RSD indicates the level of dispersion, and its optimum value is 1, suggests that both datasets (simulated and observed) have the same kind of (Mahmood and Babel, 2014; Moses and Gondwe, 2019). Both parameters are computed using daily and monthly average precipitation data of observed and downscaled reanalysis data (NCEP_CanESM2 and NCEP_HadCM3).

iv) Climate scenario generation

The calibrated model was used for generation of ensembles of the daily precipitation corresponding to the future period. Using predictors of the respective GCMs, future daily rainfall was generated under five climate change scenarios (H3A2a and H3B2a of HadCM3 and RCP 2.6, RCP4.5 and RCP8.5 of CanESM2).

3.3.4 Analysis of future changes in precipitation extreme

Future changes in extreme rainfall under climate change scenarios were assessed on the basis of four indices that were included in SDSM4.2. They are annual percentage of wet-days (wet-days%), the ratio of the sum of the values over the 95th percentile of the sum of all values (POT95), longest wet-spell (CWD) and annual total precipitation (PRECTOT). The event limit was set to 1mm/day to count the rain day with less than 1mm as dry day.

The future changes in the indices were computed using delta approach. It is a widely used method in similar studies (Choi et al., 2009; Salvacion et al., 2018; Feyissa et al., 2018). The standard delta approach for precipitation is the relative difference between GCM-simulated precipitation of the future and baseline periods, and takes the form of Equation 3.9. The analysis of the changes over the future period was carried out by dividing into two time horizons: 2020s (2021-2050) and 2050s (2051-2080). The present-day estimate (1971–2000) was considered as a base for standardizing the time-series resulting from climate change. Such approach helps to reduce the systematic bias in the mean and variance of GCMs predictors (Wilby and Dawson, 2007).

$$\Delta_{Pi} = \frac{V_{Pi} - V_{base}}{V_{base}} * 100 \qquad (3.9)$$

Where: V_{base} is the mean of all ensembles of each index for the base period (1971-2000). V_{Pi} is the mean of all ensembles of the corresponding index for the future periods (2020s, 2050s).

3.4 Analysis of extreme precipitation IDF relationship

The potential influences of climate change on future extreme rainfall characteristics were assessed by taking the present-day relationship as a bassline. This mainly involves disaggregation of daily precipitation observed and downscaled from GCMs outputs into shorter-time scales; establishment of rainfall IDF relationships; and developing IDF models and assess the possible changes in the future extreme rainfall intensity as compared to the historical condition for a range of storm durations and return periods. The flowchart depicted in Figure 3.8 was used for the analysis of changes in rainfall IDF relationships. Data used and details of methods employed for each of these analyses are explained in the following sections.

.

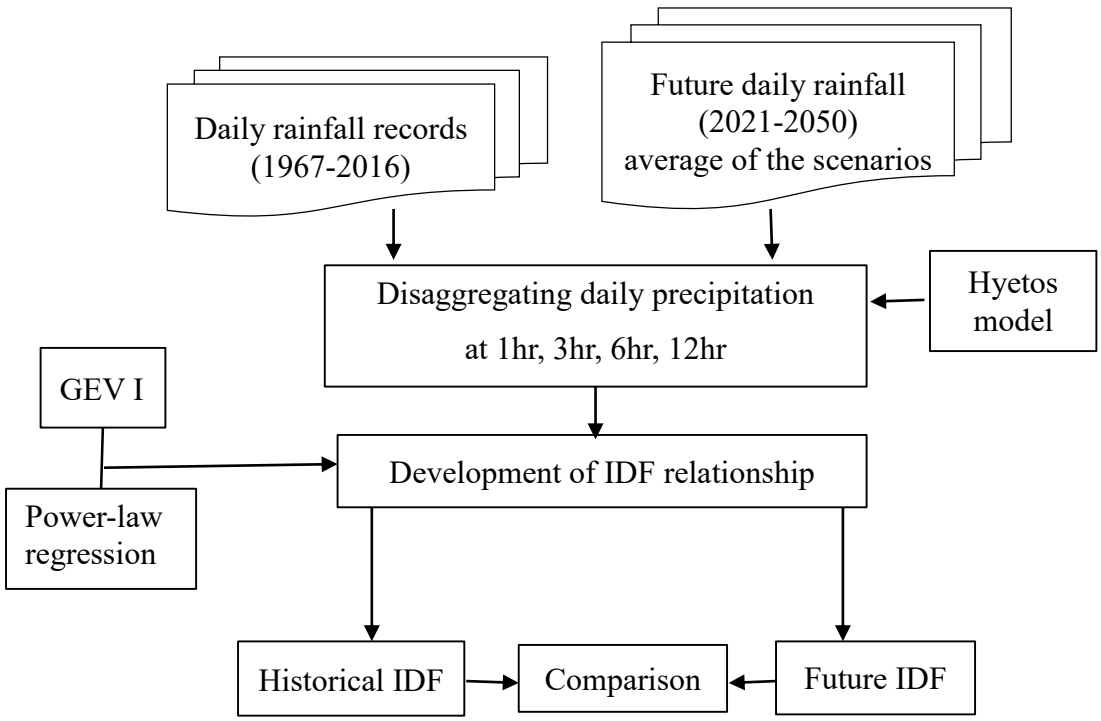

Figure 3.8 Methodological workflow of analysis of changes in extreme rainfall IDF relationship

3.4.1 Data used

Two rainfall datasets were used in this study. 50 years long (commonly used length of time-series) daily precipitation records of 1967-2016 were used for establishing IDF relationship of the historical extreme rainfall. Future daily rainfall data which have been spatially downscaled from the outputs of HadCM3 and CanESM2 in section 3.4.3 were used for establishing IDF relationship of the future period. In this regard, an average of the daily rainfall data projected under the scenarios of CanESM2 (RCP2.6, RCP4.5 and RCP8.5) and HadCM3 (A2a and B2a) were considered. Future 50 years (2021-2070) spanned time-series were used to ensure the consistency of sample sizes between the base period and future period.

3.4.2 Derivation of sub-daily precipitation and annual maximum series

Precipitation data of both the present and future periods were limited to a daily time resolution. In order to extract annual maximum precipitation at sub-daily resolution, the daily rainfall depths were disaggregated into hourly values using a Hyetos computer program. It is an easy temporal downscaling software, and freely available at http://www.itia.ntua.gr/e/softinfo/3/. Hyetos has been used in a number of studies in different regions of the world (Beyene et al., 2019; Engida and Esteves, 2011; Kossieris and Efstratiadis, 2015; Shrestha et al., 2017). Hyetos uses the Bartlett– Lewis model (BLM) and the adjustment procedures for the disaggregation process. The description of the model and the meaning of its parameters can be found in Sun et al. (2019) and is not repeated here.

In response to the existing limited hourly rainfall records to be used for the disaggregation model calibration, validated BLM parameter values (Table 3.6) for the

Addis Ababa station were adopted from (Beyene et al., 2019). It is the nearest station to the study area, among the stations with validated values available within the Awash basin. Using hourly data, thus obtained, rainfall depths for larger time-windows (3-hr, 6-hr and 12-hr) was generated. Finally, the sets of annual maximum (AMAX) corresponding to five storm durations (1-hr, 3-hr, 6-hr, 12-hr and 24-hr) for the analysis periods, 1967-2016 and 2021-2070, were extracted.

Table 3. 6 Values of BLM parameters used in disaggregation process, adopted from (Beyene et al., 2019)

Parameter	α	κ	$\emptyset$	$\lambda\,(d^{-1})$	$\mu_x\,(mm\,d^{-1})$	$v\,(d)$
Values	97.99	65.87	25	2.25	95.94	0.92839

Using the AMAX datasets, descriptive statistical analysis was conducted on the basis of skewness. The skewness index describes the shape of the distribution. It takes the value zero for a symmetrical distribution. However, a skewness of exactly zero is quite unlikely to real-world data. In this study, the skewness values between -2 and +2 were considered for normal distribution (Muzaffar, 2016). Values less than -2 and greater than +2 indicate negatively skewed and positively skewed distribution, respectively. This helped to provide an overview of the data series used in the study.

3.4.3 Developing IDF relationship

The modeling of the rainfall IDF relationships involves a series of steps that can be categorized as determining probable maximum rainfall; estimating rainfall intensity; determining the fitting model parameters; and assessing the model performance of the

fitting model (validation). In addition, correlation between return periods and model fitting parameters was assessed.

Estimation of probable maximum precipitation (PMP): It is the extreme rainfall depth for a defined period, which is meteorologically possible for a given watershed at a given time of year, without taking into account long-term climate trends. PMP is usually determined by fitting annual maximum rainfall series to a suitable theoretical probability distribution. Gumbel's extreme value distribution type I (EVI) was employed to fit each set of annual maximum rainfall series corresponding to five time-windows (1-hr, 3-hr, 6-hr, 12-hr, and 24-hr) for five periods (5-yr, 10-yr, 25-yr, 50-yr and 100-yr). EVI is the agreed probability distribution for meteorological and hydrological studies (Bhagat, 2017; Bharali, 2015; Coronado-Hernández et al., 2020; de Paola et al., 2014; Gebremedhin, 2017; Gebru, 2020; Tesfay and Quraishi, 2017). In this case, for respective storm duration and recurrence interval, PMP was computed using Equation 3.10.

$$PMP_{T_d} = \bar{X}_d + K_T S_d \qquad (3.10)$$

Where: $\bar{X}_d$ and S_d are the mean and the standard deviation of each set of annual maximum precipitation series (function of storm duration), respectively, and K_T is a frequency factor depending on the return period (T), and calculated using Equation 3.11 (Mujere, 2011).

$$K_T = -\frac{\sqrt{6}}{\pi}\left[0.5772 + \ln\left(\ln\left(\frac{T}{T-1}\right)\right)\right] \qquad (3.11)$$

Estimation of intensity: Using the values of PMP, the rainfall intensity was determined as the average precipitation depth that falls per time increment, and measured in

millimeter per hour (de Paola et al., 2014; Tesfay and Quraishi, 2017). Accordingly, the rainfall intensity was computed by dividing probable maximum precipitation for the corresponding storm duration (Equation 3.12). This helped to identify the relationships of the features of extreme rainfall (intensity, duration and return period). The relations were checked for self-similarity (Erena et al., 2018); i.e., they are assumed to have a consistent pattern for each return period.

$$I_d = \frac{PMP_{T_d}}{d} \tag{3. 12}$$

Where: PMP_{T_d} probable maximum precipitation (mm) corresponding to a T-year event for the *d*-rainfall duration, and *d* is storm duration (hour).

Deriving IDF model equations: the empirical equations (mathematical models) used to describe the IDF relationships were derived using bi-parameter power-regression model. For each return period, a functional relationship between the corresponding extreme rainfall intensity and the storm duration can be expressed as Equation 3.13 (de Paola et al., 2014). In this case, values of fitting parameters (i.e., $a(T)$ and b) are regressed for each return period, and they were calculated by Equations 3.14 and 3.15.

$$I(d,T) = a(T)d^b \tag{3. 13}$$

$$b = \frac{n\sum_{i=1}^{n}(ln\, x_i\, ln\, y_i) - \sum_{i=1}^{n}(ln\, x_i)\sum_{i=1}^{n}(ln\, y_i)}{n\sum_{i=1}^{n}(ln\, x_i)^2 - \left(\sum_{i=1}^{n} ln\, x_i\right)^2} \tag{3. 14}$$

$$a(T) = e^{\left(\frac{\sum_{i=1}^{n}(ln\, y_i) - b\sum_{i=1}^{n}(ln\, x_i)}{n}\right)} \tag{3. 15}$$

Where: *a(T)* and *b* are the regression parameters, *n* is the number of number of storm durations (time-windows) considered, x_i and y_i are storm durations (hour) and corresponding intensity (mm/hr.), respectively.

Model validation: the model of IDF relationship was validated using graphical and statistical method. First, the self-similarity of n values was checked for each return period; i.e., uniform pattern is expected (Erena and Worku, 2018). Second, the goodness-of-fit of the mathematical models was assessed using two statistical parameters: coefficient of determination (R^2) and Nash-Sutcliffe efficiency (NSE), which were determined using Equations 3.16 and 3.17, respectively. The value of R^2 ranges -1 to 1 and that of NSE can vary from -∞ to 1. The optimum value of the two chosen parameters is 1, indicating the perfect fit of the derived model to the data (Lacombe et al., 2014; Waseem et al., 2017). In this study, the minimum criteria recommended by (Moriasi et al., 2007) for both parameters (NSE > 0.5 and R^2 > 0.7) were adopted. The model is considered valid only if it satisfies these criteria at a time.

$$R^2 = \left[\frac{\sum_{i=1}^{n}(x_{O_i}-\bar{x}_O)(x_{P_i}-\bar{x}_P)}{\sqrt{\sum_{i=1}^{n}(x_{O_i}-\bar{x}_O)^2}\sqrt{\sum_{i=1}^{n}(x_{P_i}-\bar{x}_P)^2}}\right]^2 \quad (3.16)$$

$$NSE = 1 - \frac{\sum_{i=1}^{n}\left(x_{O_i}-x_{P_i}\right)^2}{\sum_{i=1}^{n}\left(x_{O_i}-\bar{x}_O\right)^2} \quad (3.17)$$

Where: x_O and x_P are observed (used for calibration) and simulated (computed using IDF equations) rainfall intensities, respectively; and $\bar{x}_O$ and $\bar{x}_P$ are the corresponding mean values

Correlation analysis: It was carried to assess the extent to which the power-law fitting parameters are linear related to the return period. It was determined based on value of

Pearson's correlation coefficient (r) computed using return periods and the values of both parameters in the validated IDF models. Moreover, the statistical significance of the relationships was assessed based on p-value statistics at 95% confidence level ($p < 0.05$).

3.4.4 Analysis of changes in precipitation intensity

The potential changes in extreme precipitation intensity were assessed in two ways. First, the changes in intensity were assessed using graphical comparison by overlaying the IDF curves of historical and future periods. Second, the magnitude of changes was determined in terms of relative percentage difference between the intensity of corresponding storm durations and return periods. For this reason, the extreme precipitation intensity for a range of storm durations and return periods were calculated using the IDF models developed in this study. The percentage of relative differences were then determined using Equation 3.18, a widely used approach in most climate change studies (Gebru, 2020; Solaiman and Simonovic, 2011; Tesfay and Quraishi, 2017).

$$Relative\ difference\ (\%) = \frac{x_F - x_H}{\frac{1}{2}(x_F + x_H)} * 100 \qquad (3.18)$$

Where: x_F and x_H are extreme rainfall intensities computed based on the future and the historical IDF relationships, respectively.

3.5 Assessment of flood hazard

Assessment of urban flood hazard and its changes under evolving land use and climate conditions requires developing flood inundation model and simulation of inundation for a range of return periods under existing and future land use and climate scenarios. In addition, it demands flood hazard determination and categorizing into different levels. The general workflow to assess the urban flood hazard assessment is depicted in Figure 3.9.

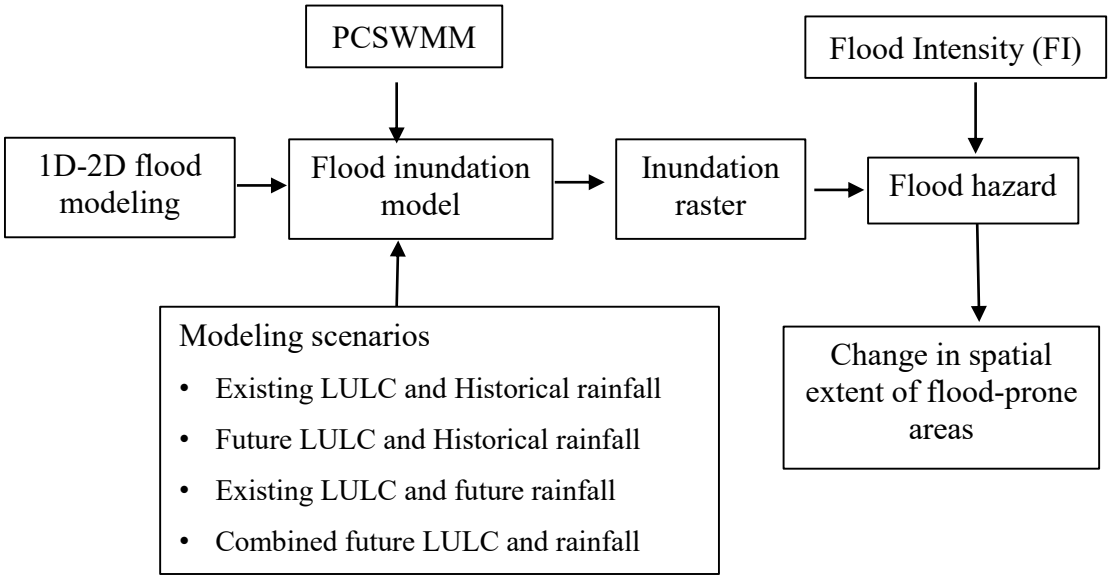

Figure 3.9 Methodological workflow of flood hazard assessment

3.5.1 Modeling flood inundation

3.5.1.1 Model description

Choosing the most proper modelling method demands balancing between accuracy, time and data availability, and also taking into account the important process of the phenomena under study (van Dijk et al., 2014). The study used 1D-2D flood modelling

approach, in which the stormwater drainage (1D) model and the overland flow (2D) model are coupled. The flow between the two systems is bi-directionally (i.e., surcharging and spilling) and takes place through coupling links such as junctions and 2D grid cells (Leandro et al., 2009; Jahanbazi and Egger, 2014; Hénonin et al., 2015). In other words, the overflowed water at the nodes is directly drained into the surface network, surcharging the surface flow. Allows representing important urban flood processes that can be represented by dual drainage concept. The details of coupled modelling approach can be found in comprehensive review conducted by Bulti and Abebe (2020).

The modelling task was realized using PCSWMM Professional 2D software package obtained from CHI water company. It integrates SWMM (1D) and 2D PCSWMM for overland flow condition. SWMM is a one-dimensional dynamic rainfall–runoff simulation model used for a single event or long-term (continuous) simulation of runoff quantity and quality from primarily urban areas (Rossman, 2015). It computes the flow and depth of flow in flow channels. Surface runoff is generated by considering individual subcatchments as a non-linear reservoir with a single inflow produced from rainfall (Jorge et al., 2010; Shen and Zhang, 2014), and regarded to completely enter the junction related to the subcatchment and to be transported through the urban drainage channels to the outlet. Overland flow from overflowing junctions is exchanged through 2D nodes at the center of each 2D cell.

SCS curve number method was chosen for estimating infiltration in computation of surface runoff of the sub-catchments. It has been tested to produce satisfactory result in hydrologic modeling in urban areas and it is useful for ungauged watershed (Pandey, 2017; Chen et al., 2017). Evaporation is considered as nil because flooding happens in

rainy season and temperature is very less (Rangari et al., 2018). The model was simulated using design storms with different frequency and under climate conditions (historical and future climate conditions). This helped to identify flood inundation information such as location, extent, flow depth and flow velocity, from which flood hazard maps were prepared.

3.5.1.2 Data sources and preprocessing

The input data required for 1D-2D modeling in this study were collected from different sources. Stormwater drainage channels and land-use were acquired from Adama City Administration; digital elevation model (DEM) was downloaded from USGS website (https://espa.cr.usgs.gov/). Field survey was conducted for establishing the stormwater drainage network and for collecting the junctions and outfall information. The processing task involves (1) representation of the minor drainage (2) delineation of subcatchments (3) determination of the model parameters and (4) rainfall hyetograph generation. Each of these are discussed below.

The stormwater drainage network consists of conduits (channels), junctions and outfalls. Municipal drainage channels were populated with channel properties such as shape, cross-sectional dimensions and construction materials. Field survey was conducted to verify this information and to establish networking (interconnection) of the channels and to collect junctions and outfall nodes. Natural drainages (Figure 3.5) with average width greater than 5m passing through the study area were not considered in the modeling process, instead they were used as receivers of the waters from minor drainage system through outfall nodes. In addition, some outfall nodes were used to discharge the flow on other subcatchments within or out of the study watershed.

Physical based rainfall-runoff models, usually operate on sub-catchments in which generation of runoff takes place. Sub-catchments are hydrologic units of land, whose topographic and drainage system elements direct surface runoff to a single discharge point. The processes of urban surface runoff, such as infiltration, depression storage and overland flow take place in the sub-catchments. Hence, the accuracy of sub-catchments delineation has a great importance of modeling urban rainfall-runoff. DEM helps to understand the terrain elevation, which reflects the surface flow direction and can provide reasonable sub-catchments of a natural basin (Dongquan et al., 2009). In urban settings, the actual watershed likely deviate from the natural watershed. The building block arrangement is not necessarily follow the natural basin and urban stormwater drainage network could transport the water in an opposite direction to the surface gradient. Hence, catchment delineation in urban settings based on only DEM may not provide satisfactory result. In this study, subcatchment discretization was conducted with the help of the DEM, building blocks, stormwater drainage system and field survey. It began with generating the natural basins, from DEM using automatic watershed delineation (AWD) tool of PCSWMM. In this case, gorges (natural channels) were digitized and incorporated using burnt-in function of PCSWMM. This helped to guide the tool to consider in delineation of the subcatchments. The resulted subcatchments were then modified based on a stormwater drainage system with the help of orthophoto and field survey to fit the actual watershed of built-up area. Finally, the study watershed was discretized into 1299 subcatchments (Figure 3.10).

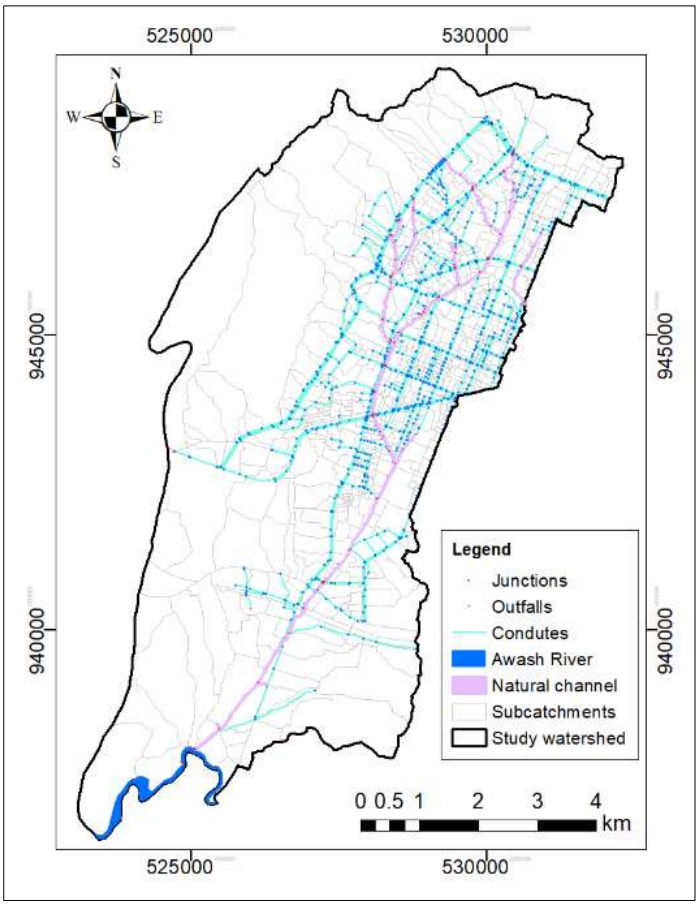

Figure 3.10 Subcatchments and drainage network in Awash sub-watershed

Urban stormwater drainages are designed for shorter durations (sub daily) and more frequent storms (2-yr, 5-yr). However, climate change-induced longer and less frequent (100-yr) storms are likely. Hence, modeling for longer and less frequent storms can provide important information for hazard assessment and planning for sustainable flood risk management. In this study, 24-hr storms design storm and five return periods: 5-yr, 10-yr, 25-yr, 50-yr and 100-yr were considered for both the historical and future projected climate conditions. A design storm is a hypothetical storm with specific duration and return period. It is usually extracted from depth-duration-frequency (DDF) or intensity-duration-frequency (IDF) relationships. The IDF models established for the Adama City (section 3.5.3) were used to determine the depth of the selected design storm (24-hr) for each scenario (Table 3.7). The rainfall hyetographs (Figure 3.11) were

generated for each scenario based on SCS-storm distribution overtime in PCSWMM. It represents a rainfall with corresponding return period and a storm duration. The model was simulated using the distributed rainfall data.

Table 3. 7 24-hr design storms (mm) for different frequencies for the historical (1967-2016) and future projection by CanESM2 (2021-2070)

Return period	5-yr	10-yr	25-yr	50-yr	100-yr
Historical climate scenario	71.4	81.8	95	104.7	114.4
Future climate scenario	62.5	89.6	124	149.5	174.9

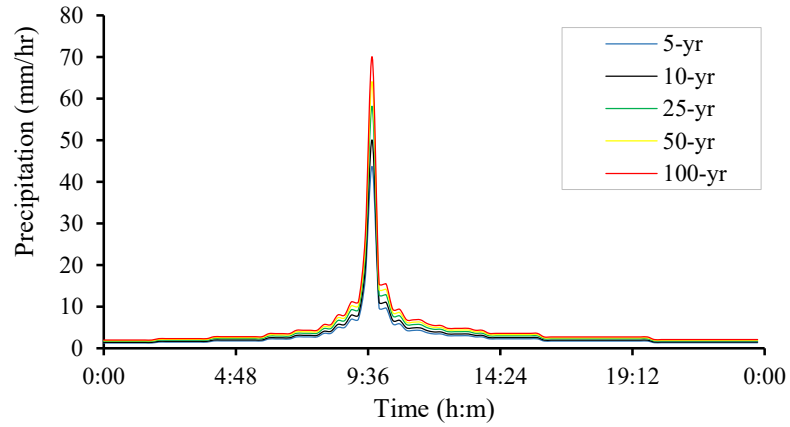

a) Historical climate scenario

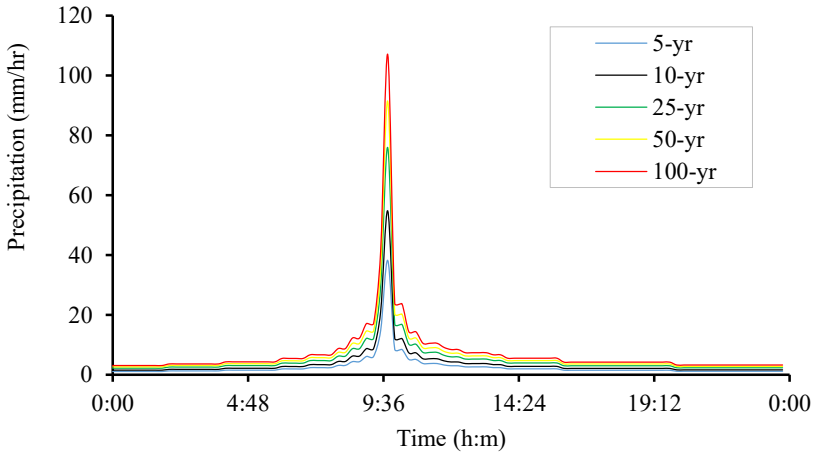

b) Future climate scenario

Figure 3.11 Rainfall hyetographs generated for 24-hr design storm for historical and future climate scenarios

Principal parameters used in the modeling process includes slope, flow width, imperviousness, curve number, manning's roughness. The slope of the subcatchments was computed by averaging the slope of each DEM pixel within the respective subcatchment. Curve number (CN) was adopted from Bulti and Abebe (2020). The characteristics width was computed on the basis of compactness factor. For subcatchments with compactness factor (Equation 3.19) greater than 1.138, the characteristics width of overland flow can be computed using Equation 3.20 (Ghazavi et al., 2016). Minimum compactness factor for subcatchments was found to be 1.131, and hence, Equation 3.20 was adopted for overland flow width computation.

$$C = 0.282 \frac{P}{\sqrt{A}} \tag{3.19}$$

$$W = \frac{C\sqrt{A}}{1.128}\left(1 - \sqrt{1 - \left(\frac{1.128}{C}\right)^2}\right) \tag{3.20}$$

Where: C= Compactness factor

A = area of the sub-catchments

P= perimeters of the sub-catchments

The imperviousness of the urbanized land is closely related to the land use land cover type (Chabaeva et al., 2009). In this study, using sub-catchment layer, land-use information was extracted from map of existing land-use prepared for the City by Adama City structural plan revision project in 2019. Future LULC condition was also adopted from land use plan of the City revised in 2019 (SP 2019). This helped to keep the consistency of data used in flood modeling. Both land use conditions are depicted in Figure 3.12.

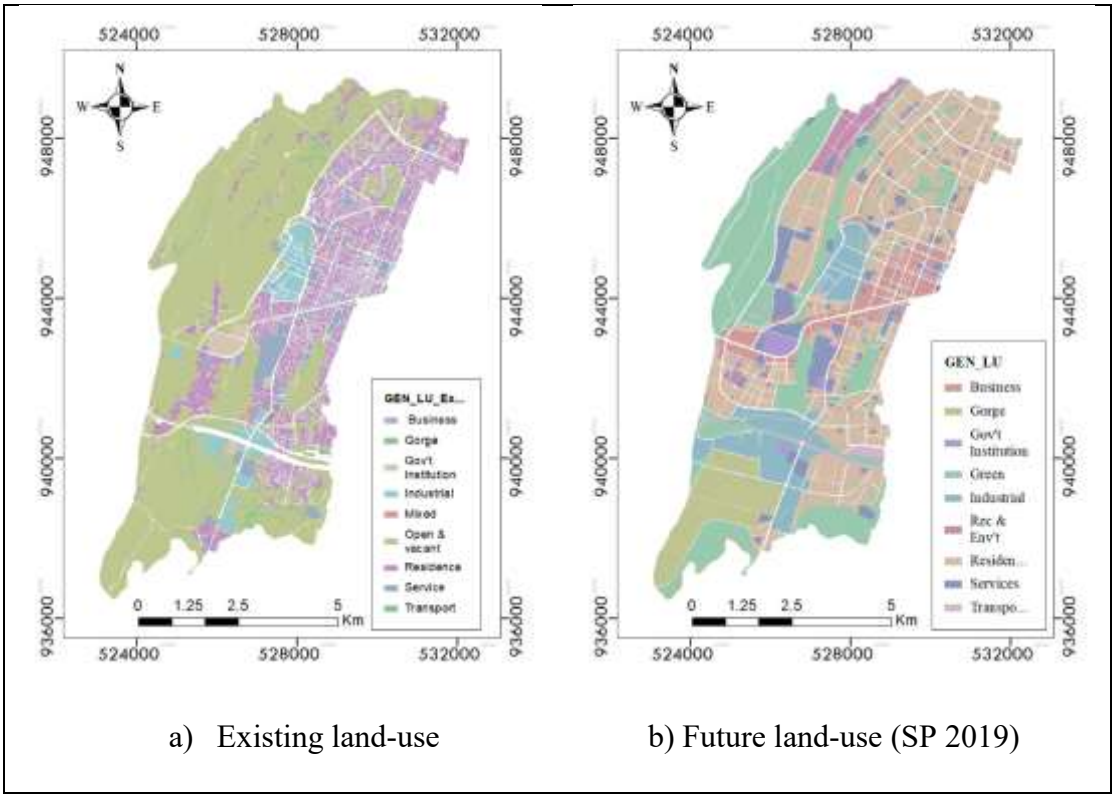

a) Existing land-use b) Future land-use (SP 2019)

Figure 3.12 Land use map of Awash sub-watershed a) existing b) structural plan proposal 2019 for future period

Imperviousness percent for each land-use were adopted from SWMM manual. Imperviousness of sub-catchments encompassing multiple types of land use were computed based on surface area weight (Equation 3.21).

$$\%Imp = \frac{\sum_{i=1}^{n} a_i I_i}{A} * 100 \qquad (3.21)$$

Where: a_i = surface area of land-use within the subcatchment

I_i = imperviousness of identified land use within the subcatchment

A = area of the subcatchment

Depth of the nodes were collected through field survey. Invert elevation was computed from surface elevation and junction depth. Elevation data were extracted from Google earth using GPS visualizer software. The accuracy of Google earth

elevation data is acceptable for different applications, such as roadway survey in transportation application (Rusli and Majid, 2012; Sharma and Gupta, 2014; Wang et al., 2017; Wei et al., 2018; Hu et al., 2020). Invert elevation values were obtained by subtracting the depth from surface elevation.

The channel roughness (manning's n) for respective types of construction material is adopted from literature (Rossman, 2015; Vojtek and Vojteková, 2016). Specifically, 0.013, 0.025 and 0.035 were used for channels made of concrete, masonry and earthen, respectively. In addition, 0.02 and 0.035 were used for impervious and pervious areas, respectively.

3.5.1.3 Model validation

Validation was conducted to establish the proof that offers reasonable information that the model result is satisfactory to represent the ground truths to the acceptable level. For this, the maximum depth of storm (i.e., 56mm) during 2016 was selected from precipitation records. However, urban flood modelling is challenging to validate, especially in developing countries where there is limited recorded data corresponding to the past flood events (Chen et al., 2009; Rosenzweig et al., 2018). Likewise, measurements, aerial photographs, or satellite data from past floods for validation were not available for the study area.

Hence, coordinates of 30 ground points in frequently flooded areas were collected using handheld GPS. The maximum water depths of the 2016 flood events at the collected points were estimated by interviewing residents. In this case, the information could be biased due to memory of affected community, yet it is the only available information. Such method has been used in several studies where the validation

information is limited (e.g., Vojtek and Vojteková, 2016; Re et al., 2019; Erena et al., 2018). The water depths of simulation result were extracted by intersecting the ground points layer with flood inundation layer. Finally, paired t-test was employed to test the water depth of the simulated inundation against field survey data at collected points to verify the reliability of the flood inundation model results. The significance of the test result was assessed at 95% ($\alpha = 0.05$) level.

3.5.2 Determination of flood hazard

Using the validated model, flood inundation was simulated for a five return periods (5, 10, 25, 50 and 100-yr) for each scenario of LULC and climate combination, namely Existing LULC and Present-day climate (Scenario-I); future LULC and present-day climate (scenario-II); Existing LULC and future climate (scenario-III) and combined future LULC and climate (scenario-IV). This helped to prepare inundation raster map of the corresponding scenarios.

Flood hazard was assessed using the output of 1D-2D modeling (inundation information). It is a potentially damaging flood that may cause the loss of life or injury, property damage, social and economic disruption or environmental degradation. The hazard level is assessed based on flood intensity (FI). In most cases, the direct relationship of inundation depth and the intensity of the hazard is considered (Dinh et al., 2012). However, the velocity of flood water adds considerable pressure to the static water pressure, causing additional harm.

In this study, FI was determined as a function of maximum water depth (d) and flow velocity (v) and expressed as Equation 3.22 (Vojtek and Vojteková, 2016). The magnitude of FI was used for describing the degree of the flood hazard. The assumption

here is that the greater the FI indicates the greater the level of the flood hazard. Depending on the characteristics of the study area, the flood hazard was categorized into three: Low ($0 < FI \leq 0.2$), Medium ($0.2 < FI \leq 0.5$) and High ($FI > 0.5$).

$$FI = \begin{cases} d, & d > 0m, v \leq 1m/s \\ d * v, & d > 0m, v > 1m/s \end{cases} \quad (3.22)$$

3.5.3 Analysis of changes in flood hazard

The change in flood hazard was assessed relative to the baseline. In this case. existing LULC and historical climate (scenario I) was considered as a baseline condition. The change in flood hazard was assessed in terms of percentage difference using Equation 3.23.

$$\%\Delta = \frac{A_{\text{i}} - A_{\text{baseline}}}{A_{\text{baseline}}} * 100 \quad (3.23)$$

3.6 Assessment of urban flood resilience

This study aims to measure urban flood resilience in view of mitigation aspect of flood hazard management. Resilience is usually inferred via "surrogates", as it cannot be measured directly. In this study, flood resilience of the study area was assessed based on the theory of urban flood resilience (Liao, 2012). The floodability of the area was used to indicate flood tolerance and a surrogate for flood resilience.

In this regard, the overall floodability of the study area is represented by urban floodability index (UFI), which indicates the portion of its floodable lands to its flood prone area (Equation 3.24). If everything else is equal, the more floodable areas the

higher the floodability. The value of UFI is 1 indicates the City is fully floodable and the value 0 means the City is entirely non-floodable.

Determining the UFI for an urban area involves identification of floodable sites and delineation of the flood-prone area. Floodable land refers to a land that can store or convey floodwater and sediments without causing harm locally or elsewhere, as well as without interrupting socioeconomic activities (Liao, 2012). It can be any type of land use and cover; e.g., open spaces, urban parks, urban green areas, sport fields, building raised on poles etc. Such areas can help to decrease the overall flood effect by reducing stormwater runoff and/or delaying its flow to the stormwater system (Nardini and Miguez 2016; Brunetta and Salata, 2019; Apud et al., 2020). They have been utilized to introduce "planned flooding," which is part of the adaptation repertoire in urban areas. Consequently, flooding that is planned is gaining traction as a supplement or replacement for traditional "hard" flood-prevention techniques (Wamsler and Brink, 2014).

The floodable lands were extracted from existing and proposed land-use maps of the City. Spatial extents of floodable lands identified from the respective land-use condition were determined. By computing the area of flood-prone sites from flood hazard maps prepared in this study, UFI was computed using Equation 3.24, for different scenarios and a range of return periods. This helped to assess the flood resilience level of the study area. Figure 3.13 also illustrates the workflow used to determine the flood resilience kevel of the City.

$$UFI = \frac{Area\ of\ floodable\ lands}{Area\ of\ flood\ prone\ sites} \quad (3.24)$$

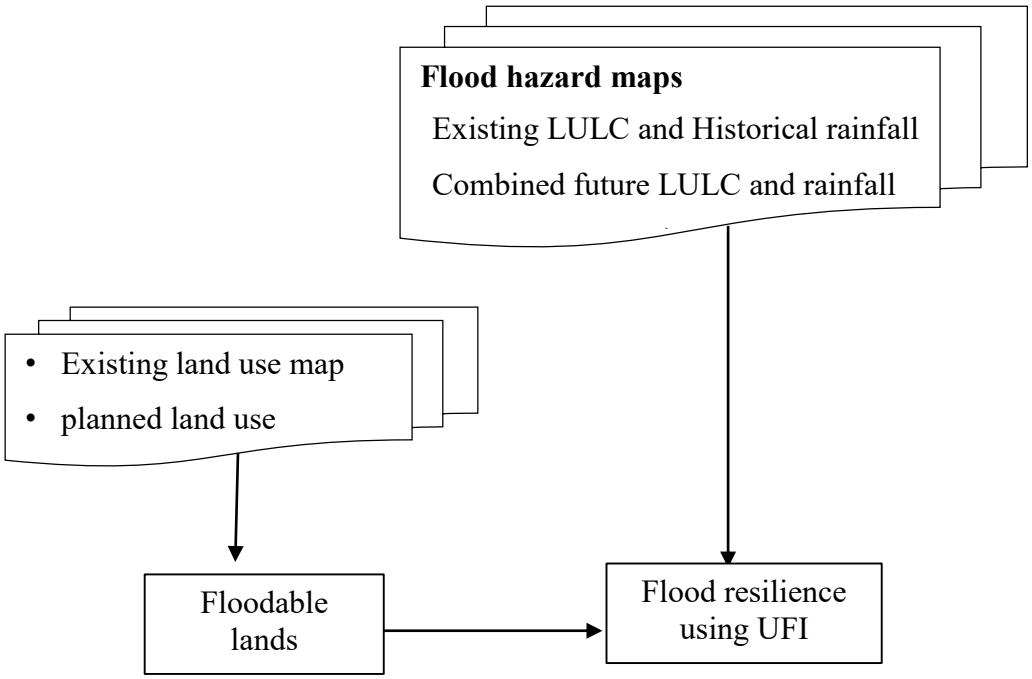

Figure 3.13 Methodological workflow of urban flood resilience assessment

3.7 Resilience-based flood hazard management planning

Planning for resilience-based flood hazard management in this study focuses on enhancing localized flood-response capacity by using the flood adaptation paradigm. It involves selection of candidate planning area; collection of spatial and nonspatial data; identifying potential localized-flood adaption measures, and analyzing their suitability to the existing and proposed future development.

Planning area was selected based on the flood hazard area defined for 100-yr return period under the combined impacts of future climate and LULC scenario. This aids in the development of long-term flood adaptation strategies. Consideration was also given

for prone-areas in the inner-city, with different flood hazard levels (i.e., high, moderate and low). Moreover, the past flood experience was considered in the selection of the candidate planning area, as it supports to identify existing local adaption approaches.

Data used in planning were collected from different sources. The building footprints were digitized from digital orthophoto with field verification. Finished ground floor level of the buildings above the surrounding ground, construction materials used for foundation and wall, present land-use, as well as existing local food adaption measures specific to the area were collected through field survey. Proposed land-uses of the area for the future period were extracted from SP 2019, through spatial overlay analysis in GIS environment. Similarly, the slope and soil type of the planning area were extracted from the corresponding maps of the City. Flood characteristics were extracted from flood inundation map of the selected flood scenario developed in this study.

Localized flood adaption strategies were identified from literatures. The feasibility of each strategy to the planning area was assessed taking the features of existing development, future land-use proposal and flood of considered scenario into account. In this case, considerations were given for the contributions of the measures to enhance localized flood-response capacity.

CHAPTER 4: RESULTS AND DISCUSSION

4.1 Results of impacts of urbanizations

4.1.1 Dynamics of land use/land cover

Figure 4.1a – f demonstrates the LULC maps of Adama City for 1995, 2000, 2005, 2010, 2015 and 2019. Overall classification accuracies are 89%, 91%, 93%, 91%, 92% and 90% for the year 1995, 2000, 2005, 2010, 2015 and 2019, respectively.

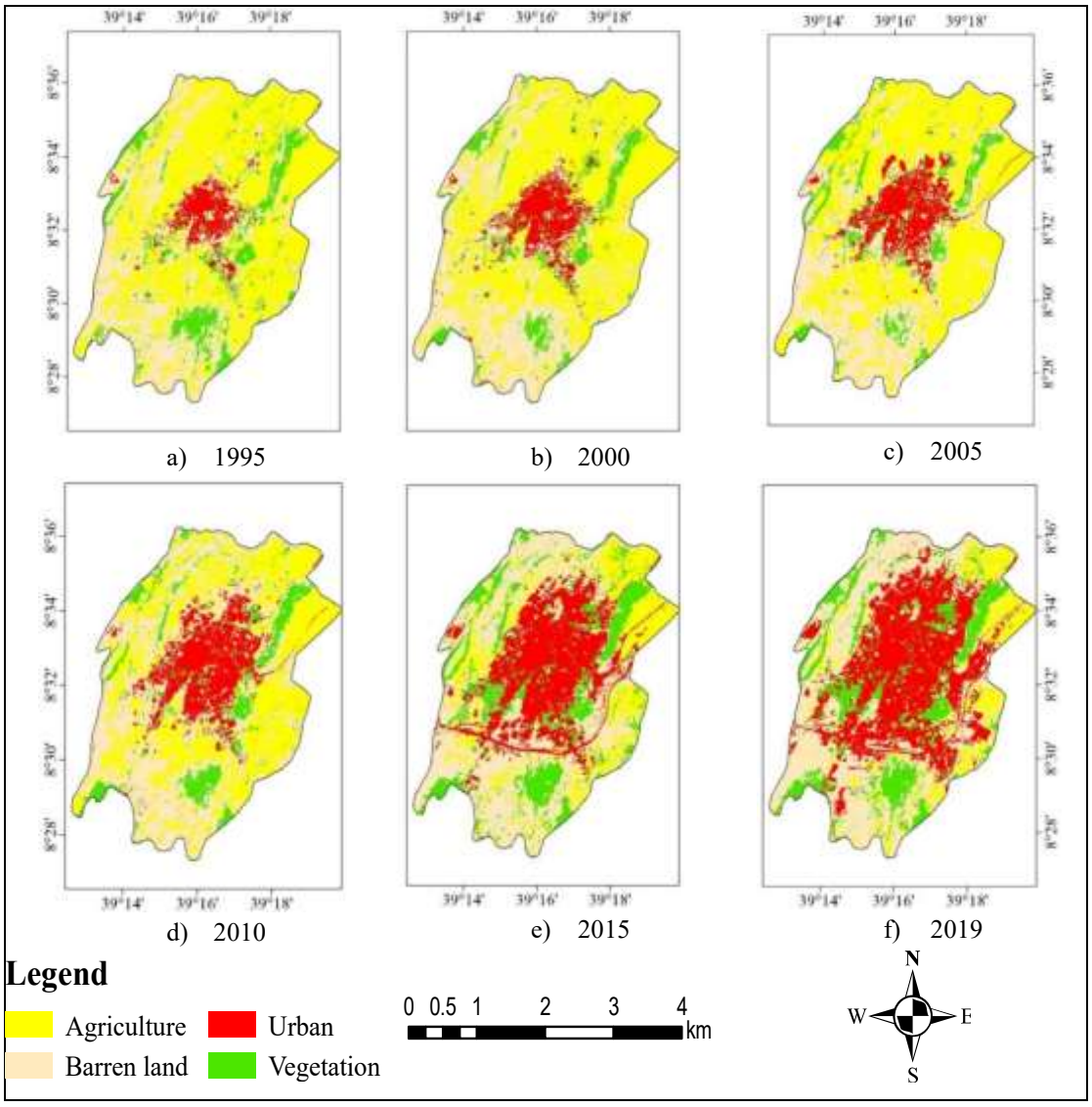

Figure 4.1 Land use/land cover maps of the study area from 1995 to 2019

The values of Kappa statistics for classified images are greater than 0.8, indicating strong agreement between the classified LULC classes and the reference data, hence the maps satisfied accuracy criteria for LULC change detection analysis.

The information summarized in Table 4.1 shows the spatial extents, percentage changes over time as well as the annual average growth of the four LULC classes (agriculture, barren land, urban and vegetation) in Adama City between 1995 and 2019. Besides Figure 4.2 demonstrates the spatio-temporal variations of the proportions of each class occurred over the span of 24 years.

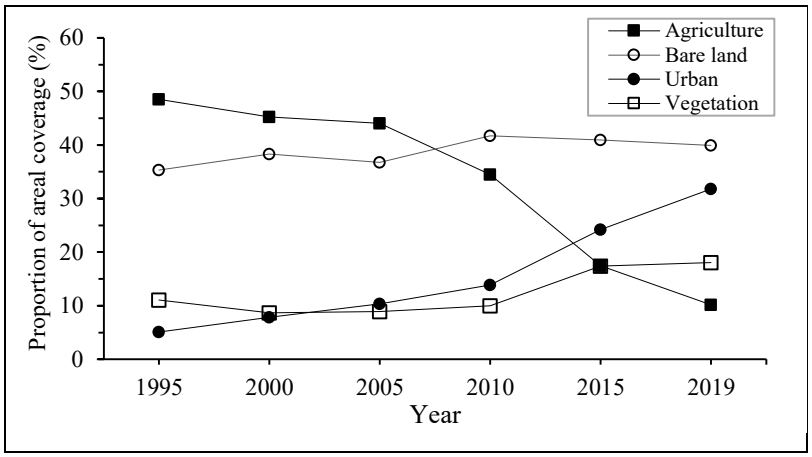

Figure 4.2 The proportions of land use/land cover classes in the study area from 1995 to 2019

Table 4. 1 Areal extents and percentage change over time of land use/land cover classes in Adama City from 1995 to 2019

LULC class	Spatial coverage												Percentage change (Δ_{LULC})					Annual average change (%) 1995-2019
	1995		2000		2005		2010		2015		2019		1995-2000	2000-2005	2005-2010	2010-2015	2015-2019	
	ha	%	ha	%	ha	%	ha	%	ha	%	ha	%						
Agriculture	6482.7	48	6044	45	5886.7	44	4608.4	34	2333.5	17	1362.8	10	-6.8	-2.6	-21.7	-49.4	-41.6	-3.3
Barren land	4724.6	35	5117.8	38	4910.6	37	5572.7	42	5475.4	41	5337.3	40	8.3	-4	13.5	-1.7	-2.5	0.5
Urban	683.3	5	1047.7	8	1381.7	10	1850.7	14	3236.1	24	4251	32	53.3	31.9	33.9	74.9	31.4	21.8
Vegetation	1475.9	11	1156.9	9	1187.5	9	1334.7	10	2321.5	17	2415.4	18	-21.6	2.6	12.4	73.9	4	2.7
Total	**13366.5**																	

Overall, the results show the extensive LULC changes in Adama City over the study period. It can be seen from Figure 4.2 and Table 4.1 that agricultural land was the dominant land use at the beginning of the study period, but declined with the continuous increase of urban land area. The rate of annual urban expansion greater by far, from the rest land use classes.

The coverage of agricultural land was slightly less than 50 % of the total area at the beginning of the study timeframe. In the following 10 years, it moderately decreased to about 44 % before it dramatically dropped to nearly 10 % in the final year. By contrast, the proportion of urban class was 5 % in 1995, this figure rose to just over 30 % in 2019, showing an increase of more than five folds of its initial spatial share. It showed 21.8 % of average annual expansion across the study period. In temporal scale, the rate of urban land expansion was comparatively low in the first fifteen years between 1995 (5.1%) and 2010 (13.8%), which showed nearly 8% increase, then it peaked 31.8 % of the total area in the last year (2019).

On the other hand, vegetation class showed a remarkable increase in spatial cover between 2010-2015 has also contributed to the increase of its share of the study area from 11 % to 18 % in the first and last years of the study period, respectively. With nearly equal proportion, the areal share of the barren land increased during the study timeframe.

4.1.2 Spatio-temporal changes of runoff depth

The computed weighted curve number for average antecedent moisture condition is summarized in Table 4.2. By converting these values to wet moisture condition, the runoff depth of each watershed at different times was computed. The results

summarized in Table 4.3 and depicted in Figure 4.3 demonstrate that the daily accumulated runoff depth in the City and its sub-watersheds from 1995 to 2019, with a more detailed look at the trend of change in runoff depth.

Table 4.2 Summary of the result of weighted curve number for average antecedent condition

Spatial boundary \ Year	1995	2000	2005	2010	2015	2019
Awash watershed	79.7	81.1	80.1	82.5	82.5	83.4
City boundary	77.4	79.0	79.2	80.6	81.0	82.3
Mermersa watershed	74.6	76.5	78.1	78.3	79.3	80.9

Table 4.3 Daily accumulated runoff depth in the City and its watersheds from 1995 to 2019 (units are in millimeter)

Spatial boundary	1995	2000	2005	2010	2015	2019	Change of runoff depth (1995-2019)	
							mm	%
Awash watershed	72.9	74.8	73.4	76.7	76.6	77.9	5.0	+6.9
Mermersa watershed	66.0	68.5	70.8	71.1	72.4	74.5	8.5	+12.9
City boundary	69.8	72.0	72.2	74.2	74.7	76.4	6.6	+9.5

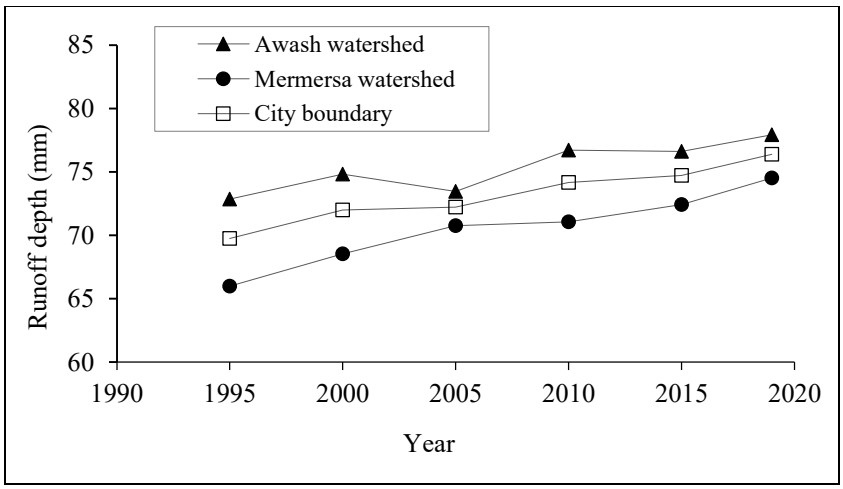

Figure 4.3 Daily runoff depth in Adama City and its sub-watersheds from 1995 to 2019

Overall, the results indicate the continued increase in runoff depth for the three analysis boundaries during the last 24-year. This rising trend is occurring across all the selected years for the analysis. In all the cases, the accumulated daily runoff depth of the Awash watershed is greater. In addition, during study timeframe, the runoff depth is increased in all areas, except for the Awash watershed that slightly decreased in 2005.

The maximum increased runoff depth is related to Mermersa sub-watershed with 12.9 %, whereas the Awash sub-watershed showed 6.9 % change. The runoff depth in Awash watershed starts at about 72.9 mm and steadily increased to 74.8 mm before it fell to 73.4 mm in 2005. Then it goes up to reach 77.9 mm at the final year. At City scale, the runoff depth starts at slightly less 70 mm in 1995, this figure is increased to reach over 76 mm in the final year, indicating about 9.5% increase in the span of 24-years.

4.1.3 Relation between the changes of PIA and runoff depth

In this study, the degree to which the temporal variations in runoff depth can be explained by the changes of PIA is examined through the regression analysis using the computed results (Table 4.4) of both variables. All percent changes at respective years are calculated with respect 1995. In all the cases, a dataset of 6 observations is used. The scatter plots overlaid with the best-fit line depicted in Figure 4.4 illustrates the relationship between the percentage changes of runoff depth and that of PIA from 1995 to 2019.

The results reveal that the observed percent change of runoff depth is directly related to the changes of PIA in both scales. Further, Pearson correlation coefficient appears a very strong correlation between the two variables. Moreover, the significance

test of the relationship between the two variables resulted in the p-value smaller than 0.05, suggests rejecting the null hypothesis. Based on this evidence it can be underlined that the observed linear relation between the percentage variation of runoff depth and the PIA is highly significant. Further, the value of the correlation coefficient is found to be 0.956, 0.826 and 0.958 for the City, Awash watershed and Mermersa watershed, respectively. From the estimated model equations, the slope of regression lines shows that the unit percentage change of PIA in the City boundary, Awash and Mermersa watersheds results the percent changes of runoff depth equal to 0.013, 0.009 and 0.018, respectively.

Table 4.4 Percentage change of PIA (Δ_{PIA}) and runoff depth in Adama City administration and its sub-watersheds from 2000 to 2019 with respect to the baseline year (1995)

	2000		**2005**		**2010**		**2015**		**2019**	
Spatial boundary	**Δ_{PIA}**	**Δ_{Q}**	**Δ_{PIA}**	**Δ_{Q}**	**Δ_{PIA}**	**Δ_{Q}**	**Δ_{PIA}**	**Δ_{Q}**	**Δ_{PIA}**	**Δ_{Q}**
City boundary	53.3	3.2	102.2	3.6	170.8	6.3	373.6	7.1	522.1	9.6
Awash sub-watershed	55.9	2.7	104.0	0.8	182.3	5.3	421.9	5.2	585.8	7.0
Mermersa sub-watershed	51.5	3.9	100.9	7.2	162.4	7.7	338.1	9.8	475.3	12.9

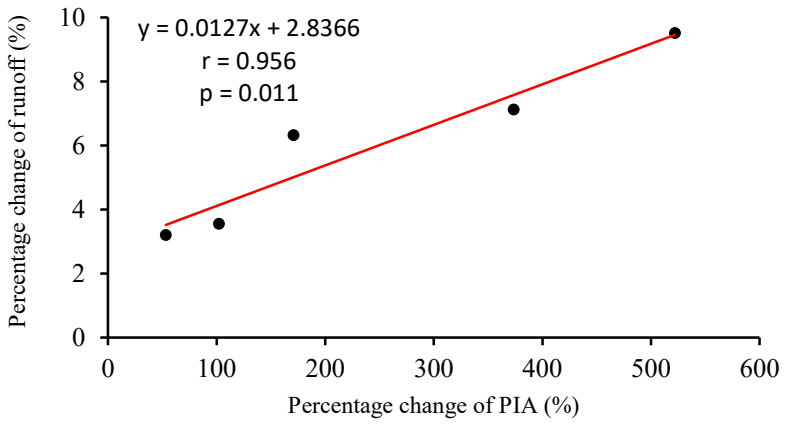

a) City boundary

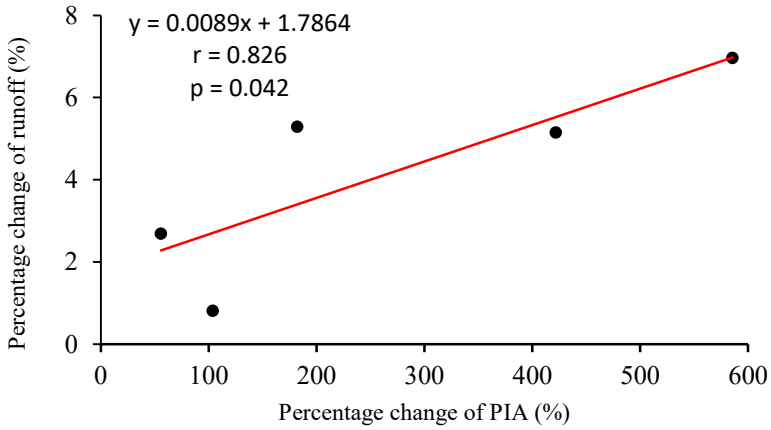

b) Awash watershed

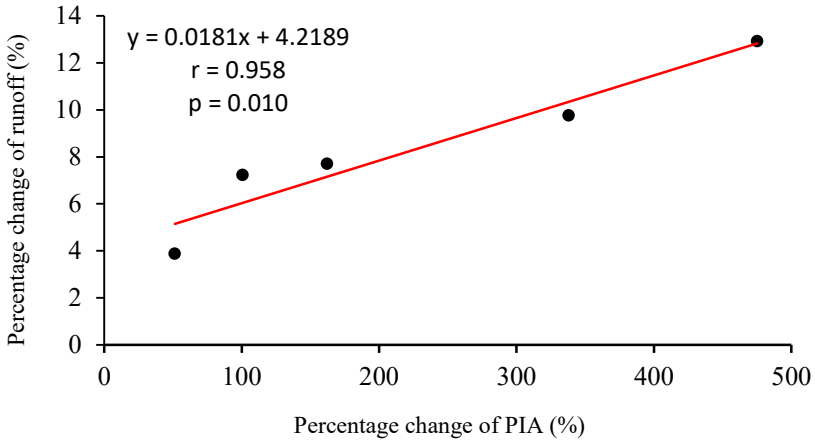

c) Mermersa watershed

Figure 4.4 Relationship between spatio-temporal changes of runoff depth and imperviousness in Adama City administration and its sub-watersheds from 1995 to 2019 with respect to the baseline year

4.1.4 Discussion

By taking the importance of short-term changes into account, LULC maps were prepared at the interval of 5 years using landsat images, and the spatio-temporal transformations of LULC were assessed. Surface runoff at respective years was computed using the SCS-CN method, and the impacts of LULC changes on hydrologic attributes of the City were examined. The relation between urbanization and change in the runoff was explored through regression analysis using the datasets of temporal changes of IAR and runoff depth.

The findings reveal extensive LULC changes during the study timeframe, particularly the extent of built-up land has expanded more than five times, indicating averagely the City undergone 21.8% urban expansion annually from 1995 to 2019. A built-up expansion rate of 7.9% during the study period, which is slightly less than the growth rate of the City's population reported by Built and Assefa (2019). On the other hand, the result is greater than the findings of Sinha et al. (2016). The disparity could be due to incorporation of transportation (gravel roads and railway) in urban classes in the case of the present study.

The LULC change occurred in the study area is due to interplay of demographic pressure, proximity factors (geographical location), and the landscape restrictions are the main drivers of LULC changes in the study area. The population growth is a key driver of the demographic element generating LULC change through the increasing needs for settlement. Recent studies have found that land cover conversion owing to demographic pressure is particularly severe in Ethiopia (Urgesa et al., 2016; Berihun et al., 2019; Anteneh et al. 2018; Degife et al. 2019; Assefa et al., 2021). Likewise, the

City has seen rapid population growth in the study period. This rise in population had a reasonable consequence of significant built-up expansion.

In the City management and analysis of LULC modifications, expansion direction is also required. Topographical and physical elements have a significant role in determining the direction of urban growth. The City has expanded towards North, North-West, South, and South-East but little more expansion towards the West, South-West and North-East because of ridges and towards the South-East due to Migra plain (wetland).

Horizontal growth of urban areas necessitates the conversion of adjacent rural areas to urban land use land cover, which has detrimental impact on other land uses such as agricultural land, green space, and forest areas (Mohan et al. 2011). Moreover, flat topography and low-lying zones are among the possible causes for LULC changes (Birhane et al., 2019). The results of the present study show that landscape restrictions such as steep slope and inaccessible high elevation areas played a vital role in maintaining and preserving vegetation covers. Agricultural land, on the other hand, has a flat to moderate slope and low-lying topography characterizes it from a topographic standpoint. These conditions have significantly contributed to the expansion of built-up area in northern and southern directions, at the expense of agricultural land throughout the study period.

The results also indicate that the observed alterations of LULC in the study area resulted in an increase in runoff depth in the City by 9.5 % over the study timeframe. This figure is less than the result of the study (Birhanu et al., 2016) reported for the impacts of LULC change in Addis Ababa City over the period of 10 years, and it is greater than that of Billi et al. (2015) noted in Dire Dawa town over 21 years. This

disparity could be underpinned by local conditions, which can be associated with socioeconomic, level of urbanization, level of spatial planning and environmental variability. At the watershed level, while an increase of 12.9 % in Mermersa, a 6.9 % increase in Awash is found. Along with other (e.g., Chen et al., 2015), the findings of this study indicate that the impacts of LULC changes on runoff can be influenced by spatial scale of the analysis. In addition, while urban land continuously increased across the study period, the runoff in Awash watershed decreased from 2000 to 2005. The opposite effect shows that the alterations in other LULC classes appears to counterbalance the impacts of urbanization in storm runoff. Moreover, the findings show an increasing in vegetation cover, and increasing runoff volume, highlighting afforestation has shown little effect on runoff. This result is consistent with the findings of Ohana-Levi et al. (2017) pertaining to Israel.

The significant linear relationship between the spatio-temporal variations of runoff and imperviousness ratio is another important finding of this study. The result is slightly different from other studies Sanyal et al. (2014) and Chen et al. (2015) in which the deviation from a linear relationship between urban expansion and runoff variation is reported for some of the analyzed watersheds pertaining to northern China. The result of this study is referred to Adama City and its watersheds.

This study would increases understanding of the cumulative impact of urbanization in the hydrologic regime of the City. By limiting the extents of future impervious surfaces that can be converted from the remaining available land through new expansion, urban renewal and infill developments, the impacts of urbanization can be arguably managed to show sustainability of the City's development. It spotlights the potential of imperviousness ratio to be used as an alternate pragmatic planning tool for

controlling the hydrologic influences attributable to urbanization and could be integrated to storm water management regulations.

4.2 Impacts of climate change on extreme precipitation events

4.2.1 Trend of extreme precipitation from 1967 to 2016

4.2.1.1 Trends of extreme precipitation indices

The computed annual statistics and trends of the selected extreme precipitation indices in Adama City over the period of 1967-2016 are summarized in Table 4.5. The graphical illustration of the trend of corresponding indices is also depicted in Figure 4.5.

Table 4.5 Statistical parameters and trends of extreme precipitation indices in Adama City from 1967 to 2016

Indices	Annual statistical parameters			Trend test	
	Minimum	Maximum	Mean	Trend (per 10 years)	P_value
PRECTOT (mm)	578.4	1357.6	868.7	30.69	0.061**
SDII (mm)	4.7	15.8	10.7	0.37	0.075**
Rx1day (mm)	30.7	104.8	61.4	-0.89	0.587
Rx5day (mm)	61	190.1	111	5.24	0.053**
R95p (mm)	0	558.2	206	13.4	0.194
R99p (mm)	0	221.3	51.1	-1.91	0.723
R10 (no of days)	10	46	28.4	1.33	0.056**
R20 (no of days)	2	29	13.3	1.11	0.026*
CDD (no of days)	25	148	74.7	-5.72	0.061**
CWD (no of days)	3	70	10.3	-2.45	0.014*

$* \; significant \; at \; \alpha = 0.05; ** \; significant \; at \; \alpha = 0.1$

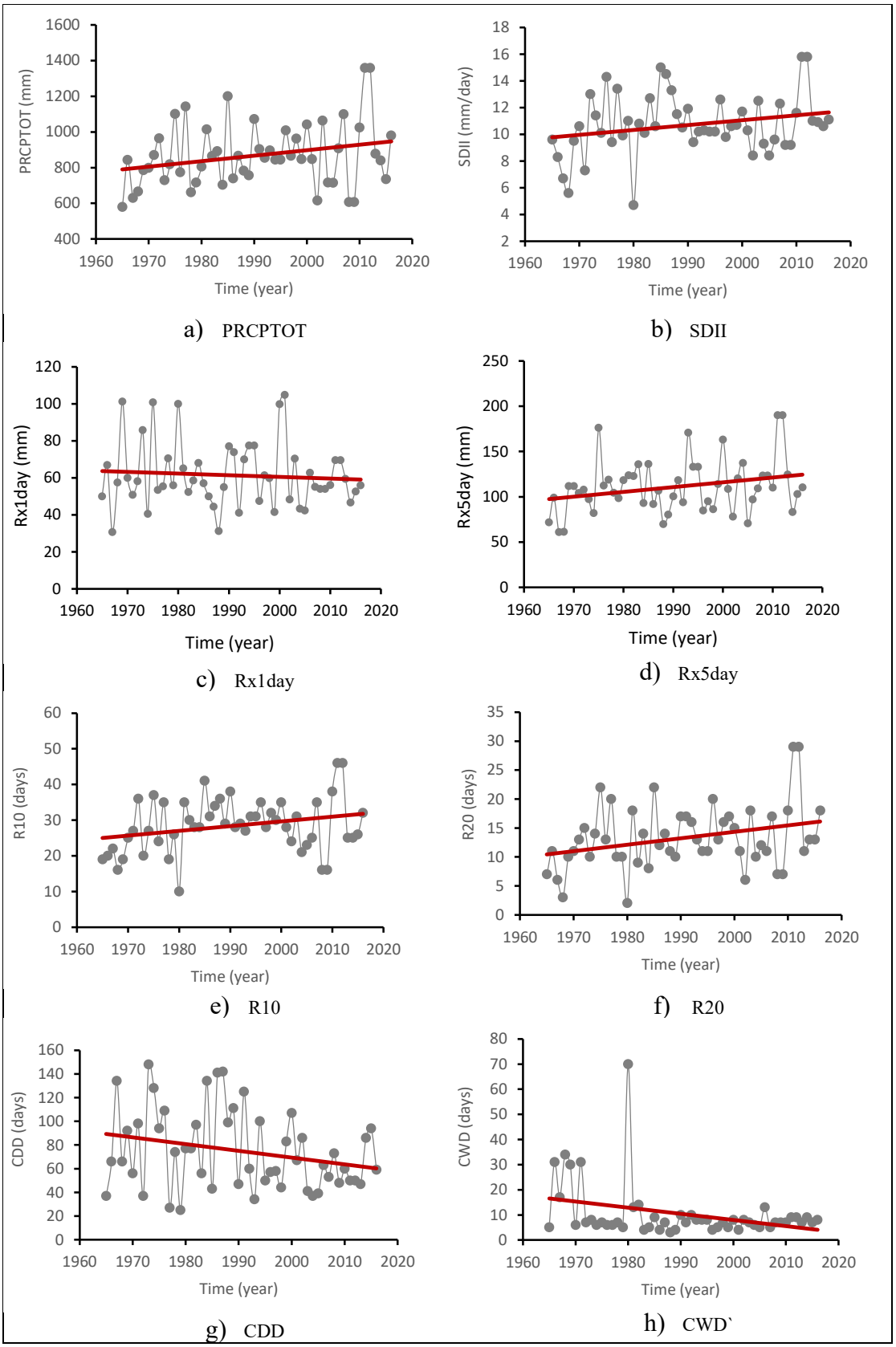
PRCPTOT (mm)
Time (year)
a) PRCPTOT
SDII (mm/day)
Time (year)
b) SDII
Rx1day (mm)
Time (year)
c) Rx1day
Rx5day (mm)
Time (year)
d) Rx5day
R10 (days)
Time (year)
e) R10
R20 (days)
Time (year)
f) R20
CDD (days)
Time (year)
g) CDD
CWD (days)
Time (year)
h) CWD`

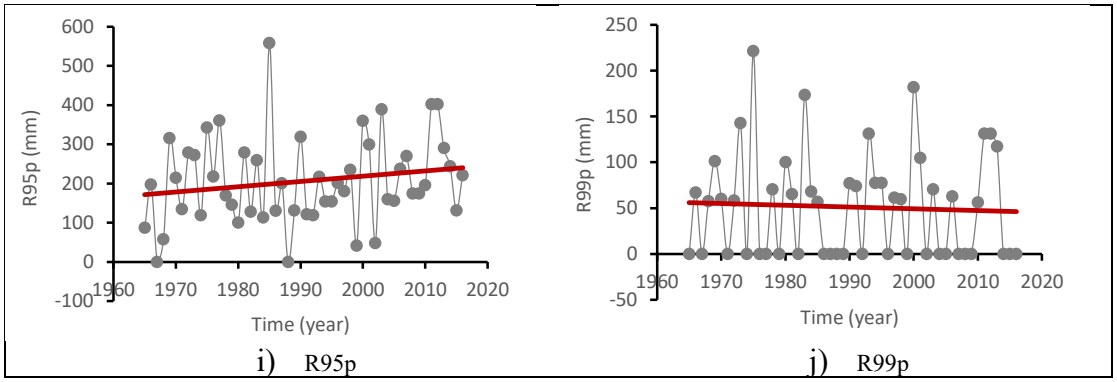

i) R95p j) R99p

Figure 4.5 Trends of standard extreme precipitation indices in Adama City between 1967 and 2016

Overall, the results show that there were statistically significant trends in the majority of the indices in the study period. The computed values of six indices (60% of the analyzed indices) showed rising trend, while the rest of the indices showed a declining trend over the span of 52 years. The p-value statistics shows that the observed trends of seven indices were significant. In contrast, no sufficient evidence was found to support the upward trend of R95p and downward trends of Rx1day and R99p.

On average, the study area received 868.7 mm annual total precipitation over the study period. The values were increasing at the rate of 30.69 mm/decade. Likewise, the amount of mean precipitation on a wet-day (SDII) varied from 4.7 mm to 15.8 mm. The values were increasing by 0.37 mm every 10 years over the study period. The observed rising trends of both indices were statistically significant ($\alpha = 0.05$).

With regard to the two absolute extreme indices (Rx1day and Rx5day), the results show that there was remarkable variation in the amount of the indices: Rx1day (30.7mm to 104.8 mm) and Rx5day (61 mm to 190.1 mm). The highest 1-day precipitation was decreasing at the rate of 0.89 mm/decade, yet the trend is not statistically significant.

On the other hand, the maximum precipitation of consecutive 5-days was showing significant ($\alpha = 0.1$) increasing trend (5.24 mm/decade) during the study period.

The results also show the values of the non-fixed (percentile) threshold indices, which represents a fraction of the total annual rainfall on wet-days attributed to the 95th and 99th percent rainfall events. Very wet-days (R95p) showed a tendency to increase, whereas extremely wet-days (R99p) decreased over the study period. However, the observed trends in both cases are not statistically significant. The annual mean values of both percentile indices were 206 mm (R95p) and 51.1 mm (R99p). The values of the indices were increasing (R95p) and decreasing (R99p) over time, respectively, yet the trends were not statistically significant.

Furthermore, it can be seen that the annual count of days with precipitation greater than fixed thresholds (heavy rainfall days and very heavy precipitation days) was increasing over the study period, ranging 10-46 days (R10) and 2-29 days (R20). The values were increasing at the rate of 1.33 days/decade for R10 and 1.11 days/decade for R20 at $\alpha = 0.1$ and 0.05 significant levels, respectively. Likewise, the two spell indices (maximum length of consecutive days with a rainfall below and above 1 mm) showed a tendency to decline over time. The values were decreasing at the rate of 5.72 days/decade (CDD) and 2.45 days/decade (CWD). The observed decreasing trends in both cases are also found to be statistically significant at $\alpha = 0.1$ and 0.05, respectively.

4.2.1.2 Correlation between extreme precipitation indices

The computed values of the correlation coefficient indicating the level of the linear relationship between the changes in the analyzed indices are shown in Table 4.6.

Overall, the results show that most of extreme rainfall indices are correlated, although the strength of the correlation varies from moderate to very strong. However, the correlation of the CDD index with other indices is found to be weak ($|r| < 0.39$). In addition, CDD is negatively correlated with the analyzed indices. Moreover, statistically significant positive correlation is found between the pattern of PRECTOT and other indices except Rx1day and CWD. Likewise, the observed positive correlations of SDII with the four indices (Rx5day, R10, R20 and R95p) and the negative correlation with CWD are also significant at the selected level of the analysis.

Table 4.6 Summary correlation analysis between the selected extreme precipitation indices in Adama City from 1967 to 2016

	PRECTOT	SDII	Rx1day	Rx5day	R10	R20	CDD	CWD	R95p	R99p
PRECTOT	1									
SDII	69.8*	1								
Rx1day	26.4	5.3	1							
Rx5day	62.4*	50.2*	48.8*	1						
R10	83.4*	82.1*	-0.6	43.3*	1					
R20	89.7*	79.8*	6.2	56.3*	85.9*	1				
CDD	-29.9*	-11.8	1.4	-22.4	-11.6	-23.3	1			
CWD	-8.5	-57.5*	31.7*	-5	-44.5*	-36.0*	5.8	1		
R95p	75.8*	66.1*	46.5*	61.4*	51.9*	66.4*	-34.8*	-14	1	
R99p	41.8*	26.7	78.4*	63.1*	19.8	26.5	-4	12.6	52.4*	1

*. Correlation is significant at the 0.05 level

4.2.2 Future daily precipitation

4.2.2.1 Selected predictors for SDSM

The candidate predictors shown in Table 4.7 were selected for calibration of SDSM for downscaling experiment in this study. In the process of screening predictors, specific humidity at 500 hPa height (s500) and divergence at 850 hPa height (p8zh) were

identified as super predictors for CanESM2 and HadCM3, respectively. Using these, additional four predictors from CanESM2 and three predictors from HadCM3 were selected.

Table 4. 7 Candidate predictors for calibration of SDSM

Short name	Long name	CanESM2	HadCM3
s500	Specific humidity at 500 hPa height	√	
r500	Relative humidity at 500 hPa height		√
p5_u	Zonal velocity component at 500 hpa	√	
p5_v	Meridional velocity component at 500 hPa height		√
shum	Near-surface specific humidity	√	√
p8_z	Vorticity at 850 hPa	√	
p8zh	Divergence at 850 hPa height		√
prcp	Total precipitation	√	

4.2.2.2 Performance of SDSM

The performance of downscaling model calibrated using the respective sets of selected predictors was evaluated on the basis of graphical and statistical parameters. Figure 4.6 illustrates the graphs of the monthly mean observed and the downscaled reanalysis data for each month of validation periods. It can be seen from the graphs that there is a good agreement between the generated and observed values of precipitation, except a slightly overestimate for July and August in the case of CanESM2 and underestimate for HadCM3.

The computed values of coefficient of determination and the ratio of the standard deviations of simulated to observed time-series data are summarized in Table 4.8. The

values of RSD show that the variations in monthly data are about the same in both GCMs. However, it can be seen that the values of the parameters computed from the daily time-series are relatively lower than the results of monthly time-series data, indicating the monthly variations are better captured by the SDSM. This is due to the fact that the amount of daily precipitation at a specific site is poorly determined by the regional climate forcing. Hence, the results of statistical parameters obtained in this study are quite respectable. In general, the overall evaluation of the SDSM performance suggests that the agreement between simulated and observed data is satisfactory, indicating a potential application of the calibrated model for downscaling future daily precipitation from the outputs of the two GCMs for the study area.

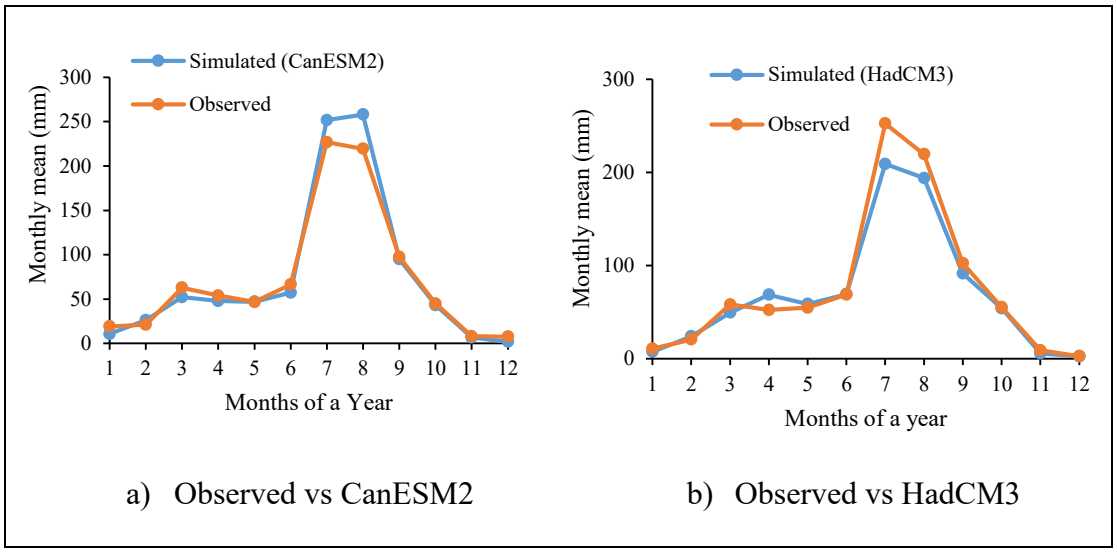

Figure 4.6 Observed versus simulated monthly mean precipitation for the period of a) 1991-2005, b) 1991-2001

Table 4.8 Performance assessment of SDSM during validation periods: 1991-2005 for NCEP_CanESM2 and 1991-2001 for NCEP_HadCM3

	NCEP_CanESM2		NCEP_HadCM3	
	Daily	**Monthly**	**Daily**	**Monthly**
R^2	0.088	0.992	0.100	0.986
RSD	0.49	1.17	0.51	0.84

4.2.2.3 Future annual precipitation scenarios

The future daily precipitation was downscaled from the outputs of the selected GCMs under five climate change scenarios. Figure 4.7 shows the plots of annual future precipitation (aggregated from daily values) in Adama City from 2021 to 2080. The statistical parameters summarized in Table 4.9 provides the descriptive information about future annual rainfall scenarios in Adama City from 2021-2080. Overall, the results show that the City will receive remarkable annual precipitation over the coming 60 years. The range of future annual precipitation is greater under the scenarios of CanESM2 than that of HadCM3 in which the highest annual mean rainfall is projected. In addition, it can be seen from the Figure 4.7 that under all climate change scenarios, the maximum annual rainfall is expected in the far-future period (2050s).

Regarding to the two ends of each statistic, the information summarized in Table 4.9 show that the City expects the maximum annual precipitation between 1065.8 mm (H3A2a) and 2251.6 mm (RCP8.5) over the coming 60 years, whereas the minimum rainfall ranging from 445.7 mm (RCP2.6) to 717.7 mm (H3A2a) is predicted within the same period. In addition, maximum and minimum values of mean annual rainfall varies between 907.1 mm (H3A2a) and 670.8 mm (RCP4.5). Further, with reference to the values of standard deviations, it can be viewed that the relative dispersion in the annual

precipitation is about the same for the two scenarios of HadCM3. However, in the case of the scenarios of CanESM2, dispersion in annual rainfall under RCP8.5 is higher than the other two scenarios (RCP2.6 and RCP4.5) which showed about similar dispersions.

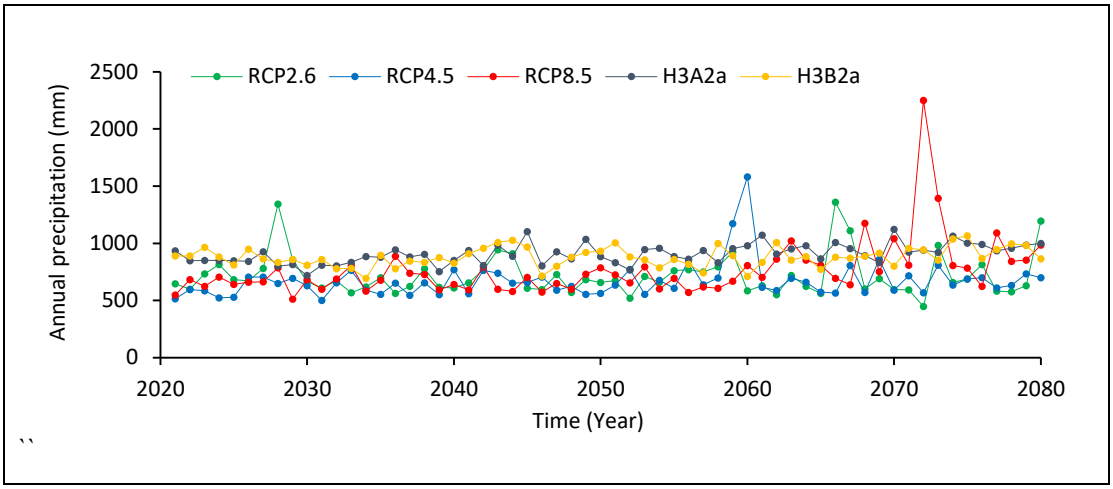

Figure 4.7 Annual rainfall in Adama City based on the projection of CanESM2 and HadCM3 for the period of 2021-2080

Table 4.9 Statistics of future annual precipitation in Adama City over the years 2021-2080 under the five climate change scenarios.

	Annual precipitation			
Scenarios	**Maximum**	**Minimum**	**Mean**	**Std. Dev**
CanESM2				
RCP2.6	1358.9	445.7	716.6	180.8
RCP4.5	1580.2	501.5	670.8	161.1
RCP8.5	2251.6	512.0	762.7	253.6
HadCM3				
H3A2a	1123.3	717.7	907.1	84.9
H3B2a	1065.8	693.2	879.7	84.1

4.2.3 Future changes in extreme precipitation

With future daily precipitation data, the likely changes of precipitation extreme in the near-future (2020s) and far-future (2050s) periods under five scenarios were assessed with respect to the conditions in the base period. Table 4.10 shows the computed future changes of extreme precipitation indices: wet-day%, POT95, CWD and PRECTOT. Overall, the future changes of the selected indices are found to be increasing under the majority of climate change scenarios over the analysis period, despite the magnitude significantly vary between GCMs, scenarios and time-windows.

Each of the three scenarios of CanESM2 projected to consistently increasing changes over the years 2021-2080 with different ranges across the indices: wet-days% (11.2% - 23.1%), POT95 (4.7%- 23.9%), CWD (9.1% – 32.5%), PRECTOT (13.1% - 55.1%). In addition, the difference between the projection of RCP2.6 and RCP4.5 will decrease in most of the analyzed indices in the far-future (2050s).

With regard to HadCM3, the consistency of increasing changes was observed throughout the study period, except in the case of wet-days% and POT95 corresponding to H3B2a. In addition, the ranges of the changes projected by H3A2a and H3B2a scenarios for the analyzed indices are relatively small, except for CWD. H3B2a projected wet-days% and POT95 decrease throughout the study period, despite the changes are small.

With the exception of CWD, CanESM2 offers maximum values of the indices in both analysis periods. In addition, the projected change by both models are more significant in the far-future, but for H3B2a results for wet-days% and POT95. In the 2020s, RCP2.6 showed a maximum of two indices (PRECTOT, POT95),

while in the 2050s, excluding CWD, the maximum in the selected indices changes were made via RCP8.5.

In all analyzed scenarios, the increase in CWD and PRECTOT indices is predicted. The maximum and minimum changes of CWD are 42.4% (H3B2a) and 9.1% (RCP2.6), respectively. With respect to the results of each model, the maximum value for CWD in CanESM2 is equal to 32.5% corresponding to RCP4.5 in the 2050s. The maximum change in total annual precipitation is also predicted to be 55.1% (RCP8.5) in 2050s, while the minimum value is predicted by the two scenarios of HadCM3 and equal to 2.5%.

Table 4.10 Percentage change of extreme precipitation indices in the future (2021-2080) with reference to a base period (1971-2000)

Model/scenarios	**Time -zone**	**Wet-days%**	**POT95**	**CWD**	**PRECTOT**
CanESM2					
RCP2.6	2020s	12.9	14.6	9.1	28.2
	2050s	13.8	17.9	15.2	31.1
RCP4.5	2020s	11.2	4.7	14.7	13.1
	2050s	14.2	16.1	32.5	29.6
RCP8.5	2020s	13.8	8.6	16.2	20.8
	2050s	23.1	23.9	28.9	55.1
HadCM3					
H3A2a	2020s	-2.2	0.0	9.8	2.5
	2050s	1.5	0.3	25.6	10.5
H3B2a	2020s	-0.5	-0.2	20.6	2.5
	2050s	-1.3	-0.5	42.4	5.4

4.2.4 Discussion

The extreme rainfall in Adama City during 1967-2016 was analyzed based on the trends of 10 selected precipitation extreme indices computed from daily time-series records. Using SDSM, the projections of GCMs (CanESM2 and HadCM3) under 5 climate change scenarios were downscaled to provide daily precipitation in the study area for the period 2021-2080. Taking the climate conditions during 1971-2000 as a base period, future changes in extreme precipitation were investigated using delta approach.

The results reveal that most of the extreme rainfall indices, including Rx5day, SDII, R10, R20, R95p and PRECTOT showed statistically significant upward trend over the years 1967-2016. Some of the findings are slightly different from the results reported by Shawul and Chakma (2020) for the rainfall time-series (1980–2012) in the upper Awash basin in which Adama station belongs. The authors reported a negative trend for SDII and R20, and no statistically significant trend for R10 over the study period for Adama station. The disparity between the findings of the present study and that of Shawul and Chakma (2020) could be because of the different periods analyzed. It has been argued that length of climate records is an important factor that affects the probability of identifying trends in any given time-series data. In the present study rather long period has been analyzed, which may include different trends within different sub-periods. The results of this study suggest that the extreme precipitation in Adama City was increasing over the past 50 years, which could explain the notable impacts of climate change. Furthermore, consistent with Lima et al. (2015), statistically significant correlation is found between PRECTOT and SDII and other indices. This indicates the trends of annual total and average daily precipitation of wetdays were changing with the changes of the trends of most of extreme precipitation indices.

The performance of the downscaling model used in this study was also found to be good in predicting the daily precipitation during the validation period. The results are comparable to that of studies conducted to inspect the impacts of climate change on future precipitation extremes in Addis Ababa City (Feyissa et al., 2018) and Amhara Regional State (Ayalew et al., 2012). The results indicate a successful application of the SDSM for downscaling local-scale daily precipitation from the estimates of large-scale atmospheric information for the study area.

Future changes in extreme precipitation in Adama City are also another important finding of this study. Under all scenarios of the GCMs, almost all of the analyzed extreme precipitation statistics are found to increase up to 2080, despite the changes will be higher in the far-future (2050-2080) than near-future (2021-2050). The changes in wet-day%, POT95 and PRECTOT could reach 23.1%, 23.9%, and 55.1%, respectively and predicted by the worst scenario of CanESM2. The changes in longest wet-spell will also increase by 42.4 % that projected by the worst scenario of HadCM3. The results suggest that the study area is expected to receive more severe extreme precipitation events over 2021-2080 as compared to the condition during 1971-2000. In accordance with this result, Feyissa et al. (2018) reported the extreme precipitation in Addis Ababa City will increase over the 21st century, while the present study is pertaining to Adama City which has been little explored. With a high rate of urbanization in Adama City that has expanded built-up area at the cost of agricultural land in the upper watershed area of the City administration, the future increase of extreme precipitation events can produce high runoff, thereby increases the chance of more severe floods to occur.

Given the importance of improved understanding of the trend of extreme precipitation in planning for sustainable flood risk management, the findings of this study can help decision-makers for early identification of potential impacts due to predicted changes. For mitigation planning, it is ideal to consider the changes under the worst scenario; however, it could not be always possible due to the existing limited resources. In this regard, the results presented here can support analysis of alternative responses to the impacts of climate change under different scenarios. Moreover, the results could also be used in various modeling studies (e.g., Flood modeling) to assess the impacts of future climate conditions. From flood modeling perspective, the relationship between the attributes of extreme events is more important.

4.3 Impacts of climate change on relationship between extreme precipitation IDF

4.3.1 Annual maximum precipitation series

Daily rainfall data recorded during 1967-2016 and predicted for the future 2021-2070 under two GCMs were disaggregated into shorter time scales. AMAX rainfall series of storm durations 1-hr, 3-hr, 6-hr, 12-hr and 24-hr was extracted for respective analysis timelines. Skewness index was computed for each dataset. The computed values of skewness are summarized in Table 4.11, and provides information about the shape of the distribution of the datasets. In all the cases, the values are found to be positive and less than 2.0; i.e., within the criteria considered for normal distribution (-2<skewness<+2). The AMAX sub-daily rainfall series obtained through disaggregation process has similar distribution, with that of the corresponding daily precipitation.

Table 4.11 Skewness of AMAX daily and sub-daily rainfall series during the past and future timelines

Scenarios	Storm duration				
	1-hr	3-hr	6-hr	12-hr	24-hr
Historical	1.279	0.997	1.370	0.772	0.806
HadCM3	0.510	0.754	0.577	0.371	0.356
CanESM2	1.314	1.160	1.561	1.699	1.616

4.3.2 Extreme precipitation IDF relationships

4.3.2.1 IDF curves

Figure 4.8 illustrates the IDF curves of extreme rainfall in Adama City for the periods 1967-2016, historical (a), HadCM3 (b) CanESM2 (c). They are developed by fitting GEV I to the respective AMAX precipitation series. The curves give information about the magnitude of rainfall intensity as a function of storm durations from 1-hr to 24-hr and return periods from 5-yr to 100yr. The IDF curves clearly show that rainfall intensity decreases, as duration of the storm increases from 1-hr to 24-hr. For storms from 1-hr to 24-hr, the rainfall intensity increases, as return period increases from 5-yr to 100-yr. The results confirm that the pattern of the IDF curves of the respective study periods satisfied self-similarity and are consistent with the expected behavior of the IDF curve. Comparatively, the HadCM3 curves do not show significant difference in intensity for storms longer than 12-hr.

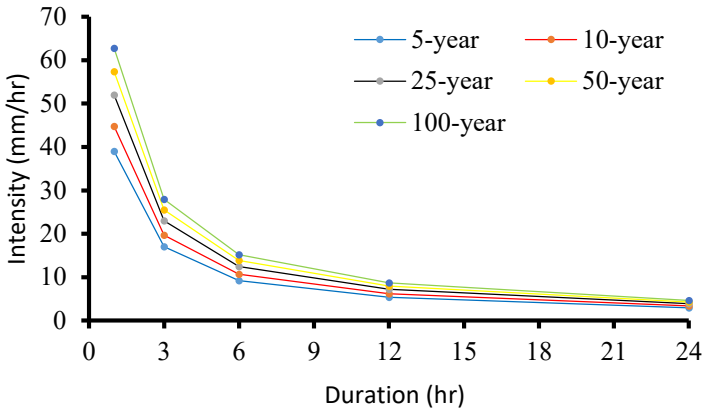

a) Historical (1967-2016)

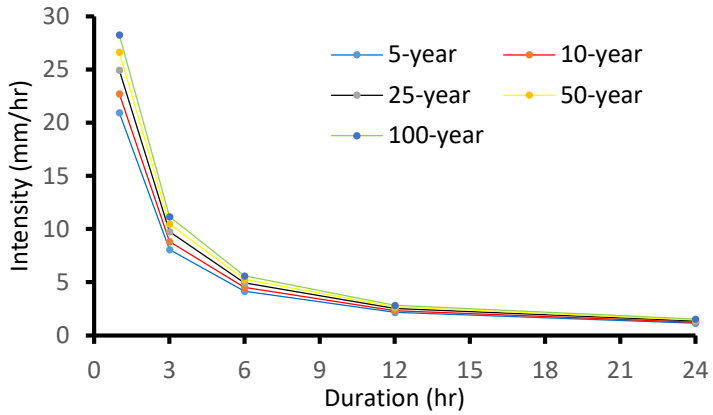

b) HadCM3 (2021-2070)

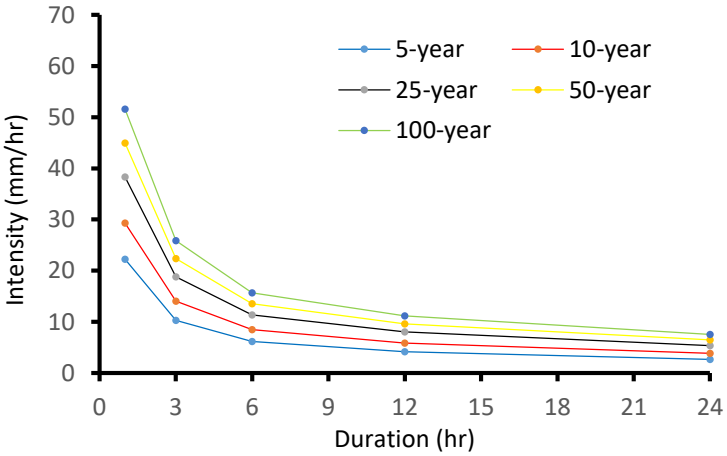

c) CanESM2 (2021-2070)

Figure 4.8 Precipitation IDF curves of the past and future timelines a) historical 1967-2016, future projection b) HadCM3, and c) CanESM2

4.3.2.2 IDF models

Results summarized in Table 4.12 show the mathematical equations of respective IDF models alongside the computed values of coefficient of determination and Nash-Sutcliffe efficiency. From the equations of the respective IDF models, it is evident that the value of coefficient parameter increases, as frequency decreases from more frequent (5-yr) to less frequent (100-yr) storms, in all datasets. Similarly, the value (absolute) of exponent parameter increases, with return period for the historical and HadCM3 datasets and on the contrary of CanESM2.

Table 4.12 Summary of the IDF model equations for the present and future rainfall in Adama City ($\boldsymbol{d}$: rainfall duration (hour)) and the corresponding results of model performance evaluation ($\boldsymbol{R^2}$: Coefficient of determination, $\boldsymbol{NSE}$: Nash-Sutcliffe efficiency)

	Historical			HadCM3			CanESM2		
T	**Equations**	**R^2**	**NSE**	**Equations**	**R^2**	**NSE**	**Equations**	**R^2**	**NSE**
5-yr	$39.8d^{-0.816}$	0.999	0.998	$21.4d^{-0.916}$	1.000	0.968	$21.5d^{-0.665}$	0.998	0.991
10-yr	$45.9d^{-0.818}$	0.999	0.998	$23.3d^{-0.920}$	0.999	0.922	$28.4d^{-0.639}$	0.997	0.939
25-yr	$53.6d^{-0.820}$	0.999	0.997	$25.7d^{-0.925}$	0.999	0.853	$37.2d^{-0.621}$	0.997	0.820
50-yr	$59.3d^{-0.821}$	0.999	0.997	$27.5d^{-0.927}$	0.999	0.803	$43.7d^{-0.613}$	0.997	0.722
100-yr	$65.0d^{-0.822}$	0.998	0.997	$29.3d^{-0.930}$	0.999	0.757	$50.1d^{-0.607}$	0.996	0.626

With regard to the results of model performance evaluation, high values are obtained for the selected statistical parameters. The computed value of coefficient of determination ranges 0.996 – 1.0 and that of Nash-Sutcliffe efficiency is between 0.584

and 0.998, for the analysis periods and datasets considered in this study. The results greater than the threshold considered for both parameters in this study (NSE > 0.5 and $R^2 > 0.7$), and satisfied all considered model performance evaluation criteria at a time.

4.3.2.3 Relationship of return periods and IDF model parameters

The extent of the relationship between return period and the individual model parameters (i.e., coefficient and exponent parameters) was also assessed using correlation analysis. The computed correlation coefficient and the p-value are shown in Table 4.13. The results show that the fitting parameters of IDF models are positively correlated with the return periods. The observed relationships are found to be very strong (i.e., r > 0.79) for most of the cases and strong (r > 0.59) for exponent parameter in the case of historical and CanESM2.

Moreover, the significance test of the linear relationship of coefficient parameter with return periods resulted in the p-value smaller than 0.05 in all of the cases, indicates the relationship is statistically significant. On the other hand, the p-value is found to be greater than 0.05 for the case of exponent parameter, indicates the observed linear relationship is not significant, at the selected analysis level.

Table 4.13 Results of correlation analysis between fitting parameters power-law function ($i = aD^b$) and return periods

Model parameters	Test Statistics	Historical (1967-2016)	Future (2021-2070)	
			HadCM3	CanESM2
Coefficient parameter (a)	*r*	0.863	0.864	0.864
	p	0.027	0.026	0.027
Exponent parameter (b)	*r*	0.757	0.796	0.683
	p	0.081	0.058	0.135

4.3.3 Future changes in rainfall intensity

The potential changes in extreme precipitation intensity in the future period as compared to the baseline period were assessed based on the two GCMs. Figure 4.9 compares the historical IDF curves with that of future period based on the selected GCMs, HadCM3 and CanESM2. Table 4.14 also provides information about the magnitude and direction of changes in the future extreme rainfall intensity relative to that of the baseline climate condition at 1-hr, 3-hr, 6-hr, 12-hr and 24-hr rainfall durations and all return periods considered in this study.

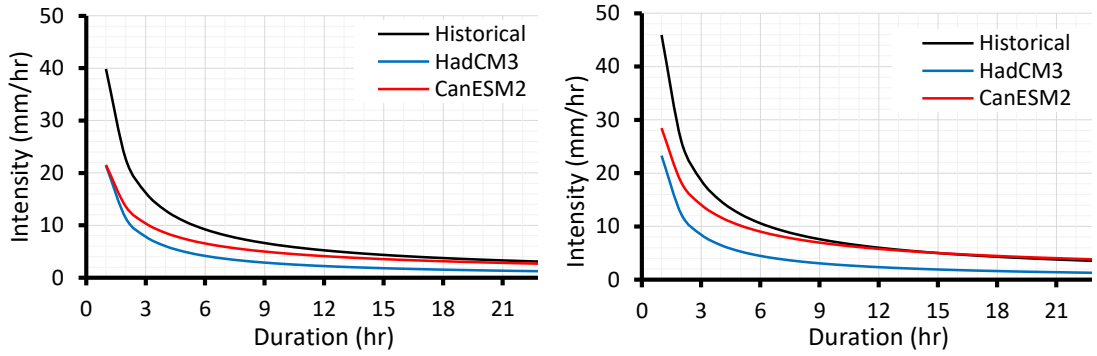

a) 5-yr b) 10-yr

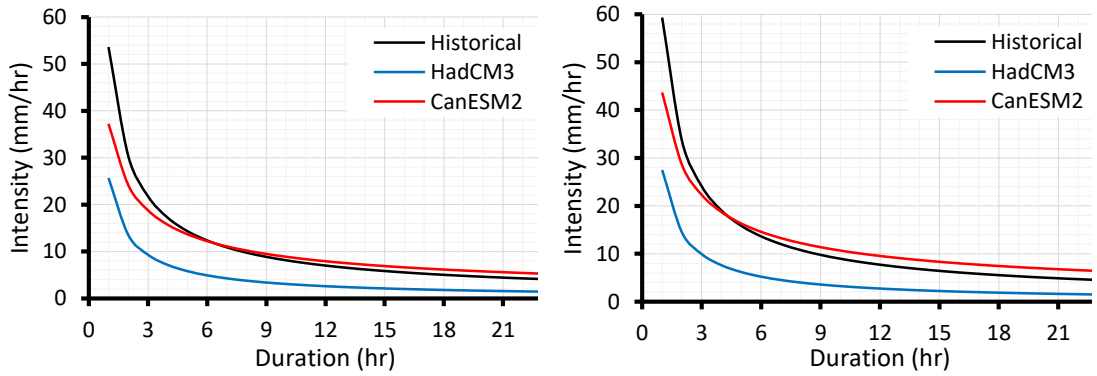

c) 25-yr d) 50-yr

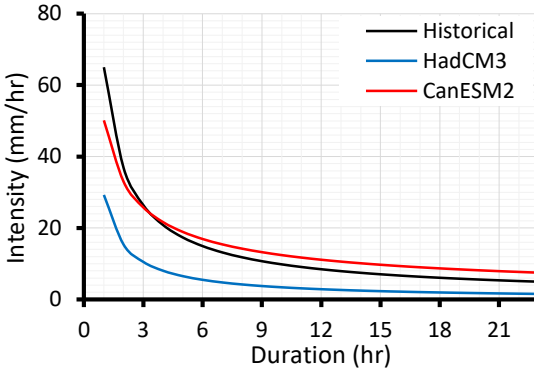

e) 100-yr

Figure 4.9 Comparison of historical IDF curves (1967-2016) with Projected IDF curves (2021-2070)

Table 4.14 Percentage change of future intensity relative to historical condition (T: return period (year), d: storm duration (hour))

T	Duration	Change in intensity (%)		T	Duration	Change in intensity (%)	
		HadCM3	CanESM2			HadCM3	CanESM2
5-yr	1	-60.3	-59.7	50-yr	1	-73.3	-30.4
	3	-70.1	-44.1		3	-83.1	-7.7
	6	-76.1	-34.0		6	-89.1	6.8
	12	-81.9	-23.7		12	-94.9	21.1
	24	-87.5	-13.3		24	-100.5	35.3
10-yr	1	-65.4	-47.0	100-yr	1	-75.7	-25.8
	3	-75.2	-28.0		3	-85.7	-2.3
	6	-81.2	-15.8		6	-91.7	12.6
	12	-87.0	-3.4		12	-97.5	27.4
	24	-92.6	9.1		24	-103.1	41.9
25-yr	1	-70.4	-36.2				
	3	-80.2	-14.7				
	6	-86.2	-0.9				
	12	-92.1	12.9				
	24	-97.7	26.5				

Overall, the IDF curves demonstrate that the rainfall intensity over the future period will be different from the baseline period. In all the cases, the HadCM3 curves show smaller intensity than that of historical and CanESM2. Except for 5-yr return

period, IDF curves corresponding to CanESM2 GCM show that intensity of the extreme rainfall will be higher, for longer storms and will be lower for shorter storms than the baseline condition. In this regard, extreme rainfall events with 15-hr, 7-hr, 5-hr and 4-hr storm durations corresponding to return periods 10-yr, 25-yr, 50-yr, and 100-yr, respectively, will approximately reproduce historical rainfall intensity. However, IDF curves HadCM3 show less intensified rainfall than that of the baseline period under all storm durations and return periods. The decreasing magnitude is maximum for the shortest storm (1-hr), despite the value is found to decline towards the longest storm (24-hr).

Turning to the results summarized in Table 4.14, rainfall intensity in Adama City will change in the future by significant percentage relative to that of the baseline period. In addition, significant difference can be seen in the identified changes by the GCMs. With regard to HadCM3 projection, future rainfall intensity will decrease by significant percentage, for all storm durations and return periods. The magnitude of percentage changes is also found to increase from more frequent rainfall of shorter duration (1-hr 5-yr) to less frequent rainfall of longer duration (24-hr 300-yr). Conversely, results based on CanESM2 projections reveal that the magnitude of decreasing change in intensity predicted by CanESM2 GCM declines and that of increasing changes increases, with return periods and respective storm durations. It is also evident that HadCM3 predicted the relative decrease future daily rainfall intensity ranges 87.5%(T=5-yr)-103.1%(T=100-yr). With similar length of storm (24-hr), CanESM2 predicted 13.3% decrease corresponding to 5-yr return period and an increase in intensity by 9.1% (T=10-yr)-41.9% (T=100-yr).

4.3.4 Discussion

Daily precipitation records of 1967-2016 and projected for 2021-2070 periods were disaggregated into shorter time scale, and used for developing rainfall IDF models. By computing rainfall intensity for a range of storm durations and return periods using the models, the percentage change of future rainfall intensity relative to the current climate condition was determined.

In the process of fitting bi-parametric power-law function ($i = a D^b$) to the data, high values are obtained for coefficient of determination in all the cases and for Nash-Sutcliffe efficiency in most of the cases, indicate a good agreement of the observed (i.e., computed from rainfall depths) and simulated rainfall intensity using the developed IDF models. The results are comparable with that of similar studies (Erena et al., 2018; Ewea et al., 2018; Gebru, 2020), and confirm a good performance of the IDF models in explaining the relationship between intensity, duration and frequency of extreme precipitation in Adama City under the study's conditions (i. e., datasets, storm durations, return periods and analysis timelines). In addition, the findings reflect the successful application of Gumbel's type I probability distribution and the bi-parametric power-regression function, for constructing IDF curves and for deriving the equations of the models, respectively.

Statistically significant direct linear relationship is obtained between the values of coefficient parameter (i.e., parameter a) and the corresponding return periods, in all models developed using the observed and projected rainfall datasets and on the contrary for exponent parameter (i.e., parameter b). This finding is consistent with the findings of (Ewea et al., 2018) who modeled IDF curves in Makkah Al Mukarramah region for designing stormwater infrastructures.

Moreover, the findings reveal that the extreme rainfall intensity in the future period in Adama City would rise or decline, depending on GCM, storm duration and return period considered. Under the projection of CanESM2, the intensity of shorter storms will decrease and that of longer storms increase, under all return periods greater than 5-yr. The results based on HadCM3 prediction reveal that the intensity of future extreme precipitation will decrease more than by half of its historical value, in all the cases. In accordance with these findings, studies have documented mixed results, decreasing and increasing, of changes in extreme rainfall intensity due to climate change in different areas of the country, including Mekele City (Gebreigziabher, 2020), some parts of Tigray region (Gebru, 2020) and Chiro and Hurso (Tesfay and Quraishi, 2017). The findings of the present study are pertaining to Adama City which has received little attention. The significant differences between the results of the GCMs used in this study could be associated with uncertainties in the GCMs in predicting rainfall pattern (Noor et al., 2018), and highlight the results of climate change impacts studies could be affected by our choice of GCMs for future climate projections.

Considering these findings, it is reasonable to conclude that extreme rainfall intensity over the coming 50 years (2021-2070) in Adama City likely to change due to climate change. An increase rainfall intensity could have an impact on the conveyance capacity of the existing stormwater drainage system, and could result more frequent and severe floods than in the past years. Moreover, the current practice of stormwater infrastructure design based on the assumption of time-invariant rainfall distribution may not provide reliable result to maintain the future potential increase in extreme rainfall due to climate change.

With respect to the increasing concern of management of climate change-induced urban flooding in general and in Adama city in particular, the significance of this study can be explained in different ways. The potential changes in extreme rainfall intensity identified here contribute to a clear understanding of the effects of climate change on the future extreme precipitation characteristics, and support local climate change adaption planning as well as decision-making. The findings can also be used in revision of the current regulations and standards for the planning and designing of urban drainage systems at local level. Moreover, they have paramount importance of future studies, particularly the assessment of flood hazard and risk of the City under the effects of changes in global climate in order to formulate effective flood mitigation and adaption strategies.

In urban settings, reliably established relationships between features of extreme rainfall has a primary importance of designing a new stormwater infrastructures and assessing the potential risk of existing drainage system. The IDF models developed in this study enable to estimate extreme precipitation intensity for a wider range of storm durations and for a number of return periods; i.e., from more frequent rainfall of shorter duration (1-hr 5-yr) to less frequent rainfall of longer duration (24-hr 100-yr) over different analysis periods. IDF models of more-frequent shorter durations can be used for stormwater management applications and a less-frequent longer-duration events are useful for flood risk management in the City under future climate conditions. Moreover, mathematical equations of the rainfall IDF relationships can reduce the dependency on the graphical versions of the models and allow to better determine any of the three features of the storm (intensity, duration, frequency) using the other two attributes, at specific duration from 1-hr to 24-hr.

Finally, the findings build on existing evidences and offers valuable insights into the influences of climate change on extreme precipitation; the uncertainties of GCMs in the predicting precipitation characteristics; the relationships between return period and fitting parameters of the power-law function and the potential application of methodology used in the present study.

4.4 Flood hazard in Awash sub-watershed

4.4.1 Validation of flood inundation model

The inundation model was validated using maximum water depth of 2016 flood collected for 30 ground points. It was used to test the agreement simulation result and real on-the-ground reality. The result of statistical test indicates correlation (r) and p-value equals 0.968 and 0.023, respectively, at 95% confidence interval of difference. The correlation (0.968) shows strong positive correlation between the simulation result and the ground truth information. The observed relationship between the two sets of data is statistically significant at 95% level. The evidences established by the validation process reveal that the model's performance is adequate in terms of representing the facts on the ground to an appropriate degree. In addition, the results reflect the successful application of PCSWMM for modeling urban flood. Figure 4.10 depicts the overlay of inundation map simulated for 2016 flood events for validation overlaid with urban drainage network and topography of the watershed. It also shows the City and Awash sub-watershed boundaries.

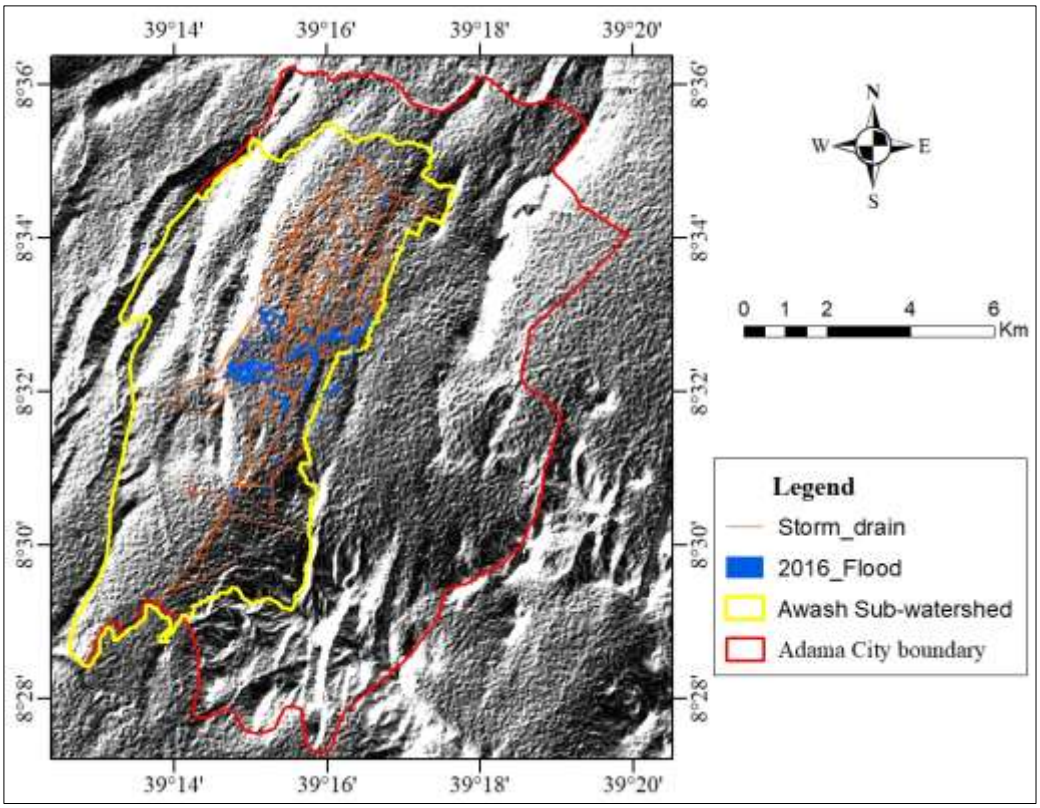

Figure 4.10 Flood inundation during 2016 for validation

4.4.2 Flood inundation

Using the validated model, flood inundation was simulated for five return periods: 5, 10, 25, 50 and 100-yr and four LULC and climate scenarios. The results reveal that the modeled study area is flooded under all scenarios considered, though the magnitudes of inundation characteristics are different from period to period. For illustration purpose, the inundated raster cells with maximum water depth and flow velocity for 5-yr and 100-yr under existing land cover and climate conditions are depicted in Figure 4.11. The complete set of inundation maps for all modeled scenarios and frequencies are included in Annex A. The maximum values of water depth and flow velocity and total extents of inundations of the study watershed for respective scenarios are summarized in Table 4.15.

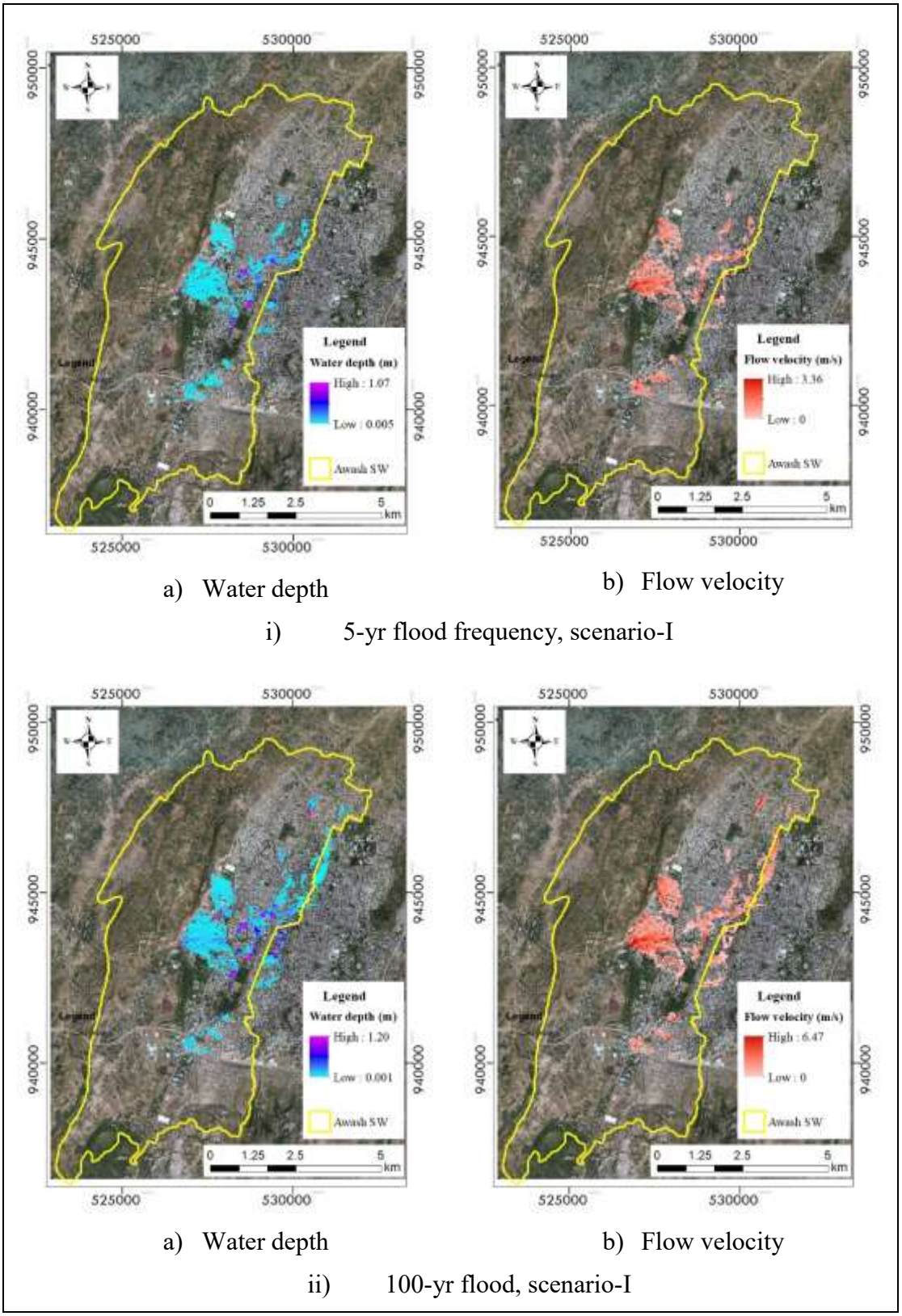

a) Water depth b) Flow velocity

i) 5-yr flood frequency, scenario-I

a) Water depth b) Flow velocity

ii) 100-yr flood, scenario-I

Figure 4. 11 Flood inundation maps for 5-yr and 100-yr floods under existing land cover and present day climate condition

Table 4.15 Flood inundation attributes for different frequencies and climate scenarios

Parameter \ Return period	5-yr	10-yr	25-yr	50-yr	100-yr
Existing LU Historical climate scenario (I)					
Depth (m)	1.07	1.12	1.15	1.18	1.20
Velocity (m/s)	3.36	5.97	6.28	6.38	6.47
Future LU Historical climate scenario(II)					
Depth (m)	1.04	1.16	1.16	1.16	1.16
Velocity (m/s)	3.17	3.29	3.41	3.47	3.53
Existing LU Future climate scenario (III)					
Depth (m)	1.06	1.14	1.22	1.27	1.29
Velocity (m/s)	3.07	6.19	6.56	6.72	6.86
Future LU Future climate scenario (IV)					
Depth (m)	1.16	1.16	1.18	1.26	1.31
Velocity (m/s)	3.04	3.36	5.43	5.93	6.17

Overall, the results reveal that storm drainage system of the study watershed is insufficient for 24-hr long storm with 5-yr and above return period under all land use and climate scenarios analyzed in this study. The high water depths are occurring around stream banks and densely urbanized areas. The velocities are also increasing towards the central area. The close look at eastern part of the study watershed reveals that the flooding in the modeled area surcharges the runoff in the adjacent sub-watershed (Mermersa). Such additional flow due to flooding of the adjacent distinct watershed is rarely considered during design of infrastructures.

Limiting the analysis of the results within the boundary of the study watershed, information summarized in Table 4.15 shows that the inundation characteristics increase as return period increases from 5-yr to 100-yr for all scenarios, despite

insignificant differences can be seen for maximum induction depth for return period greater than 5-yr. Comparison of the most frequent and less frequent scenarios reveal that 100-yr storm produces 13, 12, 23 and 15cm for scenario I, II, III and IV, respectively. In addition, maximum flow velocity of the 100-yr inundation are found to be about twice that of 5-yr for the majority of analyzed scenarios.

4.4.3 Flood hazard

Flood hazard was assessed using the values of FI of each scenario. Flood hazard maps depicted in Figure 4.12 help to visualize spatial distribution of flood prone areas of 5-yr and 100-yr flood under the four scenarios of land cove and climate conditions. The complete set of flood hazard maps are depicted in Annex B. The degree of the hazard was categorized into Low, Medium and High. The computed spatial coverage of each hazard category of respective scenarios is summarized in Table 4.16 a, b, c & d.

Overall, flood hazard in the northern part of the modeled area is less likely under 5-yr flood. It can be viewed that low flood hazard zones are covering large area relative to the other hazard categories. High and medium flood hazards are concentrated on the central part of study area, which is densely urbanized low-lying flood plain area. However, small coverage of medium and high flood hazards seen in the northern western parts in the case of 25-yr and above are around stream banks that could be due to greater water depth. The high hazard zones at western part, especially for future climate condition could be resulted due to the steep slope of the area that increases the velocity.

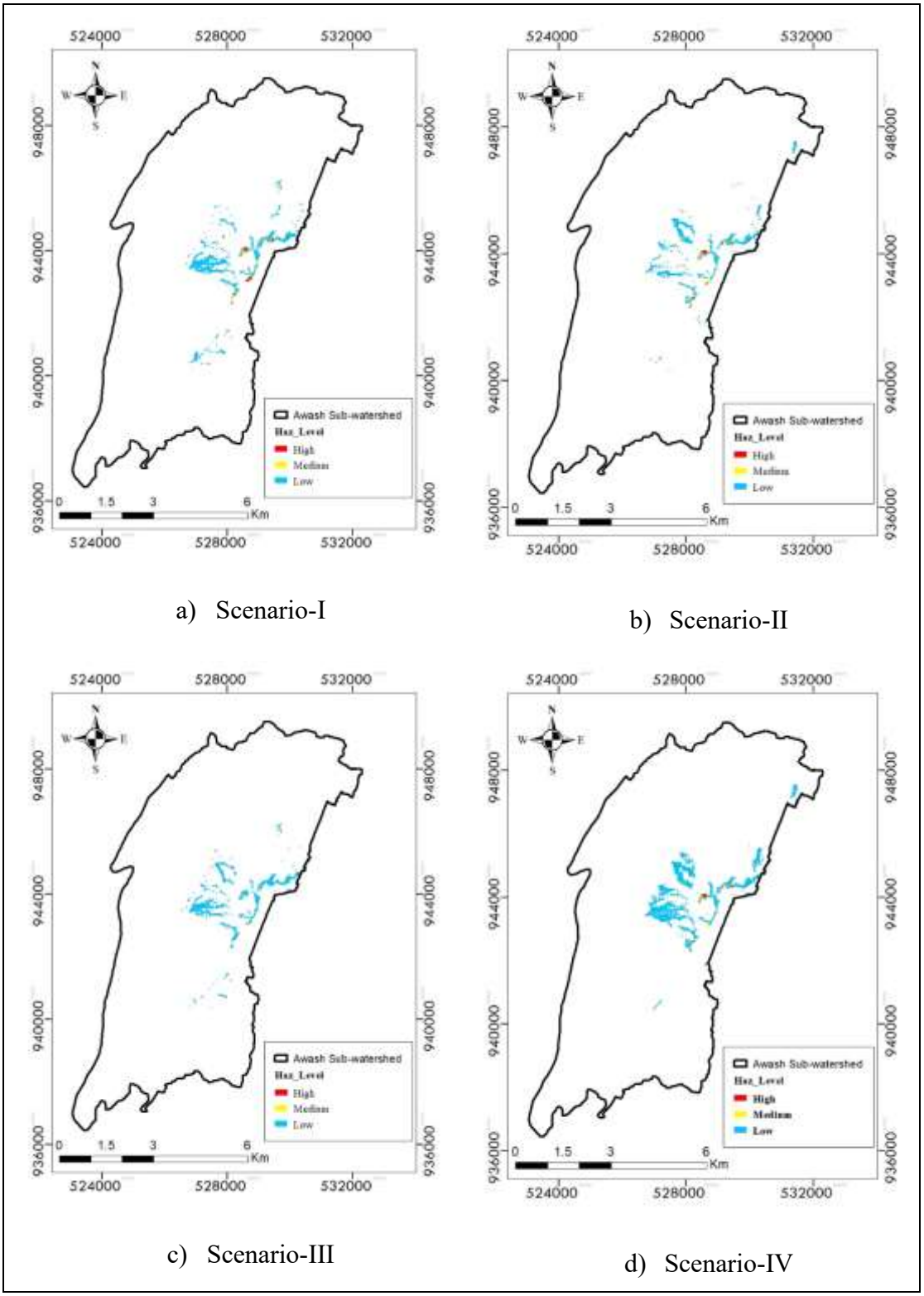

a) Scenario-I

b) Scenario-II

c) Scenario-III

d) Scenario-IV

Figure 4.12 Flood hazard map of 5-yr flood under different scenarios considered in the study

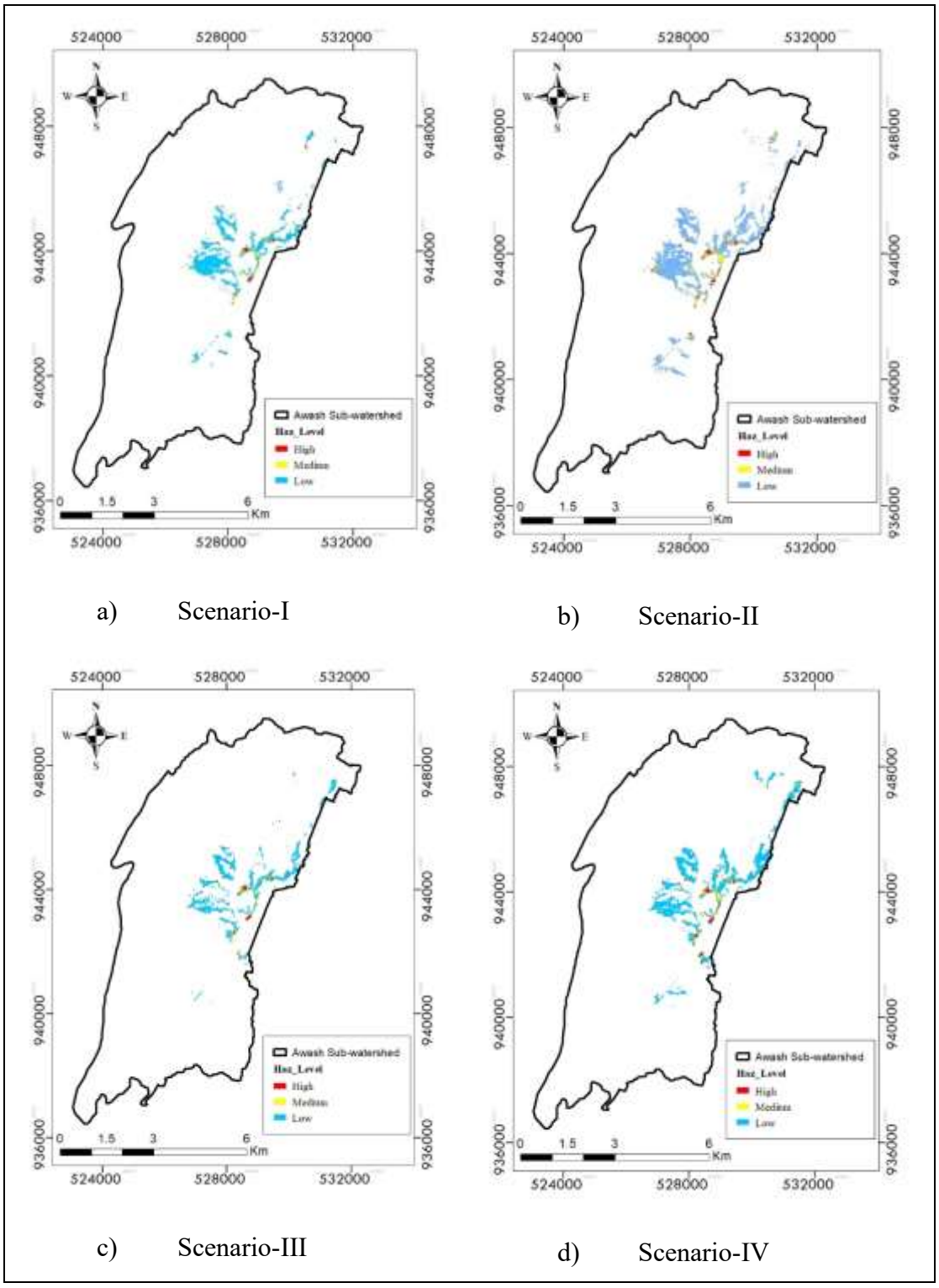

Figure 4.13 Flood hazard map of 100-yr flood under different scenarios considered in the study

It can be seen from Table 4.16 a, b, c & d that the total prone area is higher with increasing return period from 5-yr to 100-yr. In terms of the degree of the hazards, the spatial coverage increases as return period increases and severity of the hazard decrease. Under all scenarios, flood hazard is mostly low. Based on historical climate and existing LULC condition (Table 4.16a), 123.7ha of the modelled area is prone to flood of 5-yr return period whereas the figure reaches 204.3 ha for 100-yr return period. It can also be seen that storms of 5 and 10-yr recurrence periods result about equal area of high flood hazard. Scenario III- Under climate change, the spatial extent of flood prone area ranges 106.8ha (5-yr) to 319.61ha (100-yr) with different flood prone zones (Table 4.16c). High flood hazard is less likely for storms of 5-yr recurrence period.

Table 4.16 The spatial coverages of the hazard at respective levels measured in hectare

a) Historical climate and existing LULC

Return period / Hazard level	5-yr	10-yr	25-yr	50-yr	100-yr
High	5.33	5.28	5.72	6.24	7.95
Medium	9.41	11.43	14.02	16.35	18.66
Low	108.98	128.20	149.14	162.76	177.68
Total	123.72	144.91	168.88	185.35	204.29

b) Hazard under future urbanization

Return period / Hazard level	5-yr	10-yr	25-yr	50-yr	100-yr
High	4.61	5.69	7.24	7.66	7.97
Medium	9.19	10.34	11.24	13.35	15.06
Low	187.77	205.99	230.25	252.55	268.13
Total	201.57	222.02	248.73	273.56	291.16

c) existing LULC and future climate change

Hazard level \ Return period	5-yr	10-yr	25-yr	50-yr	100-yr
High	0.20	5.70	8.72	11.14	13.07
Medium	3.09	13.63	21.04	25.14	30.33
Low	103.49	141.54	190.40	229.24	276.21
Total	106.78	160.87	220.17	265.52	319.61

d) under combined effect of future urbanization and climate changes

Hazard level \ Return period	5-yr	10-yr	25-yr	50-yr	100-yr
High	3.83	6.71	8.75	11.2	12.92
Medium	6.76	10.49	15.62	19.29	23.52
Low	167.62	219.11	283.88	325.48	360.39
Total	178.21	236.31	308.25	355.97	396.83

4.4.4 Changes in flood hazard

Taking the extent of flood-prone area identified under the existing LULC and historical climate condition as a baseline, this study assessed increasing or decreasing of flood-prone areas under the other three scenarios. Information summarized in Table 4.17 shows the percentage changes in spatial extent of flood prone areas in study area due to climate change-induced increased rainfall intensity, increased impervious surface attributable to future land-use change, and due to the combined effect of the two factors. Overall, the results show that spatial extent of flood-prone areas increases over the coming years by significant percentage for majority of the return periods considered under the three scenarios.

Considering the impacts of urbanization alone, future flood-prone area increases by significant percentage. Under future climate conditions, the relative percentage increase in spatial extent rises from 11% to 56.4% as return period increases from 10-yr to 100-yr. In contrast, the coverage of prone area as a result of 5-yr flood under climate change is expected to decrease compared to the baseline.

Further comparison of the changes due to urbanization and climate change reveals that, the percentage change due to urbanization is greater than that of climate change for the recurrence interval of 5, 10, 25 and 50-yr. The difference between the percentage change can be seen decreasing as increasing flood frequency increases from 5-yr to 50-yr. However, for the less frequent storm (100-yr), the impacts of climate change-induced increased rainfall intensity on flood hazard is greater than that of the potential increase of impervious surface due to future LULC change. Moreover, the combined effect of urbanization and climate change results increasing flood-prone areas with increasing percentage as return period increases from 5-yr to 100-yr.

Table 4. 17 The percentage change in spatial extent of flood prone areas relative to the baseline (existing land use and historical climate)

Return period / **Scenarios**	**5-yr**	**10-yr**	**25-yr**	**50-yr**	**100-yr**
Future LULC and Historical climate	62.9	53.2	47.3	47.6	42.5
Future climate and Existing LULC	-13.7	11.0	30.4	43.3	56.4
Future LULC and climate	44.0	63.1	82.5	92.1	94.2

4.4.5 Discussion

The urban flood hazard assessment was conducted for Awash sub-watershed in Adama City by modeling flood inundation with coupled 1D-2D urban flood modeling method and implemented in PCSWMM. A good performance of the model was obtained during validation process, with statistically significant ($p<0.05$) strong direct correlation (0.968) between the model result and ground truths. The model was applied for simulating flood of 5, 10, 25, 50, and 100-yr return periods under four scenarios. By computing flood intensity based on the combined effect of water depth and flow velocity, flood hazard was assessed and categorized into low, medium and high. The spatial extents of the corresponding flood hazard of three scenarios were compared and contrasted with the bassline scenario.

The results of 1D-2D flood modeling show that the existing stormwater drainage system in the study watershed is associated with limited capacity to convey the runoff due to the considered frequencies and climate scenarios. This is useful information for the City in particular and for the country urban centers in general with regard to urban drainage network planning and design. The inundation raster cells provide the physical characteristics (location, spatial extent, water depth and flow velocity) of potential floods during their occurrence. This information supports effective flood hazard assessment, as well as it can be used for improving awareness of the prone community. Moreover, the results can serve as a base of assessing the floodability of the area, the surrogate measure of urban flood resilience.

Flood hazard maps produced here provides information, including location, extent and severity under different frequency and climate conditions. Such information enables stakeholders to conduct a proper flood risk assessment. By integrating flood

hazard maps into the local development plan of the City, negligent expansion and densification of construction in prone areas could be prevented. By providing information on a ranges of frequencies it helps formulation of alternatives of flood risk management strategies. They can also be used for designing and/or updating urban plans and in developing integrated natural hazard management in the City. Moreover, the results support landscape planning in the course of environmental impact assessment (EIA). Above all, this study quantified the how the impacts of urbanization and climate change affects flood hazards. This improves existing understanding on the impacts of human-nature couplings, hence informs future planning policies.

4.5 Urban flood resilience

4.5.1 Flood resilience of Awash subwatershed

The study assessed the flood resilience level of Awash sub-watershed in Adama City using surrogate measure—percent floodable area, which is represented by urban floodability index. The areas of extracted floodable lands in existing and proposed land use plan are found to be 35.78 ha and 39.12 ha, respectively. Using flood-prone area obtained in section 4.4.3, UFI of the study area was computed for 5, 10, 25, 50 and 100-yr and four scenarios. The results are summarized in Table 4.18 a & b. The values refer the capacity of the study area to tolerate floods without causing physical damages and socioeconomic disruptions. Overall the results show that the study watershed is less floodable under all scenarios considered.

The maximum and minimum values of computed floodability index are found to be 0.37 and 0.09, respectively. Following variation in the spatial extent of flood-prone

area, UFI decreases as return period increase from 5-yr to 100-yr. Comparison between the results of the scenarios reveals that the study area is more floodable under existing LULC and future climate scenario for 5-yr return periods.

Table 4.18 Summary of urban floodability index of Awash sub-watershed in Adama

a) Based on floodable lands in existing land-use

Return period / Scenario	5-yr	10-yr	25-yr	50-yr	100-yr
Existing LULC and Historical climate	0.29	0.25	0.21	0.19	0.18
Future LULC and Historical climate	0.18	0.16	0.14	0.13	0.12
Future climate and Existing LULC	0.34	0.22	0.16	0.13	0.11
Future LULC and climate	0.20	0.15	0.12	0.10	0.09

b) Based on floodable lands in proposed land use plan 2019

Return period / Scenarios	5-yr	10-yr	25-yr	50-yr	100-yr
Existing LULC and Historical climate	0.32	0.27	0.23	0.21	0.19
Future LULC and Historical climate	0.19	0.18	0.16	0.14	0.13
Future climate and Existing LULC	0.37	0.24	0.18	0.15	0.12
Future LULC and climate	0.22	0.17	0.13	0.11	0.10

4.5.2 Discussion

By extracting floodable lands and using the resulted flood hazard map, this study assessed the flood tolerance level of the study area. The results showed the resilience level of the Awash sub-watershed in Adama City is low, suggesting more efforts are required in the future period to increasing floodable lands for building the City's flood resilience. In this regard, the results of this study can be used as a benchmark for

improving the flood resilience of the City and helps to inform the existing planning practices. It is possible to increase percent floodable area by making built-up areas to convey and storing floodwater during rainy seasons through adaptive urban design. UFI can be used as a planning tool for building the resilience of the City in the long-term. In this case, higher value (for example, 1) can be set as a goal.

4.6 Resilience-based flood hazard management plan

4.6.1 Planning area and existing situation

A number of flood-prone areas have been identified under the worst flooding scenario. The selected area for planning is a neighborhood within inner-city covering 10.9 ha (Figure 4.14). Presently, the area encompasses single-floor (villa houses) and few multi-story buildings (Figure 4.15a) used for different uses, including business, residence, governmental institution, hotels/bars/restaurants, mixed residence, primary school, shops and supermarkets and workshops (Figure 4.15b).

Single-story buildings are constructed on stone masonry foundation. In multi-story buildings, stone masonry is used under grade beam, between footing columns. Hollow concrete block is used in majority of the buildings for wall construction. Solid mud block is also observed, in the case of small buildings (less than 20 m^2) within a plot and relatively old houses. According to SP 2019, the planning area is proposed for different urban land uses (Figure 4.15c) with number of floors ranging 6-8 stories. The slope of the area is found to be within 0-2% and the soil texture is clay loam. Moreover, the inundation is characterized by water depth, 0.02-1.0m and flow speed from 0.01 to 0.77m/sec.

The planning area is vulnerable due to its low-lying flat topography, its location in central business district as there are active socio-economic activities. In most of the buildings the floor finish elevation is about 30-50 cm above the ground around the buildings. For majority of the buildings the water surface level is higher than the finished floor level (Figure 4.15d), which ranges from 10 cm to 20 cm. Flow speed of the inundation of the selected area is less than 1m/sec; hence, the impacts due to the flow speed can be considered insignificant (Vojtek and Vojteková, 2016). Hence, the vulnerability of the area mainly due to the water depth, and used in selection of the adaption measures. Adaption techniques developed by the community is limited to sandbagging, which increase an existing elevation of places through which floods enter the property

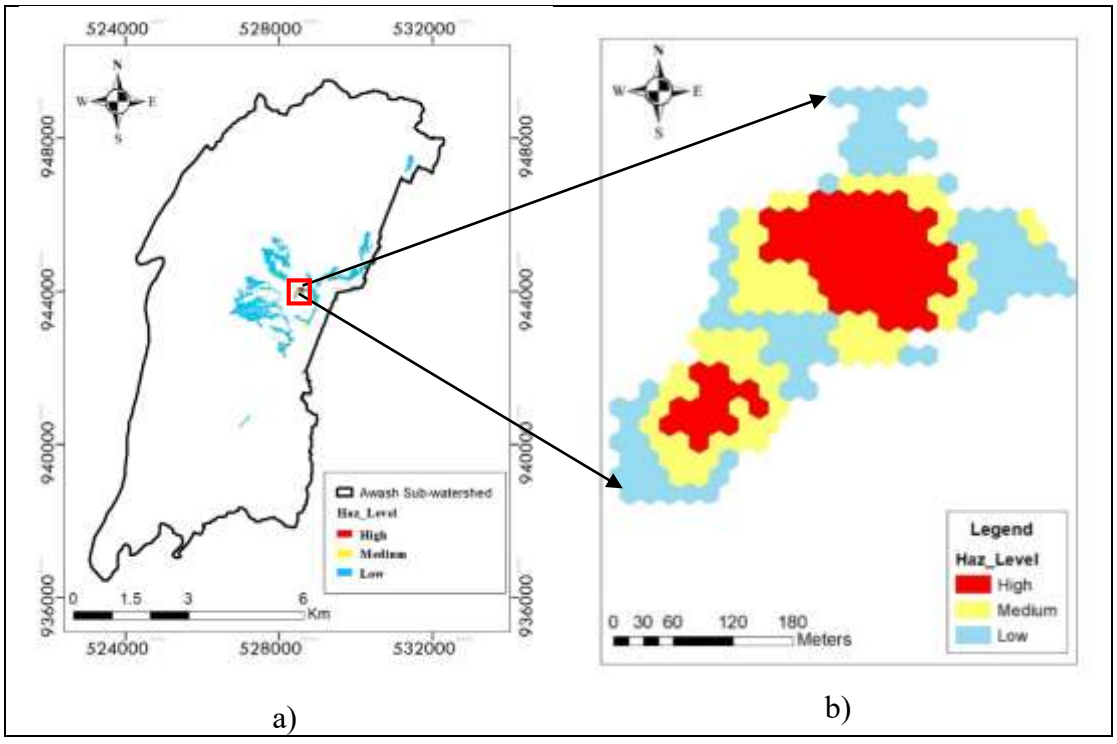

Figure 4.14 Location map of planning area a) 100-yr flood hazard map Awash sub-watershed, b) selected planning area hazard map

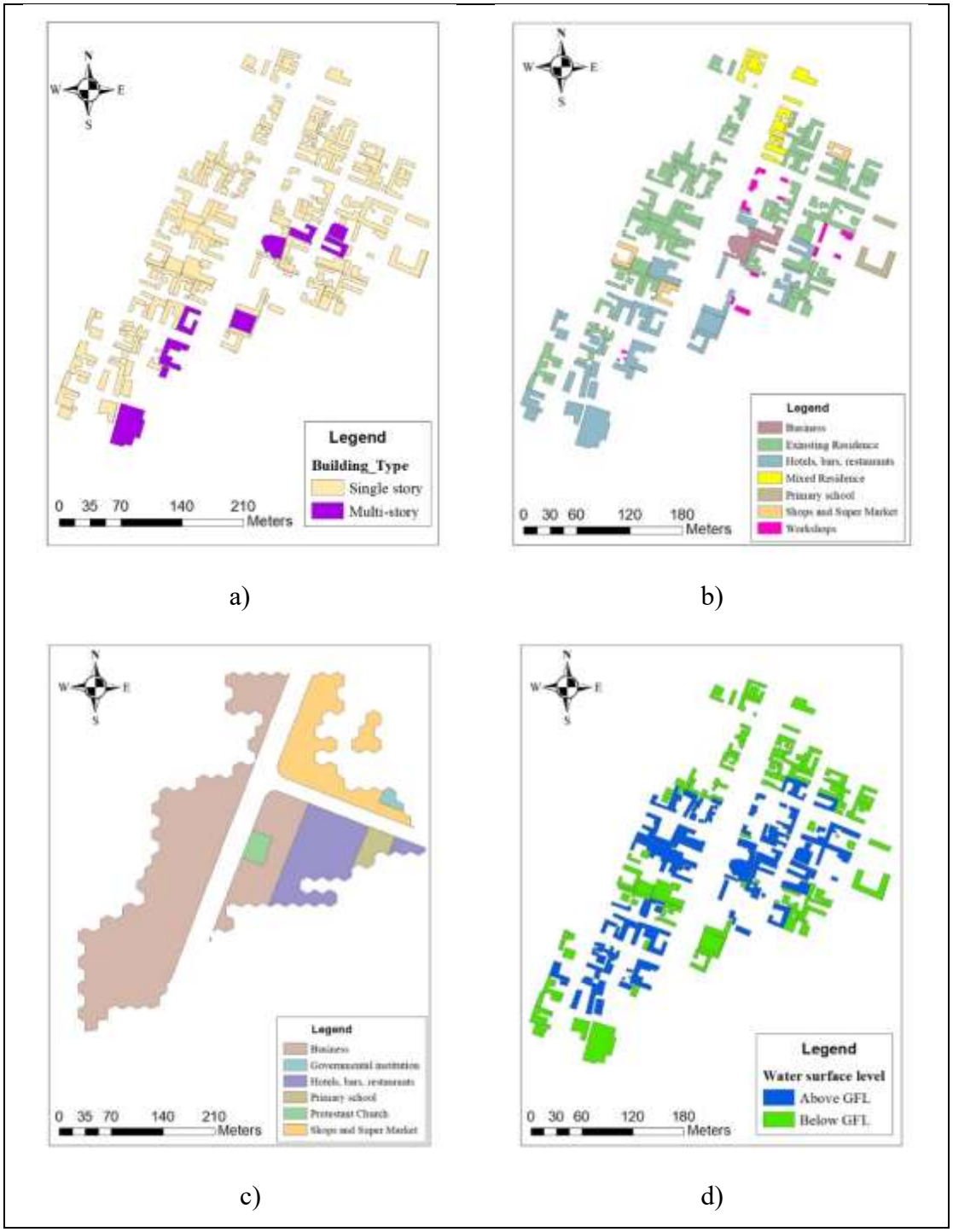

Figure 4.15 Maps of planning area a) existing buildings interns of height regulation, b) existing development, c) SP 2019 proposal, and d) water surface level with reference to finished ground floor level of the buildings

4.6.2 Proposed measures

A range of flood adaption measures are widely applied at smaller scales. Depending on the local situation and the important features of potential flood, a range of localized flood adaption strategies are proposed for the planning area. These measures can be categorized into five strategies: elevated configuration, dry-proofing, wet-proofing, temporary measures and site and landscape interventions.

Elevated configuration

Flood adaption using elevated configuration involves elevating the finished floor elevation above the flood level to prevent the entrance of flood water, e.g. by building on columns, or embankments. This adaption strategy is suitable, mainly for future developments that could be undertaken through redevelopment in the area ('brownfields') and 'infill' of the remaining open spaces in the plots. Future development projects in this area should consider non-habitable ground floor. In this case, the ground floor could be designed for flood compatible uses such as car parking, flood resilient storage, public open space etc. However, the cost to elevate an existing building by increasing the height of foundation could be prohibitive that limits the application this adaption strategy for the existing developments.

Dry-proofing

Dry-proofing is a flood adaption method, in which the flood water is kept out of the building by establishing a watertight seal on the exterior part of the building and sealing all interior spaces below the established flood level. Due to the pressure from floodwater, this method is generally used in the case of shallower flood, less than one meter. This method is suitable for existing buildings in the planning area, as majority

of them are built on stone masonry foundation, as well as the flood level is below the top of the foundation. This technique enables to reduces the exposure of the foundation walls to floodwater.

Wet-proofing

Wet-proofing is adaption approach based on the acceptance of flood water to enter the buildings. It is proposed for buildings where the water surface elevation greater than the finished ground level and when the inflow of water into the building cannot be prevented. Wet-proofing design can be used to treat the internal and external spaces of an existing or new buildings, enabling floodwaters to enter and leave quickly and easily without causing significant damage. It involves, designing to withstand floodwaters, elevating mechanical, electrical, and plumbing systems above the established flood level or otherwise.

Temporary measures

Temporary protective measures use materials or systems that can be deployed or activated when flooding is predicted and removed or stored when the flood waters have receded. Temporary measures include sandbags, temporary floodgates, and flood-wrapping systems. Sandbags are the most widely recognized tool used to protect a property from floodwater, but there are also synthetic products that function in a similar fashion. Temporary floodgates are removable barriers installed in windows, doorways, and other openings. Flood wrapping systems cover the most vulnerable portion of an existing structure to create a temporary impervious barrier.

This adaption approach is suitable for existing buildings in the planning area where the flood is shallower. They are assumed to be the most affordable localized adaption

options, yet require time and people to quickly deploy them, that limits their application in locations where flooding may occur frequently and without sufficient warning time.

Site and landscape adaptions

This approach involves basic site interventions through storm-water management systems, berms, and floodwalls to change how water moves through and around a property. For instance, flood damage to fences can be reduced by ensuring the fence is water permeable up to a height that allows water to flow through with ease, and then solid above that point. In addition, pervious surface areas can be increased by using permeable paving materials (e.g., gravel, decomposed granite, permeable pavers, permeable concrete) and/or remove any unnecessary hard surfaces to allow ground to absorb water. Protecting and maintaining buildings, site, and landscape features can also be achieved by providing proper drainage to ensure that water does not erode foundation walls, drain toward the building.

4.6.3 Discussion

Based on the situations of the selected flood-prone area, this study proposed different localized flood adaption strategies suitable for the existing and future developments in the planning area. Every strategy is associated with some sort of limitations. Due to hydrostatic forces, dry-proofing and temporary measures are only suitable for shallower floods. Site and landscape intervention enable buildings remain unaltered, yet can make flooding worse for other adjoining sites and little applications in an already fully developed sites. Wet-proofing is appropriate when the entry of flood water into the building could not be prevented, yet its suitability is limited for

buildings with inadequate ventilation. Moreover, elevated configuration is less applicable in the case of existing buildings. The maximum benefit can be attained through an appropriate combination of these strategies.

By providing protections for the buildings and properties, the proposed measures reduce flood damages and allow the operation of buildings under flood conditions. As such they contribute to reducing possible damage to buildings and properties, as well as time required for building recovery. Hence, they are suitable for building the flood resilience of the prone-community. In addition, they can be seen as means to increase floodability of the area. Moreover, these strategies impose more responsibility on property owners, which aids in the formulation of how to distribute flood hazard reduction responsibilities among various levels.

CHAPTER 5: CONCLUSIONS AND RECOMMENDATIONS

5.1 Conclusions

This study analyzed urban flood hazard in Adama City under spatiotemporal changes of LULC due to urbanization and increased extreme precipitation as a result of climate change. It also looked at the flood resilience of the City and devised a resilience-based flood hazard management strategy.

The findings reveal that Adama City administration has undergone an excessive LULC change due to urbanization over the last twenty-four years, resulting in 22% annual rise in impervious surface area. The overall effects on hydrological regime of the City show increased surface-runoff depth of the City administration by 9.5 %, whereas 12.9 % and 6.9 % increase are found in the case of Awash and Mermersa subwatersheds, respectively. At both the City watershed and subwatershed scales, the findings reveal statistically significant strong linear relationship between the changes in PIA and runoff depth. The findings suggest that the hydrological impacts of urbanization can be arguably managed by limiting the extents of impervious surfaces due to future developments. In addition, the findings spotlight the potential application of PIA as an alternative pragmatic planning tool for controlling the hydrologic influences of urbanization.

The study also shows that climate change has had an impact on historical precipitation and continue to influence future extreme precipitation in the City. Intensity of extreme rainfall in Adama City over the coming years 2021-2070 would be different from the present-day climate condition. It could increase up to 49.5% or decrease up to 106.2%, depending on GCM, storm duration and return period

considered. The findings reveal that the current practice of stormwater infrastructure design based on the assumption of time-invariant rainfall distribution may not provide reliable result to maintain the future potential increase in extreme rainfall due to climate change. An increase in rainfall intensity could have consequences of the way the City's drainage infrastructures are designed, operated and sustained, suggests updating of standards for designing drainage infrastructures. The findings also show the uncertainties of GCMs in projecting precipitation characteristics, implying that our choice of GCMs for future precipitation projections could have a significant impact on the results impact studies.

Moreover, the results also highlight that the length and quality of time-series records used and the variety of standard precipitation extreme indices examined here allowed to describe the structure and changes of extreme precipitation over the past years in Adama City. Moreover, the important large-scale datasets (i.e., quality of predictors and climate change scenarios), the spatial downscaling model, used in this study enabled to examine the changes in extreme precipitation under future period climate conditions in the City.

1D-2D flood modeling using PCSWMM enabled to assess the potential flood in Awash sub-watershed, under different frequencies. The results show that existing drainage system in modelled area is insufficient to convey storms of 24-hr 5-yr and above storms and results flood hazard ranging 123.7 to 204.3 ha as return period increases from 5-yr to 100-yr. In addition, spatial extent of flood-prone areas increases over the coming years by significant percentage under evolving LULC and climate. The findings also reveal that relative contribution of urbanization and climate change to potential increase of flood hazard are depends on return periods. The study suggests

that the existing drainage system is characterized by poor performance, and could experience more frequent floods. Moreover, the results of flood modeling provided features of potential floods, which aided to produce realistic flood hazard maps.

Moreover, the results show that the flood resilience level of the City is low. Different flood adaption strategies are proposed which include elevated configuration, dry-proofing, wet-proofing, temporary measures and site and landscape interventions. These measures enhance localized flood response capacity, and contributes to building the flood resilience of the prone-community.

Overall, Adama City has experienced devastating rainfall-induced urban floods in the past and could experience more frequent and severe floods in the future due to the possible rise in extreme precipitation intensity under changing climate, urbanization-driven increased impervious surface area, low performance of the current storm drainage system. By guiding future land development using impervious surface based regulations, utilizing flood hazard maps developed in this study and flood modeling as base of flood hazard management operations, and appropriately utilizing the proposed measures flood hazard in the City can be managed effectively.

With respect to the increasing concern of sustainable urban flood hazard management under urbanization and climate change, this study presented significant contributions, which can be explained in different ways. The influence of urbanization on runoff was examined at smaller spatiotemporal scales, and can represent improvements in the assessment of the hydrological influence of urbanization, to account for the effects of rapid urbanization. The findings also reveal that relative contribution of urbanization and climate change to potential increase of flood hazard are depends on return periods, which can provide new insight in relation to relative

contribution of urbanization-driven impervious surface and increased precipitation intensity due to climate change to urban flood. Further, the study demonstrates a successful application of the GCMs outputs for analyzing the influences of the potential increase in extreme rainfall intensity due climate change in the future period, and can be considered an important contribution to existing knowledge how to use GCM projections to study the effects of climate change on urban flood.

Moreover, the flood modeling framework of this study combines various land cover and climatic scenarios for current and future periods, and can reflect advances in urban flood modeling to incorporate the effects of urbanization and climate change. Finally, the study provides empirical evidences on measuring mitigation aspect of urban flood resilience and proposed flood adaption measures, which are effective in building localized flood response capacity, contributing operationalization of the concept of resilience in urban flood hazard management. These strategies impose more responsibility on property owners, which aids in the formulation of how to distribute flood hazard reduction responsibilities among various levels.

5.2 Recommendations

In order to realize the sustainable developments of Adama City in particular and flood-vulnerable urban areas of Ethiopia, in general, the following issues require attention of Adama City Administration, Urban policies, and future studies.

It is recommended that City's local development plans (LDP) integrate impervious surface based land-use control and building regulations to arguably manage the hydrological impacts of impervious surfaces that can be converted from remaining available land through new expansion, urban renewal and infill developments. In

addition, designing and updating the City's local development plan and building codes should aim to define flood level of different flood-prone areas along with suitable alternative flood adaptive measures. Moreover, standards and guidelines presently employed by the City for the planning and designing of stormwater management infrastructure should be updated in order to help climate-resilient drainage infrastructure design. Finally, localized flood adaptation strategies proposed in this study put more responsibility on property owners; hence, in order for the community to willingly adopt these measures, attentions should be given to enhance the community's flood risk awareness and a sense of ownership of the problem.

Policies should promote urban flood modeling as a base for urban flood hazard management operations. This aligns the country's focus on flood hazard reduction with the aims of similar initiatives in more developed countries. This should be related to enhancing collaboration between the Ethiopia and developed nations, in order to promote a more effective flood risk management methodology. It is also recommended that urban planning policies integrate impervious-surface-based urban land development regulations in order to better control hydrologic influences of urbanization. Revision of existing standards and guidelines for planning and design of drainage infrastructure is suggested, in such a way that they reflect global climate change consequences at local level. Moreover, it is suggested that the country's standards for buildings incorporate flood hazard standards to guide developments in flood-prone areas. Finally, policies should focus on promoting personal responsibility in flood safety. This could help to distribute responsibilities between different types of stakeholders, so as to take advantage of different initiatives over differing spatial scales, from the catchment level down to the individual building level.

Further studies are required in several fronts. First, the impacts of urbanization are assessed using the variations of accumulated runoff depth corresponding to variations in the volume of water yield. However, the impacts on other factors (e.g., flow rate) and their combined effect on flooding needs further investigations. Second, flood modeling is conducted for Awash sub-watershed. With incorporation of Mermersa subwatershed can provide the full picture urban flooding in the City. Furthermore, quantitative flood risk analysis is necessary to aid in the prioritizing of flood hazard management actions in various locations. The level of flood resilience was also determined using a single surrogate measure; however, assessment of resilience with more surrogate measures could provide complimentary insight into flood resilience level of the City. Finally, flood adaptation mechanisms proposed in this study are just a few of the several ways that flood-prone communities can use to build their resilience to floods. Feedbacks from application of other adaption measures could improve understanding, and support operationalization of the concept of resilience in flood hazard management.

REFERENCES

Abbasnia, M., Toros, H. 2016. Future changes in maximum temperature using the statistical downscaling model (SDSM) at selected stations of Iran. Model. Earth Syst. Environ. 2(68). http://doi.org/10.1007/s40808-016-0112-z

Abshirini, E., Koch, D., and Legeby, A. 2017. "Flood Resilient Cities : A Syntactic and Metric Novel on Measuring the Resilience of Cities against Flooding , Gothenburg ,Sweden." *Journal of Geographic Information System* 9: 505–534. https://doi.org/10.4236/jgis.2017.95032.

ACFMP 2016. Adama City Flood Mitigation Project. Adama Science and Technology

Adeogun A.G, Pathirana A, Daramola M.O. 2012. 1D-2D Hydrodynamic Model Coupling for Inundation Analysis of Sewer Overflow. Journal of Engineering and Applied Science 7(5): 356-362. https://doi.org/10.3923/jeasci.2012.356.362.

Adger, W. N., Hughes, T. P., Folke, C., Carpenter, S. R., & Rockström, J. 2005. Socialecological resilience to coastal disasters. Science, 309, 1036-1039.

Adisu M, Hailemikael M (2017) An Approach to Drainage System Sustainability in Wolaita Soddo Town: A Case Study from Southern Ethiopia. Int J Waste Resour 7: 271. doi: 10.4172/2252-5211.1000271

Adugna, D., Lemma, B., Jensen, M. B., Gebrie, G. S. 2019. Evaluating the hydraulic capacity of existing drain systems and the management challenges of stormwater in Addis Ababa, Ethiopia. Journal of Hydrology: Regional Studies 25 (2019) 100626. https://doi.org/10.1016/j.ejrh.2019.100626

Aksoy, H., Sadan, V., Kirca O, Burgan I, Kellecioglu D. 2016. Hydrological and hydraulic models for determination of flood-prone and flood inundation areas. IAHS 373: 137–141.

Alahacoon, N., Matheswaran, K., Pani, P., Amarnath, G. 2018. "A Decadal Historical Satellite Data and Rainfall Trend Analysis (2001–2016) for Flood Hazard Mapping in Sri Lanka." *Remote Sensing* 10(3).

Alemu, Y. T. 2015. "Flash Flood Hazard in Dire Dawa , Ethiopia." *Journal of Social Sciences and Humanities* 1(4): 400–414.

Amaguchi, H., Kawamura, A. 2016. Evaluation of Climate Change Impacts on Urban Drainage Systems by a Storm Runoff Model with a Vector-Based Catchment Delineation. World Environmental and Water Resources Congress 2016, 595-606

Amani, M., Brisco, B., Afshar M, Mirmazloumi SM, Mahdavi S, Mirzadeh SMJ, Huang W, Granger J. 2019. A generalized supervised classification scheme to produce provincial wetland inventory maps: an application of Google Earth Engine for big geo data processing, Big Earth Data, 3:4, 378-394, DOI: 10.1080/20964471.2019.1690404.

Anteneh, Y., Stellmacher, T., Zeleke, G., Mekuria, W., Gebremariam, E. 2018. Dynamics of land change: insights from a three-level intensity analysis of the Legedadie-Dire catchments, Ethiopia Environ Monit Assess 190:309. https://doi.org/10.1007/s10661-018-6688-1

Aryal, D., Wang, L., Adhikari, T. R., Zhou, J., Li, X., Shrestha, M., Wang, Y., & Chen, D. 2020. "A model-based flood hazard mapping on the southern slope of Himalaya." *Water* 12(540). https://doi.org/10.3390/w12020540.

Assefa, T, H. 2018. Flood Risk Assessment in Ethiopia Civil and Environmental Research. 10(1): 2224-5790

Ayalew, D., Tesfaye, K.., Mamo, G., Yitaferu, B., Bayu, W. 2012. Outlook of future climate in Northwestern Ethiopia. Agric. Sci. 3(4): 608–624. http://doi.org/10.4236/as.2012.34074

Aychiluhim M. 2016. Adama Flood Problem –Flood Risk Mitigation Option For Boku Shenen Area. Addis Ababa Institute of Technology School Of Civil And Environmental Engineering Hydraulic Engineering Stream. Thesis.

Bajracharya, A. R., Rai, R. R., Rana, S. (2015) Effects of Urbanization on Storm Water Run-off: A Case Study of Kathmandu Metropolitan City, Nepal. Journal of the Institute of Engineering 11(1): 36-49. DOI: 10.3126/jie. v11i1.14694.

Bamford, T., B, Digman C. J, Balmforth, D. J., Waller, S, Hunter, N. 2008. Modelling flood risk – an evaluation of different methods. WaPUG Autumn Conference 2008.

Bansode, A., Patil, K. A. (2014) Estimation of runoff by using SCS curve number method and arc GIS. Int J Sci Eng Res 5(7):1283–1287.

Barroca B, Pacteau C (2018) Resilience and urban design: what does the French flood of 2016 teach us? TECHNE 15(2018):31– 38. https ://doi.org/10.13128 /Techn e-23199

Bathrellos, G. D., Karymbalis, E., Skilodimou, H. D., Gaki-Papanastassiou, K., Baltas, E. A. (2016). "Urban flood hazard assessment in the basin of Athens Metropolitan

city, Greece." *Environvironmental Earth Sciences* 75:319. DOI 10.1007/s12665-015-5157-1.

Batica J, Gourbesville P and Hu F (2013) Methodology for Flood Resilience Index. International Conference on Flood Resilience: Experiences in Asia and Europe.

Batica, J., & Gourbesville, P. (2016) "Resilience in Flood Risk Management - A New Communication Tool." *Procedia Engineering* 154: 811–817. https://doi.org/10.1016/j.proeng.2016.07.411.

Bellos, V., Kourtis, I. M, Tsihrintzis, V. A. 2017. A simplified methodology for flood simulation in urban catchments. European Water 57: 307-313.

Berhane, A., Hadgu, G., Worku, W., Abrha, B. 2020. Trends in extreme temperature and rainfall indices in the semi-arid areas of Western Tigray, Ethiopia. Environ. Syst. Res. 9(3). https://doi.org/10.1186/s40068-020-00165-6

Berihun, B. L., Tsunekawa, A., Haregeweyn, N., Meshesha D. T, Adgo, E., Tsubo, M., Masunaga, T., Fenta, A. A., Sultan, D., Yibeltal, M. 2019. Exploring land use/land cover changes, drivers and their implications in contrasting agro-ecological environments of Ethiopia. Land Use Policy 87 (2019) 104052

Berihun, M. L., Tsunekawa, A., Haregeweyn, N., Meshesha, D. T., Adgo, E.,Tsubo, M., Masunaga, T. Fenta, A. A., Sultan, D., Yibeltal, M.2018.Exploring land use/land cover changes, drivers and their implications in contrasting agro-ecological environments of Ethiopia. Land Use Policy 87 (2019) 104052

Berkes, F. (2007). Understanding uncertainty and reducing vulnerability: lessons from resilience thinking. Natural Hazards, 41(2), 283-295.

Beyene, T.D., Moges, M.A., Tilahun, S.A. 2019. Development of rainfall disaggregation model in the Awash River Basin, Ethiopia, in: Advances of Science and Technology 6th EAI International Conference, ICAST 2018. Springer International Publishing, pp. 50–64. https://doi.org/10.1007/978-3-030-15357-1_4

Bhagat, N. 2017. Flood Frequency Analysis Using Gumbel's Distribution Method: A Case Study of Lower Mahi Basin, India. Journal of Water Resources and Ocean Science 6, 51–54. https://doi.org/10.11648/j.wros.20170604.11

Bharali, B. 2015. A Study on Frequency Analysis for Puthimari Catchment by Gumbel Distribution Method. Journal of Civil Engineering and Environmental Technology 2, 19–22.

Billi, P., Alemu, Y. T., Ciampalini, R. 2015. Increased frequency of flash floods in Dire Dawa, Ethiopia: Change in rainfall intensity or human impact? Nat Hazards. 76:1373–1394. DOI 10.1007/s11069-014-1554-0.

Birhanu, D., Kima, H., Jang, C, Parka, S. 2016. Flood Risk and Vulnerability of Addis Ababa City Due to Climate Change and Urbanization. In: 12th International Conference on Hydroinformatics, HIC 2016. Procedia Engineering 154 (2016): 696 – 702.

Bisht D, S, Chatterjee C, Kalakoti S, Upadhyay P, Sahoo M, Panda A 2016. Modeling urban floods and drainage using SWMM and MIKE URBAN: a case study. Natural Hazards 84(2): 749-776.

Bouvier C, Chahinian N, Adamovic M, Cassé C, Crespy A, Crès A (2017) LARGE-SCALE GIS-BASED URBAN FLOOD MODELLING: A CASE STUDY ON THE CITY OF OUAGADOUGOU. SimHydro 2017: Choosing the Right Model in Applied Hydraulics.

Buba, L.F., Kura, N.U., Dakagan, J.B., 2017. Spatiotemporal trend analysis of changing rainfall characteristics in Guinea Savanna of Nigeria. Modeling Earth Systems and Environment. https://doi.org/10.1007/s40808-017-0356-2

Bulti D, T, Assefa T 2019. Analyzing ecological footprint of residential building construction in Adama City, Ethiopia. Journal of Environmental Systems Research 8(2). https://doi.org/10.1186/s40068-019-0130-8

Bulti, D. T., Mekonnen, B., Bekele, M. 2017. Assessment of Adama City Flood Risk Using Multicriteria Approach. The Ethiopian Journal of Science and Sustainable Development (EJSSD) 4(1): 6-23.

Burns, M, J, Schubert, J, E, Fletcher, T. D., Sanders, B. F. 2015. Testing the impact of at-source stormwater management on urban flooding through a coupling of network and overland flow models. WIREs Water. doi: 10.1002/wat2.1078.

Butler, D, Davies, J. 2011. Urban Drainage. 3rd edition; Taylor and Francis Group. London.

Cao, C., Xu, P. H., Wang, Y. H., Chen, J. P., Zheng, L. J., Niu, C. C. 2016. “Flash Flood Hazard Susceptibility Mapping Using Frequency Ratio and Statistical Index Methods in Coalmine Subsidence Areas.” *Sustainability* 8(948). doi:10.3390/su8090948.

Chabaeva, A., Civco, D.L. & Hurd, J.D. 2009. “Assessment of impervious surface estimation techniques.” *Journal of Hydrologic Engineering* 14(4): 377-387.

Chattefuee, S., Hadi, A. S. (2006) Regression analysis by example, 4th edn. John Wiley and Sons Inc, Hoboken

Chemeda Y. C. 2020. Engineering Geological Investigation of Adama Town: Implication to Engineering Practice. Ethiopian Journal of Science and Sustainable Development 7(2) 103-116

Chen, A. S., Hammond, M., Domingo, N. D., Hénonin, J., Russo, B., Mark, O. et al. 2014. WP2 Urban Flood Modelling. Consistent framework for analysis of urban flood risks, CORFU.

Chen, J, Theller L, Gitau, M. W., Engel B. A., Harbor J. M. .2017. Urbanization impacts on surface runoff of the contiguous United States. Journal of Environmental Management 187: 470e481. https://doi.org/10.1016/j.jenvman.2016.11.017.

Chen, J., Hill, A. A., Urbano, L. D. 2009. “A GIS-based model for urban flood inundation.” *Journal of Hydrology* 373: 184–192. doi:10.1016/j.jhydrol.2009.04.021.

Chen, J., Theller, L., Gitau, M. W., Engel, B. A., Harbor, J. M. 2017. “Urbanization impacts on surface runoff of the contiguous United States.” *Journal of Environomental Management* 187:470–481. https ://doi.org/10.1016/j.jenvm an.2016.11.017.

Chen, X., Tian, C., Meng, X., Xu, Q., Cui, G., Zhang, Q., Xiang, X. 2015. Analyzing the effect of urbanization on flood characteristics at catchment levels. International Association of Hydrological Sciences 370: 33–38.

Chen, Y., Wang, Q., Wang, Y., Duan, S., Xu, M., Li, Z. 2016 A Spectral Signature Shape-Based Algorithm for Landsat Image Classification. ISPRS Int. J. Geo-Inf. 5(154): 1-16. doi:10.3390/ijgi5090154.

Cheng, L., AghaKouchak, A., Gilleland, E., Katz, R.W., 2014. Non-stationary extreme value analysis in a changing climate. Climatic Change. https://doi.org/10.1007/s10584-014-1254-5

Cherian, B, Das DP, John L, Devadathan M, Malakeel, G. S. 2017. A Study on Impact of Urbanization on Surface Runoff in Muvattupuzha Municipality. International Journal of Innovative Research in Science, Engineering and Technology 6(4): 5814-5821. DOI:10.15680/IJIRSET.2017.0604195.

Choi. G, Collins D, Ren G, Trewin B, Baldi M, Fukuda Y, Afzaal M, Pianmana T, Gomboluudev P, Huong PTT, et al (2009) Changes in means and extreme events of temperature and precipitation in the Asia-Pacific network region, 1955–2007. Int. J. Climatol. 29: 1906-1925. https://doi.org/10.1002/joc.1979

Chu J, T, Xia J, Xu CY, Singh VP (2010) Statistical downscaling of daily mean temperature, pan evaporation and precipitation for climate change scenarios in Haihe River, China. Theor Appl. Climatol. 99: 149–161. https://doi.org/10.1007/s00704-009-0129-6

Conference

Congalton R, G and Green K (2009) Assessing the accuracy of remotely sensed data: principles and practices, 2nd edn. CRS Press, Taylor and Francis, Baco Ratton.

Cook, L.M., McGinnis, S., Samaras, C., 2020. The effect of modeling choices on updating intensity-duration-frequency curves and stormwater infrastructure designs for climate change. Climatic Change 159, 289–308. https://doi.org/10.1007/s10584-019-02649-6

Coronado-Hernández, Ó.E., Merlano-Sabalza, E., Díaz-Vergara, Z., Coronado-Hernández, J.R., 2020. Selection of hydrological probability distributions for extreme rainfall events in the regions of Colombia. Water 12. https://doi.org/10.3390/W12051397

de Paola, F., Giugni, M., Topa, M.E., Bucchignani, E., 2014. Intensity-Duration-Frequency (IDF) rainfall curves, for data series and climate projection in African cities. SpringerPlus 3, 1–18. https://doi.org/10.1186/2193-1801-3-133

Deb P, Babel MS, Denis AF (2018) Multi-GCMs approach for assessing climate change impact on water resources in Thailand. Modeling Earth Systems and Environment. https://doi.org/10.1007/s40808-018-0428-y

Deb, P., Babel, M.S., Denis, A.F., 2018. Multi-GCMs approach for assessing climate change impact on water resources in Thailand. Modeling Earth Systems and Environment. https://doi.org/10.1007/s40808-018-0428-y

Degife, A., Worku, H., Gizaw, S., Legesse, A. 2019. Land use land cover dynamics, its drivers and environmental implications in Lake Hawassa Watershed of Ethiopia, Remote Sensing Applications: Society and Environment. https://doi.org/10.1016/j.rsase.2019.03.005.

Demeke G, G and Andualem TG (2018) Application of Remote Sensing for Evaluation of Land Use Change Responses on Hydrology of Muga Watershed, Abbay River Basin, Ethiopia. J Earth Sci Clim Change 9 (493). doi: 10.4172/21577617.1000493.

DIBABA W., T. (2018) A REVIEW OF SUSTAINABILITY OF URBAN DRAINAGE SYSTEM: TRAITS AND CONSEQUENCES. Journal of Sedimentary Environments. 3 (3): 131-137. doi: 10.12957/jse.2018.37825

Dile, Y, T, Berndtsson R, Setegn SG (2013) Hydrological response to climate change for gilgel abay river, in the lake tana basin-upper Blue Nile basin of Ethiopia. PloS one 8(10): e79296

Dinh, Q., Balica, S., Popescu, I., Jonoski, A. 2012. "Climate change impact on flood hazard, vulnerability and risk of the Long Xuyen Quadrangle in the Mekong Delta." *International Journal of River Basin Management* 10 (1): 103-120. http://dx.doi.org/10.1080/15715124.2012.663383.

Dongquan, Z., Jining, C., Haozheng, W., Qingyuan, T., Shangbing, C., Zheng, S. 2009. "GIS-based urban rainfall-runoff modeling using an automatic catchment-discretization approach: a case study in Macau." *Environvironmental Earth Sciences* 59:465–472. DOI 10.1007/s12665-009-0045-1.

Douglas I., Kurshid Alam, Maryanne Maghenda, Yasmin Mcdonnell, Louise Mclean and Jack (2008). Unjust waters: climate change, flooding and the urban poor in Africa. Environment & Urbanization Vol 20(1): 187–205. DOI: 10.1177/0956247808089156

Emilsson T and Ode Sang A (2017) Impacts of Climate Change on Urban Areas and Nature-Based Solutions for Adaptation. In Kabisch et al. (eds.), Nature-based Solutions to Climate Change Adaptation in Urban Areas, Theory and Practice of Urban Sustainability Transitions. DOI: 10.1007/978-3-319-56091-5_2.

Emiru Birhane, E., Ashfare, H., Fenta, A.A., Hishe, H.,Gebremedhin, M. A., Wahed, H. G., Solomon, N. 2019. Land use land cover changes along topographic gradients in Hugumburda national forest priority area, Northern Ethiopia. Remote Sensing Applications: Society and Environment 13: 61–68

Engida, A.N., Esteves, M., 2011. Characterization and disaggregation of daily rainfall in the Upper Blue Nile Basin in Ethiopia. Journal of Hydrology 399, 226–234. https://doi.org/10.1016/j.jhydrol.2011.01.001

Erena S, H and Worku H (2018) Flood risk analysis causes and landscape based mitigation strategies in Dire Dawa city, Ethiopia. Geoenvironmental Disasters 5(16). DOI: 10.1186/s40677-018-0110-8.

Erena, S. H., Worku, H., & Paola, F. De. 2018. "Flood hazard mapping using FLO-2D and local management strategies of Dire Dawa city, Ethiopia" *Journal of Hydrology : Regional Studies* 19: 224–239.. https://doi.org/10.1016/j.ejrh.2018.09.005.

Ewea, H.A., Elfeki, A.M., Bahrawi, J.A., Al-amri, N.S., 2018. Modeling of IDF curves for stormwater design in Makkah Al Mukarramah region , The Kingdom of Saudi Arabia. Open Geoscience 10, 954–969.

Fadhel, S., Rico-ramirez, M.A., Han, D., 2017. Uncertainty of Intensity – Duration – Frequency (IDF) curves due to varied climate baseline periods. Journal of Hydrology 547, 600–612. https://doi.org/10.1016/j.jhydrol.2017.02.013

Feyissa G, Zeleke G, Bewket W, Gebremariam E (2018) Downscaling of Future Temperature and Precipitation Extremes in Addis Ababa under Climate Change. Climate 6(58). https://doi.org/10.3390/cli6030058

Fonji S, F and Taff GN (2014) Using satellite data to monitor land-use land-cover change in North-eastern Latvia. SpringerPlus 3 (61). doi:10.1186/2193-1801-3-61.

Foody GM (2002) Status of land cover classification accuracy assessment. Remote Sensing of Environment 80 (2002) 185– 201. DOI: 10.1016/s0034-4257(01)00295-4.

Forkuo, E. K., & Quaye-ballard, J. A. 2013. "GIS Based Fire Emergency Response System." *International Journal of Remote Sensing and GIS* 2(1): 32–40.

Gebrechorkos SH, Hülsmann S, Bernhofer C (2019) Statistically downscaled climate dataset for East Africa. Scientific Data 6 (31). https://doi.org/10.1038/s41597-019-0038-1

Gebreigziabher, E.T., 2020. Analysis Rainfall Intensity-Duration-Frequencyrelationships Under Climate Change for Mekele City, Ethiopia. International Journal of Technical Research & Science 05, 1–11. https://doi.org/10.30780/ijtrs.v05.i02.001

Gebremedhin, Y.G., 2017. Development of Rainfall Intensity-Duration-Frequency (IDF) Relationships for Siti Zone , In Case of Ethiopia Somali Regional State. Civil and Environmental Research 9, 10–28.

Gebru, T.A., 2020. Rainfall Intensity-Duration-Frequency Relations under Changing Climate for Selected Stations in the Tigray Region, Ethiopia. Journal of Hydrologic Engineering 25. https://doi.org/10.1061/(asce)he.1943-5584.0001999

Gelman A (2012) P-values and statistical practice. epidemiology 24(1): 69–72.

Geremew GM, Mini S, Abegaz A (2020) Spatiotemporal variability and trends in rainfall extremes in Enebsie Sar Midir district, northwest Ethiopia. Modeling Earth Systems and Environment. https://doi.org/10.1007/s40808-020-00749-2

Getachew HE and Melesse AM (2012) The Impact of Land Use Change on the Hydrology of the Angereb Watershed, Ethiopia. International Journal of Water 1(4): 1-7. DOI: 10.5772/56266.

Getahun Y, S and Van Lanen HAJ (2015) Assessing the Impacts of Land Use-Cover Change on Hydrology of Melka Kuntrie Subbasin in Ethiopia, Using a Conceptual Hydrological Model. Hydrol Current Res 6(210). doi:10.4172/21577587.1000210.

Gharbi M, Soualmia A, Dartus D (2016) Masbernat, L. Comparison of 1D and 2D Hydraulic Models for Floods Simulation on the Medjerda Riverin Tunisia. J. Mater. Environ. Sci. 7 (8): 3017-3026.

Gharbia S, S, Gill L, Johnston P, Pilla F (2016) Multi-GCM ensembles performance for climate projection on a GIS platform. Modeling Earth Systems and Environment 2(102): 1–21. https://doi.org/10.1007/s40808-016-0154-2

Ghazavi, R., Rabori, A. M., Reveshty, M. A. 2016. "Modelling and assessment of urban flood hazards based on rainfall intensity-duration-frequency curves reformation." *Natural Hazards and Earth System Sciences Discussion.* doi:10.5194/nhess-2016-304, 2016.

Gigovi´c, L., Pamuˇcar, D., Baji´c, Z., Drobnjak, S. 2017. "Application of GIS-Interval Rough AHP Methodology for Flood Hazard Mapping in Urban Areas." *Water* 9(360). doi:10.3390/w9060360.

Gujree I, Wani I, Muslim M, Farooq M, Meraj G (2017) Evaluating the variability and trends in extreme climate events in the Kashmir Valley using PRECIS RCM simulations. Modeling Earth Systems and Environment. https://doi.org/10.1007/s40808-017-0370-4

Gunn R, Martin A, Engel B, Ahiablame L (2012) Development of two indices for determining hydrologic implications of land use changes in urban areas. Urban Water Journal 9 (4): 239e248. http://dx.doi.org/10.1080/1573062X.2012.660957.

Gupta R, S (2017) Elements of the Hydrologic Cycle: Precipitation. In: Hydrology and Hydraulic Systems 4th edn. Waveland, US, pp 39-63.

Gutman G, Huang C, Chander G, Noojipady P, Masek JG (2013) Assessment of the NASA-USGS global landsurvey (GLS) datasets. Remote Sens. Environ. 134: 249–265.

Hailemariam, M., Ajeme, A. 2014. Solid Waste Management in Adama, Ethiopia: Aspects and Challenges. International Journal of Environmental, Ecological, Geological and Mining Engineering 8(9): 603-609

Hankin B, Waller S, Astle G, Kellagher R (2008) Mapping space for water: screening for urban flash flooding. Journal of Flood Risk Management 1: 13–22.

Hénonin J, Hongtao M, Zheng-Yu Y, Hartnack J, Havnø K, Gourbesville P, Mark O (2015) Citywide multi-grid urban flood modelling: The July 2012 flood in Beijing. Urban Water Journal 12 (1): 52-66. https://doi.org/10.1080/1573062X.2013.851710.

Huang J, Zhang J, Zhang Z, Xu C, Wang B, Yao J (2011) Estimation of future precipitation change in the Yangtze River basin by using statistical downscaling method. Stoch Environ Res Risk Assess 25: 781–792. https://doi.org/10.1007/s00477-010-0441-9

Hughes J, Sharman B (2015) Flood resilient communities: a framework and case studies. In: Asia Pacific stormwater

Huong, H. T. L., Pathirana, A. (2013) Urbanization and climate change impacts on future urban flooding in Can Tho city, Vietnam

Hydrol. Earth Syst. Sci., 17, 379–394. doi:10.5194/hess-17-379-2013

IFRC, (2014). IFRC Framework for Community Resilience. International Federation of Red Cross and Red Crescent Societies, Geneva, Switzerland.

IPCC (2014) Climate change 2014: Synthesis report. Contribution of Working Groups I, II and III to the Fifth Assessment Report of the Intergovernmental Panel on Climate Change. In: Pachauri RK, Meyer LA (eds) IPCC, Geneva, Switzerland

Jaafar K, Ismail N, Tajjudin M, Adnan R (2015) Rahiman, M. H. F. A Review on Flood Modelling and Rainfall-Runoff Relationships. 2015 IEEE 6th Control and System Graduate Research Colloquium, UiTM, Shah Alam, Malaysia. 10 – 11 August 2015: 158-162.

Jacobson C, R (2011) Identification and quantification of the hydrological impacts of imperviousness in urban catchments: A review. J. Environ. Manag. 92: 1438–1448. doi: 10.1016/j.jenvman.2011.01.018.

Jahanbazi M, Egger U (2014) Application and comparison of two different dual drainage models to assess urban flooding, Urban Water Journal 11(7): 584-595. DOI: 10.1080/1573062X.2013.871041.

Jenkins, K., Surminski, S., Hall, J., and Crick, F. (2016). Assessing surface water flood risk and management strategies under future climate change: An Agent-Based Model approach, Working Paper, 1-30

Jha A, Lamond J, Bloch R, Bhattacharya N, Lopez A, et al. (2011). Five Feet High and Rising: Cities and Flooding in the 21st Century. Policy Research Working Paper 5648

Jiang L, Chen Y, Wang H (2015) Urban flood simulation based on the SWMM model. Remote Sensing and GIS for Hydrology and Water Resources 368: 186-191. https://doi.org/10.5194/piahs-368-186-2015.

Jorge, G., Larry, A.R., Lewis, A.R. & Jennifer, D. 2010. "A new applications manual for the Storm Water Management Model (SWMM)." *Environmental Modelling & Software* 25(6): 813-814.

Josef S (2012) Dynamic Modelling of Urban Rainfall Runoff and Drainage Coupling DHI MIKE URBAN and MIKE FLOOD. University of SalzBurg.

Karamouz, M., ASCE, F., Nazif, S. 2013. Reliability-Based Flood Management in Urban Watersheds Considering Climate Change Impacts. JOURNAL OF WATER RESOURCES PLANNING AND MANAGEMENT 139:520-533

Katz, R.W., 2013. Statistical Methods for Nonstationary Extremes, in: AghaKouchak, A., Easterling, D., Hsu, K., Schubert, S., Sorooshian, S. (Eds.), Extremes in a Changing Climate:Detection, Analysis and Uncertainty. Springer Dordrecht Heidelberg, New York, pp. 15–37. https://doi.org/10.1007/978-94-007-4479-0 2

Khaing, Z. M., Zhang, K., Sawano, H., Shrestha, B. B., Sayama, T., Nakamura, K. 2019. Flood hazard mapping and assessment in data-scarce Nyaungdon area, Myanmar." *PLoS ONE* 14(11): e0224558. https://doi.org/10.1371/journal.pone.0224558.

Kossieris, P., Efstratiadis, A., 2015. European Geosciences Union General Assembly 2015 Assessing the performance of Bartlett-Lewis model on the simulation of

Athens rainfall Panagiotis Kossieris , Andreas Efstratiadis , Ioannis Tsoukalas School of Civil Engineering. https://doi.org/10.13140/RG.2.2.14371.25120

Kourgialas, N. N., Karatzas, G. P. 2017. "A national scale flood hazard mapping methodology: The case of Greece – Protection and adaptation policy approaches." *Science of the Total Environment* 601–602: 441–452.

Kourtis IM, Bellos V, Tsihrintzis VA (2017) Comparison of 1D-1D and 1D-2D urban flood models. In 15th International Conference on Environmental Science and Technology. Rhodes, Greece.

Kulkarni, A. T., Mohanty, J., Eldho, T. I., Rao, E. P., & Mohan, B. K. 2014. "Computers & Geosciences A web GIS based integrated flood assessment modeling tool for coastal urban watersheds." *Computers and Geosciences* 64: 7–14. https://doi.org/10.1016/j.cageo.2013.11.002.

Lacombe, G., Douangsavanh, S., Vogel, R.M., McCartney, M., Chemin, Y., Rebelo, L.M., Sotoukee, T., 2014. Multivariate power-law models for streamflow prediction in the Mekong Basin. Journal of Hydrology: Regional Studies 2, 35–48. https://doi.org/10.1016/j.ejrh.2014.08.002

Leandro J, Chen AS, Djordjević S, Savić DA (2009) Comparison of 1D/1D and 1D/2D Coupled (Sewer/Surface) Hydraulic Models for Urban Flood Simulation. J. Hydraul. Eng 135: 495-504. https://doi.org/10.1061/_ASCE_HY.1943-7900.0000037.

Leitão J (2009) Enhancement of Digital Elevation Models and Overland Flow Path Delineation Methods for Advanced Urban Flood Modelling. Dissertation, Department of Civil Engineering - Imperial College London, London.

Li F, Chen, J., Liu, Y., Xu, P., Sun, et al. 2019. Assessment of the Impacts of Land Use/Cover Change and Rainfall Change on Surface Runo_ in China. Sustainability 2019, 11, 3535; doi:10.3390/su11133535

Li Y., Wang, C. 2009. Impacts of Urbanization on Surface Runoff of the Dardenne Creek Watershed, St. Charles County, Missouri, Physical Geography, 30:6, 556-573. http://dx.doi.org/10.2747/0272-3646.30.6.556

Li, C., Liu, M., Hu, Y. Shi, T., Qu, X., ToddWalter, M. (2018). Effects of urbanization on direct runoff characteristics in urban functional zones. Science of the Total Environment 643 (2018) 301–311

Liao, K. 2012. "A theory on urban resilience to floods—a basis for alternative planning practices." *Ecology and Society* 17(4): 48.

Liao, K.-H. (2014). From flood control to flood adaptation: a case study on the Lower Green River Valley and the City of Kent in King County, Washington. Natural Hazards, 71: 723-750.

Lima MIP, Santo FE, Ramos AM, Trigo RM (2015) Trends and correlations in annual extreme precipitation indices for mainland Portugal, 1941–2007. Theoretical and Applied Climatology 119(1–2): 55–75. https://doi.org/10.1007/s00704-013-1079-6

Liu L, Liu Y, Wang X, Yu D, Liu K, Huang H, Hu G (2015) Developing an effective 2-D urban flood inundation model for city emergency management based on cellular automata. Nat. Hazards Earth Syst. Sci. 15: 381–391. doi:10.5194/nhess-15-381-2015.

Loucks D, van Beek E, Stedinger J, Dijkman, J, Villars M (2005) Water Resources Systems Planning and Management. An Introduction to Methods, Models and Applications. UNESCO, Paris.

Lu D and Weng, Q (2007) A survey of image classification methods and techniques for improving classification performance. Int. J. Remote Sens. 28: 823–870.

Luo, P. P., Mu, D. R., Xue, H., Ngo-Duc, T., Dang-Dinh, K., Takara, K., et al. 2018. "Flood inundation assessment for the Hanoi Central Area, Vietnam under historical and extreme rainfall conditions." *Scientific Reports*. 8:12623. DOI:10.1038/s41598-018-30024-5.

Mahmood R, Babel MS (2014) Future changes in extreme temperature events using the statistical downscaling model (SDSM) in the trans-boundary region of the Jhelum river basin. Weather and Climate Extremes 5-6: 56–66. http://dx.doi.org/10.1016/j.wace.2014.09.001

Maksimović Č, Prodanović D, Boonya-Aroonnet S, Leitão JP, Djordjević S, Allitt R (2009) Overland flow and pathway analysis for modelling of urban pluvial flooding. Journal of Hydraulic Research 47 (4): 512–523. https://doi.org/10.3826/jhr.2009.3361.

Mark O, Weesakul S, Apirumanekul C, Aroonnet S, Djordjevic S (2004) Potential and limitations of 1D modelling of urban flooding. Journal of Hydrology 299: 284–299. https://doi.org/10.1016/j.jhydrol.2004.08.014.

Meerow S, Joshua P, Newell JP and Stults M (2016) Defining urban resilience: A review. Landscape and Urban Planning 147: 38–49.

Mejía AI and Moglen GE (2009) Spatial patterns of urban development from optimization of flood peaks and imperviousness-based measures. J. Hydrol. Eng. 14: 416–424.

Mekonen A. A., Berlie, A., B. 2019. Spatiotemporal variability and trends of rainfall and temperature in the Northeastern Highlands of Ethiopia. Modeling Earth Systems and Environment. https://doi.org/10.1007/s40808-019-00678-9

Mekonnen DF, Disse M (2018) Analyzing the future climate change of Upper Blue Nile River basin using statistical downscaling techniques. Hydrol. Earth Syst. Sci. 22: 2391–2408. https://doi.org/10.5194/hess-22-2391-2018

Mekonnen DF, Duan Z, Rientjes T, Disse M (2018) Analysis of combined and isolated effects of land-use and land-cover changes and climate change on the upper Blue Nile River basin's stream flow. Hydrol. Earth Syst. Sci. 22: 6187–6207. https://doi.org/10.5194/hess-22-6187-2018.

Meng, X., Zhang, M., Wen, J., Du, S., Xu, H., Wang, L., & Yang, Y. 2019. "A Simple GIS-Based Model for Urban Rainstorm Inundation Simulation." Sustainablity 11(2830). https://doi.org/10.3390/su11102830

Mentens J, Raes D, Hermy M (2006) Green roofs as a tool for solving the rainwater runoff problem in the urbanized 21st century? Landscape and Urban Planning 77: 217–226. doi:10.1016/j.landurbplan.2005.02.010.

Mirhosseini G., Srivastava P., Stefanova L., 2013. The impact of climate change on rainfall Intensity–Duration–Frequency (IDF) curves in Alabama. Reg Environ Change 13, S25–S33. https://doi.org/10.1007/s10113-012-0375-5

Mishra, B. K., Herath, S. 2014. "Assessment of Future Floods in the Bagmati River Basin of Nepal Using Bias-Corrected Daily GCM Precipitation Data." *Journal of Hydrologic Engineering* 05014027-2. DOI: 10.1061/(ASCE)HE.1943-5584.0001090.

Mohammed M, Biazn B, Belete MD (2020) Hydrological Impacts of Climate Change in Tikur Wuha Watershed, Ethiopian Rift Valley Basin. Journal of Environment and Earth Science 10(2): 28-49. https://doi.org/10.7176/JEES/10-2-04

Mohammed Y, Yimer F, Tadesse M, et al (2018) Variability and trends of rainfall extreme events in north east highlands of Ethiopia. Int J Hydro. 2(5): 594–605. https://doi.org/10.15406/ijh.2018.02.00131

Moriasi, D.N., Arnold, J.G., Liew, M.W. Van, Bingner, R.L., Harmel, R.D., Veith, T.L., 2007. MODEL EVALUATION GUIDELINES FOR SYSTEMATIC QUANTIFICATION OF ACCURACY IN WATERSHED SIMULATIONS. American Society of Agricultural and Biological Engineers ISSN 50, 885–900.

Moses O, Gondwe M (2019) Simulation of changes in the twenty-first century maximum temperatures using the statistical downscaling model at some stations in Botswana. Modeling Earth Systems and Environment. https://doi.org/10.1007/s40808-019-00571-5

Moujahid, M., Stour, L., Agoumi, A., Saidi, A., 2018. Regional approach for the analysis of annual maximum daily precipitation in northern Morocco. Weather and Climate Extremes 21, 43–51. https://doi.org/10.1016/j.wace.2018.05.005

Mujere, N., 2011. Flood Frequency Analysis Using the Gumbel Distribution. International Journal on Computer Science and Engineering (IJCSE) 3, 2774–2778.

Mulatu Liyew Berihun, M. L., Tsunekawa, A., Haregeweyn, N., Meshesha, D. T.,Adgo, E. Tsubo, M., Masunaga, T., Fenta, A. A., Sultan, D., Yibeltal, M. 2019. Exploring land use/land cover changes, drivers and their implications in contrasting agro-ecological environments of Ethiopia. Land Use Policy 87 (2019) 104052

Muzaffar, M.B., 2016. The Development and Validation of a Scalte to Measure Training Culture: The TC Scale. Journal of Culture, Society and Development 23, 49–58.

Natarajan, S., Radhakrishnan, N., 2019. Simulation of extreme event - based rainfall – runoff process of an urban catchment area using HEC - HMS. Modeling Earth Systems and Environment. https://doi.org/10.1007/s40808-019-00644-5

Navarro-Racines C, Tarapues J, Thornton P, Jarvis A, Ramirez-Villega J (2020) High-resolution and bias-corrected CMIP5 projections for climate change impact assessments 7(7). https://doi.org/10.1038/s41597-019-0343-8

NDRMC 2018. “Federal Democratic Republic of Ethiopia National Disaster Risk Management Commission , Early Warning and Emergency Response Directorate Revised Flood Alert (Issue May)”.

Ngongondo C, Chong Y, Lottschalk L, Alemaw B (2011) Evaluation of spatial and temporal characteristics of rainfall in Malawi: a case of data scarce region. Theor Appl Climatol. 106(1–2): 79–93

Nie N., Lindholm, O., Lindholm, G., Syversen, E. 2009. Impacts of climate change on urban drainage systems – a case study in Fredrikstad, Norway, Urban Water Journal, 6:4, 323-332. http://dx.doi.org/10.1080/15730620802600924

Nigusse, A. G., Adhanom, O. G. 2019. "Flood Hazard and Flood Risk Vulnerability Mapping Using Geo-Spatial and MCDA around Adigrat, Tigray Region, Northern Ethiopia." Momona Ethiopian Journal of Science 11(1):90-107. http://dx.doi.org/10.4314/mejs.v11i1.6.

Noor, M., Ismail, T., Chung, E.-S., Shahid, S., Sung, J.H., 2018. Uncertainty in rainfall intensity duration frequency curves of Peninsular Malaysia under changing climate scenarios. Water 10. https://doi.org/10.3390/w10121750

Ogato, G. S., Bantider, A., Abebe, K., Geneletti, D. 2020. "Geographic information system (GIS)-Based multicriteria analysis of flooding hazard and risk in Ambo Town and its watershed, West shoa zone, oromia regional State, Ethiopia." *Journal of Hydrology: Regional Studies* 27(100659).

Ohana-Levi, N., Givati, A., Alfasi, N., Peeters, A., Karnieli, A. 2017. Predicting the effects of urbanization on runoff after frequent rainfall events, Journal of Land Use Science, DOI: 10.1080/1747423X.2017.1385653

Pandey AC (2017) Geospatial technique for runoff estimation based on scs-cn method in upper south koel river basin of Jharkhand (India). Int J Hydro. 1(7): 213–220. DOI: 10.15406/ijh.2017.01.00037.

Parece TE and Campbell JB (2013) Comparing Urban Impervious Surface Identification Using Landsat and High-Resolution Aerial Photography. Remote Sens. 5: 4942-4960. doi:10.3390/rs5104942.

Parsasyrat L., Jamali A. (2015). The Effects of Impermeable Surfaces on the Flooding Possibility in ZarrinShahr, Isfahan Municipal Watershed, J. Appl. Environ. Biol. Sci., 5(1)28-38, 2015

Patel, D. P., Ramirez, J. A., & Srivastava, P. K. 2017. "Assessment of flood inundation mapping of Surat city by coupled 1D/2D hydrodynamic modeling: a case application of the new HEC-RAS 5." *Natural Hazards.* https://doi.org/10.1007/s11069-017-2956-6.

Pathirana A., Denekew H., Veerbeek W., Zevenbergen C., Banda A. (2014). Impact of urban growth-driven land-use change on microclimate and extreme precipitation-A sensitivity study. Journal of Atmospheric Research. 138, 59-72.

Pervez S, Henebry GM (2014) Projections of the Ganges-Brahmaputra precipitation—downscaled from GCM predictors, Journal of Hydrology. http://doi.org/10.1016/j.jhydrol.2014.05.016

Phiri D and Morgenroth J (2017) Developments in Landsat Land Cover Classification Methods: A Review. Remote Sens 9(967). doi:10.3390/rs9090967.

Pinos, J., Timbe, L. 2019. "Performance assessment of two-dimensional hydraulic models for generation of flood inundation maps in mountain river basins." *Water Science and Engineering* 12 (1):11–8.

Quinlan A. E., Blazquez M. B., Haider L. J., Peterson G. D. (2016). Measuring and assessing resilience. Journal of Applied Ecology. 53. 677- 687.

Ramamurthy P, Bou-Zeid E (2014) Contribution of impervious surfaces to urban evaporation. Water Resour. Res. 50: 2889–2902. doi:10.1002/2013WR013909.

Rangari VA, Gonugunta R, Umamahesh NV, Patel AK, Bhatt CM (2018) 1D-2D Modeling of Urban Floods and Risk Map Generation for The Part of Hyderabad City. The International Archives of the Photogrammetry, Remote Sensing and Spatial Information Sciences XLII-5: 445-450. https://doi.org/10.5194/isprs-archives-XLII-5-445-2018.

Rangari, V. A., Gonugunta, R., Umamahesh, N. ., Patel, A. K., & Bhatt, C. M. 2018. "1D-2D MODELING OF URBAN FLOODS AND RISK MAP GENERATION FOR THE PART OF HYDERABAD CITY." *The International Archives of the Photogrammetry, Remote Sensing and Spatial Information Sciences* XLII–5: 445–450. https://doi.org/https://doi.org/10.5194/isprs-archives-XLII-5-445-2018.

Rao GS, Giridhar MVSS, Mohan S, Sowmya P (2017) SCS-CN Method and Geomatics Approach for Fully distributed Runoff Modelling. International Journal of Computational Engineering Research (IJCER) 7(9): 20-26.

Rao YRS, Ramana RV (2015) Storm Water Flood Modeling in Urban Areas. International Journal of Research in Engineering and Technology 4(11): 18-21.

Rao, Y.R.S., Ramana, R.V., 2015. STORM WATER FLOOD MODELING IN URBAN AREAS. IJRET: International Journal of Research in Engineering and Technology 04, 18–21.

Re, M., Kazimierski, L. D., Badano, N. D. 2019. "High-resolution urban flood model for risk mitigation validated with records collected by the affected community." *Journal of Flood Risk Management*. doi: 10.1111/jfr3.12524.

Rosenberg, E. A., Keys, P. K., Booth D. B., Hartley D., Burkey, J., Steinemann, A. C., Lettenmaier, D. P. 2010. Precipitation extremes and the impacts of climate change on stormwater infrastructure in Washington State. Climatic Change (2010) 102:319–349. DOI 10.1007/s10584-010-9847-0

Rosenzweig BR, McPhillips L, Chang H, Cheng C, Welty C, Matsler M, Iwaniec D (2018) Davidson, C. I. Pluvial flood risk and opportunities for resilience. WIREs Water e1302. https://doi.org/10.1002/wat2.1302.

Rossman, L. A. 2015. "Storm Water Management Model User's Manual Version 5.1, EPA/600/R-14/413b" *US EPA National Risk Management Research Laboratory,Cincinnati*, Ohio, USA.

Rukundo E, Doğan A (2016) Assessment of climate and land use change projections and their impacts on flooding. Pol. J. Environ. Stud. 25: 2541–2551

Rusli, N., Majid, M. R. 2012. "Digital Elevation Model (DEM) Extraction from Google Earth: a Study in Sungai Muar Watershed." *Applied Geoinformatics for Society and Environment* 24-28.

Saberifar R. and Shokri H. (2016). Analyzing the effects of urban development on flooding in the cities: case of Birjand city. Natural Environment Change. 2(2): 177-186.

Salvacion AR, Magcale-Macandog DB, Sta. Cruz PC, Saludes RB, Pangga IB, Cumagun CJR (2018) Evaluation and spatial downscaling of CRU TS precipitation data in the Philippines. Modeling Earth Systems and Environment. https://doi.org/10.1007/s40808-018-0477-2

Samuale T, Raj A, Girmay G (2014) Assessment of climate change impact on the hydrology of Geba catchment, Northern Ethiopia. Am. J. Environ. Eng. 4: 25–31

Santo FE, Ramos AM, Lima MIP, Trigo RM (2013) Seasonal changes in daily precipitation extremes in mainland Portugal from 1941 to 2007. Reg Environ Change. https://doi.org/10.1007/s10113-013-0515-6

Sañudo, E., Cea, L., Puertas, J. 2020. "Modelling Pluvial Flooding in Urban Areas Coupling the Models Iber and SWMM." *Water* 12(2647). doi:10.3390/w12092647.

Sanyal, J, Densmore AL, Carbonneau P (2014) Analyzing the effect of land-use/cover changes a sub-catchment levels on downstream flood peaks: A semi-distributed modelling approach with sparse data, Catena 118: 28–40. https://doi.org/10.1016/j.catena.2014.01.015.

Schlauß S, Grottker M (2016) Coupling Process for 1D-2D Numerical Flash Flood Simulation: A Parameter Study of Involved Variables for Gullies and Manholes. International Junior Researcher and Engineer Workshop on Hydraulic Structures. https://doi.org/10.15142/T3759N.

Seltman HJ (2018) Experimental design and analysis. http://www.stat.cmu. edu/hselt man/309/Book/. Accessed 5 Sept 2018

Semenov MA, Stratonovitch P (2010) Use of multi-model ensembles from global climate models for assessment of climate change impacts. Climate Research 41: 1–14. https://doi.org/10.3354/cr00836

Sepehri, M., Malekinezhad, H., Hosseini, S. Z., Ildoromi, A. R. 2017. "Assessment of flood hazard mapping in urban areas using entropy weighting method: a case study in Hamadan city, Iran." Acta Geophysica. https://doi.org/10.1007/s11600-019-00342-x.

Serre, D., Barroca, B., Balsells, M., Becue, V. 2018. Contributing to urban resilience to floods with neighbourhood design: the case of Am Sandtorkai/Dalmannkai in Hamburg. J Flood Risk Management 11 (2018) S69–S83

Sertel E and Akay SS (2015) High resolution mapping of urban areas using SPOT-5 images and ancillary data. International Journal of Environment and Geoinformatics 2(2): 63-76.

Shang H, Yan J, Gebremichael M, Ayalew SM (2011) Trend analysis of extreme precipitation in the Northwestern Highlands of Ethiopia with a case study of Debre Markos. Hydrol Earth Syst Sci 15:1937–1944. https ://doi.org/10.5194/hess-15-1937-2011

Sharma, A., Gupta, D. 2014. "DERIVATION OF TOPOGRAPHIC MAP FROM ELEVATION DATA AVAILABLE IN GOOGLE EARTH." Civil Engineering and Urban Planning: An International Journal (CiVEJ) 1(2): 14-21.

Shawul A. A., Chakma, S. 2020. Trend of extreme precipitation indices and analysis of long-term climate variability in the Upper Awash basin, Ethiopia. Theoretical and Applied Climatology. https://doi.org/10.1007/s00704-020-03112-8

Shen, J., Zhang, Q. 2014. "Parameter estimation method for SWMM under the condition of incomplete information based on GIS and RS." EJGE 20(14): 6095-6108.

Shewangizaw D and Michael Y (2010) Assessing the Effect of Land Use Change on the Hydraulic Regime of Lake Awassa. Nile Basin Water Science & Engineering Journal 3(2): 110-118.

Shiferaw H, Gebremedhin A, Gebretsadkan T, Zenebe A (2018) Modelling hydrological response under climate change scenarios using SWAT model: the case of Ilala watershed, Northern Ethiopia. Model. Earth Syst. Environ. http://dx.doi.org/10.1007/s40808-018-0439-8

Shin S, Lee S, Judi DR, Parvania M, Goharian E, McPherson T, Burian SJ (2018) A systematic review of quantitative resilience measures for water infrastructure systems. Water 10:164. https://doi.org/10.3390/w1002 0164

Shrestha, A., Babel, M.S., Weesakul, S., Vojinovic, Z., 2017. Developing Intensity-Duration-Frequency (IDF) curves under climate change uncertainty: The case of Bangkok, Thailand. Water 9. https://doi.org/10.3390/w9020145

Sillmann, J., Thorarinsdottir, T., Keenlyside, N., Schaller, N., Alexander, L. V, Hegerl, G., Seneviratne, S.I., Vautard, R., Zhang, X., Zwiers, F.W., 2017. Understanding , modeling and predicting weather and climate extremes : Challenges and opportunities. Weather and Climate Extremes 18, 65–74. https://doi.org/10.1016/j.wace.2017.10.003

Simões N, Ochoa S, Leitão J, Pina R, Sá Marques A, Maksimović Č (2011) Urban drainage models for flood forecasting: 1D/1D, 1D/2D and hybrid models. In 12th International Conference of Urban Drainage, Porto Alegre/Brasil.

Singh, T. B., Sephu , Khwairakpam , D. 2016. Investigation on Urban DrainageSystem inSululta City,Ethiopia. International Journal of Engineering Studies 8(1):1-10

Sinha P., Verma N.K., Ayele E. (2016). Urban Built-up Area Extraction and Change Detection of Adama Municipal Area using Time-Series Landsat Images. International Journal of Advanced Remote Sensing and GIS. 5 (8): 1886-1895. https://doi.org/10.23953/cloud.ijarsg.67.

Smits, A. J. M., P. H. Nienhuis, and H. L. F. Saeijs. (2006). Changing estuaries, changing views. Hydro-biologia. 565:339-355.

Solaiman, T.A., Simonovic, S.P., 2011. Development of Probability Based Intensity-Duration-Frequency Curves under Climate Change. London, Canada.

Steffen M (2019) CRAN-Package imputeTS. R J. 1: 207–218.

Su W, Ye G, Yao S, Yang G (2014) Urban land pattern impacts on floods in a new district of China. Sustainability 6: 6488–6508. doi:10.3390/su6106488.

Subramanya K (2008) Engineering Hydrology. 3rd Edition; McGraw-Hill Education, India.

Sui D, Maggio R (1999) Integrating GIS with hydrological modeling: practices, problems, and prospects. Computers, Environment and Urban Systems 23: 33-51.

Sun, Y., Wendi, D., Kim, D.E., Liong, S.Y., 2019. Deriving intensity – duration – frequency (IDF) curves using downscaled in situ rainfall assimilated with remote sensing data. Geoscience Letters 6. https://doi.org/10.1186/s40562-019-0147-x

Tabbutt V and Ambrogi M (2013) Estimates of Current and Future Impervious Area and Forest Lands Vulnerable to Urban Conversion for Watershed Based Land Use Planning Thurston County. United States, Environmental Protection Agency.

Tayefi V, Lane SN, Hardy RJ, Yu D (2007) A comparison of one- and two-dimensional approaches to modelling flood inundation over complex upland floodplains. Hydrol. Process 21: 3190–3202. https://doi.org/10.1002/hyp.6523.

Tesfay, A., Quraishi, S., 2017. Impact of Climate Change on the Development of Rainfall Intensity, Duration and Frequency Curves in Chiro and Hurso Stations of Eastern Ethiopia. Earth Sciences 6, 97–105. https://doi.org/10.11648/j.earth.20170605.16

Tiepolo M (2014) Flood Risk Reduction and Climate Change in Large Cities South of the Sahara. In Macchi S and Tiepolo M (eds.) Climate Change Vulnerability in Southern African Cities, Springer Climate, DOI: 10.1007/978-3-319-00672-7_2

Tilahun A and Teferie B (2015) Accuracy Assessment of Land Use Land Cover Classification using Google Earth. American Journal of Environmental Protection 4(4): 193-198. doi: 10.11648/j.ajep.20150404.14.

Tingsanchali T (2012) Urban flood disaster management. Procedia Engineering 32: 25-37. doi:10.1016/j.proeng.2012.01.1233.

Tran, H.D., Molavi, S., Muttil, N. 2011. Assessment Framework for the Impacts of Climate Change and Urbanization on Urban Drainage Systems. Pipelines 2011: A Sound Conduit for Sharing Solutions. ASCE 2011, pp1403-1412

UN (2018) Handbook of statistics. In: United Nations conference on trade and development (UNCTAD). United Nations, New York

Urgesa, A. A., Abegaz, A., Bahir, A. L., Antille, D. L. 2016. Population growth and other factors affecting land-use and land-cover changes in north-eastern Wollega, Ethiopia. Trop. Agric. (Trinidad) 93(4): 298-311

van Dijk, E., van der Meulen, J., Kluck, J., Straatman, J. H. M. 2014. "Comparing modelling techniques for analysing urban pluvial flooding." Water Science & Technology 69 (2): 305-311. doi:10.2166/wst.2013.699.

Vojinovic Z, Tutulic D (2009) On the use of 1D and coupled 1D-2D modelling approaches for assessment of flood damage in urban areas, Urban Water Journal 6(3): 183-199. https://doi.org/10.1080/15730620802566877.

Vojtek, M., Vojtekova´, J. 2016. "Flood hazard and flood risk assessment at the local spatial scale: a case study." Geomatics, Natural Hazards and Risk 7(6):1973–92. https://doi.org/10.1080/19475705.2016.1166874

Wang, Y., Zou, Y., Henrickson, K., Wang, Y., Tang, J., Park, B-J. 2017. "Google Earth elevation data extraction and accuracy assessment for transportation applications." PLoS ONE 12(4): e0175756. https://doi.org/10.1371/journal.pone.0175756.

Waseem, M., Mani, N., Andiego, G., Usman, M., 2017. a Review of Criteria of Fit for Hydrological Models. International Research Journal of Engineering and Technology 04, 1765–1772.

Wei, H., Luan, X., Li, H., Jia, J., Chen, Z., Han, L. 2018. "Elevation Data Fitting and Precision Analysis of Google Earth in Road Survey." AIP Conference Proceedings 1967 020031. https://doi.org/10.1063/1.5039003.

Weifeng L, Qiuwen C, Jingqiao M (2009) Development of 1D and 2D coupled model to simulate urban inundation: An application to Beijing Olympic Village. Chinese Science Bulletin 54 (9).

Weng Q (2010) Remote Sensing and GIS Integration: Theories, Methods, and Applications. McGraw-Hill, New York.

Wilby R. L, Dawson CW (2013) The statistical downscaling model (SDSM): Insights from one decade of application. Int. J. Clim. 33: 1707–1719

Wilby RL, Dawson CW (2007) SDSM 4.2-A decision support tool for the assessment of regional climate change impacts. https://sdsm.org.uk/software.html. Accessed 12 May 2020

Willems, P. 2013. Revision of urban drainage design rules after assessment of climate change impacts on precipitation extremes at Uccle, Belgium. Journal of Hydrology 496 (2013) 166–177

Woldetsadik, A. A. 2017. Practices of Solid Waste Management by Municipality and Community in Oromia Regional State of Ethiopia: a Case of Adama City, Ethiopia. SSRG International Journal of Agriculture & Environmental Science (SSRG – IJAES) 4(1)

XIONG, L., YAN, L., DU, T., YAN, P., LI, L., XU, W. 2018.. IMPACTS OF CLIMATE CHANGE ON URBAN EXTREME RAINFALL AND DRAINAGE INFRASTRUCTURE PERFORMANCE: A CASE STUDY IN WUHAN CITY, CHINA. IRRIGATION AND DRAINAGE

Yeo S (2013). A review of flood resilience in Fiji. In: International conference on flood resilience: experiences in Asia and Europe 5–7 September 2013, Exeter, UK

Yilmaz, A.G., Hossain, I., Perera, B.J.C., 2014. Effect of climate change and variability on extreme rainfall intensity-frequency-duration relationships: A case study of Melbourne. Hydrology and Earth System Sciences 18, 4065–4076. https://doi.org/10.5194/hess-18-4065-2014

Yohannes AW, Cotter M, Kelboro G, Dessalegn W (2018) Land Use and Land Cover Changes and Their Effects on the Landscape of Abaya-Chamo Basin, Southern Ethiopia. Land 7(2): 1-17. doi:10.3390/land7010002.

Yu H, Zhao Y, Fu Y, Li L (2018) Spatiotemporal Variance Assessment of Urban Rainstorm Waterlogging Affected by Impervious Surface Expansion: A Case Study of Guangzhou, China. Sustainability 10 (3761). doi:10.3390/su10103761

Zahiri, E.-P., Bamba, I., Famien, A.M., Koffi, A.K., Ochou, A.D., 2016. Mesoscale extreme rainfall events in West Africa: The cases of Niamey (Niger) and the Upper Ouémé Valley (Benin). Weather and Climate Extremes 13, 15–34. https://doi.org/10.1016/j.wace.2016.05.001

Zeder, J., Fischer, E.M., 2020. Observed extreme precipitation trends and scaling in Central Europe. Weather and Climate Extremes 29. https://doi.org/10.1016/j.wace.2020.100266

Zevenbergen, C., and Gersonius B. (2007). Challenges in urban flood management. Advances in urban flood management. 1-11

Zhang H, Wang T, Zhang Y, Dai Y, Jia J, Yu C, Li G, Lin Y, Lin H, Cao Y (2018) Quantifying Short-Term Urban Land Cover Change with Time-Series Landsat Data: A Comparison of Four Different Cities. Sensors 18 (4319): 1-23. doi:10.3390/s18124319.

Zhang X, Alexander L, Hegerl GC, Jones P, Tank AK, Peterson TC, Trewin B, Zwiers FW (2011) Indices for monitoring changes in extremes based on daily temperature and precipitation data. Wiley Interdiscip Rev Clim Chang 2(6): 851–870

Zhang, D-w., Quan, J., Zhang, H-b., Wang, F., Wang, H., He, X-y. 2015. "Flash flood hazard mapping: A pilot case study in Xiapu River Basin, China." Water Science and Engineering 8(3):195–204. https://doi.org/10.1016/j.wse.2015.05.002.

Zhou Q, Leng G, Huang M (2018) Impacts of future climate change on urban flood volumes in Hohhot in northern China: benefits of climate change mitigation and adaptations. Hydrol. Earth Syst. Sci., 22, 305–316. https://doi.org/10.5194/hess-22-305-2018

Zinabie, A., Kebede, B. 2020. Hydraulic Analysis of Storm Water Drainage System in Alamata Town, South Tigray, Ethiopia. Iranian (Iranica) Journal of Energy & Environment 11(1): 40-50

ANNEX

A: Flood inundation maps

Scenario-I: Existing LULC and Historical rainfall

	Water depth	Flow velocity
5-yr	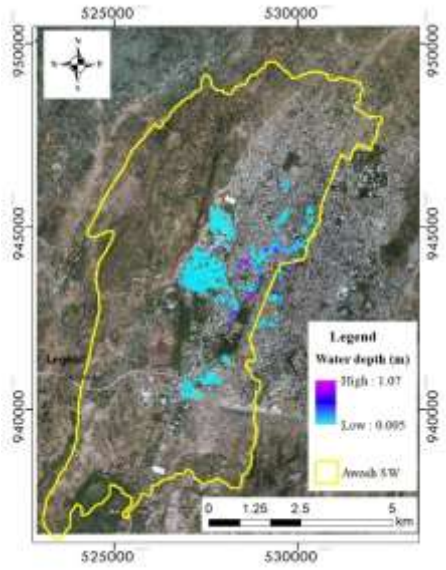	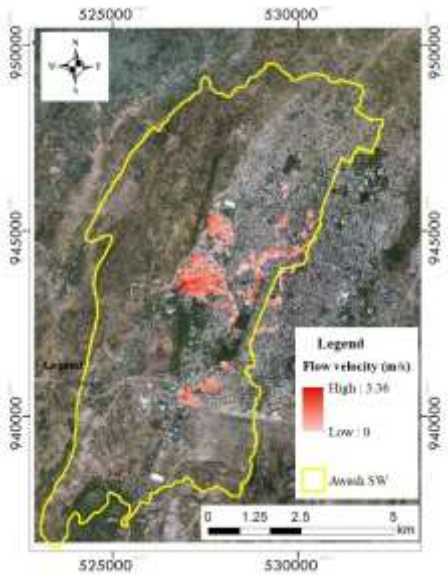
10-yr	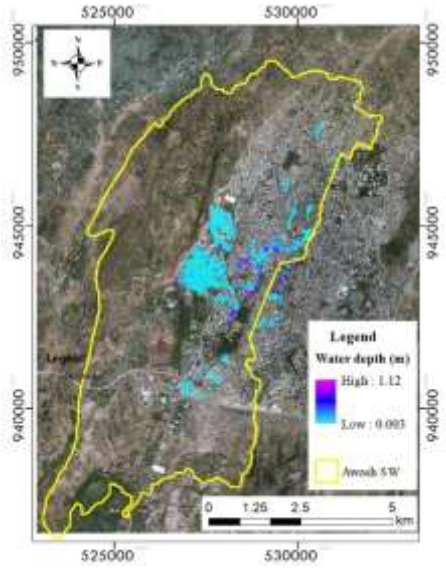	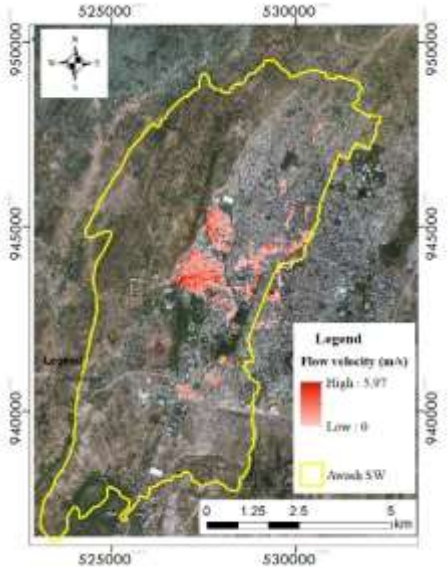

25-yr	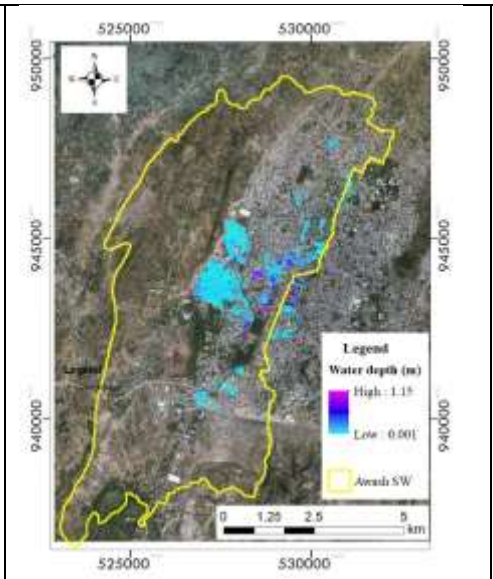	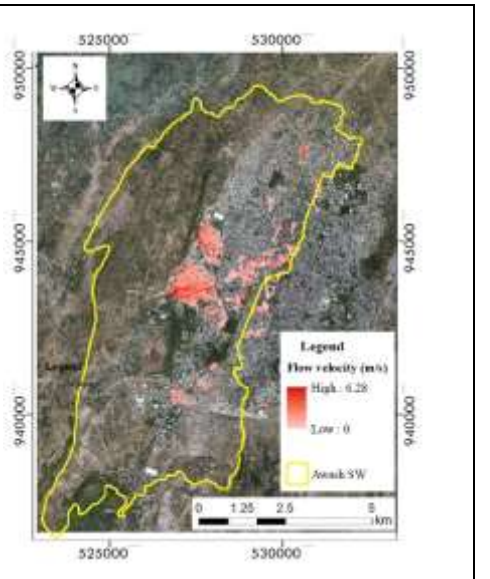
50-yr	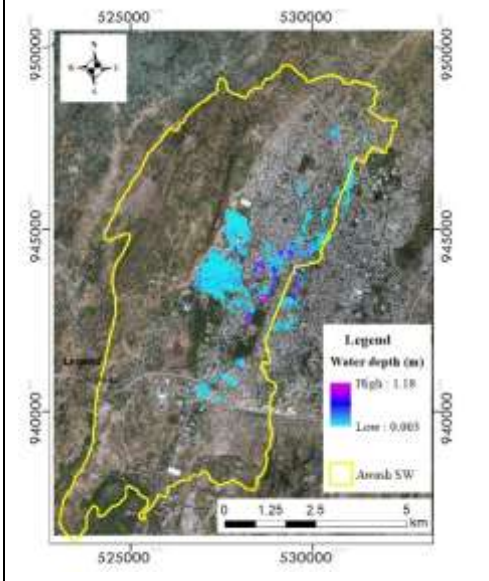	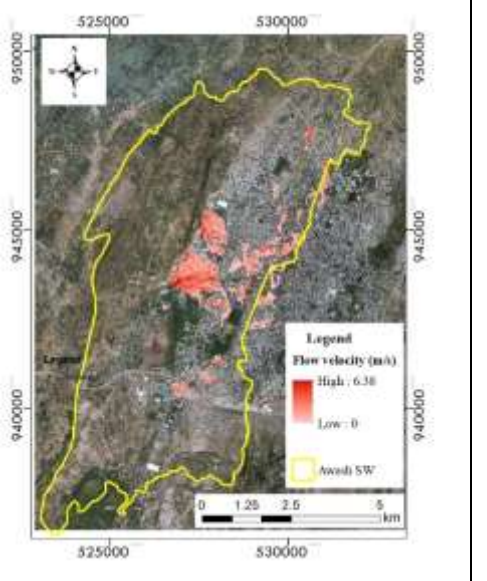
100-yr	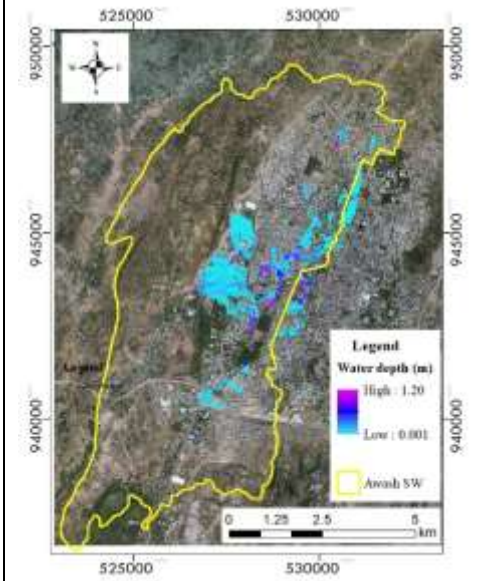	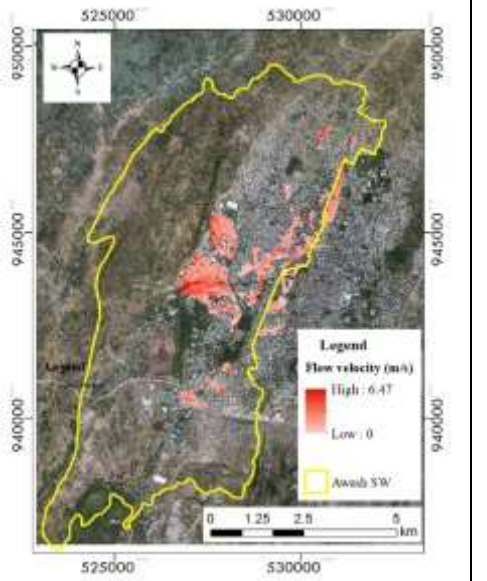

Scenario-II: Future LULC and Historical rainfall

	Water depth	Flow velocity
5-yr	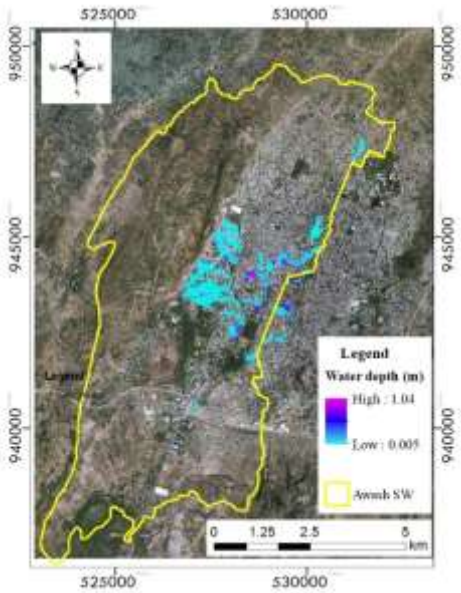	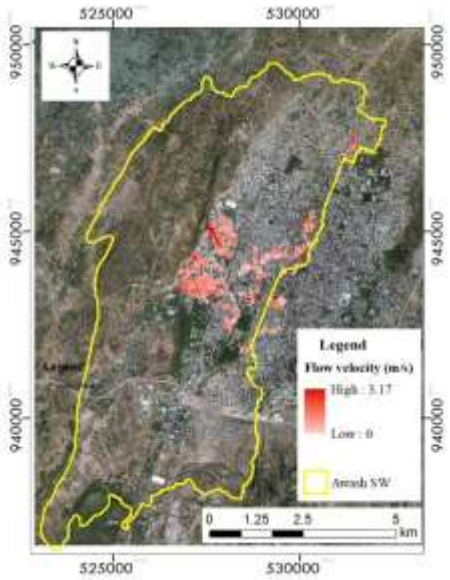
10-yr	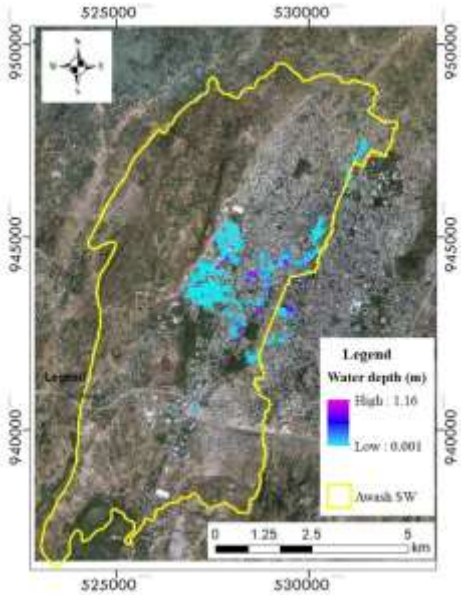	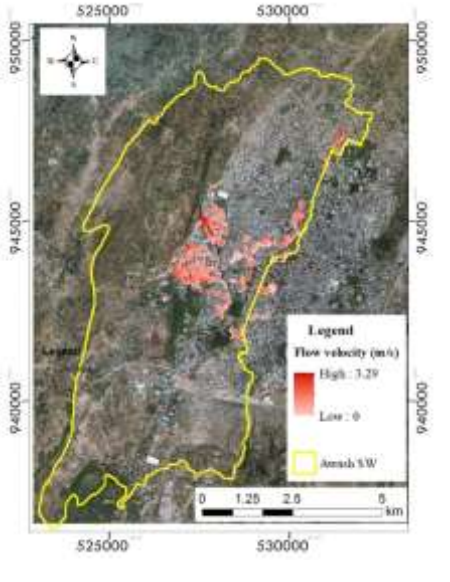

25-yr	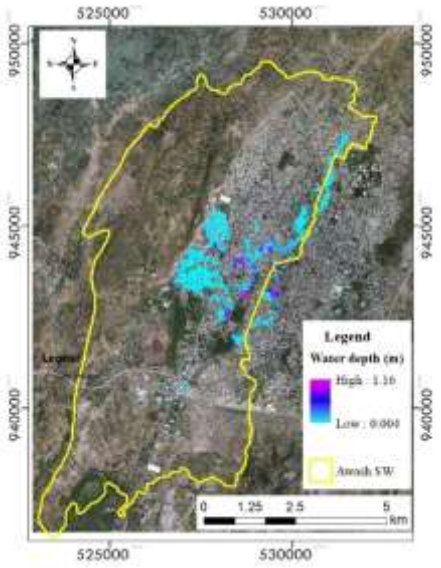	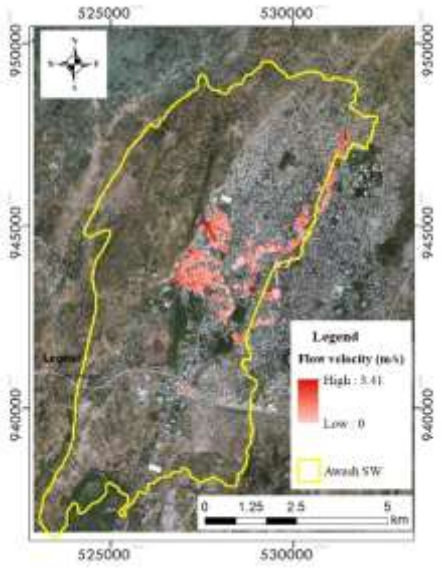
50-yr	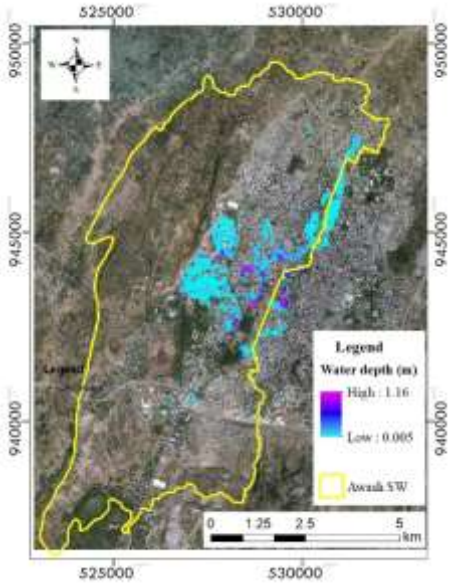	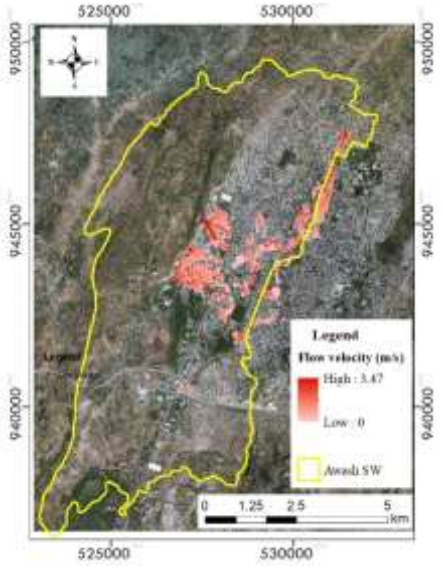
100-yr	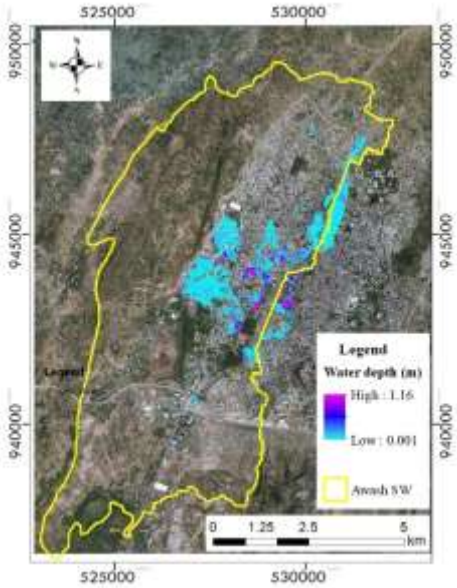	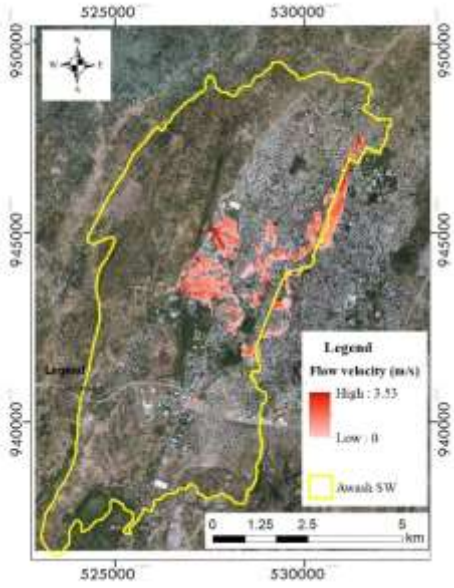

Scenario-III: Existing LULC and future rainfall

	Water depth	Flow velocity
5-yr	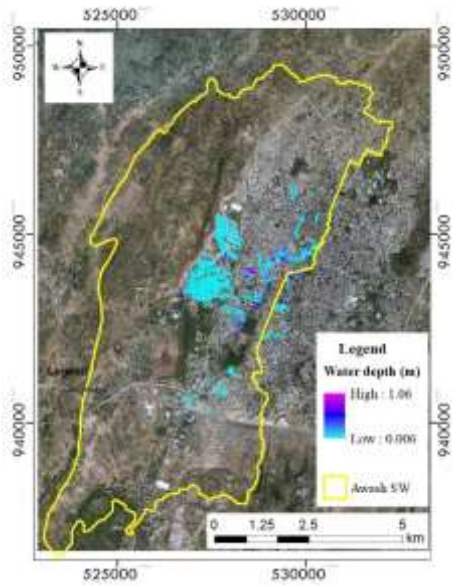	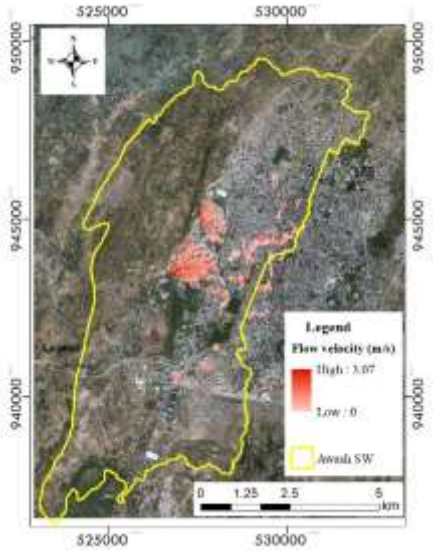
10-yr	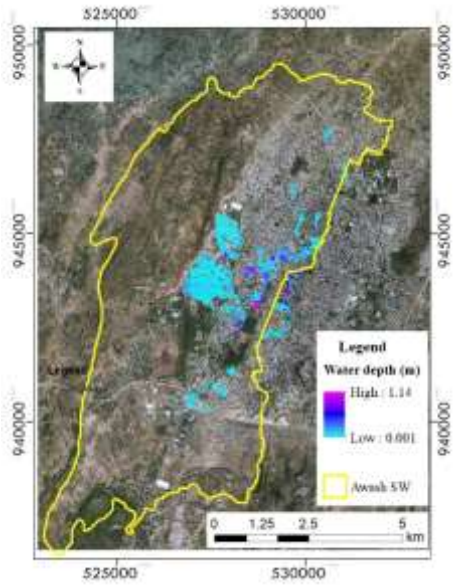	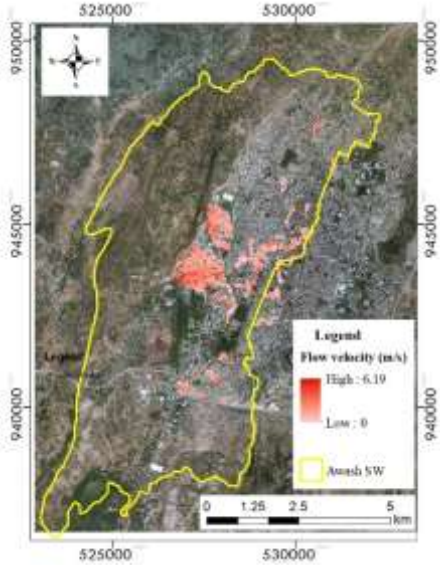

25-yr	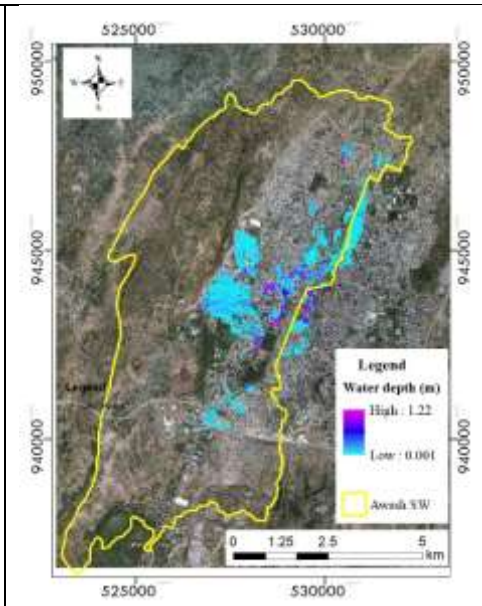	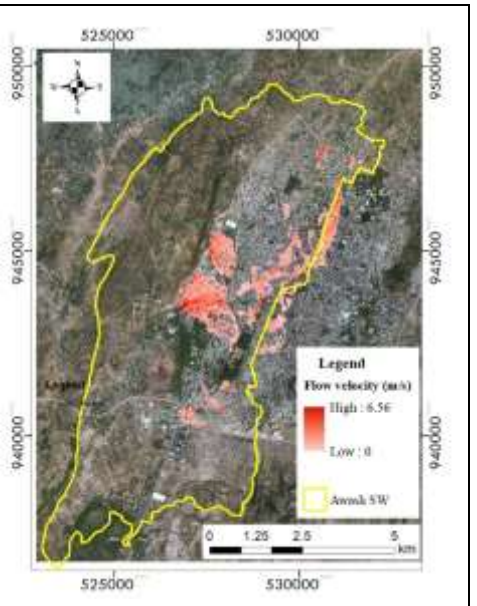
50-yr	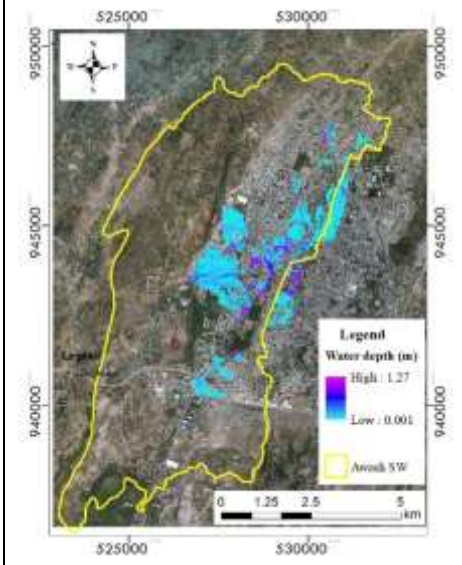	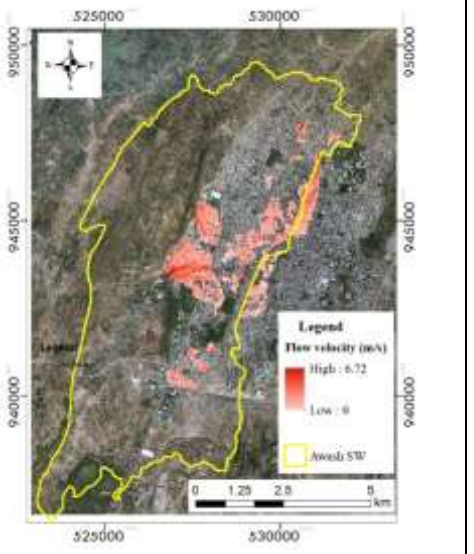
100-yr	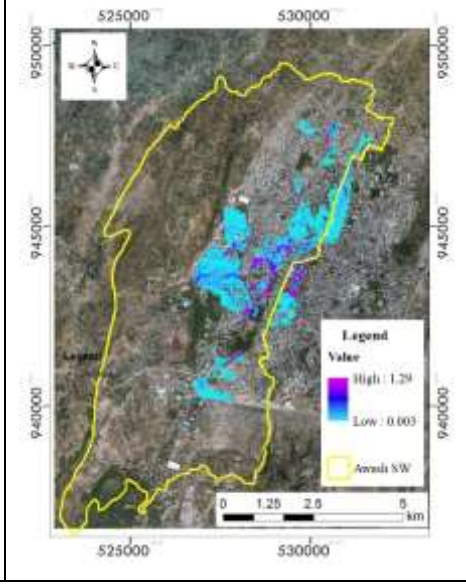	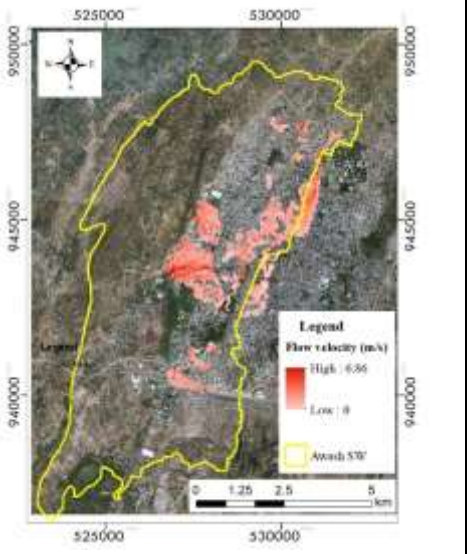

Scenario-IV: Combined future LULC and rainfall

	Water depth	Flow velocity
5-yr	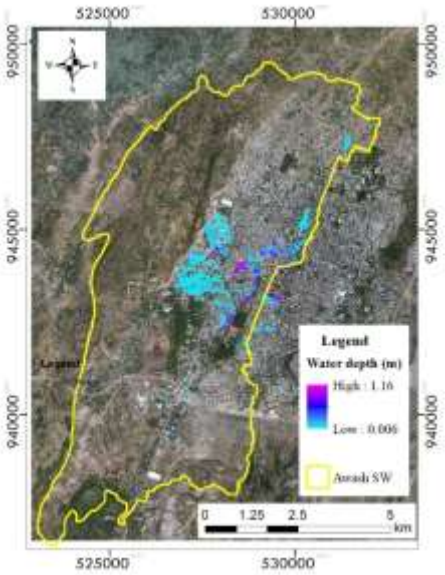	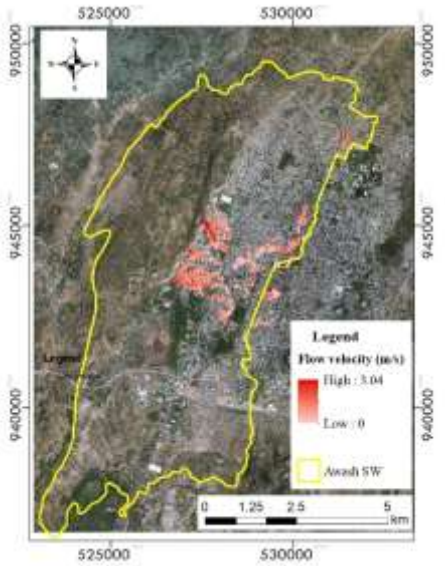
10-yr	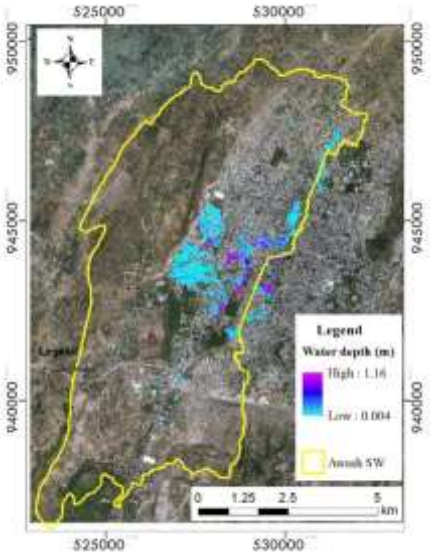	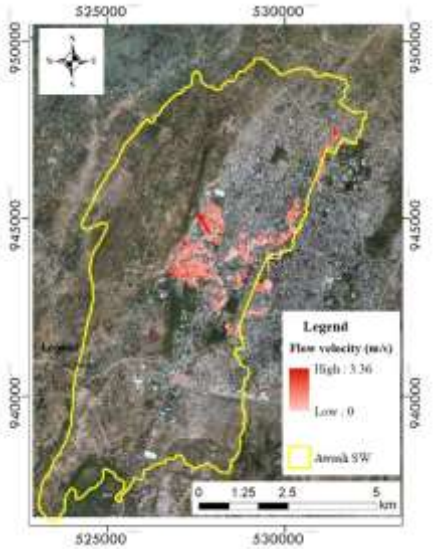

25-yr	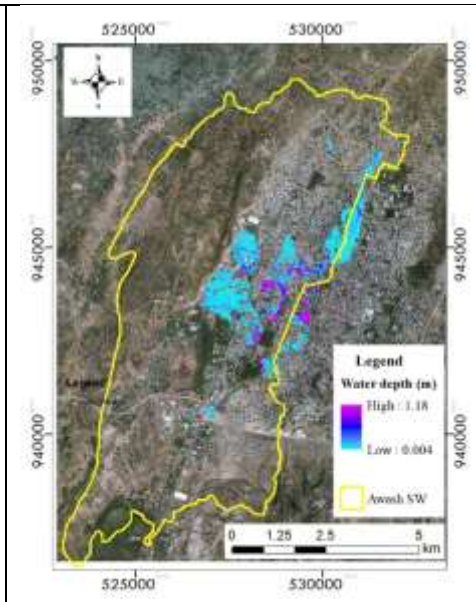	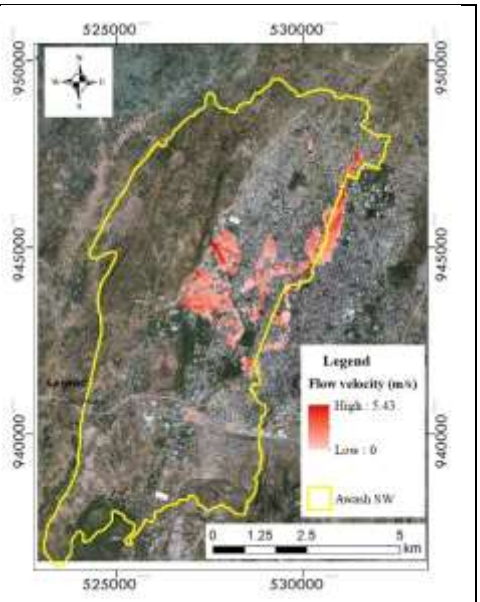
50-yr	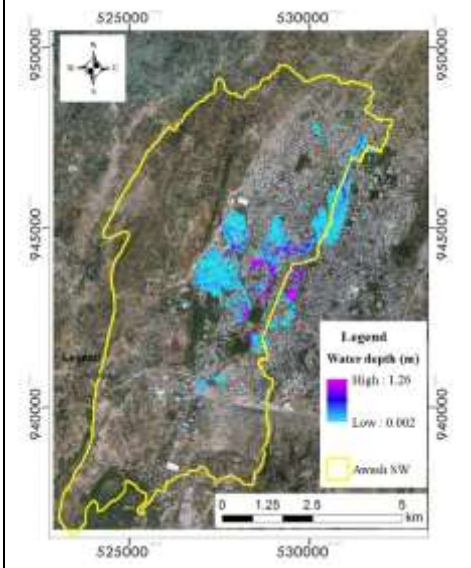	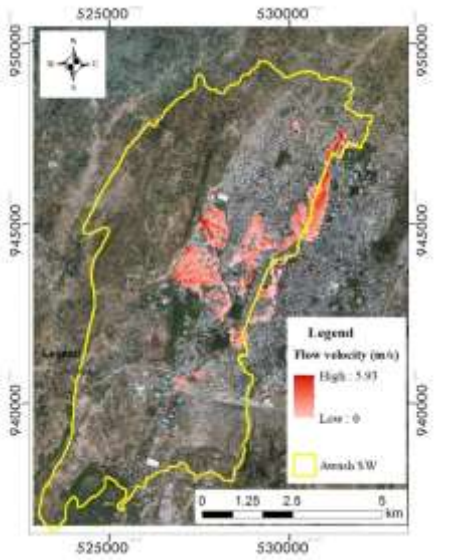
100-yr	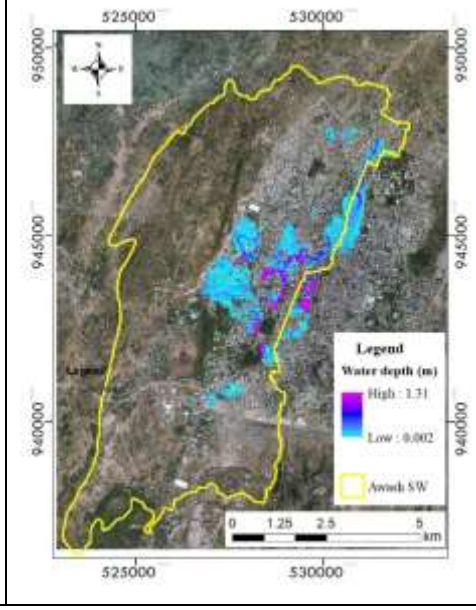	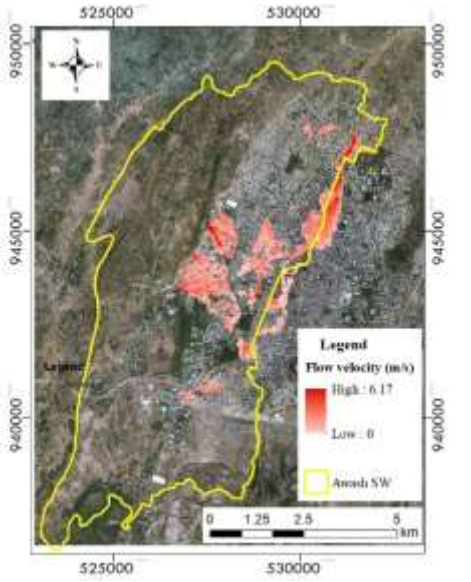

B: Flood hazard maps

5-yr

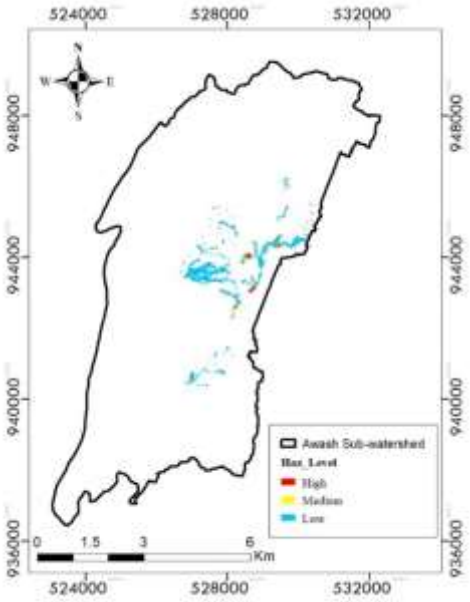

c) Scenario-I

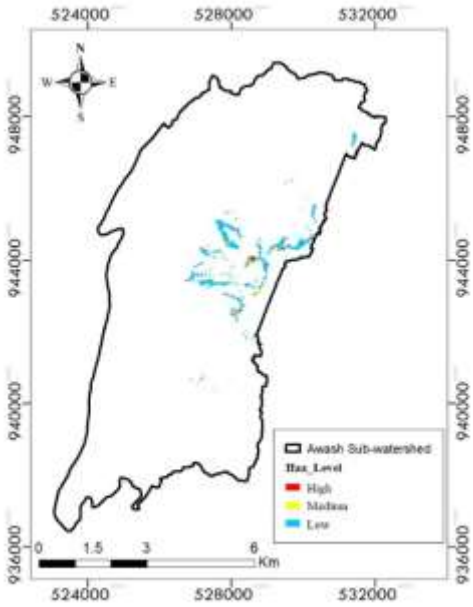

d) Scenario-II

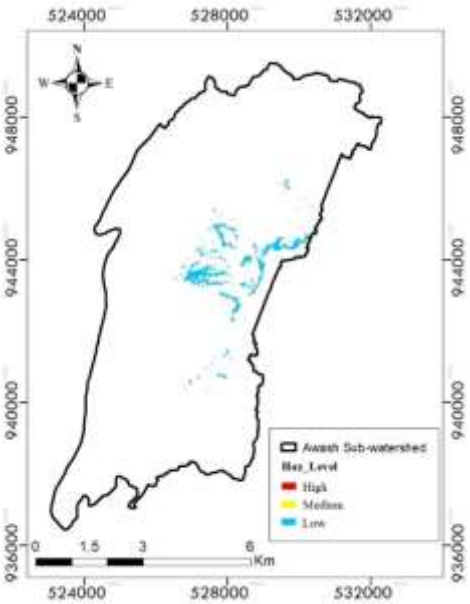

e) Scenario-III

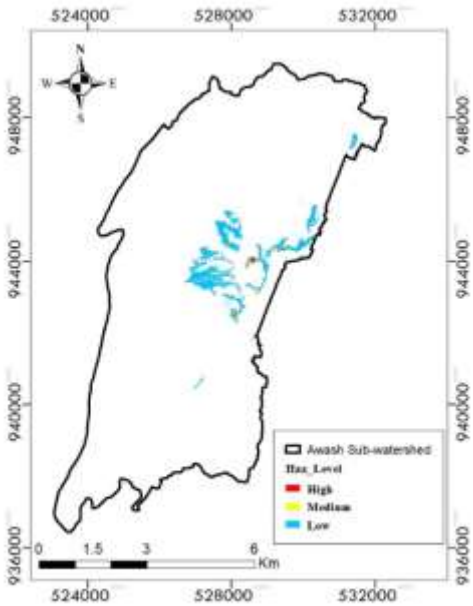

f) Scenario-IV

10-yr

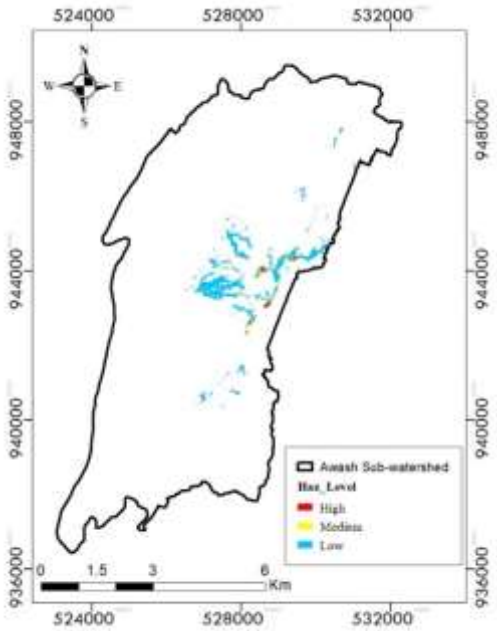

a) Scenario-I

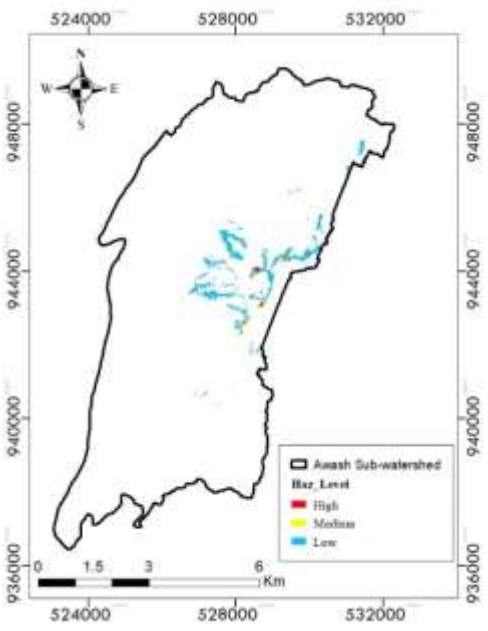

b) Scenario-II

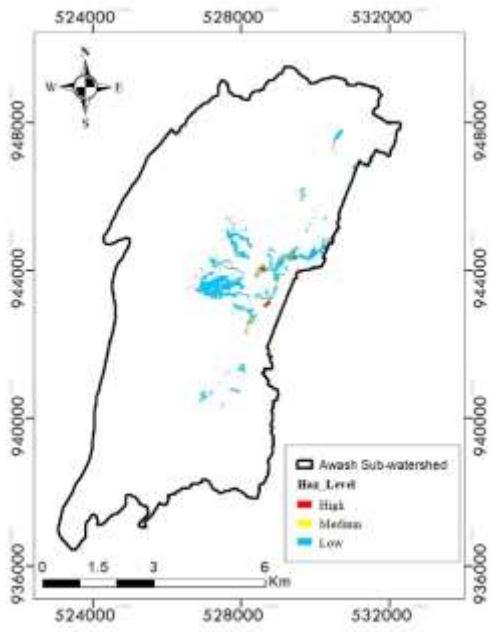

c) Scenario-III

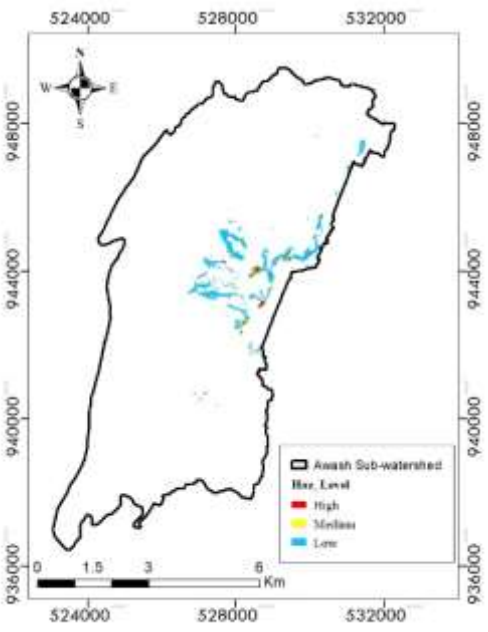

d) Scenario-IV

25-yr

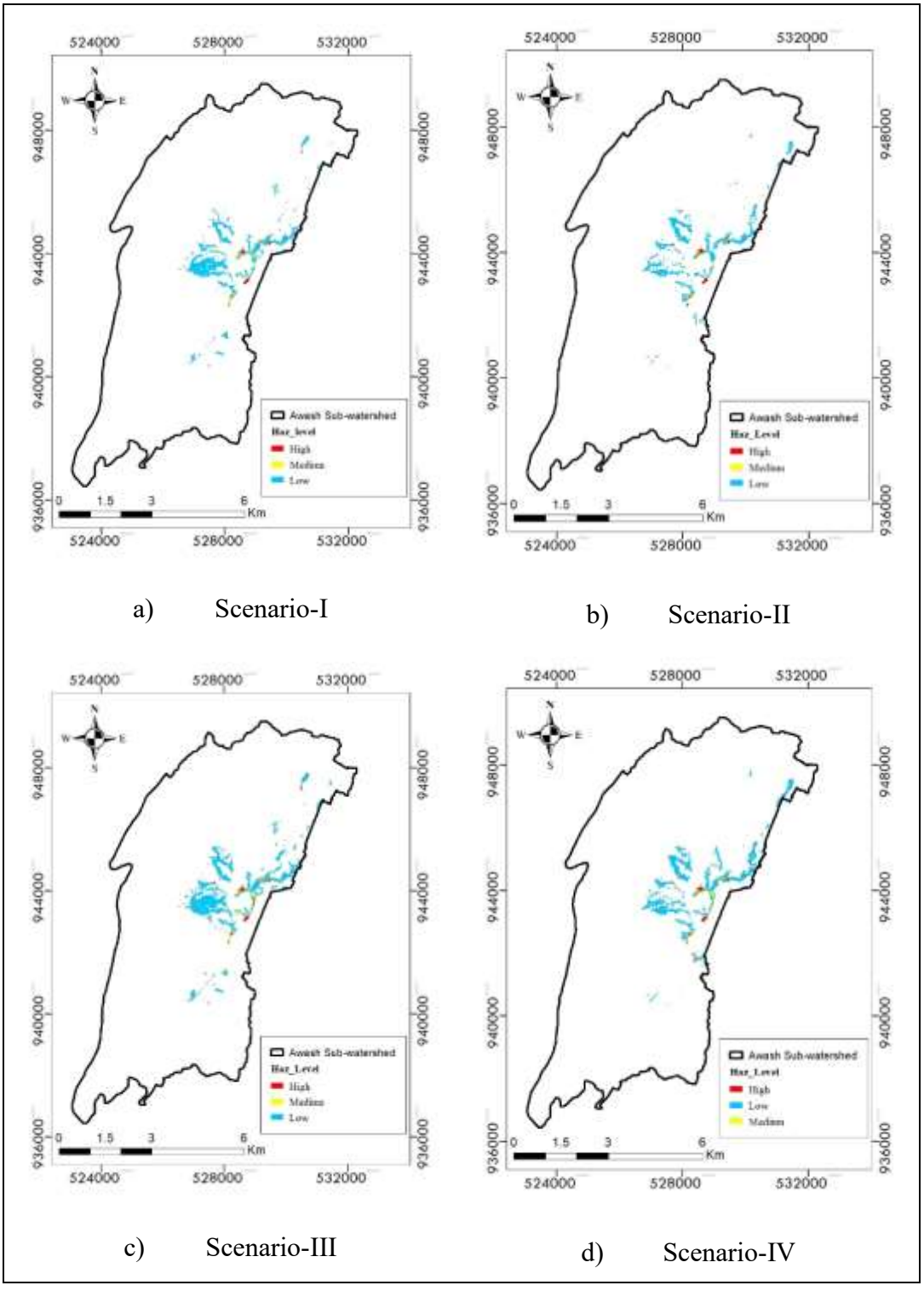

a) Scenario-I

b) Scenario-II

c) Scenario-III

d) Scenario-IV

50-yr

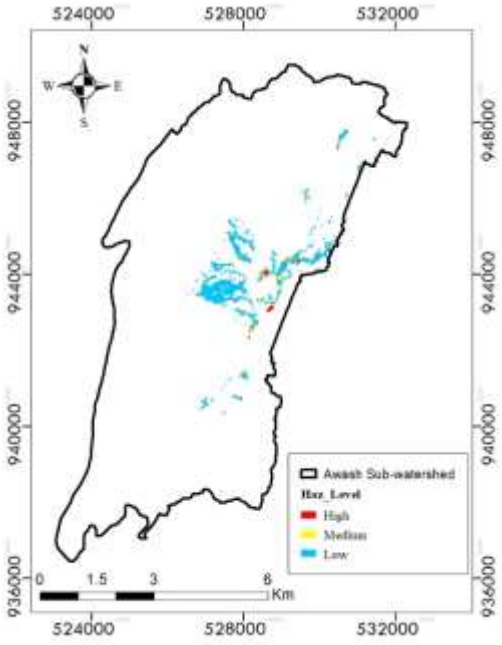

a) Scenario-I

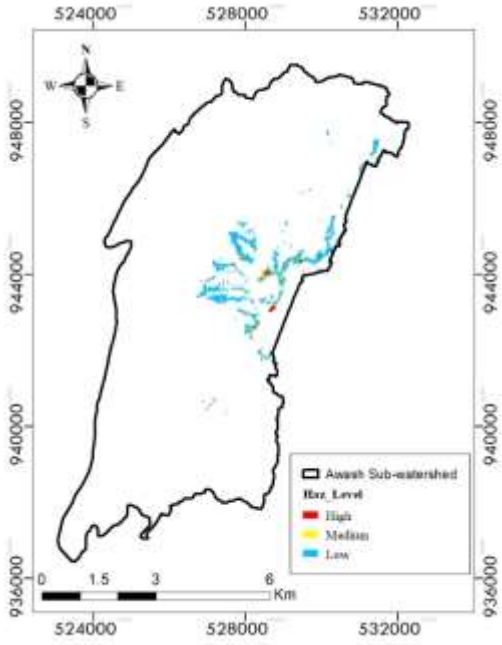

b) Scenario-II

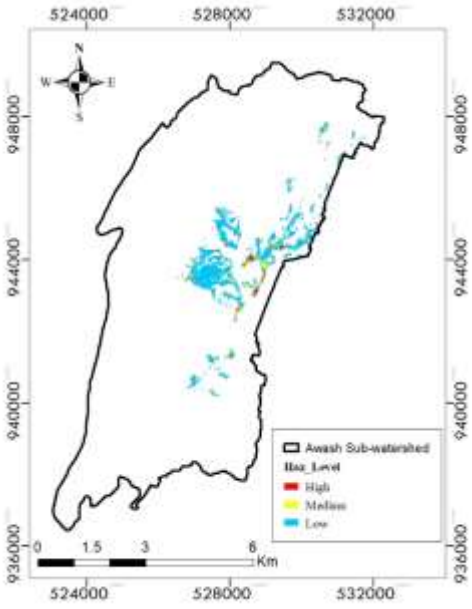

c) Scenario-III

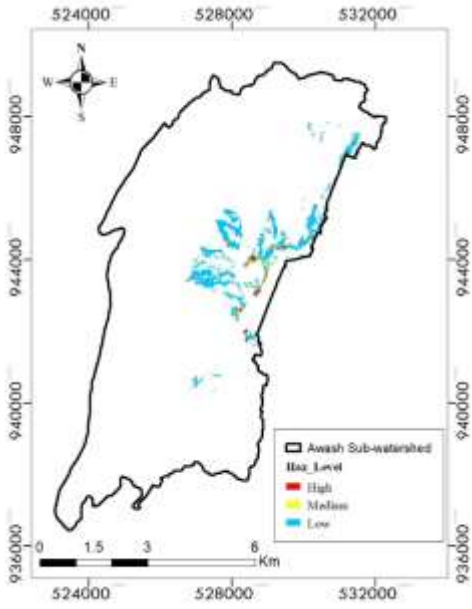

d) Scenario-IV

100-yr

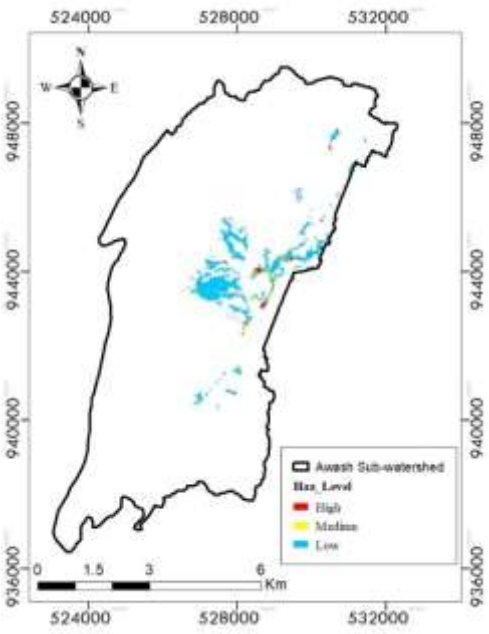

a) Scenario-I

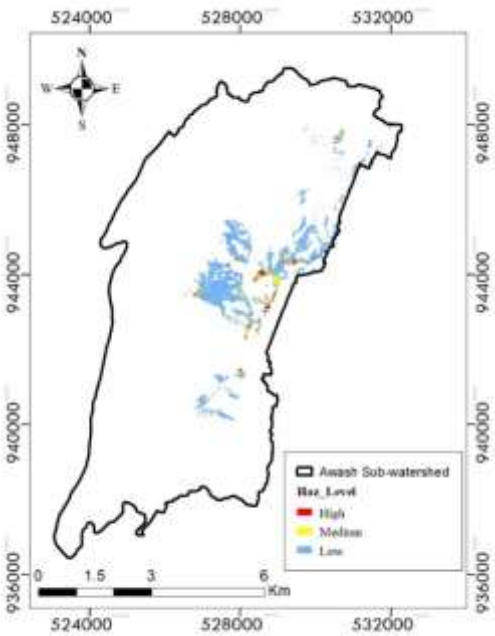

b) Scenario-II

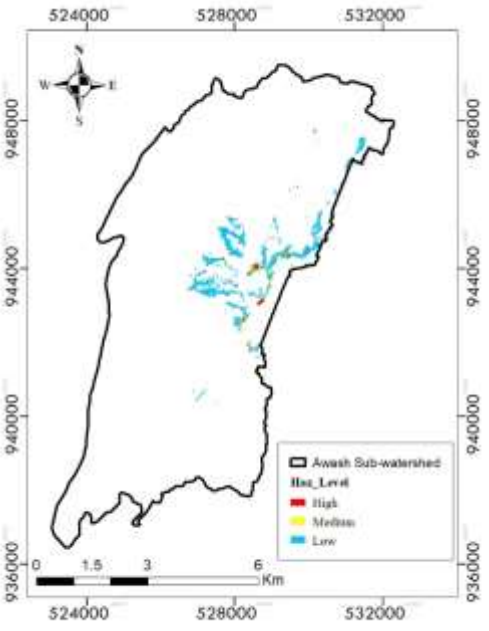

c) Scenario-III

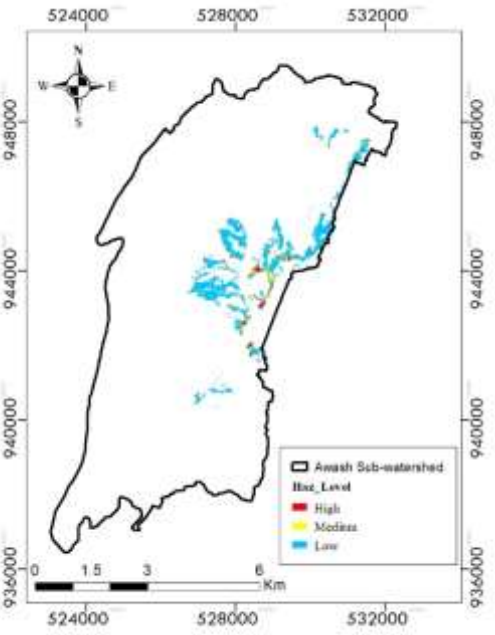

d) Scenario-IV

C: Published Articles

Analysis of the changes in historical and future extreme precipitation under climate change in Adama city, Ethiopia

Dejene Tesema Bulti, Birhanu Girma Abebe & Zelalem Biru

Modeling Earth Systems and Environment

ISSN 2363-6203
Volume 7
Number 4

Model. Earth Syst. Environ. (2021)
7:2575-2587
DOI 10.1007/s40808-020-01019-x

Springer

Modeling Earth Systems and Environment (2021) 7:2575–2587
https://doi.org/10.1007/s40808-020-01019-x

ORIGINAL ARTICLE

Analysis of the changes in historical and future extreme precipitation under climate change in Adama city, Ethiopia

Dejene Tesema Bulti[1] · **Birhanu Girma Abebe**[1] · **Zelalem Biru**[2]

Received: 6 August 2020 / Accepted: 17 October 2020 / Published online: 5 November 2020

Abstract

Under the conditions of climate change, extreme events occur more frequently with higher energy for devastation. Planning for effective management of climate-related risks demands clear information at the local scale. This study aims to characterize the extreme events in the daily precipitation records and to assess the changes under future climate conditions in flood vulnerable city of Adama. For this, the extreme rainfall events during 1965 and 2016 were analyzed on the basis of 10 selected extreme precipitation indices. Using a statistical downscaling model (SDSM), future daily precipitation in the city for the period 2021–2080 was downscaled from the outputs of two Global Circulation Models (CanESM2 and HadCM3) under five climate change scenarios. Taking the climate conditions during 1971 and 2000 as a base, changes in precipitation extreme events in future periods (2021–2050 and 2051–2080) were investigated using the delta approach. The study reveals that the extreme precipitation events in Adama city were increasing over the period of 1965–2016. The results also indicate a successful application of the SDSM for downscaling local-scale future daily precipitation from the outputs of large-scale atmospheric information for the study area. Moreover, under future climate change scenarios, the extreme precipitation would increase up to 2080, despite the changes will be highest during 2050 and 2080, indicates the study area could experience frequent and more severe floods during the coming 60 years due to the changes in global climate. This study would support planning for effective management of flood risks due to the impacts of climate change on extreme precipitation in Adama city.

Keywords Climate change · Sustainability · Statistical downscaling · Flood risk · Climate extreme

Introduction

The augmentation of climatic change due to global warming has become a major concern of climate scientists (Mekonen and Berlie 2019; Geremew et al. 2020). Climate change alters the frequency and intensity of extremes with high variability across the spatial scales. According to the report of the Intergovernmental Panel on Climate Change (IPCC), in many regions of the world, intensity and frequency of extreme precipitation events will increase until the end of this century (IPCC 2014). In Ethiopia, climate extremes have been considered as a major trigger for climate-related natural disasters (e.g., flood) (Mekasha et al. 2014; Dawit et al. 2019).

Information about extreme precipitation has a significant role in the management of flood risk effectively. Reliably identified the trend of extreme precipitation and its potential alteration in the future due to the changes in global climate allows to assess and model the influences of climate change on hydrological characteristics of a particular area (Supharatid et al. 2016; Mohammed et al. 2020). Consequently, it helps to identify potential risks at an early stage and supports planning for mitigation and adaptation. In most regions of the world, however, it is not yet possible to make concrete assessments of how climate change has affected extremes as compared to mean climate, and how it will modify extremes in the future (Basistha et al. 2009; Shang et al. 2011).

✉ Dejene Tesema Bulti
dejenetesema@yahoo.com

Birhanu Girma Abebe
birhanu.girma@eiabc.edu.et

Zelalem Biru
zelalembgd2016@gmail.com

[1] Ethiopian Institute of Architecture, Building Construction, and City Development, Addis Ababa University, Addis Ababa, Ethiopia

[2] Adama Science and Technology University, Adama, Ethiopia

In the context of Ethiopia, the trend of extreme precipitation in time-series records has been assessed for different areas of the country, such as Debre Markos town (Shang et al. 2011), north-east highlands of Ethiopia (Mohammed et al. 2018); upper Awash basin (Shawul and Chakma 2020); Northeastern Highlands of Ethiopia (Mekonen and Berlie 2019) and Northwest Ethiopia (Geremew et al. 2020). These studies emphasize that the trend of long-term precipitation extreme is less uniform when it comes to a smaller scale (local scale), indicating a small-scale analysis is necessary to adequately address the climate-related risks.

Climate information for the future period is projected by several global circulation models (GCMs) and readily available for the end of the twenty-first century, yet at a coarser resolution, 70 km or more (Gharbia et al. 2016; Deb et al. 2018; Navarro-Racines et al. 2020). Hence, it does not fit the desires of impact studies that usually demand climate information at finer-scale (tens or hundreds of square kilometers) (Pervez and Henebry 2014). As more emphasis is placed on evaluating potential circumstances for future climate change at the local scale, several researchers have downscaled long-term future climate conditions projected by GCMs using statistical downscaling methods (Abbasnia and Toros 2016; Shiferaw et al. 2018; Salvacion et al. 2018; Moses and Gondwe 2019). The statistical downscaling method assumes the present-day empirical relationship between the local observed climate variable (e.g., Precipitation) and its estimates by GCMs remains unchanged under the future climatic conditions. This method provides station-based climate information with a low computational cost (Wilby and Dawson 2013; Gharbia et al. 2016).

To this point, some attempts have been made to downscale the outputs of GCMs to provide the long-term future climate conditions in Ethiopia for hydrological applications (Dile et al. 2013; Samuale et al. 2014; Rukundo and Doğan 2016; Mohammed et al. 2020). However, the downscaling of GCMs estimates for cities is limited, although there is an example to the contrary (Feyissa et al. 2018). Given the importance of information about local climate conditions for the planning of sustainable management of risks posed by the changes in global climate, future changes in precipitation extreme under changing climate in flood vulnerable area, Adama city, deserves further analysis.

Hence, the aim of this study is to analyze the trend of extreme precipitation in Adama city and its future variability under climate change. More specifically, the study is conducted (1) to analyze the trend of extreme precipitation in Adama city over the period of 1965–2016; (2) to statistically downscale future daily precipitation from the estimates of GCMs for the years 2021–2080; and (3) to investigate the future changes in precipitation extreme in the city.

Materials and Methods

Study Area

Adama city is one of the fast-growing urban areas in Ethiopia with a population growth rate of about 9% between 2004 and 2016 (Bulti and Asefa 2019). The city is located at 8° 33′ north latitude and 39° 16′ east longitude. It is suited on the flat terrain of the Rift Valley and surrounded by mountains and ridged topography. Urban flood has been a regular feature of Adama City during rainy seasons with substantial damages (Bulti et al. 2017). Figure 1 shows the study area along with the nearby metrological stations. In this study, Adama observation station is selected as a representative station due to its location and available length of time-series precipitation data. The station is located at 8.55-degree latitude and 39.28-degree longitude with an altitude of 1622 m.

Data used

Data used in this study were collected from different sources. The daily rainfall data recorded at Adama weather observation station were obtained from the National Meteorological Agency (NMA). Due to extended missing observation (i.e., more than 1 year), only 52 years (1965–2016) time-series precipitation data were selected and acted on. First, the proportion of missing observation in the selected time-series data was checked and found to be 7.47%. It is within the maximum flexible threshold values adopted by other studies (Ngongondo et al. 2011; Mohammed et al. 2018). Next, the missing data were filled using the Kalman Smoothing function in R-based ImputeTS package. This function provides acceptable results and it is recommended for long time-series data (Steffen 2019).

In addition, three large-scale datasets (described below) were used: NCEP reanalysis dataset for the calibration and validation, and CanESM2 and HadCM3 datasets for the baseline and climate scenario generation. They are chosen because they are freely available online and predictors are organized in such a way that they can directly be used in the statistical downscaling model (SDSM) presented in Sect. 2.3.2. In addition, they have been widely applied in similar studies (Dile et al., 2013; Mekonnen and Disse 2018; Deb et al. 2018; Mohammed et al. 2020).

- *CanESM2* (second generation Canadian Earth System Model) is coupled atmosphere–ocean global climate model developed by the Canadian Centre for Climate Modelling and Analysis (CCCma). CanESM2 pro-

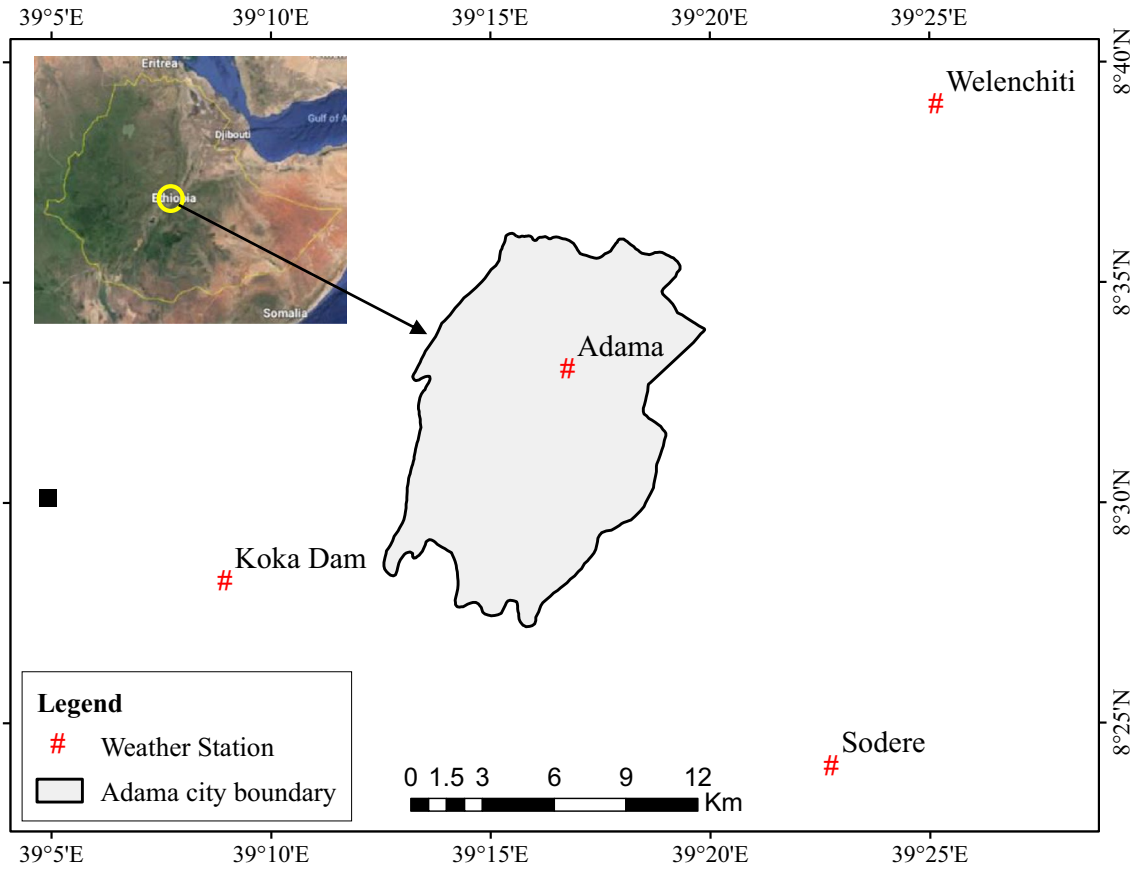

Fig. 1 Location map of the study area

vided long-term climate simulation based on the three greenhouse gases (GHG) emission scenarios (Representative Concentration Pathways, RCPs), including a stringent mitigation scenario (RCP2.6); medium stabilization scenario (RCP4.5) and high emission scenario (RCP8.5). The CanESM2 model has a resolution of 2.79^0 latitude and 2.81^0 longitude. More descriptions can be found in IPCC (2014).

- *HadCM3* (third-generation Hadley center Climate Model) is a coupled atmosphere–ocean general circulation model developed at the Hadley Centre in the United Kingdom. The model generated climate variable using two emission scenarios in the future atmosphere: medium–high (A2) and medium–low (B2). This GCM has a resolution of 2.5° latitude by 3.75° longitude. More description can be found in Semenov and Stratonovitch (2010).
- *NCEP* (National Centre for Environmental Prediction) reanalysis dataset contains large-scale atmospheric variables representing the present-day condition, and it was used for calibration and validation of the downscaling model in this study. The NCEP dataset was normalized over the complete 1961–1990 period data and interpolated to the equal grid as CanESM2 and HadCM3 from its horizontal resolution of 2.5° latitude and 2.5° longitude (Mekonnen and Disse 2018).

The archives of large-scale datasets were downloaded from the Environment Canada website (https://ccdsdscc.ec.gc.ca/?page=pred-canesm2) for the grid box containing the study area (CanESM2_BOX_015X_36Y and HadCM3_BOX_11X_31Y). The archive of CanESM2 include historical large-scale simulation data (CanESM2_historical_1961_2005) and predicted data corresponding to three emission scenarios (RCP2.6, RCP4.5 and RCP8.5) for the years 2006–2100. HadCM3 archive also includes data for both scenarios (H3A2a and H3B2a) spanning from 1961 to 2099 (the "a" in A2a and B2a refers the ensemble member in the HadCM3 A2 and B2 experiments). In addition, archives of both datasets contain reanalysis data (NCEP-NCAR_1961_2005 for CanESM2 and NCEP_1961-2001 for HadCM3). The datasets include 26 predictor variables under each of the emission scenarios of respective GCMs and reanalysis data. However, the NCEP-derived predictor's data and the predictors supplied for the GCMs were slightly vary (Table 1).

Table 1 Gridded predictors of CanESM2 and HadCM3 datasets

Variable	Description	Variable	Description
temp	Mean temperature at 2 m	s850[b]	Specific humidity at 850 hPa height
mslp	Mean sea level pressure	r850 [a]	relative humidity at 850 hPa height
p500	500 hPa geopotential height	*_f	Geostrophic air flow velocity
p850	850 hPa geopotential height	*_z	Vorticity
shum	Near-surface specific humidity	*_u	Zonal velocity component
rhum [a]	Near-surface relative humidity	*_v	Meridional velocity component
prec[b]	Total precipitation	*zh	Divergence
s500[b]	Specific humidity at 500 hPa height	*thas	Wind direction
r500[a]	Relative humidity at 500 hPa height		

[a]Found only for HadCM3

[b]Found only for CanESM2

*Refers to different atmospheric levels: the surface (p_), 850 hPa height (p8) and 500 hPa height (p5)

Methods

Analysis of extreme precipitation

Extreme precipitation indices Extreme precipitation in Adama city was analyzed using standard indices for the extreme precipitation defined by Expert Team on Climate Change Detection and Indices (ETCCDI). These indices are easy to calculate and understand, and they provide scientifically robust measures of the variability of rainfall extremes (Zhang et al. 2011). Moreover, they have been widely used in several similar studies in different regions of the world for recent years (e.g., Lima et al 2015; Gujree et al. 2017; Shawul and Chakma 2020; Berhane et al. 2020; Geremew et al. 2020). The definitions of the indices used in this study are presented in Table 2. The linear trends of the indices were computed from daily precipitation data using the R-based RClimDex software package, and the statistical significance of the trends was assessed at $\alpha = 0.1$amd$\alpha = 0.05$.

Correlation analysis The linear relationship between extreme precipitation indices was also assessed using Pearson correlation analysis. In essence, it was conducted to compare the precipitation indices for mean conditions (SDII and PRECTOT) and other extreme indices. Such analysis may also help to identify the data with irregular behavior as a result of a few individuals, highly faulty daily values in time-series data, which affect overall data statistics (Santo et al. 2013); hence, it helped as an additional tool for examining the data closely. In this case, the correlation coefficient (r) was calculated to determine the extent to which the indices are linearly related. Based on the recommendation of Evans (1996), the strength of observed correlation was described: very weak ($|r|<0.19$), weak ($|r|<0.39$), moderate ($|r|<0.59$), strong ($|r|<0.79$), very strong ($|r|<1$). The statistical significance of the correlations was determined using the two-tailed test of the Student's distribution and evaluated at the $\alpha = 0.05$ level.

Downscaling future precipitation

Statistical downscaling model (SDSM) The choice of the proper downscaling method relies on the needed temporal and spatial resolutions of the climate variability, as well as the resource and time constraints. In this study, the statisti-

Table 2 Definitions of indices for analysis of extreme precipitation in Adama city

ID	Indicator name	Indicator definitions	Units
PRECTOT	Annual total wet-day precipitation	Total wet-day precipitation ≥ 1 mm	mm
SDII	Simple daily intensity index	Mean precipitation amount on wet-day (≥ 1 mm)	mm/day
Rx1day	Max 1-day precipitation amount	Maximum 1-day precipitation	mm
Rx5day	Max 5-day precipitation amount	Maximum 5 consecutive days precipitation	mm
R10	Number of heavy precipitation days	Annual count when precipitation ≥ 10 mm	days
R20	Number of very heavy precipitation days	Annual count when precipitation ≥ 20 mm	days
CDD	Consecutive dry days	Maximum number of consecutive days when precipitation < 1 mm	days
CWD	Consecutive wet days	Maximum number of consecutive days when precipitation ≥ 1 mm	days
R95p	Very wet days	Annual total precipitation from days > 95th percentile	mm
R99p	Extremely wet days	Annual total precipitation from days > 99th percentile	mm

cal downscaling model (SDSM) was selected to downscale local daily precipitation from the outputs of selected GCMs. The structure of the model for climate scenario generation is depicted in Fig. 2. The downscaling experiment was realized using SDSM4.2 software. It is a freely available Windows-based decision support tool for generating single-site daily climate variables under the current and future regional climate forcing (Wilby and Dawson 2007). It provides a robust scenario building technique for a specific location for which there are archived GCMs outputs and adequate observed daily local variable for calibrating the model (Gebrechorkos et al. 2019). In general, downscaling experiment using SDSM in this study involves the selection of candidate predictors; model calibration and validation; and synthesizing future precipitation.

Selection of predictors Statistical downscaling methods require appropriate large-scale atmospheric variables that enable identification of robust empirical associations between gridded predictor variables and site-scale predictands. However, choosing a predictor is one of the most challenging tasks, as the explanatory power of each variable varies in both spatial and temporal scales, indicating the selection process can be exposed to some level of subjectivity. To reduce this, a quantitative approach presented in other similar studies (Huang et al. 2011; Mahmood and Babel 2014), was used to examine the predictive variables.

Initially, the correlations between the daily rainfall (predictand) and each of the 26 NCEP atmospheric variables

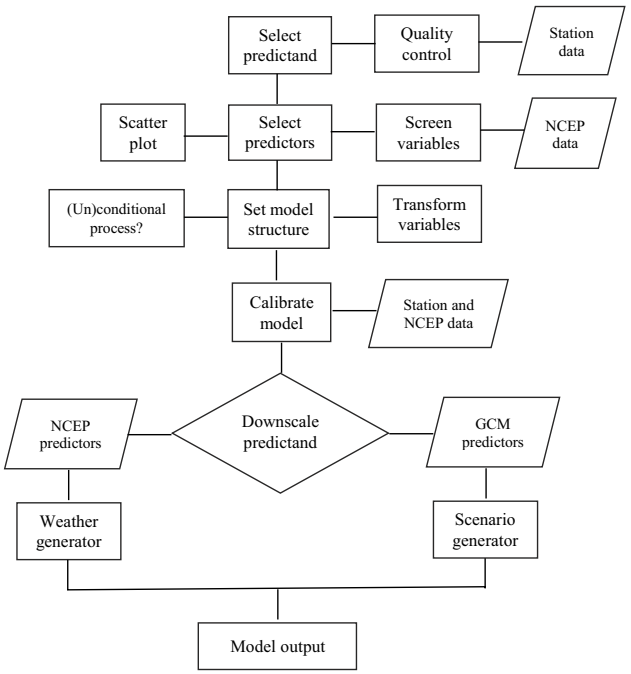

Fig. 2 SDSM Version 4.2 climate scenario generation, adapted from Wilby and Dawson (2007)

were identified. Then, 11 variables with relatively large values of absolute correlation were selected, from which the variable with the highest correlation coefficient is assigned as a superior predictor (SP). Then, the absolute correlation between predictor variables (r), the partial correlation coefficient (Pr) and the P values were determined in the presence of SP. Then, the percentage reduction (PR) for each variable was calculated using Eq. 1. The second candidate predictor was determined using a combination of the correlation coefficient (r), p value and the percent reduction (PR). In this case, a predictor with, $r < 0.7$, $p < 0.05$, and minimum PR. By repeating this procedure, further additional predictors were selected. Due to variation in the supplied predictors for the two GCMs, two sets of predictors were selected one for each GCM for calibration of the models. In most cases, 3–5 predictors are considered sufficient to detect the variation of a predictand during SDSM calibration (Chu et al. 2010; Feyissa et al. 2018). Because in the regression equation, an increase in the number of predictors can increase the probability of multiple co-linearity (Mahmood and Babel 2014):

$$\mathrm{PR} = \frac{(\mathrm{Pr} - r)}{r} \times 100. \tag{1}$$

Model calibration and validation Using the respective sets of selected NCEP predictors, two precipitation models (for each of the GCMs) were developed under conditional processes on the monthly timescale with a fourth root transformation of the predictand. The models were calibrated for daily rainfall data observed over the period of 1965–1990, and used for historical rainfall generation (i.e., downscaling of NCEP reanalysis data). The models were validated over the years 1990–2005 (CanESM2) and 1990–2001 (HadCM3). The variation of the length of the validation periods is due to the availability of NCEP data corresponding to the GCMs. The performance of the models was evaluated using graphical and statistical methods. First, the models were validated by plotting the observed against simulated monthly mean precipitation. Second, two statistical parameters: the coefficient of determination (R^2) and the ratio of the standard deviation of the simulated data to the observed data (RSD) were used. RSD indicates the level of dispersion, and its optimum value is 1, suggests that both datasets (simulated and observed) have the same kind of (Mahmood and Babel 2014; Moses and Gondwe 2019). Both parameters are computed using daily and monthly average precipitation data of observed and downscaled reanalysis data (NCEP_CanESM2 and NCEP_HadCM3).

Climate scenario generation The calibrated model was used for the generation of ensembles of the daily precipitation corresponding to the future period. Using predictors

of the respective GCMs, future daily rainfall was generated under five climate change scenarios (H3A2a and H3B2a of HadCM3 and RCP 2.6, RCP4.5 and RCP8.5 of CanESM2).

Analysis of future changes in precipitation extreme

Future changes in extreme rainfall under climate change scenarios were assessed on the basis of four indices that were included in SDSM4.2. They are the annual percentage of wet-days (wet-days%), the ratio of the sum of the values over the 95th percentile of the sum of all values (POT95), longest wet-spell (CWD) and annual total precipitation (PRECTOT). The event limit was set to 1 mm/day to count the rain day with less than 1 mm as dry day.

The future changes in the indices were computed using the delta approach. It is a widely used method in similar studies (Choi et al. 2009; Salvacion et al. 2018; Feyissa et al. 2018). The standard delta approach for precipitation is the relative difference between GCM-simulated precipitation of the future and baseline periods, and takes the form of Eq. 2. The analysis of the changes over the future period was carried out by dividing into two-time horizons: 2020s (2021–2050) and 2050s (2051–2080). The present-day estimate (1971–2000) was considered as a base for standardizing the time-series resulting from climate change. Such an approach helps to reduce the systematic bias in the mean and variance of GCMs predictors (Wilby and Dawson 2007):

$$\Delta_{\mathrm{Pi}} = \frac{V_{\mathrm{Pi}} - V_{\mathrm{base}}}{V_{\mathrm{base}}} \times 100. \quad (2)$$

where: V_{base} is the mean of all ensembles of each index for the base period (1971–2000). V_{Pi} is the mean of all ensembles of the corresponding index for the future periods (2020s, 2050s).

Results

Trend of extreme precipitation from 1965 to 2016

Trends of extreme precipitation indices

The computed annual statistics and trends of the selected extreme precipitation indices in Adama city over the period of 1965–2016 are summarized in Table 3. The graphical illustration of the trend of corresponding indices is also depicted in Fig. 3. Overall, the results show that there were statistically significant trends in the majority of the indices in the study period. The computed values of six indices (60% of the analyzed indices) showed a rising trend, while the rest of the indices showed a declining trend over the span of 52 years. The p-value statistics shows that the observed trends of seven indices were significant. In contrast, no sufficient evidence was found to support the upward trend of R95p and downward trends of Rx1day and R99p.

Table 3 Statistical parameters and trends of extreme precipitation indices in Adama city from 1965 to 2016

Indices	Annual statistical parameters			Trend test	
	Minimum	Maximum	Mean	Trend (per 10 years)	*p* value
PRECTOT (mm)	578.4	1357.6	868.7	30.69	0.061**
SDII (mm)	4.7	15.8	10.7	0.37	0.075**
Rx1day (mm)	30.7	104.8	61.4	− 0.89	0.587
Rx5day (mm)	61	190.1	111	5.24	0.053**
R95p (mm)	0	558.2	206	13.4	0.194
R99p (mm)	0	221.3	51.1	− 1.91	0.723
R10 (no of days)	10	46	28.4	1.33	0.056**
R20 (no of days)	2	29	13.3	1.11	0.026*
CDD (no of days)	25	148	74.7	− 5.72	0.061**
CWD (no of days)	3	70	10.3	− 2.45	0.014*

∗ Significant at $\alpha = 0.05$; ∗∗ significant at $\alpha = 0.1$

On average, the study area received 868.7 mm annual total precipitation over the study period. The values were increasing at a rate of 30.69 mm/decade. Likewise, the amount of mean precipitation on a wet-day (SDII) varied from 4.7 to 15.8 mm. The values were increasing by 0.37 mm every 10 years over the study period. The observed rising trends of both indices were statistically significant ($\alpha = 0.05$).

With regard to the two absolute extreme indices (Rx1day and Rx5day), the results show that there was remarkable variation in the amount of the indices: Rx1day (30.7–104.8 mm) and Rx5day (61–190.1 mm). The highest 1-day precipitation was decreasing at the rate of 0.89 mm/decade, yet the trend is not statistically significant. On the other hand, the maximum precipitation of consecutive 5-days was showing significant ($\alpha = 0.1$) increasing trend (5.24 mm/decade) during the study period.

The results also show the values of the non-fixed (percentile) threshold indices, which represents a fraction of the total annual rainfall on wet-days attributed to the 95th and 99th percent rainfall events. Very wet-days (R95p) showed a tendency to increase, whereas extremely wet-days (R99p) decreased over the study period. However, the observed trends in both cases are not statistically significant. The annual mean values of both percentile indices were 206 mm (R95p) and 51.1 mm (R99p). The values of the indices were

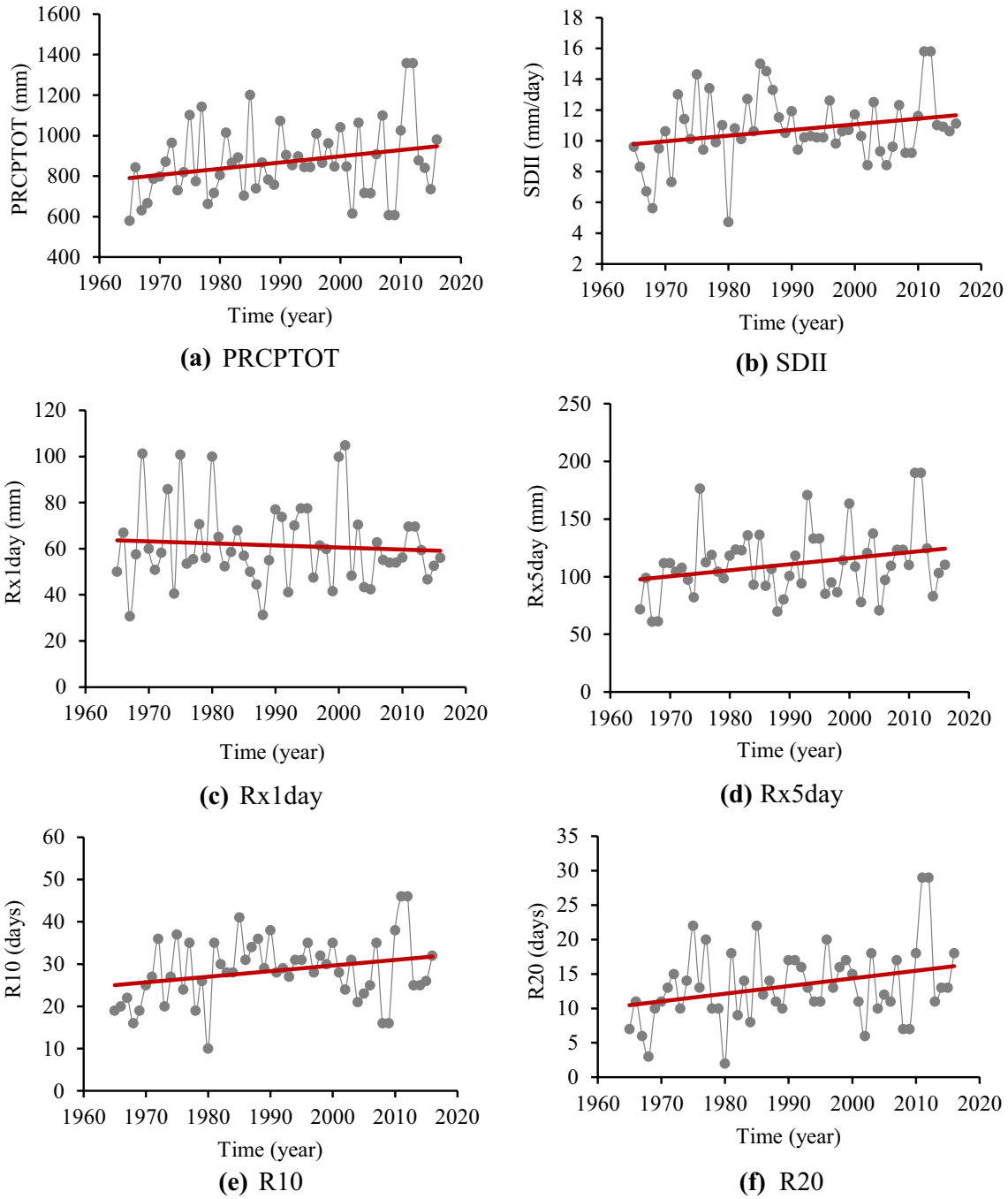

Fig. 3 Trends of standard extreme precipitation indices in Adama city between 1965 and 2016

increasing (R95p) and decreasing (R99p) over time, respectively, yet the trends were not statistically significant.

Furthermore, it can be seen that the annual count of days with precipitation greater than fixed thresholds (heavy rainfall days and very heavy precipitation days) was increasing over the study period, ranging 10–46 days (R10) and 2–29 days (R20). The values were increasing at the rate of 1.33 days/decade for R10 and 1.11 days/decade for R20 at $\alpha = 0.1$ and 0.05 significant levels, respectively. Likewise, the two spell indices (maximum length of consecutive days with a rainfall below and above 1 mm) showed a tendency to decline over time. The values were decreasing at the rate of 5.72 days/decade (CDD) and 2.45 days/decade (CWD). The observed decreasing trends in both cases are also found to be statistically significant at $\alpha = 0.1$ and 0.05, respectively.

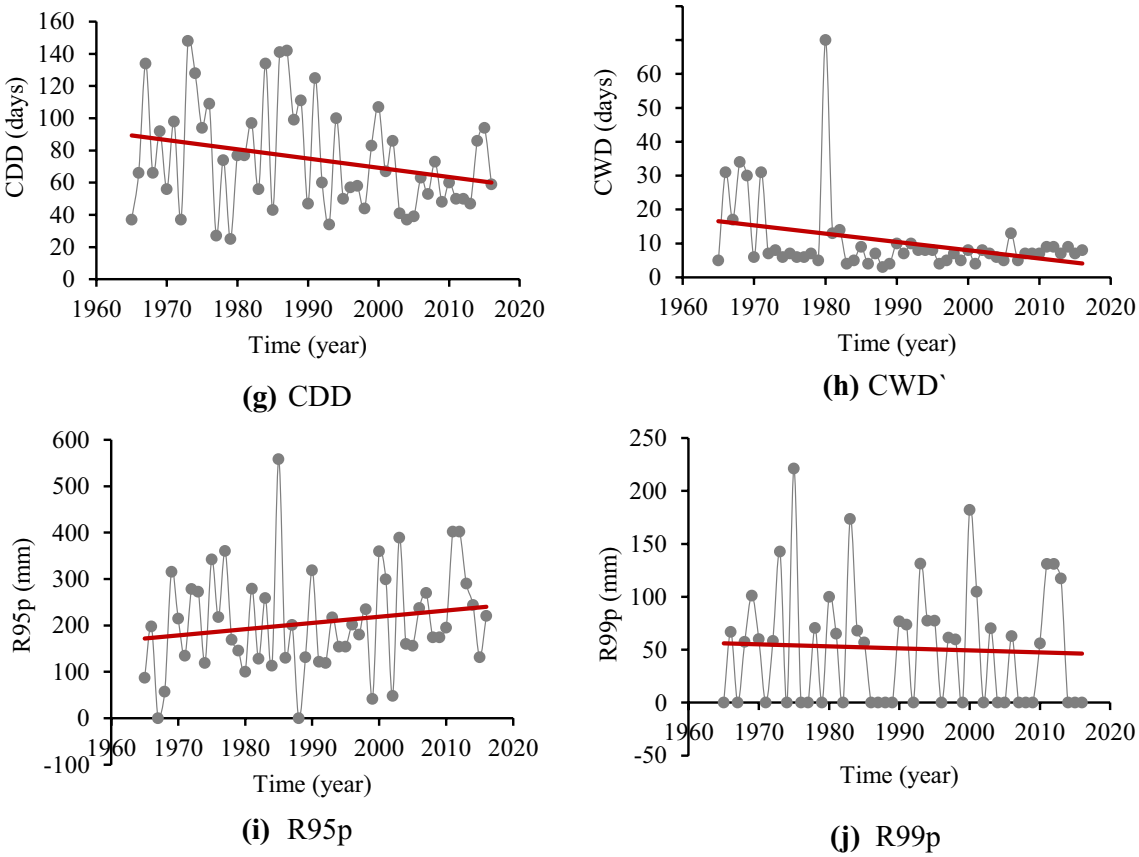

Fig. 3 (continued)

Correlation between extreme precipitation indices

The computed values of the correlation coefficient indicating the level of the linear relationship between the changes in the analyzed indices are shown in Table 4. Overall, the results show that most of thhhe extreme rainfall indices are correlated, although the strength of the correlation varies from moderate to very strong. However, the correlation of the CDD index with other indices is found to be weak ($|r|<0.39$). In addition, CDD is negatively correlated with the analyzed indices. Moreover, a statistically significant positive correlation is found between the pattern of PRECTOT and other indices except Rx1day and CWD. Likewise, the observed positive correlations of SDII with the four indices (Rx5day, R10, R20 and R95p) and the

Table 4 Summary correlation analysis between the selected extreme precipitation indices in Adama city from 1965 to 2016

	PRECTOT	SDII	Rx1day	Rx5day	R10	R20	CDD	CWD	R95p	R99p
PRECTOT	1									
SDII	69.8*	1								
Rx1day	26.4	5.3	1							
Rx5day	62.4*	50.2*	48.8*	1						
R10	83.4*	82.1*	− 0.6	43.3*	1					
R20	89.7*	79.8*	6.2	56.3*	85.9*	1				
CDD	− 29.9*	− 11.8	1.4	− 22.4	− 11.6	− 23.3	1			
CWD	− 8.5	− 57.5*	31.7*	− 5	− 44.5*	− 36.0*	5.8	1		
R95p	75.8*	66.1*	46.5*	61.4*	51.9*	66.4*	− 34.8*	− 14	1	
R99p	41.8*	26.7	78.4*	63.1*	19.8	26.5	− 4	12.6	52.4*	1

*Correlation is significant at the 0.05 level

Table 5 Candidate predictors for calibration of SDSM

Short name	Long name	CanESM2	HadCM3
s500	Specific humidity at 500 hPa height	√	
r500	Relative humidity at 500 hPa height		√
p5_u	Zonal velocity component at 500 hpa	√	
p5_v	Meridional velocity component at 500 hPa height		√
shum	Near-surface specific humidity	√	√
p8_z	Vorticity at 850 hPa	√	
p8zh	Divergence at 850 hPa height		√
prcp	Total precipitation	√	

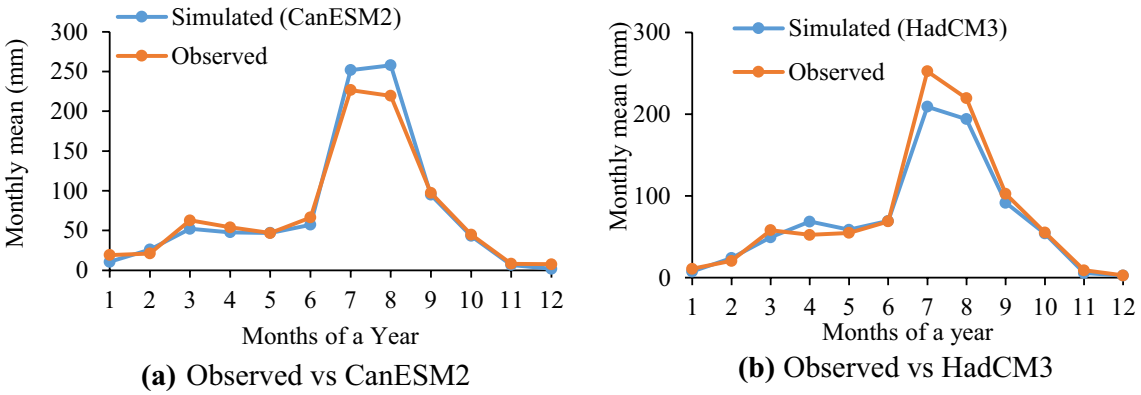

Fig. 4 Observed versus simulated monthly mean precipitation for the period of **a** 1991–2005, **b** 1991–2001

negative correlation with CWD are also significant at the selected level of the analysis.

Future precipitation

Selected predictors for SDSM

With the procedures described in Sect. 2.3.2, the candidate predictors shown in Table 5 were selected for calibration of SDSM for a downscaling experiment in this study. In the process of screening predictors, specific humidity at 500 hPa height (s500) and divergence at 850 hPa height (p8zh) were identified as super predictors for CanESM2 and HadCM3, respectively. Using these, additional four predictors from CanESM2 and three predictors from HadCM3 were selected.

Performance of SDSM

The performance of the downscaling model calibrated using the respective sets of selected predictors was evaluated on the basis of graphical and statistical parameters. Figure 4 illustrates the graphs of the monthly mean observed and the downscaled reanalysis data for each month of validation periods. It can be seen from the graphs that there is a good agreement between the generated and observed values of precipitation, except a slightly overestimate for July and August in the case of CanESM2 and underestimate for HadCM3.

Table 6 Performance assessment of SDSM during validation periods: 1991–2005 for NCEP_CanESM2 and 1991–2001 for NCEP_HadCM3

	NCEP_CanESM2		NCEP_HadCM3	
	Daily	Monthly	Daily	Monthly
R^2	0.088	0.992	0.100	0.986
RSD	0.49	1.17	0.51	0.84

The computed values of the coefficient of determination and the ratio of the standard deviations of simulated to observed time-series data are summarized in Table 6. The values of RSD show that the variations in monthly data are about the same in both GCMs. However, it can be seen that the values of the parameters computed from the daily time-series are relatively lower than the results of monthly time-series data, indicating the monthly variations are better captured by the SDSM. This is due to the fact that the amount of daily precipitation at a specific site is poorly determined by

the regional climate forcing. Hence, the results of the statistical parameters obtained in this study are quite respectable. In general, the overall evaluation of the SDSM performance suggests that the agreement between simulated and observed data is satisfactory, indicating a potential application of the calibrated model for downscaling future daily precipitation from the outputs of the two GCMs for the study area.

Future annual precipitation scenarios

The future daily precipitation was downscaled from the outputs of the selected GCMs under five climate change scenarios. Figure 5 shows the plots of annual future precipitation (aggregated from daily values) in Adama city from 2021 to 2080. The statistical parameters summarized in Table 7 provides the descriptive information about future annual rainfall scenarios in Adama city from 2021–2080. Overall, the results show that the city will receive remarkable annual precipitation over the coming 60 years. The range of future annual precipitation is greater under the scenarios of CanESM2 than that of HadCM3 in which the highest annual mean rainfall is projected. In addition, it can be seen from Fig. 5 that under all climate change scenarios, the maximum annual rainfall is expected in the far-future period (2050s).

Regarding the two ends of each statistic, the information summarized in Table 7 shows that the city expects the maximum annual precipitation between 1065.8 mm (H3A2a) and 2251.6 mm (RCP8.5) over the coming 60 years, whereas the minimum rainfall ranging from 445.7 mm (RCP2.6) to 717.7 mm (H3A2a) is predicted within the same period. In addition, maximum and minimum values of mean annual rainfall varies between 907.1 mm (H3A2a) and 670.8 mm (RCP4.5). Further, with reference to the values of standard deviations, it can be viewed that the relative dispersion in the annual precipitation is about the same for the two scenarios of HadCM3. However, in the case of the scenarios of CanESM2, dispersion in annual rainfall under RCP8.5 is higher than the other two scenarios (RCP2.6 and RCP4.5) which showed about similar dispersions.

Table 7 Statistics of future annual precipitation in Adama city over the years 2021–2080 under the five climate change scenarios

	Annual precipitation			
	Maximum	Minimum	Mean	Std. dev.
CanESM2				
RCP2.6	1358.9	445.7	716.6	180.8
RCP4.5	1580.2	501.5	670.8	161.1
RCP8.5	2251.6	512.0	762.7	253.6
HadCM3				
H3A2a	1123.3	717.7	907.1	84.9
H3B2a	1065.8	693.2	879.7	84.1

Future changes in extreme precipitation

With future daily precipitation data, the likely changes of precipitation extreme in the near-future (2020s) and far-future (2050s) periods under five scenarios were assessed with respect to the conditions during 1971–2000. Table 8 shows the computed future changes of extreme precipitation indices: wet-day%, POT95, CWD and PRECTOT. Overall, the future changes of the selected indices are found to be increasing under the majority of climate change scenarios over the analysis period, despite the magnitude significantly vary between GCMs, scenarios and time-windows.

Each of the three scenarios of CanESM2 projected to consistently increasing changes over the years 2021–2080 with different ranges across the indices: wet-days% (11.2–23.1%), POT95 (4.7–23.9%), CWD (9.1–32.5%), PRECTOT

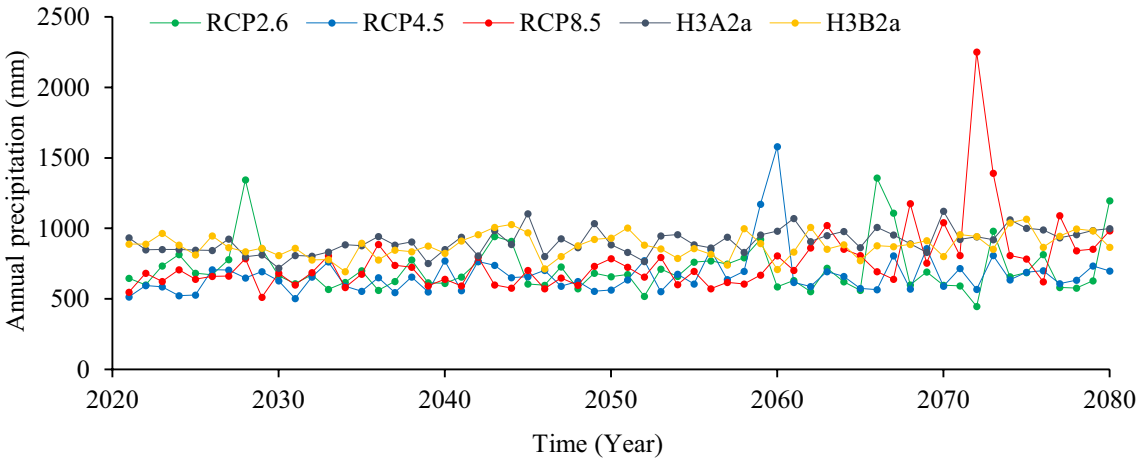

Fig. 5 Annual rainfall in Adama city based on the projection of CanESM2 and HadCM3 for the period of 2021–2080

Table 8 Percentage change of extreme precipitation indices in the future (2021–2080) with reference to a base period (1971–2000)

Model/scenarios	Time-zone	Wet-days%	POT95	CWD	PRECTOT
CanESM2					
RCP2.6	2020s	12.9	14.6	9.1	28.2
	2050s	13.8	17.9	15.2	31.1
RCP4.5	2020s	11.2	4.7	14.7	13.1
	2050s	14.2	16.1	32.5	29.6
RCP8.5	2020s	13.8	8.6	16.2	20.8
	2050s	23.1	23.9	28.9	55.1
HadCM3					
H3A2a	2020s	− 2.2	0.0	9.8	2.5
	2050s	1.5	0.3	25.6	10.5
H3B2a	2020s	− 0.5	− 0.2	20.6	2.5
	2050s	− 1.3	− 0.5	42.4	5.4

(13.1–55.1%). In addition, the difference between the projection of RCP2.6 and RCP4.5 will decrease in most of the analyzed indices in the far-future (2050s).

With regard to HadCM3, the consistency of increasing changes was observed throughout the study period, except in the case of wet-days% and POT95 corresponding to H3B2a. In addition, the ranges of the changes projected by H3A2a and H3B2a scenarios for the analyzed indices are relatively small, except for CWD. H3B2a projected wet-days% and POT95 decrease throughout the study period, despite the changes are small.

With the exception of CWD, CanESM2 offers maximum values of the indices in both analysis periods. In addition, the projected change by both models are more significant in the far-future, but for H3B2a results for wet-days% and POT95. In the 2020s, RCP2.6 showed a maximum of two indices (PRECTOT, POT95), while in the 2050s, excluding CWD, the maximum in the selected indices changes were made via RCP8.5.

In all analyzed scenarios, the increase in CWD and PRECTOT indices is predicted. The maximum and minimum changes in CWD are 42.4% (H3B2a) and 9.1% (RCP2.6), respectively. With respect to the results of each model, the maximum value for CWD in CanESM2 is equal to 32.5% corresponding to RCP4.5 in the 2050s. The maximum change in total annual precipitation is also predicted to be 55.1% (RCP8.5) in 2050s, while the minimum value is predicted by the two scenarios of HadCM3 and equal to 2.5%.

Discussion

In general, the results reveal that most of the extreme rainfall indices, including Rx5day, SDII, R10, R20, R95p and PRECTOT showed a statistically significant upward trend over the years 1965–2016. Some of the findings are slightly different from the results reported by Shawul and Chakma (2020) for the rainfall time-series (1980–2012) in the upper Awash basin in which Adama station belongs. The authors reported a negative trend for SDII and R20, and no statistically significant trend for R10 over the study period for Adama station. The disparity between the findings of the present study and that of Shawul and Chakma (2020) could be because of the different periods analyzed. It has been argued that the length of climate records is an important factor that affects the probability of identifying trends in any given time-series data. In the present study, rather long period has been analyzed, which may include different trends within different sub-periods. The results of this study suggest that the extreme precipitation in Adama city was increasing over the past 52 years, which could explain the notable impacts of climate change. Furthermore, consistent with Lima et al. (2015), a statistically significant correlation is found between PRECTOT and SDII and other indices. This indicates the trends of annual total and average daily precipitation of wet-days were changing with the changes in the trends of most of the extreme precipitation indices.

The performance of the downscaling model used in this study was also found to be good in predicting the daily precipitation during the validation period. The results are comparable to that of studies conducted to inspect the impacts of climate change on future precipitation extremes in Addis Ababa city (Feyissa et al. 2018) and Amhara Regional State (Ayalew et al. 2012). The results indicate a successful application of the SDSM for downscaling local-scale daily precipitation from the estimates of large-scale atmospheric information for the study area.

Future changes in extreme precipitation in Adama city are also another important finding of this study. Under all scenarios of the GCMs, almost all of the analyzed extreme precipitation statistics will increase up to 2080, despite the changes will be higher in the far-future (2050–2080) than near-future (2021–2050). The changes in wet-day%, POT95 and PRECTOT could reach 23.1%, 23.9%, and 55.1%, respectively and predicted by the worst scenario of CanESM2. The changes in the longest wet-spell will also increase by 42.4% that projected by the worst scenario of HadCM3. The results suggest that the study area is expected to receive more severe extreme precipitation events over 2021–2080 as compared to the condition during 1971–2000. In accordance with this result, Feyissa et al. (2018) reported the extreme precipitation in Addis Ababa city will increase over the twenty-first century, while the present study is pertaining to Adama city which has been little explored. With a high rate of urbanization in Adama city that has expanded built-up area at the cost of agricultural land in the upper watershed area of the city administration (Bulti and Abebe 2020), the future increase of extreme precipitation events

can produce high runoff, thereby increases the chance of more severe floods to occur.

Given the importance of improved understanding of the trend of extreme precipitation in planning for sustainable flood risk management, the findings of this study can serve as a springboard for decision-makers for early identification of potential impacts due to predicted changes. For mitigation planning, it is ideal to consider the changes under the worst scenario; however, it could not be always possible due to the existing limited resources. In this regard, the results presented here can support the analysis of alternative responses to the impacts of climate change under different scenarios. Moreover, the results could also be used in various modeling studies (e.g., Flood modeling) to assess the impacts of future climate conditions.

Conclusions

The intent of this study was to provide information about the characteristics of extreme precipitation events in the observed daily precipitation records in flood vulnerable city of Adama and its changes under future climate conditions. For this, the extreme rainfall in Adama city during 1965–2016 was analyzed based on the trends of 10 selected precipitation extreme indices computed from daily time-series records. Using SDSM, the projections of GCMs (CanESM2 and HadCM3) under 5 climate change scenarios were downscaled to provide daily precipitation in the study area for the period 2021–2080. Taking the climate conditions during 1971–2000 as a base period, future changes in extreme precipitation were investigated using delta approach.

The study reveals that the extreme precipitation events in Adama city were increasing over the period of 1965–2016. The results also indicate a successful application of the SDSM for downscaling local-scale future daily precipitation from the outputs of large-scale atmospheric information for the study area. Moreover, under future climate change scenarios, the extreme precipitation would increase up to 2080, despite the changes will be higher during 2050–2080. The findings infer that as compared to the past period, Adama city could experience frequent and more severe floods during the coming 60 years due to the changes in global climate.

The length and quality of time-series records used and the variety of precipitation extreme indices examined here allowed to describe the structure and changes of extreme precipitation over the past 52 years in Adama city. Moreover, the important large-scale datasets (i.e., quality of predictors and climate change scenarios), the downscaling model and the statistics/indices used in this study enabled to examine the changes in extreme precipitation under future climate conditions in the city. The findings of this study would support planning for effective management of flood risks due to the impacts of climate change on extreme precipitation in Adama city.

Acknowledgements This paper is a part of ongoing Ph.D. dissertation by Dejene Tesema Bulti at Ethiopian Institute of Architecture, Building Construction and City Development (EiABC), Addis Ababa University, Ethiopia. We would like to thank the anonymous reviewers and the editor for their genuine comments and corrections which helps the paper to be in its present form.

Author contributions DTB has conceived of the study and made contributions in design, analysis, interpretation of the results and draft the manuscript. BGA and ZB supervised the study and reviewed the whole content. Both authors read and approved the manuscript.

Funding No funding was received.

Compliance with ethical standards

Conflict of interest The authors declare that they have no competing interests.

Ethics approval and consent to participate Not applicable.

Consent for publication We have agreed to submit for Modeling Earth Systems and Environment journal and approved the manuscript for submission.

Availability of data and material Not applicable.

References

Abbasnia M, Toros H (2016) Future changes in maximum temperature using the statistical downscaling model (SDSM) at selected stations of Iran. Model Earth Syst Environ. https://doi.org/10.1007/s40808-016-0112-z

Ayalew D, Tesfaye K, Mamo G, Yitaferu B, Bayu W (2012) Outlook of future climate in Northwestern Ethiopia. Agric Sci 3(4):608–624. https://doi.org/10.4236/as.2012.34074

Basistha A, Arya DS, Goyal NK (2009) Analysis of historical changes in rainfall in the Indian Himalayas. Int J Climatol 29(4):555–572. https://doi.org/10.1002/joc.1706

Berhane A, Hadgu G, Worku W, Abrha B (2020) Trends in extreme temperature and rainfall indices in the semi-arid areas of Western Tigray, Ethiopia. Environ Syst Res. https://doi.org/10.1186/s40068-020-00165-6

Bulti DT, Assefa T (2019) Analyzing ecological footprint of residential building construction in Adama City, Ethiopia. J Environ Syst Res. https://doi.org/10.1186/s40068-019-0130-8

Bulti DT, Abebe BG (2020) Analyzing the impacts of urbanization on runoff characteristics in Adama city, Ethiopia. SN Appl Sci 1:1. https://doi.org/10.1007/s42452-020-2961-3

Bulti DT, Mekonnen B, Bekele M (2017) Assessment of Adama city flood risk using multicriteria approach. Ethiop J Sci Sustain Dev 4(1):6–23

Choi G, Collins D, Ren G, Trewin B, Baldi M, Fukuda Y, Afzaal M, Pianmana T, Gomboluudev P, Huong PTT et al (2009) Changes in means and extreme events of temperature and precipitation in the Asia–Pacific network region, 1955–2007. Int J Climatol 29:1906–1925. https://doi.org/10.1002/joc.1979

Chu JT, Xia J, Xu CY, Singh VP (2010) Statistical downscaling of daily mean temperature, pan evaporation and precipitation for climate change scenarios in Haihe River, China. Theor Appl Climatol 99:149–161. https://doi.org/10.1007/s00704-009-0129-6

Dawit M, Halefom A, Teshome A, Sisay E, Shewayirga B, Dananto M (2019) Changes and variability of precipitation and temperature in the Guna Tana watershed, Upper Blue Nile Basin, Ethiopia. Model Earth Syst Environ. https://doi.org/10.1007/s40808-019-00598-8

Deb P, Babel MS, Denis AF (2018) Multi-GCMs approach for assessing climate change impact on water resources in Thailand. Model Earth Syst Environ. https://doi.org/10.1007/s40808-018-0428-y

Dile YT, Berndtsson R, Setegn SG (2013) Hydrological response to climate change for gilgel abay river, in the lake tana basin-upper Blue Nile basin of Ethiopia. PLoS ONE 8(10):e79296

Evans JD (1996) straightforward statistics for the behavioral science. Brooks/Cole Publishing, Pacific Grove

Feyissa G, Zeleke G, Bewket W, Gebremariam E (2018) Downscaling of future temperature and precipitation extremes in Addis Ababa under climate change. Climate. https://doi.org/10.3390/cli6030058

Gebrechorkos SH, Hülsmann S, Bernhofer C (2019) Statistically downscaled climate dataset for East Africa. Sci Data. https://doi.org/10.1038/s41597-019-0038-1

Geremew GM, Mini S, Abegaz A (2020) Spatiotemporal variability and trends in rainfall extremes in Enebsie Sar Midir district, northwest Ethiopia. Model Earth Syst Environ. https://doi.org/10.1007/s40808-020-00749-2

Gharbia SS, Gill L, Johnston P, Pilla F (2016) Multi-GCM ensembles performance for climate projection on a GIS platform. Model Earth Syst Environ 2(102):1–21. https://doi.org/10.1007/s40808-016-0154-2

Gujree I, Wani I, Muslim M, Farooq M, Meraj G (2017) Evaluating the variability and trends in extreme climate events in the Kashmir Valley using PRECIS RCM simulations. Model Earth Syst Environ. https://doi.org/10.1007/s40808-017-0370-4

Huang J, Zhang J, Zhang Z, Xu C, Wang B, Yao J (2011) Estimation of future precipitation change in the Yangtze River basin by using statistical downscaling method. Stoch Environ Res Risk Assess 25:781–792. https://doi.org/10.1007/s00477-010-0441-9

IPCC (2014) Climate change 2014: Synthesis report. In: Pachauri RK, Meyer LA (eds) Contribution of working groups I, II and III to the fifth assessment report of the intergovernmental panel on climate change. IPCC, Geneva

Lima MIP, Santo FE, Ramos AM, Trigo RM (2015) Trends and correlations in annual extreme precipitation indices for mainland Portugal, 1941–2007. Theor Appl Climatol 119(1–2):55–75. https://doi.org/10.1007/s00704-013-1079-6

Mahmood R, Babel MS (2014) Future changes in extreme temperature events using the statistical downscaling model (SDSM) in the trans-boundary region of the Jhelum river basin. Weather Clim Extremes 5–6:56–66. https://doi.org/10.1016/j.wace.2014.09.001

Mekasha A, Tesfayed K, Duncan AJ (2014) Trends in daily observed temperature and precipitation extremes over three Ethiopian eco-environments. Int J Climatol 34:1990–1999. https://doi.org/10.1002/joc.3816

Mekonen AA, Berlie AB (2019) Spatiotemporal variability and trends of rainfall and temperature in the Northeastern Highlands of Ethiopia. Model Earth Syst Environ. https://doi.org/10.1007/s40808-019-00678-9

Mekonnen DF, Disse M (2018) Analyzing the future climate change of Upper Blue Nile River basin using statistical downscaling techniques. Hydrol Earth Syst Sci 22:2391–2408. https://doi.org/10.5194/hess-22-2391-2018

Mohammed Y, Yimer F, Tadesse M et al (2018) Variability and trends of rainfall extreme events in north east highlands of Ethiopia. Int J Hydrol 2(5):594–605. https://doi.org/10.15406/ijh.2018.02.00131

Mohammed M, Biazn B, Belete MD (2020) Hydrological impacts of climate change in Tikur Wuha watershed, Ethiopian Rift Valley Basin. J Environ Earth Sci 10(2):28–49. https://doi.org/10.7176/JEES/10-2-04

Moses O, Gondwe M (2019) Simulation of changes in the twenty-first century maximum temperatures using the statistical downscaling model at some stations in Botswana. Model Earth Syst Environ. https://doi.org/10.1007/s40808-019-00571-5

Navarro-Racines C, Tarapues J, Thornton P, Jarvis A, Ramirez-Villega J (2020) High-resolution and bias-corrected CMIP5 projections for climate change impact assessments. Sci Data 7(7):1–14. https://doi.org/10.1038/s41597-019-0343-8

Ngongondo C, Chong Y, Lottschalk L, Alemaw B (2011) Evaluation of spatial and temporal characteristics of rainfall in Malawi: a case of data scarce region. Theor Appl Climatol 106(1–2):79–93

Pervez S, Henebry GM (2014) Projections of the Ganges–Brahmaputra precipitation—downscaled from GCM predictors. J Hydrol. https://doi.org/10.1016/j.jhydrol.2014.05.016

Rukundo E, Doğan A (2016) Assessment of climate and land use change projections and their impacts on flooding. Pol J Environ Stud 25:2541–2551

Salvacion AR, Magcale-Macandog DB, Sta Cruz PC, Saludes RB, Pangga IB, Cumagun CJR (2018) Evaluation and spatial downscaling of CRU TS precipitation data in the Philippines. Model Earth Syst Environ. https://doi.org/10.1007/s40808-018-0477-2

Samuale T, Raj A, Girmay G (2014) Assessment of climate change impact on the hydrology of Geba catchment, Northern Ethiopia. Am J Environ Eng 4:25–31

Santo FE, Ramos AM, Lima MIP, Trigo RM (2013) Seasonal changes in daily precipitation extremes in mainland Portugal from 1941 to 2007. Reg Environ Change. https://doi.org/10.1007/s10113-013-0515-6

Semenov MA, Stratonovitch P (2010) Use of multi-model ensembles from global climate models for assessment of climate change impacts. Clim Res 41:1–14. https://doi.org/10.3354/cr00836

Shang H, Yan J, Gebremichael M, Ayalew SM (2011) Trend analysis of extreme precipitation in the Northwestern Highlands of Ethiopia with a case study of Debre Markos. Hydrol Earth Syst Sci 15:1937–1944. https://doi.org/10.5194/hess-15-1937-2011

Shawul AA, Chakma S (2020) Trend of extreme precipitation indices and analysis of long-term climate variability in the Upper Awash basin, Ethiopia. Theor Appl Climatol. https://doi.org/10.1007/s00704-020-03112-8

Shiferaw H, Gebremedhin A, Gebretsadkan T, Zenebe A (2018) Modelling hydrological response under climate change scenarios using SWAT model: the case of Ilala watershed, Northern Ethiopia. Model Earth Syst Environ. https://doi.org/10.1007/s40808-018-0439-8

Steffen M (2019) CRAN-Package imputeTS. R J 1:207–218

Supharatid S, Aribarg T, Supratid S (2016) Assessing potential flood vulnerability to climate change by CMIP3 and CMIP5 models: case study of the 2011 Thailand great flood. J Water Clim Change 07(1):52–67

Wilby RL, Dawson CW (2007) SDSM 4.2—a decision support tool for the assessment of regional climate change impacts. https://sdsm.org.uk/software.html. Accessed 12 May 2020

Wilby RL, Dawson CW (2013) The statistical downscaling model (SDSM): Insights from one decade of application. Int J Clim 33:1707–1719

Zhang X, Alexander L, Hegerl GC, Jones P, Tank AK, Peterson TC, Trewin B, Zwiers FW (2011) Indices for monitoring changes in extremes based on daily temperature and precipitation data. Wiley Interdiscip Rev Clim Chang 2(6):851–870

A review of flood modeling methods for urban pluvial flood application

Dejene Tesema Bulti & Birhanu Girma Abebe

Modeling Earth Systems and Environment

ISSN 2363-6203
Volume 6
Number 3

Model. Earth Syst. Environ. (2020)
6:1293-1302
DOI 10.1007/s40808-020-00803-z

Springer

Modeling Earth Systems and Environment (2020) 6:1293–1302
https://doi.org/10.1007/s40808-020-00803-z

REVIEW ARTICLE

A review of flood modeling methods for urban pluvial flood application

Dejene Tesema Bulti[1] · **Birhanu Girma Abebe**[1]

Received: 21 January 2020 / Accepted: 25 April 2020 / Published online: 5 May 2020

Abstract

Pluvial flood has been increasingly understood as a major threat that has presented a significant risk for many cities worldwide. Regarding flood risk management, flood modeling enables to understand, assess and forecast flood conditions and their impact. Likewise, several hydrodynamic models have been developed and their application has been spread. With respect to effective flood modeling, particularly in urbanized floodplains, the choice of an appropriate method, considering contextual requirements, is challenging. This paper gives an overview of prevailing flood modeling approaches in view of their potentials and limitations for modeling pluvial flood in urban settings. The existing methods are categorized into: rapid flood spreading, one-dimensional sewer, overland flow (1D and 2D), sewer-surface coupling approaches (1D–1D and 1D–2D). Each of these techniques is described, by taking aspects influencing the selection of a proper flood modeling method for a particular application into account. This paper would help urban flood managers, and potential users undertake effective flood modeling tasks, balancing between their needs, model complexity and requirements of both input data and time.

Keywords Urban flood · Flood risk · Hydrodynamic model · Flood hazard · Floodplain

Introduction

Nowadays, flood has become the supreme catastrophic natural hazard with significant economic damage and loss of lives, particularly in urban areas (Tsubaki and Fujita 2010; Bulti et al. 2019; Natarajan and Radhakrishnan 2019). Flooding in urban areas is associated with pluvial flood (Tingsanchali 2012; Bouvier et al. 2017; Rosenzweig et al. 2018; Meng et al. 2019), usually occurs when the volume of runoff exceeds the conveyance capacity of the storm sewer. Since recent decades, pluvial flood has been increasingly considered as a major threat and presented a substantial risk for many cities (Fritsch et al. 2016; Rangari et al. 2018).

In response to this adversity, flood inundation modeling has significant contributions. Flood modeling provides the distribution and extent of inundation alongside its dynamics. These are helpful input information for planning to mitigate the flood and reduce its effects (Tsubaki and Fujita 2010; Fan et al. 2017; Meng et al. 2019). The yields of real-time flood simulations can help emergency operations (Jiang et al. 2015; Gharbi et al. 2016). Modeling flood inundation has also been regarded as an effective way to plan, design and analyze the storm sewer in cities (Fan et al. 2017; Ahamed and Agarwal 2019; Laouacheria et al. 2019). It can support to assess the performance of the stormwater sewer network under severe events as well as to test and appraise the success of the operational and structural solutions. Besides, it has been applied in planning for environmental flows to uphold healthy aquatic ecosystems (Teng et al. 2017; Sisay et al. 2017; Abdulkareem et al. 2018).

Despite its benefits, reliable flood inundation modeling is not as simple as it sounds, due to the chaotic and multifaceted nature of flooding (Basnayaka and Sarukkalige 2011; Freer et al. 2013; Bellos et al. 2017; Fan et al. 2017). Numerous hydrodynamic models have been developed for determining the flood conditions through diverse methods. Their applications have also been realized through commercial and open-source simulation tools (Henonin et al. 2013; Jiang et al. 2015). From application point of view, different applications require diverse kinds of information and level

✉ Dejene Tesema Bulti
dejenetesema@yahoo.com

Birhanu Girma Abebe
birhanu.girma@eiabc.edu.et

[1] Ethiopian Institute of Architecture, Building Construction, and City Development, Addis Ababa University, Addis Ababa, Ethiopia

of accuracy. As an example, flood risk assessment in urban areas relies on the precision of critical flow representation. The flow velocity should be sensibly modeled for flood damage assessment, while the maximum water depth and extent of inundation could be sufficient for hazard mapping, water resource planning and environmental flow assessment. Moreover, shorter computational time is needed for real-time applications, as precise information could be unusable if it is not accessible at the required time. Of these reflections, imply the users to reasonably select a model, balancing between their needs, modeling requirements and computational efficiency. This poses more demand for knowledge about the aspects of the underlying modeling methods attributed to the available hydrodynamic models.

The present paper aims to provide an overview of the existing flood inundation modeling methods for application for pluvial flood in urban settings. The relation between rainfall and runoff has been discussed, largely in hydrological literature. In order to assist urban-oriented readers in coming to grasp with this vast literature, the rainfall–runoff process in urban areas and the primer of urban pluvial flooding are presented. Following this, a review of existing flood modeling approaches is presented while discussing their advantages and limitations towards modeling urban pluvial flood.

Urban hydrological process

Rainfall-runoff in urban areas

Flood modeling needs an adequate understanding of important processes that occur in the drainage system from the input (rainfall) to the output (outflow) (Josef 2012; Jaafar et al. 2015). Figure 1 demonstrates the rainfall–runoff process in urban regions. Rainfall, a prominent type of precipitation, is the main source of runoff in most urban areas (Butler and Davies 2011; Tingsanchali 2012). It is usually expressed as a depth of liquid water measured in millimeters, indicating the water depth that would store on the ground surface, if all the rain remained where it had dropped. The amount of the rainfall fluctuates over time and space. The variation is small for storms with short duration and small distances (Loucks et al. 2005; Subramanya 2008). Intense rainfall tends to originate from small rain cells, approximately one kilometer in diameter. Such storms, usually last for a short period and their intensity changes considerably in space. Conversely, the fluctuation in intensity is smaller for extended storm events, arising from the larger rainfall cells.

Not all rainwater falling on the catchment surface is converted to runoff, rather it is subjected to initial and continuing losses. Initial loss refers to the portion of stormwater conserved on vegetation and buildings. It also includes rainwater trapped in surface puddles, and ditches occur on any surfaces, paved or otherwise. The volume of initial loss is commonly considered as a minimum quantity of rainfall causing runoff (Loucks et al. 2005). On the other hand, continuing loss occurs as a result of the processes of infiltration and evapotranspiration, and they are assumed to proceed as far as the stormwater is available on the surface of the ground. The amount of both types of losses relies on the catchment characteristics and duration of the storm. For instance, in urbanized catchment with dominant impervious surfaces, the loss prior to runoff is smaller for periods with intense rainfall (Josef 2012). Infiltration is usually higher at

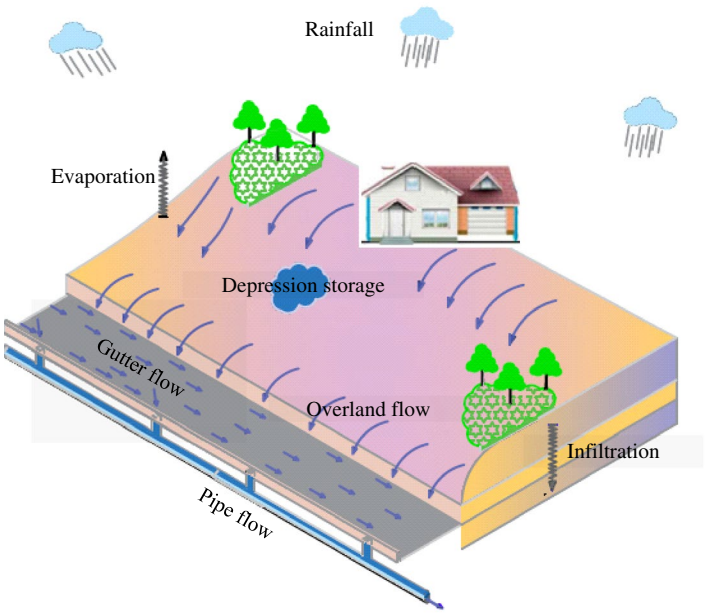

Fig. 1 Schematic representation of rainfall–runoff processes in urban areas

the start of a rain and tends to diminish exponentially, once the soil became saturated (Gupta 2017).

If the amount of precipitation exceeds the combined initial and continuing losses, the excess rain known as runoff starts flowing across the surface to enter the drainage network. The flow will be changed to gutter flow as it reaches streets or natural flow paths. Finally, it becomes pipe flow once it enters the storm water drainage system.

Urban pluvial flooding

The main processes explained in "Rainfall-runoff in urban areas" section are useful in flow modeling in urban settings if the discharge is less than the conveyance capacity of the storm sewer system. However, when the capacity is reached or exceeded, the exceedance flow is induced refers to *pluvial flood*. The exceedance can occur either before the water reaches the minor drainage system or when outflow from the system occurs, or as the combination of the two cases (Rosenzweig et al. 2018).

The dual-drainage concept is usually used to explain the exceedance flow (Fig. 2). It divides the urban drainage system into two components: minor system and major system (Maksimović et al. 2009; Simões et al. 2011; Rao and Ramana 2015). The minor drainage system encompasses the traditional storm drainage hardware (manholes, gully inlets, storm sewer and roadside ditches) and culverted watercourses. This drainage system is generally capable of conveying the flow during more frequent storm conditions with the flow kept below the ground surface. The major drainage system is the route followed by stormwater when the conveyance capacity of the minor drainage system is surpassed (Jahanbazi and Egger 2014). It consists of the flow pathways along the surface whose primary purpose is generally not to convey flow, such as streets and other artificial and natural channels and temporary storage areas (e.g., Playing Fields).

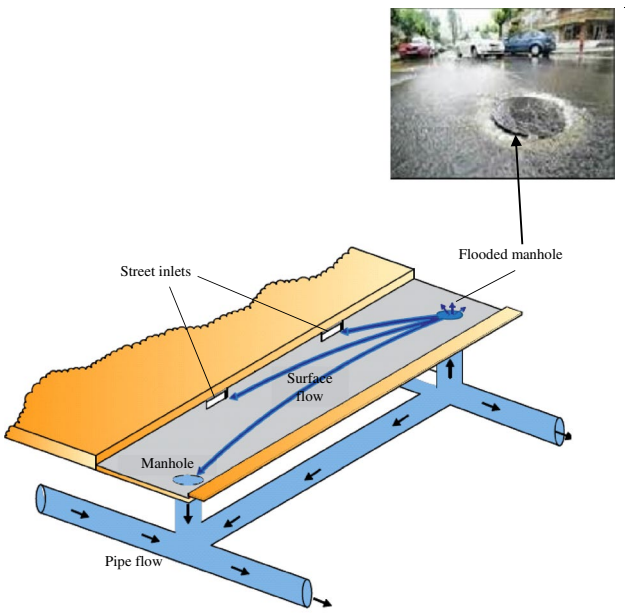

Fig. 2 Illustration of dual-drainage concept

The interface points of the minor and major systems are vital features of exceedance. The flow exchange between the two systems takes place at gully inlets, manholes and river outfalls (Leandro et al. 2009; Hénonin et al. 2015). Generally, gully inlets are provided for runoff to enter into the storm sewer and manholes are access points for maintenance and services of the storm sewer. Nonetheless, if the conveyance capacity of the storm sewer is reached or the inlets are obstructed, water cannot enter into the system and will be retained on the surface. Likewise, if the capacity of the sewer is surpassed, the water can exit the system at the inlets and manholes. The river outfalls are also used as outlet points for the minor system, yet if the level of water in the receiving watercourse rises, a backwater can be formed and induces exceedance.

Flood modeling approaches

There are various underlying approaches for modeling flood inundation attributed to the existing hydrodynamic models. They can be categorized as: rapid flood spreading (RFS), one-dimensional sewer (1D-S), one-dimensional overland (1D), two-dimensional overland (2D), coupling sewer-overland (1D–1D and 1D–2D). The selection of a proper method for a particular flood modeling application needs to take various factors into account. The underlying modeling technique should be capable of representing important flood processes, as accurate results of flood modeling can only be derived if no important process is missed out (Butler and Davies 2011). Potential outputs are also needed to meet requirements of the intended applications in terms of quality and type (Chen et al. 2014; RainGain 2015). Further, the time required for computation should be feasible to meet the run-time requirements of the planned applications (Moore et al. 2015; Teng et al. 2017), as accurate information would be useless, if it is not available at the right time. Finally, the collection and processing of the required input data must be feasible within the modeling project period and also the availability of other kinds of resources, like hardware, technical skills and simulation tools. These facets were taken into concern to guide the extraction of information from the documents, such as journal articles, guidelines and reports related to the respective approaches. The features of each of the inundation modeling methods are discussed within the remainder of this section, and Tables 1 and 2 show the summary of the main features of the methods.

Table 1 Potentials of modeling approaches to represent dominant flow process and likely outputs

Modelling approach	Overland flow representation	Outputs (Inundation characteristics)				Main spatial data required
		Overflow Location	Inundation extent	Inundation depth	Flow velocity	
RFS	No	No	Yes, but only the final state	Yes, but only the final state	No	DTM
1D surface	Yes, but only in surface networks	No	Yes, but only in surface networks	Yes, but only in surface networks	Yes, but in one-direction	DTM, Surface networks (major system)
1D sewer	No	Yes	Yes, but approximation with virtual storage	Yes, but approximation with virtual storage	No	DTM, Stormwater drainage network (minor system)
2d surface	Yes, in 2D	No	Yes	Yes	Yes, in two-direction	DTM and Topographic data
1D–1D coupled	Yes, but only in surface networks	Yes	Yes, but only in surface networks	Yes, but only in surface networks	Yes, one directional	DTM, surface networks and stormwater drainage network
1D–2D coupled	Yes, in 2D	Yes	Yes	Yes	Yes, two directional	Surface network, sewer network and Topographic data, DTM

Table 2 Relative accuracy, run-time requirements and suitable scale of applications of flood modeling approaches

Model type	Accuracy for flood risk analysis	Run-time	Suitable spatial scale of application
	Low	*One minute*	*Macro*
RFS 1D surface 1D sewer 1D-1D coupled 2D surface 1D-2D coupled	↓	↓	↓
	High	*Hours*	*Micro*

Rapid flood spreading

Rapid flood spreading (RFS) method is the simplified flood simulation approach that takes the total floodwater volume as an input and spread over the floodplain (Liu and Pender 2010; Bernini and Franchini 2013). The spreading of the floodwater is carried out based on the flat-water supposition, in which the levels of water in neighboring cells are equalized (Yang et al. 2015). The floodwater is assigned to local low points in the respective impact zones and can also cross the boundaries of the zones.

The overall process involves two stages: pre-calculation routine and inundation routine. In the former stage, areas where the storm water accumulates during flood events known as impact zones are delineated using a digital terrain model (DTM). In addition, an array of grid cells (storage cells) is established on the floodplain (Fig. 3), and then, the cell with lower elevation is identified in which the spreading of floodwater starts. In the later stage, using the total volume of floodwater from respective zones, the inundation is computed by spreading the volume over the individual grid cells (Krupka et al. 2007). The process starts by filling the lowest cell adjacent to the input points and spilling the excess to the neighboring cells. This process is repeated till the inundation reaches its final state, i.e., no excess volume of water. The output is a gird of the floodwater depth of the floodplain area.

This approach mainly requires terrain data and two minutes or less, for computation (Liu et al. 2015; Yang et al. 2015; Shen et al. 2016), enabling a several scenarios to be built and

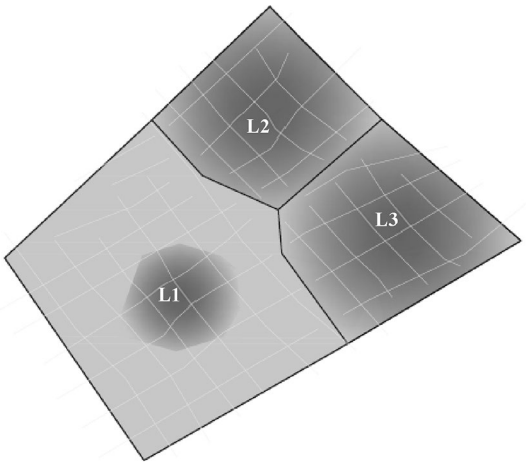

Fig. 3 Illustration of flood catchment delineation for rapid flood spreading (L: pit cell)

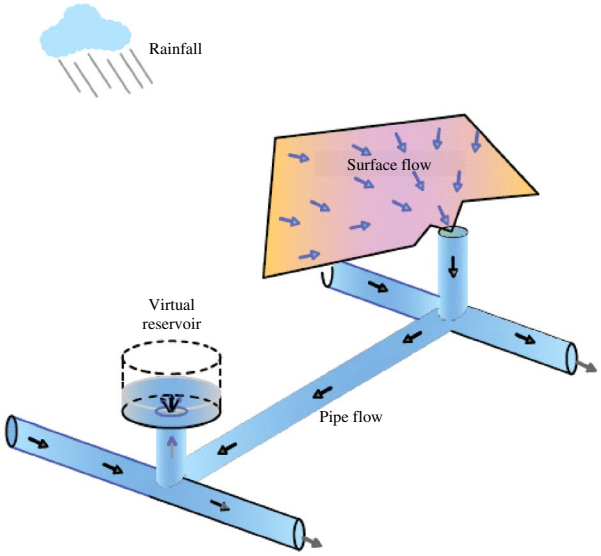

Fig. 4 Illustration of 1D sewer flow modeling approach, showing the virtual reservoir at the flooded manhole

run. However, the result can only show the final state of inundation and fail to describe actual flood information, such as sources of the flood, flow pathways, flow velocity and duration (Lhomme et al. 2009; Fritsch et al. 2016). Moreover, it does not contemplate the effects of the flow in the minor drainage system. RFS method is recommended when an overview of the flooding condition in the general basin is required, and for rapid assessment, specifically when adequate input data to run complex models are not available (Aksoy et al. 2016). It can also be used in probabilistic models that consider defense failure, involving the analysis of a range of loading with various defense failure combinations (Liu and Pender 2012).

One-dimensional sewer

One-dimensional (1D) for sewer flow modeling approach attempts to simulate the flow in the storm sewer and simplify the situations when the system conveyance capacity is exceeded. It represents the minor system as a set of links (represent conduits) and nodes (represent manhole or gullies). With this approach, the overflow is considered as stagnant water temporarily stored in a virtual storage on the top of the manholes (Fig. 4), and it is supposed that the water starts returning from the storage when the situation of hydraulic head in the node permits (Henonin et al. 2013). The hydraulics are solved using the Saint–Venant equations: continuity equation (Eq. 1) and dynamic equation (Eq. 2).

$$\frac{\partial A}{\partial t} + \frac{\partial Q}{\partial x} = 0 \tag{1}$$

$$\frac{\partial Q}{\partial t} + \frac{\partial\left(\frac{Q^2}{A}\right)}{\partial x} + gA\frac{\partial y}{\partial x} - gA\left(S_0 - S_f\right) = 0 \tag{2}$$

where Q discharge (m^3/s), t time (s), A area of the wet cross section (m^2), x distance (m), y flow depth (m), B water surface width (m), g gravity acceleration; S_0 bed slope, S_f friction slope.

Storm sewer network and DTM are the main spatial data for modeling flood inundation using this method. The required time for computation ranges from 1 min to 1 h (Chen et al. 2014; Henonin et al. 2013), allowing to run multiple scenarios. This approach enables to identify the potential overflow locations and the corresponding volume of floodwater accurately. The volume of overflowed water at each node can help to identify the distribution of hotspots. It can also be used for approximating the average inundation depth over the storage cross section. Nonetheless, besides the challenges associated to, how to define the dimensions of the virtual storage, the floodwater depth computed in the reservoir rarely represents the realistic behavior of the floodwater (Mark et al. 2004; Jiang et al. 2015). Therefore, the floodwater depth may not be determined precisely.

This modeling approach is suitable for urban applications, normally for planning and management of storm water drainage (Walsh et al. 2014; Zhu et al. 2016; Ahamed and Agarwal 2019). They are also recommended for rapid studies that do not require too much precision of surface runoff routing, including real-time application, emergency operation and early warning (Jiang et al. 2015; Gharbi et al. 2016).

Overland flow modeling

One-dimensional surface

One-dimensional (1D) modeling of surface flow aims to represent the major system flow in one dimension. In this case, the floodplain is discretized as a set of linked nodes (Leandro et al. 2009; RainGain 2015). The links represent surface flow pathways, and characterized by linear geometry. The nodes represent ponds and junctions, and characterized by storage capacity and represented by nodes. The surface network is extracted manually or automatically from digital elevation models (DEM) of the floodplain using different tools, such as Automatic Overland Flow Delineation. With this technique, the floodplain is deemed as a user-defined network of open channels and ponds. The governing equations are solved similar to pipe flow ("one-dimensional sewer" section).

Modeling flood inundation using this approach requires few types of input data (DTM and surface networks) and short run-time (Abderrezzak et al. 2009; RainGain 2015), but the setup of models of this type seems to be time demanding (Henonin et al. 2013). This modeling technique allows to determine the characteristics of inundation as far as the flow is well channeled and the water is confined within the surface network (RainGain 2015). However, it is not capable of simulating multidirectional flow conditions, for instance, when the flow overtops the street curbs (Basnayaka and Sarukkalige 2011; Chen et al. 2014). Besides, since it does not take the impacts of the flow in the minor drainage system into account, the accuracy of the output information can be affected. Accordingly, the application of 1D modeling of overland flow is limited when it comes to the development of precise and reliable flood maps.

Two-dimensional surface

Two-dimensional (2D) modeling of surface flow attempts to model the overland flow propagation, by taking the two orthogonal components of the flow into account. In this approach, the catchment is discretized as a structured or unstructured mesh of hydraulic grid cells. Structured mesh usually consists quadrilateral cells, whereas unstructured type is composed of triangular or mixed triangular and quadrilateral cells (Kim et al. 2014). Every grid cell is depicted by a point with coordinates (X, Y, Z), and the catchment parameters and rainfall are assumed to be spatially homogeneous within each element (RainGain 2015). The hydraulics are solved using the two-dimensional shallow water equations: continuity equation (Eq. 3) and dynamic equations.

$$\frac{\partial h}{\partial t}+\frac{\partial (hu)}{\partial x}+\frac{\partial (hv)}{\partial y}=0 \tag{3}$$

$$\frac{\partial (hu)}{\partial t}+\frac{\partial (hu^2+\frac{1}{2}gh^2)}{\partial x}+\frac{\partial (huv)}{\partial y}=gh\left(S_{0x}-S_{fx}\right) \tag{4}$$

$$\frac{\partial (hv)}{\partial t}+\frac{\partial (huv)}{\partial x}+\frac{\partial (hv^2+\frac{1}{2}gh^2)}{\partial y}=gh\left(S_{0y}-S_{fy}\right) \tag{5}$$

where h water depth (m); g acceleration of gravity (m^2/s); u and v depth-averaged velocity (m/s) components in X and Y directions, respectively; S_{0x} and S_{fx} water surface gradient and friction resistance in X direction; S_{0y} and S_{fy} water surface gradient and friction resistance in Y direction.

2D modeling of surface flow enables to determine maximum inundation extent and dynamics of the flow, such as water depth and velocity (Liu et al. 2012). In addition, the capability of representing the flow around small scale topographic features is the main advantage of this method that makes it suitable for application in urban settings (Hénonin et al. 2015; Nkwunonwo et al. 2020). Nonetheless, the accuracy is at the expense of high capability of the computing tools, high-resolution DEM and more computational time, generally more than one hour (Moore et al. 2015; Chang et al. 2015).

Urban applications require a fine 2D grid, usually less than 5 m for accurate simulation of the flow on streets and around the buildings (Mark et al. 2004). Likewise, high-resolution topographic data are needed to represent small urban features (Nielsen et al. 2008; Gourbesville 2009). However, it should be noted that decreasing the size of hydraulic grid cells increases the density of the mesh, and requires more run-time (Fewtrell et al. 2008; Liu and Pender 2012; Shen et al. 2015; Gharbi et al. 2016). Although 2D surface flow models can provide descriptions of the overland flow propagation, it fails to provide overflow locations and to represent in channel flow, particularly for narrow watercourses. Further, such models do not consider the influences of the flow in the minor drainage system, and therefore, the accuracy of the output information could be affected. Accordingly, this approach is more suitable for applications in urban areas where there is no actual stormwater drainage or the influence of stormwater drainage is considered insignificant on the flood phenomenon under the study.

Coupled sewer-surface

1D–1D

1D–1D (sewer-surface) coupling is a condition in which a one-dimensional for minor system flow is coupled with a

one-dimensional representation of surface flow. In this case, the floodplain is treated as a user-defined network of open channels and ponds connected to the stormwater drainage system (Fig. 5). This approach enables to capture the interaction between the belowground flow and aboveground flow (Mark et al. 2004). The flow exchanges bi-directionally (i.e., Surcharging and spilling) between the two systems and takes place through coupling links: gully inlets and manholes (Leandro et al. 2009; Hénonin et al. 2015). In this case, the overflowed water at the nodes is directly discharged on the surface network to surcharge the surface flow.

The main input data include surface network, stormwater drainage network and DTM. Using moderate computation time, ranging from 5 min to 1 h, this approach enables to determine overflow location, flow-depth and velocity (one-dimension) with sufficient accuracy, assuming that the surface flowpaths are well defined (Henonin et al. 2013; Bisht et al. 2016; Kourtis et al. 2017). Conversely, it is not capable of providing the flood information when the water leaves the defined surface flow pathways. Accordingly, this modeling approach is suggested for planning and management of storm sewer, early warning and emergency operation.

1D–2D

1D–2D (sewer–surface) coupled method is a condition in which a 1D sewer flow is connected with a 2D surface flow representation. The flow interaction between the two systems takes place at the gullies and manholes and 2D grid cells (Jahanbazi and Egger 2014). In this approach, the flow

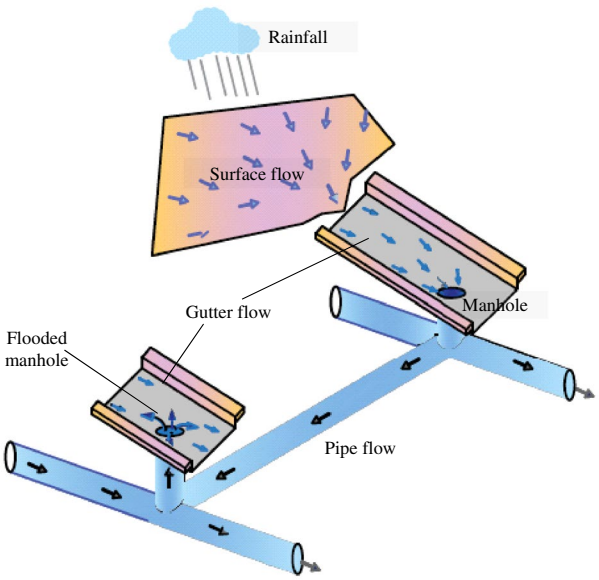

Fig. 5 Illustration of 1D–1D coupled modeling approach, simulating the flow in major and minor drainage systems

in the minor system is modeled in one-dimensional, while the surface flow is modeled as a two-dimensional problem.

The applications of 1D–2D coupled modeling method for a complex urban topography have been realized (Tayefi et al. 2007; Leitão 2009; Aksoy et al. 2016; Schlauß and Grottker 2016). This mode of coupling enables to determine the flood information (overflow location, extent, depth and velocity). The results of the simulations using this technique are more accurate than other methods (Hankin et al. 2008; Rangari et al. 2018), yet it attains this accuracy at the cost of high computational burden in terms of run-time and data requirements (Bamford et al. 2008; Leandro et al. 2009; Schlauß and Grottker 2016; Kourtis et al. 2017). This is usually considered as the main limitation of 1D–2D modeling approach when it comes to real-time simulations. Moreover, it leads to applications for smaller catchments or the use of a coarser-resolution terrain data in order to have an acceptable period of calculation.

This modeling approach is more suitable for the design/analysis of complex systems, in which a fully interactive analysis is required with on-site verification as appropriate and the capacity of the inlets is explicitly modeled (Vojinovic and Tutulic 2009; Butler and Davies 2011). The outputs of 1D–2D can also be used for calibrating a 1D–1D model in the absence of adequate field data (Leandro et al. 2011).

Strength of coupling

In model coupling process, the relationship between the belowground and aboveground flows can be defined in a loose or tight manner. For each of the coupling approaches (1D–1D and 1D–2D), both loose and tight coupling are possible. In a loose coupling mode, the sewer model is seen as a pre-processor to create input data for the surface model (Butler and Davies 2011). Therefore, the models can be operated in isolation and the results of the two models could be derived from different simulation software packages. This mode of coupling has been used in several urban studies (Adeogun et al. 2012; Burns et al. 2015; Bellos et al. 2017; Rangari et al. 2018). It can also be applied for analyzing and designing large systems with lower precision. For instance, the minor system can be designed accurately using 1D sewer, and then, surface conveyance capacity is defined by flow pathways determined in the field and modeled without detailed consideration of the interaction between the minor and major systems. It can also be used when explicit modeling of inlet capacity is not required, or when the flood risk level is expected in terms of areal extent or groups of properties.

In tight coupling mode, the interaction between the sewer and surface models cannot be split into distinct processes (Sui and Maggio 1999; WeiFeng et al. 2009), indicating a

high level of nonlinearity. This way of coupling enables to implement real-time interactions between the two models. Governing equations for network nodes, channel ends, pipes and surface channel flow are solved simultaneously. Tightly coupled models could be operated as a single unit (single simulation package). There are several commercial and open-source simulation packages that provide such access (e.g., XPSWMM and MIKE FLOOD).

Conclusions

This paper gives a review of the state-of-the-art of prevailing flood modeling approaches in view of their potentials and limitations for modeling pluvial flood in urban settings. It shows that there are various flood modeling approaches, each of which has benefits and drawbacks for applications in urban areas. The rapid flood spreading modeling approach is easy to use and required limited data and short run-time, yet it provides only the final state of inundation. The outputs of 1D sewer encompass the overflow locations and maximum floodwater volume. In addition, by simplifying the situation of the overflow using a virtual reservoir, it helps to estimate the maximum inundation extent and floodwater depth. Still, as it is not capable of describing the surface flow, the actual flood conditions could not be predicted precisely.

Flood modeling methods for surface flow can give the dynamics of the floodwater. Nonetheless, the results of 1D surface are limited to the surface network profile and one-dimensional flow velocity, and the 2D approach requires more computation time and detailed data. Besides, both approaches do not consider the influence of the flow in the stormwater drainage system, and the accuracy of the output information can be affected. In fact, the sewer-surface coupling approach enables to represent the urban dual-drainage system, as it considers the flow exchange between the major and minor systems, and provides accurate descriptions of flood conditions. However, the 1D–1D approach cannot provide information about surface flow velocities when the flow overtops the defined surface networks. On the other hand, although the 1D–2D coupling approach is capable of providing the most accurate and detailed information, it is computationally expensive both in terms of run-time and data requirements.

Given the importance of flood modeling in flood risk management, this paper provides a comprehensive understanding of the main features of existing modeling methods, such as capabilities to represent dominant flood processes, input data requirements, potential output information and run-time requirements. Accordingly, it would help urban flood managers and potential users undertake effective modeling tasks, balancing between their needs and modeling requirements.

Acknowledgements This paper is a part of ongoing PhD dissertation by Dejene Tesema Bulti at Ethiopian Institute of Architecture, Building Construction and City Development (EiABC), Addis Ababa University, Ethiopia. We would like to thank the anonymous reviewers and the editor for their genuine comments and corrections which helps the paper to be in its present form.

Author contributions DTB has conceived of the study and made contributions in design, analysis, interpretation of the results and drafted the manuscript. BGA supervised the study and reviewed the whole content. Both authors read and approved the manuscript.

Compliance with ethical standards

Conflict of interest The authors declare that they have no competing interests.

Consent for publication We have agreed to submit for Modeling Earth Systems and Environment journal and approved the manuscript for submission.

References

Abderrezzak KEK, Paquier A, Mignot E (2009) Modelling flash flood propagation in urban areas using a two-dimensional numerical model. Nat Hazards 50:433–460. https://doi.org/10.1007/s11069-008-9300-0

Abdulkareem JH, Pradhan B, Sulaiman WNA, Jamil NR (2018) Review of studies on hydrological modelling in Malaysia. Model Earth Syst Environ. https://doi.org/10.1007/s40808-018-0509-y

Adeogun AG, Pathirana A, Daramola MO (2012) 1D–2D hydrodynamic model coupling for inundation analysis of sewer overflow. J Eng Appl Sci 7(5):356–362. https://doi.org/10.3923/jeasci.2012.356.362

Ahamed SMF, Agarwal S (2019) Urban flood modeling and management using SWMM for New R. R. Pet Region, Vijayawada, India. Int Jo Recent Technol Eng: IJRTE 7(6C2):317–322

Aksoy H, Sadan V, Kirca O, Burgan I, Kellecioglu D (2016) Hydrological and hydraulic models for determination of flood-prone and flood inundation areas. IAHS 373:137–141

Bamford TB, Digman CJ, Balmforth DJ, Waller S, Hunter N (2008) Modelling flood risk—an evaluation of different methods. In: WaPUG autumn conference 2008

Basnayaka AP, Sarukkalige R (2011) Comparing hydrology and hydraulics surface routing approaches in modeling an urban catchment. In: 2nd international conference on environmental engineering and applications, vol 17, pp 123–127

Bellos V, Kourtis IM, Tsihrintzis VA (2017) A simplified methodology for flood simulation in urban catchments. Eur Water 57:307–313

Bernini A, Franchini M (2013) A rapid model for delimiting flooded areas. Water Resour Manag 27:3825–3846

Bisht DS, Chatterjee C, Kalakoti S, Upadhyay P, Sahoo M, Panda A (2016) Modeling urban floods and drainage using SWMM and MIKE URBAN: a case study. Nat Hazards 84(2):749–776

Bouvier C, Chahinian N, Adamovic M, Cassé C, Crespy A, Crès A, Alcoba M (2017) Large-scale GIS-based urban flood modelling: a case study On the City of Ouagadougou. SimHydro 2017: Choosing the right model in applied hydraulics, 14–16 June 2017

Bulti DT, Girma B, Megento TL (2019) Community flood resilience assessment frameworks: a review. SN Appl Sci 1(1663):1–17. https://doi.org/10.1007/s42452-019-1731-6

Burns MJ, Schubert JE, Fletcher TD, Sanders BF (2015) Testing the impact of at-source stormwater management on urban flooding through a coupling of network and overland flow models. WIREs Water. https://doi.org/10.1002/wat2.1078

Butler D, Davies J (2011) Urban drainage, 3rd edn. Taylor and Francis Group, London

Chang TJ, Wang CH, Chen AS (2015) A novel approach to model dynamic flow interactions between storm sewer system and overland surface for different land covers in urban areas. J Hydrol 524:662–679. https://doi.org/10.1016/j.jhydrol.2015.03.014

Chen AS, Hammond M, Domingo ND, Hénonin J, Russo B, Mark O et al (2014) WP2 urban flood modelling. Consistent framework for analysis of urban flood risks, CORFU

Fan Y, Ao T, Yu H, Huang G, Li X (2017) A coupled 1D–2D hydrodynamic model for urban flood inundation. Adv Meteorol. https://doi.org/10.1155/2017/2819308

Fewtrell TJ, Bates PD, Horritt M, Hunter NM (2008) Evaluating the effect of scale in flood inundation modelling in urban environments. Hydrol Process 22:5107–5118. https://doi.org/10.1002/hyp.7148

Freer J, Beven KJ, Neal J, Schumann G, Hall J, Bates P (2013) Flood risk and uncertainty. In: Rougier J, Sparks S, Hill L (eds) Risk and uncertainty assessment for natural hazards. Cambridge, UK, pp 190–233

Fritsch K, Assmann A, Tyrna B (2016) Long-term experiences with pluvial flood risk management. FLOOD risk 2016. In: 3rd European conference on flood risk management. https://doi.org/10.1051/e3sconf/20160704017

Gharbi M, Soualmia A, Dartus D, Masbernat L (2016) Comparison of 1D and 2D hydraulic models for floods simulation on the Medjerda Riverin Tunisia. J Mater Environ Sci 7(8):3017–3026

Gourbesville P (2009) Data and hydroinformatics: new possibilities and challenges. J Hydroinform 11:3–4

Gupta RS (2017) Elements of the hydrologic cycle: precipitation. Hydrology and hydraulic systems, 4th edn. Waveland, USA, pp 39–63

Hankin B, Waller S, Astle G, Kellagher R (2008) Mapping space for water: screening for urban flash flooding. J Flood Risk Manag 1:13–22

Hénonin J, Hongtao M, Zheng-Yu Y, Hartnack J, Havnø K, Gourbesville P, Mark O (2015) Citywide multi-grid urban flood modelling: the July 2012 flood in Beijing. Urban Water J 12(1):52–66. https://doi.org/10.1080/1573062X.2013.851710

Henonin J, Russo B, Mark O, Gourbesville P (2013) Real-time urban flood forecasting and modelling—a state of the art. J Hydroinform 15(3):717–736. https://doi.org/10.2166/hydro.2013.132

Jaafar K, Ismail N, Tajjudin M, Adnan R, Rahiman MHF (2015) A review on flood modelling and rainfall-runoff relationships. In: 2015 IEEE 6th control and system graduate research colloquium, UiTM, Shah Alam, Malaysia. 10–11 August 2015, pp 158–162

Jahanbazi M, Egger U (2014) Application and comparison of two different dual drainage models to assess urban flooding. Urban Water J 11(7):584–595. https://doi.org/10.1080/1573062X.2013.871041

Jiang L, Chen Y, Wang H (2015) Urban flood simulation based on the SWMM model. Remote Sens GIS Hydrol Water Resour 368:186–191. https://doi.org/10.5194/piahs-368-186-2015

Josef S (2012) Dynamic Modelling Of Urban Rainfall Runoff And Drainage Coupling DHI MIKE URBAN and MIKE FLOOD. University of SalzBurg, SalzBurg

Kim B, Sanders BF, Schubert JE, Famigliet JS (2014) Mesh type tradeoffs in 2D hydrodynamic modeling of flooding with a Godunov-based flow solver. Adv Water Resour 68:42–61. https://doi.org/10.1016/j.advwatres.2014.02.013

Kourtis IM, Bellos V, Tsihrintzis VA (2017) Comparison of 1D–1D and 1D–2D urban flood models. In 15th international conference on environmental science and technology. Rhodes, Greece

Krupka M, Wallis S, Pender S, Neélz S (2007) Some practical aspects of flood inundation modeling. Publ Inst Geophys Pol Acad Sci E 7:129–135

Laouacheria F, Kechida S, Chabi M (2019) Modelling the impact of design rainfall on the urban drainage system by Storm Water Management Model. J Water a Land Dev 40(I–III):119–125. https://doi.org/10.2478/jwld-2019-0013

Leandro J, Chen AS, Djordjević S, Savić DA (2009) Comparison of 1D/1D and 1D/2D coupled (sewer/surface) hydraulic models for urban flood simulation. J Hydraul Eng 135:495–504. https://doi.org/10.1061/_ASCE_HY.1943-7900.0000037

Leandro J, Djordjević S, Chen AS, Savić DA, Stanić M (2011) Calibration of a 1D/1D urban flood model using 1D/2D model results in the absence of field data. Water Sci Technol 64:1016–1024

Leitão J (2009) Enhancement of digital elevation models and overland flow path delineation methods for advanced urban flood modelling. Dissertation, Department of Civil Engineering—Imperial College London, London

Lhomme J, Sayers PB, Gouldby BPS, Marti JM (2009) Recent developments and application of a rapid flood spreading method. In. European conference flood risk management: research and practice. Taylor and Francis

Liu L, Liu Y, Wang X, Yu D, Liu K, Huang H, Hu G (2015) Developing an effective 2-D urban flood inundation model for city emergency management based on cellular automata. Nat Hazards Earth Syst Sci 15:381–391. https://doi.org/10.5194/nhess-15-381-2015

Liu Y, Pender G (2010) A new rapid flood inundation model. In Proceedings of the first IAHR European Congress, Edinburgh, Scotland, UK, 4–6 May 2010

Liu Y, Pender G (2012) Carlisle 2005 urban flood event simulation using cellular automata-based rapid flood spreading model. Soft Comput. https://doi.org/10.1007/s00500-012-0898-1

Liu Y, Zhang W, Cui X (2012) Flood emergency management using hydrodynamic modelling. In: 2012 international conference on modern hydraulic engineering, vol 28, pp 50–753

Loucks D, van Beek E, Stedinger J, Dijkman J, Villars M (2005) Water resources systems planning and management. An introduction to methods, models and applications. UNESCO, Paris

Maksimović Č, Prodanović D, Boonya-Aroonnet S, Leitão JP, Djordjević S, Allitt R (2009) Overland flow and pathway analysis for modelling of urban pluvial flooding. J Hydraul Res 47(4):512–523. https://doi.org/10.3826/jhr.2009.3361

Mark O, Weesakul S, Apirumanekul C, Aroonnet S, Djordjevic S (2004) Potential and limitations of 1D modelling of urban flooding. J Hydrol 299:284–299. https://doi.org/10.1016/j.jhydrol.2004.08.014

Meng X, Zhang M, Wen J, Du S, Xu H, Wang L, Yang Y (2019) A Simple GIS-based model for urban rainstorm inundation simulation. Sustainability. https://doi.org/10.3390/su11102830

Moore RJ, Cole SJ, Dunn S, Ghimire S, Golding BW, Pierce CE, Roberts NM, Speight L (2015) Surface water flood forecasting for urban communities, CREW report CRW2012_03. www.crew.ac.uk/publications

Natarajan S, Radhakrishnan N (2019) Simulation of extreme event-based rainfall–runoff process of an urban catchment area using HEC-HMS. Model Earth Syst Environ. https://doi.org/10.1007/s40808-019-00644-5

Nielsen NH, Jensen LN, Linde JJ, Hallager P (2008) Urban flooding assessment. In: International conference on urban drainage, Edinburgh, Scotland, UK

Nkwunonwo UC, Whitworth M, Baily B (2020) A review of the current status of flood modelling for urban flood risk management in the developing countries. Sci Afr. https://doi.org/10.1016/j.sciaf.2020.e00269

RainGain (2015) Urban pluvial flood modelling: current theory and practice. review document related to work package 3—Action 13

Rangari VA, Gonugunta R, Umamahesh NV, Patel AK, Bhatt CM (2018) 1D–2D modeling of urban floods and risk map generation for the part of Hyderabad city. Int Arch Photogr Remote Sens Spat Inf Sci 5:445–450. https://doi.org/10.5194/isprs-archives-XLII-5-445-2018

Rao YRS, Ramana RV (2015) Storm water flood modeling in urban areas. Int J Res Eng Technol 4(11):18–21

Rosenzweig BR, McPhillips L, Chang H, Cheng C, Welty C, Matsler M, Iwaniec D, Davidson CI (2018) Pluvial flood risk and opportunities for resilience. WIREs Water 1:1. https://doi.org/10.1002/wat2.1302

Schlauß S, Grottker M (2016) Coupling process for 1D–2D numerical flash flood simulation: a parameter study of involved variables for gullies and manholes. International junior researcher and engineer workshop on hydraulic structures. doi:10.15142/T3759N

Shen D, Wang J, Cheng X, Rui Y, Ye S (2015) Integration of 2-D hydraulic model and high-resolution lidar-derived DEM for floodplain flow modeling. Hydrol Earth Syst Sci 19:3605–3616. https://doi.org/10.5194/hess-19-3605-2015

Shen J, Tong Z, Zhu J, Liu X, Yan F (2016) A new rapid simplified model for urban rainstorm inundation with low data requirements. Water. https://doi.org/10.3390/w8110512

Simões N, Ochoa S, Leitão J, Pina R, Sá Marques A, Maksimović Č (2011) Urban drainage models for flood forecasting: 1D/1D, 1D/2D and hybrid models. In: 12th international conference of urban drainage, Porto Alegre/Brasil

Sisay E, Halefom A, Khare D, Singh L, Worku T (2017) Hydrological modelling of ungauged urban watershed using SWAT model. Model Earth Syst Environ 1:1. https://doi.org/10.1007/s40808-017-0328-6

Subramanya K (2008) Engineering hydrology, 3rd edn. McGraw Hill, New Delhi. ISBN 0-07-064855-7

Sui D, Maggio R (1999) Integrating GIS with hydrological modeling: practices, problems, and prospects. Comput Environ Urban Syst 23:33–51

Tayefi V, Lane SN, Hardy RJ, Yu D (2007) A comparison of one- and two-dimensional approaches to modelling flood inundation over complex upland floodplains. Hydrol Process 21:3190–3202. https://doi.org/10.1002/hyp.6523

Teng J, Jakeman AJ, Vaze J, Croke BFR, Dutta D, Kim S (2017) Flood inundation modelling: a review of methods, recent advances and uncertainty analysis. Environ Model Softw 90:201–2016. https://doi.org/10.1016/j.envsoft.2017.01.006

Tingsanchali T (2012) Urban flood disaster management. Procedia Eng 32:25–37. https://doi.org/10.1016/j.proeng.2012.01.1233

Tsubaki R, Fujita I (2010) Unstructured grid generation for urban flood inundation. Hydrol Process 24:1404–1420. https://doi.org/10.1002/hyp.7608

Vojinovic Z, Tutulic D (2009) On the use of 1D and coupled 1D–2D modelling approaches for assessment of flood damage in urban areas. Urban Water J 6(3):183–199. https://doi.org/10.1080/15730620802566877

Walsh T, Pomeroy AC, Burian S (2014) Hydrologic modeling analysis of a passive, residential rainwater harvesting program in an urbanized, semi-arid watershed. J Hydrol 508:240–253

Weifeng L, Qiuwen C, Jingqiao M (2009) Development of 1D and 2D coupled model to simulate urban inundation: an application to Beijing Olympic Village. Chin Sci Bull 54(9):1613–1621. https://doi.org/10.1007/s11434-009-0208-1

Yang TH, Chen YC, Chang YC, Yang SC, Ho JY (2015) Comparison of different grid cell ordering approaches in a simplified inundation model. Water 7:438–454. https://doi.org/10.3390/w7020438

Zhu Z, Chen Z, Chen X, He P (2016) Approach for evaluating inundation risks in urban drainage systems. Sci Total Environ 553:1–12